## **DISSERTATION**

 $submitted\ to\ the$ 

Combined Faculty of Mathematics, Engineering and Natural Sciences of Heidelberg University, Germany

for the degree of

Doctor of Natural Sciences

## $\label{eq:put forward by}$ TIM WERNER MATHIAS HERBERMANN

born in: Dissen a.T.W., Germany Oral examination: 28.10.2025

# The Universe as a neutrino laboratory: Probing neutrino nature and interactions in cosmology and astrophysics

Referees: Prof. Dr. Dr. h.c. Manfred LINDNER

Prof. Dr. Joerg JAECKEL

#### Abstract

Understanding neutrino properties remains a key open question in particle physics. This thesis explores how cosmology and astrophysics constrain or support a possible Dirac nature of neutrinos and probe neutrino interactions with dark matter (DM).

Explaining a Dirac mass for neutrinos requires new fields and symmetries. These lead to an experimentally constrained excess in  $\Delta N_{\rm eff}$  from production of right-handed neutrinos in the early Universe. We develop a Monte Carlo-based scheme for integrated Boltzmann equations and apply it to Dirac neutrino models. First, we study Z' extensions, finding them subject to strong and generic constraints from  $\Delta N_{\rm eff}$  that are only avoided if the thermal history of the Universe was non-standard or it reheated to  $T_{\rm reh} \ll m_{Z'}$ .

We also introduce a Dirac-Type-I seesaw family as a unified framework of Dirac seesaws and a generalization of the Majorana Type-I seesaw family. We study two minimal UV completions with a spontaneously broken global symmetry yielding the Diracon as a Nambu-Goldstone boson. The production of light degrees of freedom is suppressed compared to gauged models, which leads to weaker bounds from  $\Delta N_{\rm eff}$  in direct comparison. Astrophysical and laboratory-based flavor observables involving the Diracon and complementary to  $\Delta N_{\rm eff}$  are identified. Minimal Dirac models with a global symmetry appear as a viable alternative to a gauge symmetry, due to the strong and generic constraints we find on the latter.

In a separate study, we turn to astrophysical tests of neutrino-DM interactions. We investigate the upscattering of MeV-scale DM by the diffuse supernova neutrino background (DSNB), focusing on model dependence and improved flux attenuation modeling. The strength of neutrino-DM interactions preferred by cosmological data is below current experimental sensitivities. We discuss the role of DSNB upscattering in probing such interactions and its wider implications for DM direct detection. Unlike cosmological tests, upscattering offers a direct experimental window into neutrino-DM interactions.

#### Zusammenfassung

Viele Neutrinoeigenschaften sind weiterhin ungeklärt. Diese Arbeit untersucht, wie kosmologische und astrophysikalische Beobachtungen Hinweise auf eine mögliche Dirac-Natur von Neutrinos liefern und wie sich ihre Wechselwirkungen mit Dunkler Materie (DM) untersuchen lassen.

Das Erzeugen von Dirac-Massen für Neutrinos erfordert neue Felder und Symmetrien. Diese führen zur Produktion rechtshändiger Neutrinos im frühen Universum und zu einem messbaren Überschuss in  $\Delta N_{\rm eff}$ . Wir entwickeln ein Monte-Carlo-basiertes Verfahren zur Lösung integrierter Boltzmann-Gleichungen und wenden es auf Dirac-Neutrinomodelle an. Zunächst untersuchen wir Z'-Erweiterungen und zeigen, dass diese starken und generischen Einschränkungen unterliegen, die nur vermieden werden können, wenn das frühe Universum vom Standardmodell abwich oder die Wiederaufheiztemperatur bei  $T_{\rm reh} \ll m_{Z'}$  lag.

Wir generalisieren das Konzept der Type-I Seesaw Familie als kompakte Beschreibung verschiedener Seesaw-Modelle auf den Dirac-Fall. Zwei minimale, UV-vollständige Modelle mit spontan gebrochener globaler Symmetrie und dem Diracon als Nambu-Goldstone-Boson werden analysiert. Die Produktion leichter Freiheitsgrade ist hier im direkten Vergleich gehemmt, wodurch diese Modelle mit Messungen von  $\Delta N_{\rm eff}$  verträglicher erscheinen. Komplementäre flavor-verletzende Observablen im Labor und in der Astrophysik werden identifiziert. Minimale Dirac-Modelle mit einer globalen Symmetrie bieten sich als eine Alternative an, um die starken und generischen Einschränkungen für Varianten mit Eichsymmetrien zu umgehen.

In einer separaten Studie wenden wir uns astrophysikalischen Tests von Neutrino-DM-Wechselwirkungen zu. Wir untersuchen die Aufwärtsstreuung von DM im MeV-Bereich durch den diffusen Supernova-Neutrinohintergrund (DSNB) mit Fokus auf Modellabhängigkeit und verbesserter Modellierung der Abschwächung des DM-Flusses in Materie. Wechselwirkungen von Neutrino und DM, wie sie von kosmologischen Daten nahegelegt werden, liegen unterhalb experimenteller Empfindlichkeiten. Wir analysieren die Rolle der DSNB-Aufwärtsstreuung beim Testen solcher Wechselwirkungen sowie ihre Bedeutung für den Nachweis von Dunkler Materie. Im Gegensatz zu kosmologischen Tests bietet die Aufwärtsstreuung einen direkten experimentellen Zugang zu Neutrino-DM-Wechselwirkungen.

## Contents

$\mathbf{D}^{i}$	isclai	mer	vii				
1	Intr	roduction	1				
2	Neutrinos in the Standard Model and beyond						
	2.1	Neutrinos in the Standard Model	5				
		2.1.1 Electroweak theory	6				
	2.2	Phenomenology of massive neutrinos	9				
		2.2.1 Dirac and Majorana masses	10				
		2.2.2 Lepton mixing	10				
		2.2.3 Neutrino oscillations	11				
		2.2.4 Matter effects and adiabatic flavor conversion	13				
		2.2.5 Neutrinoless double beta decay	14				
		2.2.6 Helicity and chirality	15				
	2.3	Massive neutrinos are new physics	16				
		2.3.1 No neutrino masses in the SM	16				
		2.3.2 Neutrino masses slightly beyond SM	17				
3	Hov	v neutrinos shape the Universe	21				
•	3.1	An early Universe primer	21				
	0.1	3.1.1 The $\Lambda$ CDM model	21				
		3.1.2 A brief timeline of the early Universe	22				
		3.1.3 Cosmological Boltzmann equations	23				
	3.2	Neutrinos in the early Universe	$\frac{20}{24}$				
	0.2	3.2.1 Neutrino decoupling and $\Delta N_{\rm eff}$	25				
		3.2.2 Neutrino masses in cosmology	28				
	3.3	Neutrinos in the late Universe	29				
	5.5	3.3.1 Supernovae	29				
		3.3.2 Diffuse supernova neutrino background	31				
		5.5.2 Diffuse supernova fleutrino background	91				
4		e Monte Carlo approach to Boltzmann equations	35				
	4.1	General framework	35				
	4.2	Thermal corrections	37				
	4.3	Resonances	39				
		4.3.1 The narrow width approximation	39				
		4.3.2 Mediators in thermal equilibrium	41				
5	$\mathbf{Cos}$	mology of Dirac neutrinos with a $Z'$	43				
	5.1	A minimal B-L model	44				
		5.1.1 Particle content	44				
		5.1.2 Cosmology	45				
		5.1.3 Results	45				
		5.1.4 Probing Dirac neutrinos up to the GUT scale?	47				

	5.2	Cosmology revisited	47
		5.2.1 Extra degrees of freedom	49
		5.2.2 Phase transitions and other early dark energies	49
		5.2.3 Early matter dominated era	51
		5.2.4 Reheating	52
	5.3	The future of gauge symmetries and Dirac neutrinos	54
6	The	e Dirac Type-I seesaw family	57
	6.1	The Type-I Dirac seesaw family	. 58
	6.2	Minimal realizations	60
		6.2.1 Scalar sector	
		6.2.2 Canonical model	62
		6.2.3 Enhanced model	63
	6.3	Phenomenology of the Dirac Type-I seesaw	64
		6.3.1 Invisible Higgs decays	64
		6.3.2 Lepton flavor violation	65
	6.4	Cosmology of the Dirac Type-I seesaw	. 68
		6.4.1 General setup	. 68
		6.4.2 Phase transition dynamics	
		6.4.3 Process details and the degenerate BSM approximation	. 70
		Scalar sector	71
		Yukawa sector	73
	6.5	Results	. 74
		6.5.1 Model I: Canonical model	. 74
		6.5.2 Model II: Enhanced Diracon model	. 80
	6.6	Summary and future directions	84
7	Boo	osted Dark Matter from the Diffuse Supernova Neutrino Background	87
	7.1	From boost to detection	. 88
		7.1.1 Upscattering	. 88
		7.1.2 Attenuation	. 89
		7.1.3 Detection and statistical analysis	90
	7.2	Models and the role of energy dependence	91
	7.3	Results	93
	7.4	Summary and future directions	96
8	Sun	nmary and Outlook	99
${f A}$	Coll	lision operator	103
		Implementation	
		A.1.1 $2 \rightarrow 2$ processes	
		A.1.2 $1 \rightarrow 2$ processes	
В	Dira	acon-charged lepton interactions	107
Ad	cknov	wledgements	109
		graphy	111
וע	שטונעו	LI ADII V	

### Disclaimer

This thesis is mainly based on three publications that are published in peer-reviewed journals or, at time of writing, are in the peer-review process. The scientific results of these publications are the basis of the Chapters 4, 5, 6 and 7,

- [1] Anirban Das et al. "Energy-dependent boosted dark matter from diffuse supernova neutrino background". In: JCAP 07 (2024), p. 045. DOI: 10.1088/1475-7516/2024/07/045. arXiv: 2403.15367 [hep-ph],
- [2] Tim Herbermann and Manfred Lindner. "Improved cosmological limits on Z' models with light right-handed neutrinos". In: accepted for publication in JCAP (May 2025). arXiv: 2505.04695 [hep-ph],
- [3] Salvador Centelles Chuliá et al. "Flavour and cosmological probes of Diracon models". In: accepted for publication in JHEP (June 2025). arXiv: 2506.06449 [hep-ph],

all of which were done by the author in collaboration with others.

In addition, the the following study that was done by the author in collaboration with others, but is not part of this doctoral thesis, was published in a peer-reviewed journal

[4] Tim Herbermann, Manfred Lindner, and Manibrata Sen. "Attenuation of cosmic ray electron boosted dark matter". In: *Phys. Rev. D* 110.12 (2024), p. 123023. DOI: 10.1103/PhysRevD.110.123023. arXiv: 2408.02721 [hep-ph].

Some results of Refs. [1, 4] were also presented by the author at the Neutrino Oscillation Workshop 2024 and published in a conference proceedings

[5] Anirban Das et al. "Energy-dependent boosted DM from DSNB". in: *PoS* NOW2024 (2025), p. 014. DOI: 10.22323/1.473.0014.

## Chapter 1

## Introduction

After proposing the existence of a new, feebly interacting, and neutral particle to explain the energy spectrum of  $\beta$ -decay, Wolfgang Pauli is said to have remarked in 1930 that "I've done a terrible thing today, something which no theoretical physicist should ever do. I have suggested something that can never be verified experimentally." [6]. Only around 26 years later, Pauli was proven wrong. F. Reines and C. L. Cowan found the neutrino in the inverse  $\beta$ -decay  $\bar{\nu}_e + p \rightarrow e^+ + n$ , utilizing a nuclear reactor as a  $\bar{\nu}_e$  source [7].

Once feared as practically undetectable, neutrinos are now routinely measured. Just a decade after the first direct neutrino detection, the HOMESTAKE experiment observed solar neutrinos [8, 9], establishing the solar neutrino problem, which was later confirmed by Kamiokande and Super-Kamiokande [10–12], and the Sudbury neutrino observatory (SNO) [13, 14].

From the 1990s, various experiments began to show evidence of neutrino flavor transformations and oscillations. In 1998, Super-Kamiokande (SK) hinted at first evidence for flavor oscillations in atmospheric neutrinos [15–18] and later in reactor neutrinos in Double Chooze [19, 20] and Daya Bay [21, 22]. KamLAND and others firmly established neutrino flavor oscillations [23], and experiments like T2K marked the beginning of the precision era for neutrino oscillation parameters [24, 25] and global fits [26–28].

More recent advances include the detection of coherent elastic neutrino nucleus scattering (CE $\nu$ NS) [29, 30]. Next-generation facilities like the Jiangmen Underground Neutrino Observatory (JUNO) [31], Hyper-Kamiokande (HK) [32], and the Deep Underground Neutrino Experiment (DUNE) [33], which are currently under construction, will push the experimental landscape to new levels of precision.

What once made Pauli doubt that the neutrino could ever be detected is still a limiting factor when studying neutrinos in Earth-bound experiments – the feebleness of their interaction. Novel neutrino-matter interactions are predicted by many models beyond the standard model. However, this is anything but guaranteed. Parameters like detector scale and exposure time are, in principle, in our control, but more often than not, there are external constraints on the experiments we can pursue. Even then, sources of neutrinos available to us are limited in their luminosity and at the energy frontier.

At this point, cosmological and astrophysical observations become crucial. Many Earthbound experiments already utilize neutrinos from the heavens, such as solar neutrinos, but also high-energy neutrinos of known and unknown astrophysical sources are routinely studied in terrestrial detectors. Similarly, neutrinos from galactic supernovae as well as the diffuse supernova neutrino background (DSNB) are in reach, both with important consequences for fundamental neutrino physics and astrophysics [34, 35]. But Earth-bound detection facilities remain a limiting factor.

This is where we take the neutrinos from the heavens one step further and turn astrophysical systems themselves into a neutrino laboratory. Ideas revolving around these indirect probes of new physics are at the heart of astroparticle physics. These systems typically provide competitive limits from a combination of strong neutrino fluxes and dense host systems, or potentially large volumes, and thus partially compensate for small neutrino interactions by an effectively increased number of available targets. A particularly difficult to study benchmark case is interactions between neutrinos and dark matter (DM). Many models of extended neutrino sectors predict such interactions, and testing them necessarily requires the use of cosmological and astrophysical probes.

By now, neutrinos are not only measured and studied for their own sake, but they provide valuable input on astrophysics, too. With the supernova SN1987A and only around  $\mathcal{O}(10)$  detected events [36, 37], it paved the way for establishing the standard picture of neutrino driven core collapse supernovae [38]. A future supernova observation will not only improve insights on supernova physics but also fundamental neutrino physics. Observing astrophysical events like neutron star mergers in electromagnetic radiation, gravitational waves, and neutrinos heralds the beginning of true multi-messenger astronomy [39].

On cosmological scales, the large scale structure as well as global properties of the Universe can be used to constrain neutrino physics. Recently, cosmological neutrino mass limits were improved by DESI to  $\sum m_{\nu} < 0.064\,\mathrm{eV}$  [40]. This new result is stronger than the current best limit from the laboratory by KATRIN, which constrains the effective mass in  $\beta$ -decay  $m_{\beta} < 0.45\,\mathrm{eV}$  [41], and cosmology begins to put pressure on the inverted mass hierarchy, and there is even a mild tension with the minimal expectation from flavor oscillations in normal mass ordering.

Beyond neutrino masses, cosmology also constrains abundances of light additional degrees of freedom in the early Universe, and therefore, light right-handed neutrinos and their interactions. Early results already disfavored a fourth light neutrino flavor [42, 43], and limits continuously tightened to a current  $\Delta N_{\rm eff} \simeq 0.17$  from either CMB only [44, 45] or CMB and BBN combinations [46, 47]. At the current stage, both the presence of light neutrinos and other particles are strongly constrained from measurement and the precise prediction for the SM [48–51]. Cosmology effectively constrains neutrino properties from the large volumes under consideration. Indeed, the effect of neutrinos in cosmology is small but measurable because of the integrated effect of neutrinos on cosmological evolution at the global and the perturbative level. Thus, cosmological time and length scales allow for a compensation of small neutrino interactions, gravitational, weak, or otherwise.

Despite the enormous experimental and theoretical progress since inception and first detection, neutrino physics remains among the most active fields in (astro-)particle physics. The Standard Model (SM) of particle physics predicts massless neutrinos. When extending the SM to allow for massive neutrinos compatible with oscillation data, neutrino masses can be of either Dirac or Majorana type. Observation of neutrinoless double beta decay [52, 53] could clarify

this situation, but it remains unobserved thus far. As it is generally believed that differences between Dirac and Majorana neutrinos are neutrino mass suppressed [54], there is no clear experimental indication as to what option is preferred at the moment. Indeed, both options have been and continue to be studied widely. Important early contributions to Majorana masses are e.g. Refs. [55–63].

Historically, the Dirac option received less coverage, but gained more popularity in recent years and is now a very active field of research, see for instance Refs. [64–105] for a non-exhaustive collection of recent studies. These models routinely predict other properties of neutrinos, such as non-standard interactions among neutrinos or with other SM particles, or interactions with the elusive DM. All these additional predictions serve as potential observables to discriminate between different proposed models.

In this thesis, we advance the study of neutrinos in cosmology and astrophysical systems. The focus here is not on well-established standard properties of neutrinos, such as their mass, but rather to assess the potential of cosmology and, to a lesser extent astrophysics, to constrain and possibly distinguish between different well-motivated models of neutrino masses and interactions.

Of particular interest to us are models of Dirac neutrinos. Observing neutrinoless double beta decay would clarify the question of the nature of neutrinos. However, it has not been observed thus far, and even if neutrinos are Majorana in nature, it may be possible that rates are observationally inaccessible to us. This motivates us to study the Dirac hypothesis in light of the aforementioned advantages of cosmological and astrophysical probes. Perhaps it is possible that we can compensate for the neutrino mass suppressed difference between the two by looking for other signatures that could be attributed to Dirac neutrinos. While it is not possible to conclusively prove the Dirac nature of neutrinos from such an observation, just as we cannot infer the Dirac nature from non-observation of  $0\nu\beta\beta$ -decay, it can nevertheless be a clue towards a possible Dirac nature.

Models of Dirac neutrinos typically have two desirable features. Just as in the case for Majorana neutrinos, we wish for a natural explanation of the smallness of neutrino masses, e.g. by a seesaw mechanism. The introduction of light right-handed neutrinos also raises the question of why a Majorana mass term for them is absent. Indeed, right-handed neutrinos are SM gauge singlets, and therefore, nothing forbids them from having a Majorana mass a priori. Usually, this issue is addressed by protecting the Dirac nature by symmetry. This can be done either by a global symmetry [106–112] or a gauge symmetry [43, 113–116]. In either case, extended models generically contain new interactions and light degrees of freedom, such as right-handed neutrinos, and for the global symmetry option, potential Nambu-Goldstone bosons. Therefore, we identify an excess in the effective number of neutrinos  $\Delta N_{\rm eff}$  as a strong hint for light new physics and a suggestive clue to a possible Dirac nature of neutrinos.

In this thesis, we study a gauged  $U(1)_{B-L}$  as a benchmark for generic Z' extensions that protect the Dirac nature and compute the strongest limits on such extensions thus far. The constraints we find are generic and strong, but sensitive to the underlying cosmology. We focus on the intertwined relationship between cosmology and Dirac neutrinos, and study the role of non-standard cosmological histories. We highlight how constraints can be generically avoided

when moving to non-standard thermal histories, or how in return Dirac neutrinos would equip us with a unique probe of the otherwise inaccessible pre-BBN era, if they are protected by a gauge symmetry.

We also introduce the notion of a Dirac Type-I seesaw family that generalizes an analogous result from Majorana neutrinos and offers a unified framework to systematically study different Dirac seesaw models. Two minimal realizations with a global symmetry that protects the neutrino nature are studied in more detail. We find that flavor observables and cosmology provide complementary results. Moreover, results for such minimal models with global symmetries tend to be less generic, and constraints are weaker than for their gauged variants in direct comparison. We find that cosmological signatures are essentially suppressed by the imposed seesaw condition, and conjecture that similar results can be expected for other minimal models. This seems like an appealing alternative to protect the Dirac nature and also avoid generic bounds from gauged variants, however, we also acknowledge the conjectured breaking of global symmetries by gravity. We discuss possible implications for the Dirac hypothesis more generally in light of the generic constraints on gauged variants.

In an additional research project, we investigate interactions between DM and neutrinos irrespective of the neutrino nature. Different cosmological data sets show a slight preference for such interactions [117–120]. However, they are only probed indirectly, and degeneracies between cosmological parameters make definitive conclusions difficult. When considering an MeV-scale DM candidate, it is possible to directly study such interactions. We utilize the concept of boosted dark matter (BDM) [121] and apply it to upscattering by the diffuse supernova neutrino background (DSNB). Here we pivot towards toy models that mimic realistic interactions, and we highlight the importance of model-dependent interactions and attenuation of dark matter fluxes beyond boosting by the DSNB. This analysis embeds well into a larger active body of research that studies neutrino-DM interactions by upscattering of dark matter from different neutrino sources [122–130]. It is not only a building block towards a more complete picture of neutrino-DM interactions, but also for the landscape of BDM more generally.

This thesis is structured as follows: In Chapter 2, we discuss neutrinos in the SM and beyond with a focus on massive neutrino phenomenology, and an extended discussion of why neutrino masses hint at physics beyond the standard model (BSM). Chapter 3 addresses how neutrinos shape cosmological and astrophysical environments. In Chapter 4, we develop a Monte Carlo approach for solving integrated Boltzmann equations. We use it in Chapter 5 to study Dirac neutrinos protected by a gauged  $U(1)_{B-L}$ . We provide the strongest limits on such scenarios thus far and address the symbiotic relationship between cosmology and neutrino physics. In Chapter 6, we introduce the Dirac Type-I seesaw family. We study the phenomenology of two minimal realizations that protect the Dirac nature through a global symmetry and find complementarity between cosmology and flavor observables. Chapter 7 considers upscattering of MeV-scale dark matter by the DSNB. We highlight the strong model dependence of limits in such upscattering scenarios and identify upscattering more generally as a unique and direct probe of dark matter-neutrino interactions. We conclude in Chapter 8.

## Chapter 2

## Neutrinos in the Standard Model and beyond

In this Chapter, we give a high-level overview of the Standard Model of particle physics with a particular focus on leptons and specifically neutrinos. We also work out how neutrinos point towards BSM physics, and outline some well-motivated extensions in the neutrino sector. The presentation at hand is by no means complete, nor does it attempt to be. It is rather intended to make the present thesis a self-contained work, and perhaps more importantly, we wish to motivate aspects of the research undertaken during the preparation of this thesis.

#### 2.1 Neutrinos in the Standard Model

The Standard Model of particle physics is a gauge theory based on the gauge group  $\mathcal{G}_{SM} = SU(3)_C \times SU(2)_L \times U(1)_Y$ . With the exception of gravity, as described by the theory of General Relativity (GR), the forces arising from the SM suffice to explain close to all phenomena occurring in the realm of particle physics. The strong interaction is connected to the color gauge group  $SU(3)_C$  and is often referred to as quantum chromodynamics (QCD). Its gauge bosons are the eight massless gluons, coupled to the color charged quarks, and strong interactions play a supreme role in the structure of the material world. However, as far as neutrinos are concerned, they are uncharged under the color group and, therefore, we do not study QCD in more detail here.

The part of the SM that is most important to us here is the gauge group  $SU(2)_L \times U(1)_Y$ , and the theory is also referred to as the Glashow-Salam-Weinberg theory [131–133]. It is a chiral theory, since  $SU(2)_L$  only couples to left chirality, and also the  $U(1)_Y$  charges differ

Fields	$SU(3)_C$	$SU(2)_L$	$U(1)_Y$
$Q_L = \begin{pmatrix} u_L \\ d_L \end{pmatrix}$	3	2	1/3
$L = \begin{pmatrix} \nu_L \\ e_L \end{pmatrix}$	1	2	-1
$u_R$	3	1	4/3
$d_R$	3	1	-2/3
$\ell_R$	1	1	-2

Table 2.1: Fields of the SM and charge assignments under the gauge group.

between left- and right-handed fields. The presence of chiral gauge interactions forbids explicit mass terms due to gauge invariance, a problem that is resolved by the Brout-Englert-Higgs mechanism (or Higgs mechanism for short) [134–136]. A scalar doublet under  $SU(2)_L$  undergoes spontaneous symmetry breaking and develops a vacuum expectation value (VEV), which in return grants an effective mass to fermions and gauge bosons due to their couplings to the Higgs field.

We start by reviewing the Glashow-Salam-Weinberg or simply electroweak (EW) theory with a particular focus on the leptonic sector, and then follow with a detailed summary of neutrinos in the SM.

#### 2.1.1 Electroweak theory

We identify the electroweak part of the theory as the Lagrangian density

$$\mathcal{L} \supset \mathcal{L}_{\text{gauge}} + \mathcal{L}_{\text{fermion}} + \mathcal{L}_{\text{scalar}} + \mathcal{L}_{\text{Yukawa}},$$
 (2.1)

where gauge includes gauge field kinetic terms, fermion refers to the fermionic kinetic terms as well as their gauge interactions, scalar is the Higgs doublet associated kinetic terms and scalar potential and finally, Yukawa refers to the Yukawa interactions between the fermions and the Higgs field.

The EW part contains the correct fields and interaction structure required to explain observations, but it comes with a rather severe shortcoming. Experimental results show that the EW gauge bosons are massive, and only the photon is consistent with being massless. Moreover, mass terms in  $\mathcal{L}_{\text{fermion}}$  are not consistent with gauge invariance. Indeed, it is obvious that left-and right-handed fermion fields transform under different representations of  $SU(2)_L \times U(1)_Y$ . An explicit mass term  $m\bar{f}f = m(\bar{f}_L f_R + \bar{f}_R f_L)$  is manifestly not gauge invariant – a mass term written as such is a doublet under  $SU(2)_L$ .

The resolution of this problem comes from the Brout-Englert-Higgs mechanism, which postulates the spontaneous breakdown of electroweak symmetry

$$SU(2)_L \times U(1)_Y \to U(1)_{EM}$$
, (2.2)

where  $U(1)_{EM}$  is the unbroken abelian group of quantum electrodynamics (QED) with one massless gauge boson that is identified as the photon. The spontaneous breaking results from the Higgs field H developing a non-zero VEV.

In the SM, the scalar part of the Lagrangian,

$$\mathcal{L}_{\text{scalar}} = (D_{\mu}H)^{\dagger}(D^{\mu}H) - \mu^{2}H^{\dagger}H - \lambda(H^{\dagger}H)^{2}, \qquad (2.3)$$

is compatible with the gauge charge assignment. For  $\mu^2 > 0$ , the potential describes an EW doublet of mass  $\mu$ , however, if  $\mu^2 < 0$  the situation changes. The potential is of "Mexican hat" type, and the ground state of the potential no longer coincides with zero field value. Instead, the minimum is at some  $\langle H \rangle \neq 0$ , and interactions of other fields with the Higgs doublet give rise to masses.

To reproduce the correct low energy theory, the VEV should be in the neutral component, i.e.

$$H = \begin{pmatrix} G_W \\ \frac{1}{\sqrt{2}}(v+h+iG_Z) \end{pmatrix}, \qquad \langle H \rangle = \frac{1}{\sqrt{2}} \begin{pmatrix} 0 \\ v \end{pmatrix}, \qquad (2.4)$$

where we made manifest the degrees of freedom of the complex scalar doublet by introducing the auxiliary parametrization in terms of the complex scalar  $G_W$ , and the two real scalars h and  $G_Z$ . Our notation already suggests that three of the four degrees of freedom are not physical, but rather, they are the would-be Nambu-Goldstone bosons giving rise to the longitudinal modes of the massive EW gauge bosons. It is straightforward to work out the mass of the physical scalar degree of freedom h by expanding the potential accordingly. We find  $m_h^2 = -2\mu^2$ , which may be used to replace  $\mu^2$ .

It becomes evident that the remaining scalar degrees of freedom are not physical if we choose a different parametrization of the Higgs doublet.<sup>2</sup> We write in terms of real fields  $\zeta_i$ , **h** 

$$H = \exp\left(i\zeta_i/v\tau_i\right) \begin{pmatrix} 0\\ \frac{1}{\sqrt{2}}(v+\mathbf{h}) \end{pmatrix}, \qquad (2.5)$$

where i = 1, 2, 3 and  $\tau_i$  are the generators of  $SU(2)_L$ . It is no coincidence that the exponential in this parametrization resembles a gauge transformation. In fact, it can readily be gauged away, which corresponds to going to the unitary gauge that makes the physical degrees of freedom manifest. We can observe that they must become the longitudinal modes of the massive gauge bosons, by showing that indeed, the gauge bosons are massive upon developing a VEV in the Higgs doublet. Consider the kinetic terms

$$(D_{\mu}H)^{\dagger}(D^{\mu}H) \supset \frac{v^2}{8} \left[ g^2 W_{\mu}^1 W^{1\mu} + g^2 W_{\mu}^2 W^{2\mu} + \left( g W_{\mu}^3 - g' B_{\mu} \right) \left( g W^{\mu 3} - g' B^{\mu} \right) \right] , \qquad (2.6)$$

which, due to non-zero VEV, give rise to a gauge boson mass matrix. We identify the physical gauge bosons by their mass eigenstates, which is obtained by a simple field space rotation. The physical bosons are

$$W_{\mu}^{\pm} = \frac{1}{\sqrt{2}} (W_{\mu}^{1} \mp W_{\mu}^{2}), \qquad (2.7)$$

$$Z_{\mu} = \cos \theta_W W_{\mu}^3 - \sin \theta_W B_{\mu} \,, \tag{2.8}$$

$$A_{\mu} = \sin \theta_W W_{\mu}^3 + \cos \theta_W B_{\mu} \,, \tag{2.9}$$

<sup>&</sup>lt;sup>1</sup>After all, the ground state of our Universe seemingly respects electromagnetic charges.

<sup>&</sup>lt;sup>2</sup>Equivalence of the theories is guaranteed by field re-parametrization invariance, and the  $\mathbf{h}$  of the "radial" Higgs is not to be confused with the Cartesian h. However, both choices give rise to exactly the same S-matrix and therefore are equally good choices of the physical Higgs.

where  $\sin \theta_W = g'/\sqrt{g^2 + g'^2}$  and  $\cos \theta_W = g/\sqrt{g^2 + g'^2}$ . The gauge boson masses are

$$M_W^2 = \frac{g^2 v^2}{4} \,, \tag{2.10}$$

$$M_Z^2 = (g^2 + g'^2)\frac{v^2}{4},$$
 (2.11)

$$M_A^2 = 0. (2.12)$$

Thus, we observe that the Higgs mechanism gives rise to two massive, physical gauge bosons, associated with weak interactions, and one massless boson that is identified as the photon.

Since the Higgs field is a doublet under  $SU(2)_L$ , we can have Yukawa terms between left-handed doublets and right-handed singlets under  $SU(2)_L$ . We define a conjugate Higgs field  $\tilde{H} = -i\tau_2 H^*$ , and the most general Yukawa terms we can write in the SM are given by

$$\mathcal{L}_{\text{Yukawa}} = -Y_{ij}^u \bar{Q}_{iL} \tilde{H} u_{jR} - Y_{ij}^d \bar{Q}_{iL} H d_{jR} - Y_{ij}^\ell \bar{L}_i H \ell_{jR} + \text{h.c.}$$
(2.13)

The indices i, j run over the generations and we note that, in general, nothing forbids Yukawa couplings across generations, i.e. the  $Y_{ij}$  are arbitrary complex matrices.

Due to the Higgs field VEV, the fermions acquire mass terms of the form

$$\mathcal{L}_{\text{Yukawa}} \supset -Y^u \frac{v}{\sqrt{2}} \bar{u}_L u_R - Y^d \frac{v}{\sqrt{2}} \bar{d}_L d_R - Y^\ell \frac{v}{\sqrt{2}} \bar{\ell}_L \ell_R + \text{h.c.}$$
 (2.14)

The mass matrices  $M = Yv/\sqrt{2}$  are in general neither symmetric nor hermitian, though they can be diagonalized by biunitary transformations such that

$$S^{\dagger}MT = \widehat{M} \,, \tag{2.15}$$

where  $\widehat{M}$  is diagonal and with positive eigenvalues. Correspondingly, we denote by  $\widehat{u}$  etc. the mass basis rotated fields that are eigenstates of the mass matrix.

Let us ignore the leptonic part for the time being, after all, it is somewhat simpler due to the absence of  $\nu_R$  in the SM. Instead, we study the charged current interaction between upand down-type quarks mediated by the physical W-boson. The gauge basis eigenstates relate to the mass basis eigenstates by  $u_L = S_u \widehat{u}_L$  and  $d_L = S_d \widehat{u}_d$ . Then, the charged current

$$J^{\mu} = \bar{u}_L \gamma^{\mu} d_L = \bar{\hat{u}}_L \gamma^{\mu} \left[ S_u^{\dagger} S_d \right] \hat{d}_L \tag{2.16}$$

is not diagonal in the mass basis – we observe mixing between different quark flavors in charged current interactions. We capture the mixing by defining the Cabibbo-Kobayashi-Maskawa (CKM) matrix [137, 138]

$$V_{\text{CKM}} = S_u^{\dagger} S_d \,. \tag{2.17}$$

The implications for quark physics are enormous, and we will not touch here on the plethora of phenomena associated with the quark mixing.

If it were not for the absence of  $\nu_R$  in the SM, the same pattern of lepton mixing and mass generation could occur. Without the right-handed neutrino, we only generate a mass term for

the charged leptons, and the issue of simultaneous diagonalization does not arise. Hence, we should not expect mixing in the lepton sector.

However, neutrino oscillations are an experimental reality. They do not strictly prove that neutrinos are massive, but the observed E/L dependence of oscillations and all other experimental observations are well fit by neutrino masses. We note that alternative explanations are possible [139], but nevertheless, the existence of at least two massive neutrino states is generally accepted and considered the simplest explanation of observation (see also Ref. [140]). In the next section, we explore in more detail why the SM cannot accommodate a non-zero neutrino mass, and why neutrino flavor oscillations, and by extension neutrino masses as the generally accepted explanation, can be considered a herald of BSM physics.

#### 2.2Phenomenology of massive neutrinos

In this section, we discuss some of the phenomenological implications of neutrino masses. For more details, see e.g. Ref. [141]. As we discussed before, neutrino flavor oscillations do not strictly prove the existence of neutrino masses. The global experimental landscape, however, is well described by the presence of neutrino masses, and it is generally assumed that neutrinos are massive with experimentally determined mass difference values of [28]<sup>3</sup>

$$\Delta m_{21}^2 = 7.50_{-0.20}^{+0.22} \times 10^{-5} \,\text{eV}^2,$$
 (2.18)

$$\Delta m_{21}^2 = 7.50_{-0.20}^{+0.22} \times 10^{-5} \,\text{eV}^2 \,,$$

$$\left| \Delta m_{31}^2 \right| = 2.55_{-0.03}^{+0.02} \times 10^{-3} \,\text{eV}^2 \,.$$
(2.18)

Since the sign of  $\Delta m_{31}^2$  is unknown, there are two different possible mass orderings called normal ordering (NO) and inverted ordering (IO),

$$m_1 < m_2 < m_3 \text{ (NO)}$$
 and  $m_3 < m_1 < m_2 \text{ (IO)}$ . (2.20)

Despite its smallness, the mass splitting plays an important role for the phenomenology of massive neutrinos. The absolute scale of neutrino masses is still unknown, but tight upper limits exist showing that neutrinos are expected to have masses below eV scale. The Karlsruhe Tritium Neutrino (KATRIN) experiment provides the most stringent upper bound from the laboratory by means of direct measurement of the  $\beta$ -decay spectrum endpoints, finding [41]

$$m_{\beta} < 0.45 \,\text{eV} \,(90\% \,\text{CL})\,,$$
 (2.21)

for the effective electron anti-neutrino mass  $m_{\beta} = \sum_i |U_{ei}| \, m_i^2$  visible in the experiment.

Indirect cosmological probes are even stronger. Here, we must acknowledge the inherent difficulty of inferring neutrino masses from cosmological data due to model dependence and parameter degeneracies. We discuss how cosmology is sensitive to neutrino masses in more

<sup>&</sup>lt;sup>3</sup>We quote here best-fit values for normal mass ordering from global fits, see also the following discussion. The best-fit for inverted mass ordering is slightly different.

detail in Sec. 3.2.2. The current cosmological bounds by DESI [40] and ACT [44] give

$$\sum m_{\nu} < 0.064 \,\text{eV} \,(95\% \,\text{DESI}) \,, \tag{2.22}$$
$$\sum m_{\nu} < 0.089 \,\text{eV} \,(95\% \,\text{ACT}) \,, \tag{2.23}$$

$$\sum m_{\nu} < 0.089 \,\text{eV} \,(95\% \,\text{ACT})\,,$$
 (2.23)

but the minimal sum of neutrino masses inferred from flavor oscillations should be approximately  $\sum m_{\nu} > 0.06 \,\mathrm{eV}$  for NO and  $\sum m_{\nu} > 0.1 \,\mathrm{eV}$  for IO. This is already in tension with IO and suggests that even for NO the absolute scale of neutrino masses cannot significantly exceed the mass splitting.

#### 2.2.1Dirac and Majorana masses

Let us consider a massive fermion, tentatively called  $\nu$ , but the discussion that follows is general. We discuss the Dirac mass term, as we already encountered it for the other SM fermions. Such a mass term in the Lagrangian is of the form

$$\mathcal{L} \supset -m\bar{\nu}\nu = m(\bar{\nu}_L + \bar{\nu}_R)(\nu_L + \nu_R), \qquad (2.24)$$

so it couples the left- and the right-handed components of  $\nu$ , and a massive field requires the existence of both,  $\nu_L$  and  $\nu_R$ . However, combining two distinct Weyl spinors  $\nu_L$  and  $\nu_R$  to form a Dirac spinor is not the only way to include a mass term.

Another option comes from the observation that the particle-anti-particle conjugated field defined by  $\nu \to \nu^c = C\bar{\nu}^T$ ,  $C = i\gamma^2\gamma_5$  implies  $(\nu_L)^c = (\nu^c)_R$ , i.e. it is right-handed.<sup>4</sup> Thus, instead of having a distinct right-handed Weyl spinor, we can replace  $\nu_R$  with the right-handed  $(\nu_L)^c$  to build

$$\nu = \nu_L + e^{i\phi}(\nu_L)^c \,, \tag{2.25}$$

with an arbitrary phase factor  $e^{i\phi}$ . It can be used to construct a mass term of the form in Eq. (2.24), but with  $\nu_R$  replaced by the conjugate of  $\nu_L$ .

The particle-anti-particle conjugate of  $\nu$  is  $\nu^c = e^{-i\phi}\nu$ , and so particle and anti-particle coincide up to a phase factor. Similar to a real scalar field, particle and anti-particle coincide and, therefore, this Majorana field is neutral and cannot carry electric or color charges. In addition, we note that a Majorana field is constructed only from one independent Weyl spinor. It contains only two degrees of freedom, whereas a Dirac spinor is constructed from two independent Weyl spinors with a total of four internal degrees of freedom.

#### 2.2.2Lepton mixing

As was the case for the quark sector discussed before, the non-vanishing neutrino masses give rise to mixing in the lepton sector. The computation is completely analogous and will not be repeated here. The mixing matrix is referred to as the (Pontecorvo-)Maki-Nakagawa-Sakata matrix ((P)MNS matrix) [142, 143]. A subtle difference can arise due to the possibility of

<sup>&</sup>lt;sup>4</sup>We note here that for chiral fields, charge conjugation and particle-anti-particle conjugation are in general distinct. See e.g. discussions in Ref. [141].

Majorana neutrinos, in which case two additional Majorana phases that cannot be rotated away appear. The PMNS matrix can be parametrized as [144]

$$U_{\text{PMNS}} = \begin{pmatrix} c_{12}c_{13} & s_{12}c_{13} & s_{13}e^{-i\delta} \\ -s_{12}c_{23} - c_{12}s_{23}s_{13}e^{i\delta} & c_{12}c_{23} - s_{12}s_{23}s_{13}e^{i\delta} & s_{23}c_{13} \\ s_{12}s_{23} - c_{12}c_{23}s_{13}e^{i\delta} & -c_{12}s_{23} - s_{12}c_{23}s_{13}e^{i\delta} & c_{23}c_{13} \end{pmatrix},$$
(2.26)

where  $c_{ij} = \cos \theta_{ij}$ ,  $s_{ij} = \sin \theta_{ij}$ , and  $\theta_{ij}$  are the mixing angles. We include the CP-violating phase  $\delta$ , and in the case of Majorana neutrinos, we multiply Eq. (2.26) from the right by

$$\begin{pmatrix} e^{i\eta_1/2} & 0 & 0\\ 0 & e^{i\eta_2/2} & 0\\ 0 & 0 & 1 \end{pmatrix}, \tag{2.27}$$

containing the Majorana phases  $\eta_{1,2}$  that cannot be absorbed.

#### 2.2.3 Neutrino oscillations

For a coherent mixture of mass eigenstates, the mismatch between flavor and mass eigenstates allows for flavor oscillations. It turns out that in the case of neutrinos, coherent states are realized in weak interactions, and the microscopic properties allow for flavor oscillations to manifest on macroscopic scales.

In the following, we derive the probability of flavor oscillations  $\nu_{\alpha} \to \nu_{\beta}$ . We shall distinguish neutrino flavor states by indices  $\alpha = e, \mu, \tau$  and mass eigenstates by i = 1, 2, 3. The result is standard, but our derivation takes inspiration from Ref. [145], which gives a comprehensive presentation and addresses many of the misconceptions about neutrino flavor oscillations at a depth and detail we cannot present here.

We begin by quoting the master formula for the probability of a neutrino in flavor state  $|\nu_{\alpha}\rangle$  to be detected in the state  $|\nu_{\beta}\rangle$  after traveling distance L,

$$P_{\nu_{\alpha}\to\nu_{\beta}}(L) = |\langle \nu_{\beta}(L)| \ \nu_{\alpha} \rangle|^2 = \left| \sum_{i} U_{\beta i} e^{-i\frac{m_i^2}{2E}L} U_{\alpha i}^{\star} \right| = \sum_{i,j} U_{\alpha i} U_{\beta i}^{\star} U_{\alpha j}^{\star} U_{\beta j} \ e^{-i\frac{\Delta m_{ij}^2}{2E}L} \,, \qquad (2.28)$$

where  $\Delta m_{ij}^2 = m_i^2 - m_j^2$ , L is the baseline, and  $U_{\alpha i}$  indicates elements of the lepton mixing matrix. The result is commonly derived by describing neutrinos incorrectly as plane waves and although the obtained result is correct, it comes with conceptual problems [145].

In the following, we sketch a simplified but more rigorous derivation from quantum mechanics using finite wave packets. We recall that for a free particle, we have

$$\Psi(\vec{x},t) = \int \frac{d^3p}{(2\pi)^3} \Psi_p \, e^{i\vec{p}\cdot\vec{x} - iEt} \,, \tag{2.29}$$

where  $\Psi(\vec{x},t) = \langle x | \Psi \rangle$  is the wave function in coordinate space and  $\Psi_p$  is the momentum distribution.

We consider a neutrino produced in flavor state  $|\nu_{\alpha}\rangle$ , which is a superposition of mass eigenstates  $|\nu_{i}\rangle$  with their respective wave functions, i.e.

$$|\nu_{\alpha}(\vec{x},t)\rangle = \sum_{i} U_{\alpha i}^{\star} \Psi_{i}(\vec{x},t) |\nu_{i}\rangle ,$$
 (2.30)

and for oscillations in vacuum  $\Psi_i(\vec{x},t)$  obeys the free Schrödinger equation. Likewise, the detected neutrino state should also be described as a wave packet. The oscillation amplitude is given by

$$\langle \nu_{\beta}(L) | \nu_{\alpha} \rangle = \sum_{i} U_{\alpha i}^{\star} U_{\beta i} \int d^{3}p \Psi_{p}^{\star(\beta)} \Psi_{p}^{\alpha} e^{-iE_{i}t + i\vec{p}\cdot\vec{L}}, \qquad (2.31)$$

which after integrating out time t, as we remain agnostic about the precise time of production, gives rise to the transition amplitude for a given baseline L. Note that in order to compute the transition probability, we need to prescribe the shape of the wave function – which is a priori not known to us. It will include information about uncertainty in energy and momentum of the produced and detected states and allows for an analysis of coherence and decoherence phenomena associated to flavor oscillations, for example, by adopting a Gaussian wave packet.<sup>5</sup>

For a Gaussian momentum space distribution centered around  $\vec{p'}$  and with spread  $\sigma_p$ , the coordinate space wave function can be written analytically as

$$\Psi(\vec{x},t) = \frac{1}{(2\pi\sigma_p^2)^{3/4}} \exp\left(-\frac{(\vec{x}-v_g t)^2}{4\sigma_x^2}\right) e^{i\vec{p}'\vec{x}-iEt}, \qquad (2.32)$$

where  $\sigma_x = 1/(2\sigma_p)$  is the spatial width of the wave packet. For the oscillation probability with relativistic mass eigenstates, we find [145, 147]

$$P_{\nu_{\alpha} \to \nu_{\beta}}(L) \propto \sum_{i,j} U_{\alpha i} U_{\beta i}^{\star} U_{\alpha j}^{\star} U_{\beta j} e^{-i\frac{\Delta m_{ij}^{2}}{2E}L} e^{-\Delta E_{ij}^{2}/8\sigma_{E}^{2}} e^{-L^{2}/l_{\text{coh}}^{2}}, \qquad (2.33)$$

which coincides with Eq. (2.28) up to normalization and the two exponential factors. However, their meaning is rather intuitive, and without going into too much detail, we briefly highlight their significance. For more details, see Refs. [145, 147].

The exponential damping factors describe deviations from coherence conditions in production, propagation, and detection. The first factor relates a production and detection process dependent energy uncertainty  $\sigma_E$  to differences in the energy of the mass eigenstates  $\Delta E_{ij}$ . For  $\Delta E_{ij}/\sigma_E \ll 1$ , this inherent uncertainty in production and detection is large against the energy difference of the mass eigenstates, and coherence is not violated by production and detection.

Likewise, if the baseline is small against the coherence length scale

$$l_{\rm coh} = 2\sqrt{2} \frac{2E^2}{\left|\Delta m_{ij}^2\right|} \sigma_x \,, \tag{2.34}$$

the separation of wave packets remains small against the spatial spread of the packets. It is

<sup>&</sup>lt;sup>5</sup>This still does not solve the issue of correct normalization of the wave functions, which has to be introduced by hand, see e.g. Ref. [145]. These conceptual problems can be solved by a fully self-consistent QFT description [146].

a theoretical distance over which coherence for flavor oscillations is maintained. As long as  $L \ll l_{\rm coh}$  holds, damping is negligible and oscillations take place.

#### 2.2.4 Matter effects and adiabatic flavor conversion

When traveling through a medium, neutrinos are subject to forward scattering. This interaction generates an effective mean potential. When considering SM matter only, due to charged current interactions, a potential difference between (anti-)electron flavors and the non-electron flavors is generated. This effect is known as the Mikheyev-Smirnov-Wolfenstein (MSW) effect [148, 149].

Naively, we may be inclined to believe that this effective mean potential of first order in  $G_F$  is negligible when compared to typical neutrino energies. However, it is important to note that the potential need only be relevant when compared to the differences in kinetic energies, which are of order  $\Delta m^2/2E$ , and so matter effects on flavor can be of great importance.

Applying a Fierz transformation, the Hamiltonian of charged current interactions can be written as

$$H_{\rm CC} \supset \frac{G_F}{\sqrt{2}} \left[ \bar{e} \gamma_{\mu} (1 - \gamma_5) e \right] \left[ \bar{\nu}_e \gamma^{\mu} (1 - \gamma_5) \nu_e \right] .$$
 (2.35)

We obtain a matter-induced mean potential by averaging out the electron contribution, i.e.  $\langle H_{\rm CC} \rangle = \bar{\nu}_e V_e \nu_e$ , and it can be shown that for an unpolarized, zero net momentum medium with electron number density  $n_e$ , the effective potential is given by [141]

$$V_e = \sqrt{2}G_F n_e \,. \tag{2.36}$$

Similarly, neutral current potentials can be obtained. In an electrically neutral medium, proton and electron contributions cancel and only the neutron induced part  $V_n = -G_F n_n/\sqrt{2}$  remains. It is evident how the generated potential is not flavor universal due to the charged current part, and therefore we obtain an additional contribution to the mixing between mass and flavor states. The eigenstates of propagation in medium are different from the mass eigenstates in vacuum.

In many situations, it suffices to study an effective two flavor system, since we have a strong hierarchy in the mass squared differences. We can approximately neglect the oscillations resulting from the smaller mass squared difference  $\Delta m_{21}^2 \ll |\Delta m_{31}^2|$ . Then, we study the system defined by  $\nu_e$  and  $\nu_x$ , where  $\nu_x$  is a combination of  $\nu_\mu$  and  $\nu_\tau$ . Let us consider the time evolution in the flavor basis [141]

$$i\frac{d}{dt} \begin{pmatrix} \nu_e \\ \nu_x \end{pmatrix} = \begin{bmatrix} \begin{pmatrix} -\frac{\Delta m^2}{4E} \cos 2\theta & \frac{\Delta m^2}{4E} \sin 2\theta \\ \frac{\Delta m^2}{4E} \sin 2\theta & \frac{\Delta m^2}{4E} \cos 2\theta \end{pmatrix} + \begin{pmatrix} \sqrt{2}G_F n_e & 0 \\ 0 & 0 \end{pmatrix} \end{bmatrix} \begin{pmatrix} \nu_e \\ \nu_x \end{pmatrix}, \qquad (2.37)$$

where we neglect all flavor universal contributions to the potential, since only potential differences between the flavors are important here. The first part of the Hamiltonian defines the mass eigenstates in vacuum, the second term gives the mixing contribution in medium. The medium dependent mixing also affects flavor oscillations in medium, which are in general different when compared to oscillations in vacuum. Of particular importance is the so-called adiabatic flavor conversion. Let us consider a medium that gradually varies in density as neutrinos propagate. Let us also consider a neutrino that is an eigenstate of Eq. (2.37) initially. Upon propagation, the matter potential varies. If the change is sufficiently slow, the state can adjust adiabatically to the changing background. Thus, it remains in its initial mass eigenstate. However, the potential and therefore mixing and the flavor composition of that eigenstate changes. We do not discuss this effect in more detail here, but note that it was later identified as the correct solution to the solar neutrino problem, which was the unexpected appearance of  $\mu$  and  $\tau$  flavors from the sun and a reduced flux of  $\nu_e$  compared to theoretical prediction (e.g. Ref. [141] for a pedagogic overview).

Neutrinos in the sun are produced in an extremely dense environment, and due to the matter potential  $\nu_e \simeq \nu_m$  holds, where  $\nu_m$  is one of the mass eigenstates at that density. The condition of adiabaticity is fulfilled in the sun and the neutrino initially produced as  $\nu_e$  moves outward. It remains in the propagation eigenstate  $\nu_m$ , therefore changing its flavor composition leading to the apparent mismatch in the observed neutrino flux. We note here that this adiabatic flavor conversion is non-oscillatory in nature, see e.g. detailed discussions in Ref. [140].

#### 2.2.5 Neutrinoless double beta decay

It is well known that for some nuclei a double beta  $(2\nu\beta\beta)$  decay is possible. This process is higher order in weak interactions and therefore long-lived. It is only observable in nuclei where ordinary  $\beta$ -decay is kinematically forbidden. A special case arises when lepton number is explicitly violated and neutrinoless double beta decay  $(0\nu\beta\beta)$  becomes possible.

We will not discuss this process here in great detail, and instead refer to e.g. Ref. [53] for a review. However, we want to give some overview here as it is a unique signature for determining the nature of neutrinos, and is connected to the motivation of some of the research projects undertaken for this thesis. This process can only occur for a Majorana neutrino as we will see below and, therefore, it would be a key observation for establishing the nature of neutrinos, and its ongoing non-observation motivates some of the projects undertaken in this thesis.

If  $0\nu\beta\beta$  occurs, the nuclear recoil is typically negligible and so we have a unique experimental signature where the electrons/positrons have a discrete energy spectrum and their sum is the total energy released in the process. We show a possible corresponding diagram in Fig. 2.1, where  $0\nu\beta\beta$  is directly mediated by lepton number violating Majorana neutrinos. This diagram is not the only way to have  $0\nu\beta\beta$ . Many extended BSM theories allow for such a decay, but they do not need to be connected to Majorana neutrinos directly [150].

The significance of this decay mode becomes clear when we take into account the Schechter-Valle-black-box theorem [52]. It guarantees that, if there exists a diagram leading to  $0\nu\beta\beta$ , it implies that we also always generate a Majorana mass term for neutrinos involving the same process. Thus, if  $0\nu\beta\beta$  is observed, neutrinos cannot be Dirac particles.

It is noteworthy that the mass term guaranteed by the black-box theorem is only 4-loop. If  $0\nu\beta\beta$  is mediated by a different process from Fig. 2.1, we could have Dirac neutrinos up to 3-loop before we generate the Majorana mass term. It is possible then that right and left components are nearly degenerate, and while fundamentally Majorana, they experimentally appear as almost Dirac-like. This option is often referred to as pseudo-Dirac neutrinos [151].

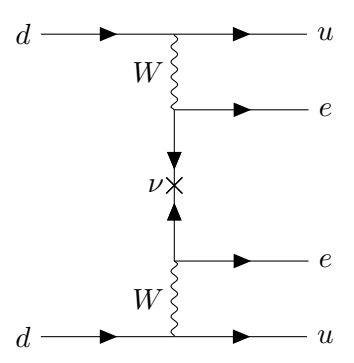


FIGURE 2.1: Feynman diagram for  $2\beta 0\nu$  violating lepton number  $\Delta L=2$ .

If  $0\nu\beta\beta$  is mediated by SM weak interactions, the amplitude scales as

$$\mathcal{A}_{0\nu\beta\beta} \propto \sum_{i} U_{ei}^2 m_i \,.$$
 (2.38)

Here we omitted the in general complicated nuclear part of the matrix element. The amplitude is explicitly neutrino mass suppressed, which makes the experimental observation challenging. The appearance of  $U_{ei}^2$  over  $|U_{ei}|^2$  is no coincidence, and potentially significant cancellations in the amplitude are possible. Therefore, even non-observation  $0\nu\beta\beta$  cannot rule out the possibility that neutrinos are Majorana fermions.

#### 2.2.6 Helicity and chirality

The subtle difference between helicity and chirality for massive but light neutrinos has caused some confusion in the literature. We use this opportunity to briefly highlight important differences, as it is also relevant to avoid some misconceptions regarding research topics in this thesis. Although a standard text book problem, we highlight here the two recent Refs. [152, 153], which address the problem for light neutrinos in great detail.

We first begin by briefly reviewing helicity and chirality [154]. Helicity is the projection of particle spin on the direction of motion,  $\vec{\Sigma} \cdot \hat{p}$ , where  $\hat{p} = \vec{p}/|\vec{p}|$  and  $\vec{\Sigma}$  is the spin operator acting on a Dirac spinor  $\Psi$ . It has eigenvalues  $\lambda = \pm 1$ .

The helicity operator obeys

$$\left[\vec{\Sigma} \cdot \hat{p}, H\right] = 0, \qquad (2.39)$$

so it commutes with the (free) Dirac Hamiltonian and is a good quantum number and conserved for a particle. However, it is manifestly not Lorentz-invariant, so it is a good quantum number only in a fixed frame of reference. This statement holds irrespective of the mass of  $\psi$ . We can use the helicity operator to define a helicity projection operator

$$P_{\mp} = \frac{1}{2} \left( 1 \mp \vec{\Sigma} \cdot \hat{p} \right) \,, \tag{2.40}$$

that projects onto eigenstates of definite helicity.

Chirality on the other hand is Lorentz invariant, as it is related to representations of the Lorentz group. We can project out left- and right-handed components of a Dirac spinor by defining a projection operator

$$P_{L/R} = (1 \mp \gamma_5)/2. \tag{2.41}$$

However, it is straightforward to show that  $[\gamma_5, H] \propto m$ , so unless m = 0, chirality is not a good quantum number. In the limit m = 0, helicity and chirality coincide, and particles of negative helicity are identical with left-handed chirality and vice versa.

Let us consider Dirac neutrinos. For finite mass, the left-handed weak interaction produces a neutrino that is a combination of positive and negative helicity eigenstates, where, due to typical energies  $m_{\nu} \ll E_{\nu}$ , the admixture of the opposite helicity is strongly suppressed. The wrong helicity neutrino is an almost sterile state under weak interactions, as its interactions are now suppressed by the admixture of the left-handed chirality. This phenomenon has been studied in context of energy loss in astrophysical systems that results from production of wrong helicity neutrinos in weak interactions [155–157].

Later in this thesis, we will frequently refer to the production of  $\nu_R$  in models of Dirac neutrinos. While this is common jargon, it is important to clarify the matter to avoid confusion about its meaning. The models we will introduce have interactions that explicitly couple to  $\nu_R$ . In a similar fashion to how weak interactions coupled to  $\nu_L$  produce predominantly  $\nu_-$ , the  $\nu_R$ -coupled interactions give rise to primarily  $\nu_R \sim \nu_+$  because of neutrino mass suppression. Thus, the actually produced state is mostly sterile under weak interactions. For simplicity, we will usually refer to  $\nu_R$  being produced and cosmological abundances of  $\nu_R$  even though chirality is not a good quantum number. The admixture is negligibly small and of no particular significance for any result we derive.

#### 2.3 Massive neutrinos are new physics

We want to conclude this Chapter by motivating why the existence of neutrino masses implies BSM physics. To this end, we first highlight how we cannot accommodate neutrino masses in the SM. We continue with some comments regarding the direction of BSM physics that neutrino masses point to.

#### 2.3.1 No neutrino masses in the SM

It seems deceptively simple to claim the SM should include  $\nu_R$  and write down appropriate Yukawa couplings such that upon symmetry breaking a Dirac neutrino mass matrix that is consistent with oscillation data is generated. One may wish to argue on grounds of "symmetry" that, just as for the quark sector, the inclusion of right-handed neutrinos would resolve the apparent mismatch between the quark and lepton sectors. However, we stress here that there is no fundamental reason to believe in the necessity of such an extension. The existence of right-handed quark fields is required to cancel gauge anomalies in the SM. The right-handed neutrinos would be true singlets under the SM gauge group, and we have no grounds for arguing based on internal consistency of the theory.

Moreover, the true singlet  $\nu_R$  would have to come without any Majorana mass terms, although they are true SM singlets, and unless any extended symmetry forbids their presence,

we have no reason to assume their absence. The masses of the active neutrinos are small compared to those of the other fermions, and it would be desirable for a model of neutrino masses to explain this aspect of the flavor puzzle.

While not pressing per se, the introduction of small Yukawa couplings  $\sim 10^{-12}$  to be consistent with neutrino mass bounds motivates additional structures in the neutrino mass sector. In either case, the presence of a Dirac mass term for neutrinos not only points to new physics beyond the SM (at least two  $\nu_R$ ), but also motivates additional components to explain the absence of Majorana masses.

The other possibility would be that of Majorana masses. Consider the Majorana mass term

$$\mathcal{L} \supset \frac{1}{2} \bar{\nu_L^c} M \nu_L + \text{h.c.} = \frac{1}{2} \bar{\nu_L^T} C M \nu_L + \text{h.c.},$$
 (2.42)

where  $\nu_L = (\nu_L^1, \nu_L^2, \nu_L^3)^T$ . The mass term has weak isospin  $I_3 = 1$ , and therefore is part of an isotriplet operator made from lepton doublets with  $\sim (3, -2)$ . However, the SM does not contain an isotriplet Higgs field and thus, such an operator can at most be generated at loop level, if at all. Indeed, the celebrated dimension five Weinberg operator [158],

$$\mathcal{L}_5 = \frac{\lambda}{\Lambda} (L^T C i \tau_2 \vec{\tau} L) (H^T i \tau_2 \vec{\tau} H), \qquad (2.43)$$

is the lowest order operator to give rise to Majorana masses for neutrinos, here written in the form to contract the iso-triplet bilinear to the iso-triplet Higgs composite operator. The Weinberg operator breaks lepton number  $\Delta L = 2$  and therefore B - L, as indeed it should, since Majorana mass terms break lepton number. Thus, unsurprisingly, we cannot create this or similar operators at higher order or even non-perturbatively in the SM.

Before we move to rather generic considerations of neutrino masses (slightly) beyond the SM, we note the possible role that gravity plays in neutrino mass generation. It is conjectured that gravity breaks all global symmetries, and hence B - L, if not gauged in any extension, will be broken by gravity too. It would be an enticing option to consider mass generation by means of a theory of quantum gravity, in which a small Majorana mass of the neutrino would be connected to Planck-scale physics.

#### 2.3.2 Neutrino masses slightly beyond SM

We established that neutrino masses cannot be generated in the SM alone and necessarily call for an extension of the SM field content or symmetry group. In the following, we study more carefully a general mass matrix for neutrinos and point to certain strategies for generating small masses for the active neutrinos.

Let us consider  $\nu_L = (\nu_L^1, \nu_L^2, \nu_L^3)^T$  active neutrino flavors, and m singlet fermions  $N_R = (N_R^1, ..., N_R^m)$  that we may refer to as sterile neutrinos. The general mass term can be written as

$$-\mathcal{L} \supset \frac{1}{2} \begin{pmatrix} \overline{\nu_L} & \overline{(N_R)^c} \end{pmatrix} \begin{pmatrix} M_L & M_D \\ M_D^T & M_N \end{pmatrix} \begin{pmatrix} (\nu_L)^c \\ N_R \end{pmatrix} + \text{h.c.}$$
 (2.44)

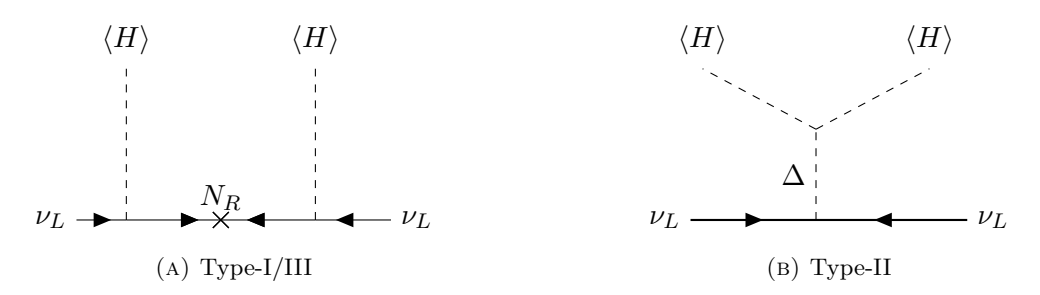


FIGURE 2.2: Neutrino mass generating diagrams for the Type-I/III seesaw (left) and Type-II seesaw (right). For Type-I/III, the heavy fermion  $N_R$  is either a singlet/triplet under  $SU(2)_L$ , and the scalar  $\Delta$  in the Type-II mechanism is a triplet.

A few comments are in order. As we have argued before, the SM does not induce  $M_L$ , but extensions of the SM may generate it, e.g. if there is an electroweak triplet. The matrix  $M_N$  is a  $m \times m$  symmetric Majorana mass matrix, and  $M_D$  is an arbitrary  $3 \times m$  matrix. Upon diagonalization, we obtain the diagonal neutral lepton mass matrix  $\widehat{\mathcal{M}}$ , which should contain the three light active neutrino flavors, and possibly additional sterile neutrinos. We note here that, only if  $M_L = M_N = 0$ , i.e. no Majorana masses are present, the active neutrinos are Dirac in nature.

There exists a variety of models that give rise to a neutral lepton mass matrix as we show in Eq. (2.44). Here, we briefly explore the options for generating a mass matrix from the Weinberg operator in Eq. (2.43) at tree level by enlarging the SM. We therefore do not consider a loop generated Weinberg operator, nor do we discuss mass generation from other higher order effective operators. There exist three tree-level realizations that give rise to small Majorana masses for the active neutrinos, and they are called seesaw mechanisms of Type-I [55–58], Type-II [59–62], and Type-III [63]. They are all based on the observation that the operator in Eq. (2.43) combines two doublets in different ways by means of the SU(2) completeness relation to form triplets/singlets under  $SU(2)_L$ . The seesaw mechanisms correspond to different triplet/singlet extensions of the SM that can be used to provide a UV-completion of Eq. (2.43) (or its equivalent other contractions) at tree level.

The Type-I and Type-III seesaws realize the operator by connecting two LH operators through their singlet (Type-I) and triplet (Type-III) components through a fermion multiplet. Neutrino masses can be suppressed from heavy masses of the respective multiplets. The Type-II seesaw is conceptually different, as it connects operators  $\sim LL$  and  $\sim HH$  with a scalar triplet. Then, EWSB induces a small VEV for the neutral component of the triplet. The suppression of the VEV due to large masses in the scalar triplet leads to small neutrino masses. We illustrate all three seesaw mechanisms by their mass generating diagram in Fig. 2.2.

It will be instructive to study this in more detail. As an example, we consider the Type-I seesaw with a neutrino mass matrix

$$\mathcal{M}_{\nu} = \begin{pmatrix} 0 & M_D \\ M_D^T & M_R \end{pmatrix} . \tag{2.45}$$

This neutrino mass matrix defines an entire family of Type-I seesaws that can be studied in generality, and it is possible to show that many alternative seesaw realizations belong to this

family [159].

Apart from assuming the matrix in Eq. (2.45), we assume the hierarchy  $(M_D M_R^{-1})_{ij} \ll 1$ , which allows for a perturbative diagonalization of Eq. (2.45) and guarantees small Majorana masses  $m_{\nu} \ll \Lambda_{\rm EW}$ . Note that this does not necessarily imply  $(M_D)_{ij}/(M_R)_{ij} \ll 1$ . Therefore, the seesaw expansion is not inconsistent with low scales in the mass matrix, giving rise to low-scale variants of the Type-I seesaw such as the linear [160–162] and inverse seesaws [163, 164], and a review on low-scale seesaws can be found in Ref. [165]. The matrix  $\mathcal{M}$  is symmetric and admits a Takagi decomposition  $\widehat{\mathcal{M}} = U^T \mathcal{M} U$ , which diagonalizes  $\mathcal{M}$  with non-negative entries on the diagonal. Since U is unitary, we decompose

$$U = \begin{pmatrix} U_l & 0 \\ 0 & U_h \end{pmatrix} \begin{pmatrix} \sqrt{1 - PP^{\dagger}} & P \\ -P^{\dagger} & \sqrt{1 - P^{\dagger}P} \end{pmatrix}, \qquad (2.46)$$

where P is a  $3 \times m$  matrix, and  $U_{l/h}$  are  $3 \times 3$  and  $m \times m$  and unitary. This parametrization allows to first block diagonalize  $\mathcal{M}$  into a light and a heavy sector, and subsequently diagonalize the blocks independently through  $U_{l/h}$ . Finding the exact matrix to diagonalize a given mass matrix is a difficult problem, however, the assumed seesaw hierarchy allows for a perturbative block diagonalization. We expand in powers of  $\epsilon \sim M_D M_R^{-1}$ , i.e.  $P = \sum_n P_n$ , where  $P_n = \mathcal{O}(\epsilon^n)$ . At leading order,  $\sqrt{1 - PP^{\dagger}} = \sqrt{1 - P^{\dagger}P} = 1 + \mathcal{O}(\epsilon^2)$ . If we perform the block diagonal transformation at leading order, we obtain conditions on P for demanding the off diagonal blocks to vanish at this order. This gives

$$P = M_D^{\star}(M_R^{-1})^{\dagger} + \mathcal{O}(\epsilon^2), \qquad (2.47)$$

and we find the block diagonal mass matrix

$$\mathcal{M}_{\text{block}} = \begin{pmatrix} -M_D M_R^{-1} M_D^T & 0\\ 0 & M_R \end{pmatrix} + \mathcal{O}(\epsilon^2). \tag{2.48}$$

We obtain the well-known neutrino mass formula for the Type-I seesaw

$$M_{\nu} = -M_D M_B^{-1} M_D^T + \mathcal{O}(\epsilon^2) ,$$
 (2.49)

which is explicitly suppressed by the potentially high scale fermion mass matrix. We note here that  $U_l$ , which diagonalizes the light neutrino mass matrix, can be identified with the PMNS matrix Eq. (2.26) at this order of the seesaw expansion. We will refer back to these results when we discuss the formal analogies between the Type-I seesaw family here and the generalization to a Type-I Dirac seesaw family in Chapter 6.

## Chapter 3

## How neutrinos shape the Universe

Despite their feeble interactions, neutrinos play an important role in virtually all aspects of how the Universe appears to us. They are abundantly created in stars, determine the dynamics of supernovae, and on even larger scales, affect the large scale structure and ultimately global expansion of the entire Universe – no observation could be reconciled without the crucial role neutrinos play in all of these systems.

The following Chapter attempts to give an (ultimately incomplete) overview of the role neutrinos play on the cosmic stage. We try to be as self-contained as possible, and focus in particular on systems and concepts important for this thesis. Occasionally, we will not shy away from exploring some topics beyond what is strictly needed in this thesis, so that we can truly appreciate the prime position of neutrinos in cosmology and astrophysics, and also to motivate future directions beyond what has been explored in this thesis.

#### 3.1 An early Universe primer

We begin with a few remarks on the early Universe by establishing some terminology of the  $\Lambda$ CDM model and the timeline of the early Universe, followed by an introduction to cosmological Boltzmann equations tailored to our needs in later Chapters of this thesis. The treatment is by no means complete, and for an exhaustive overview, we refer to standard textbooks (e.g. Ref. [166]) on the subject.

#### 3.1.1 The $\Lambda$ CDM model

The cosmological standard model, or  $\Lambda$ CDM model for its main unknown ingredients, models the Universe as homogeneous and isotropic on large scales. The metric describing such a spacetime is the Friedmann-Lemaître-Robertson-Walker (FLRW) metric,

$$ds^{2} = -dt^{2} + a(t)^{2} \left( \frac{dr^{2}}{1 - kr^{2}} + r^{2} d\Omega \right).$$
 (3.1)

The spatial curvature parameter k is consistent with a flat (k = 0) Universe by observation, so we only work in the limit of k = 0 [42]. Fortunately, the ten Einstein equations related to this metric simplify considerably, with only two independent equations remaining. They are

referred to as the Friedmann equations,

$$\left(\frac{\dot{a}}{a}\right)^2 = \frac{8\pi G}{3}\rho + \frac{\Lambda}{3}\,,\tag{3.2}$$

$$\frac{\ddot{a}}{a} = -\frac{4\pi G}{3} \left(\rho + 3p\right) + \frac{\Lambda}{3} \,, \tag{3.3}$$

where the dot denotes derivatives with respect to the time coordinate, and we define the Hubble expansion parameter  $H = \dot{a}/a$ . We made the cosmological constant explicit instead of absorbing it into the energy momentum tensor. Spatial homogeneity and isotropy also enforce a perfect fluid form for the energy-momentum tensor  $T^{\mu}_{\nu} = \text{diag}(-\rho, p, p, p)$ , and from  $\nabla_{\mu}T^{\mu\nu} = 0$  a continuity equation,

$$\dot{\rho} + 3H(\rho + p) \equiv \dot{\rho} + 3H(1+w)\rho = 0,$$
 (3.4)

is obtained. We also defined the equation of state parameter  $w = p/\rho$ . The dilution of an energy density with expansion follows directly from Eq. (3.4),

$$\rho \propto a^{-3(1+w)} \,. \tag{3.5}$$

Important equation of states are that of radiation w = 1/3 with  $\rho_{\rm rad} \propto a^{-4}$ , non-relativistic matter  $w \approx 0$  with  $\rho_{\rm mat} \propto a^{-3}$ , and vacuum energy w = -1 with  $\rho_{\rm vac} = {\rm const.}$ 

#### 3.1.2 A brief timeline of the early Universe

It is generally assumed that the early Universe, after a likely early phase of exponential expansion from cosmic inflation, was dominated by radiation energy density. While we only have a clear indication of radiation domination around the time of Big Bang nucleosynthesis (BBN), this remains one of the key assumptions that is commonly made when studying the early Universe. Non-standard scenarios, where the Universe was not always in a radiation dominated phase between inflation and BBN, are also subject of interest and in many instances well motivated.

Assuming that the Universe was as hot as  $T\gg 100\,\mathrm{GeV}$  initially, thermal corrections restore EW symmetry and only when the Universe cools down to  $T\sim 100\,\mathrm{GeV}$ , the Higgs field develops a vacuum expectation value that leads to EWSB and generates masses for SM fermions and gauge bosons.

At temperatures near  $T \sim 200 \,\mathrm{MeV}$ , the strong interaction becomes confining and free quarks and gluons disappear from the SM plasma to form hadrons and mesons. The leftovers of this transition are the protons and neutrons, which later form the primordial elements.

Neutrinos decouple at around  $T \sim 1 \, \mathrm{MeV}$  and proceed to free-stream, shortly followed by electron-positron annihilation at  $T \sim 0.5 \, \mathrm{MeV}$ , which heats up the plasma once again. Since neutrinos have decoupled at this stage, we find that relic neutrinos and the primordial photons have differing temperatures.

BBN takes place down to temperatures as low as  $T \sim 100 \, \mathrm{keV}$ . In a delicate balance of different processes, the primordial abundance of mostly hydrogen and helium (and traces of some heavier elements) is set by nuclear reactions.

We find the Universe transitioning from the radiation dominated era to the matter dominated era, where DM and baryonic matter take the lead, at around  $T \sim 1 \,\mathrm{eV}$ , before photons decouple at  $T \sim 0.3 \,\mathrm{eV}$ . Electrons and protons recombine to form neutral hydrogen, and photons free-stream until today and are observable to us as the cosmic microwave background (CMB), leaving a detailed imprint of the Universe in the moment of last-scattering.

At even lower temperatures, and depending on the unknown value of the neutrino masses, at least two of the three active neutrino mass eigenstates cool down enough to become non-relativistic. They act as a subdominant, warm DM component and influence structure formation. We will explore the role of (massive) neutrinos on the CMB and structure formation in Sec. 3.2.

#### 3.1.3 Cosmological Boltzmann equations

A coherent picture of the evolution of the Universe from its early hot and dense state to the diverse observations of the current epoch emerges in the language of thermodynamics, applied to a FLRW Universe. The tools of choice to track the abundance of species and their interactions in the primordial particle soup are phase space distributions. Here, particles are described by statistical ensembles, and the central object of interest for a species  $\phi$  is its phase space distribution or phase space density  $f_{\phi}(t, \vec{x}, \vec{p})$ , which is a function of time, physical coordinate  $\vec{x}$ , and physical momentum  $\vec{p}$ .

The phase space density can be interpreted as a particle number density in phase space, i.e.  $dN = g_{\phi} f_{\phi}(t, \vec{x}, \vec{p}) \frac{d^3 p}{(2\pi)^3} d^3 x$  [167]. The evolution of the phase space distribution is given by the Boltzmann equation, which can be written abstractly as  $\hat{L}(f_{\phi}) = \hat{C}(f_{\phi})$ , where  $\hat{L}$  is the Liouville operator that encodes the change of the phase space distribution in absence of particle interactions, and the collision operator  $\hat{C}$  captures changes coming from microphysical interactions.

We can understand the Liouville operator as the change of the phase space distribution along a world-line  $x^{\mu}(\lambda)$  of particle  $\phi$ ,

$$\hat{L}(f_{\phi}) = \frac{df_{\phi}}{d\lambda} = \frac{\partial f_{\phi}}{\partial x^{\mu}} \frac{dx^{\mu}}{d\lambda} + \frac{\partial f_{\phi}}{\partial v^{i}} \frac{dp^{i}}{d\lambda}, \qquad (3.6)$$

where  $\lambda$  is the affine parameter of the world line. This definition of the Liouville operator holds in any spacetime. The computation for the FLRW metric is a standard result, see e.g. Ref. [168]. In a homogeneous and isotropic FLRW Universe, we find

$$\hat{L}(f_{\phi}) = E_{\phi} \frac{\partial f_{\phi}}{\partial t} - H E_{\phi} p \frac{\partial f_{\phi}}{\partial p} , \qquad (3.7)$$

where t is cosmic time, and p is the modulus of the spatial part of physical momentum.

To complete the Boltzmann equation, we need the collision operator for particle  $\phi$  in a bath that may contain additional particle species  $\psi_i$ . It can be written as [166]

$$\hat{C}(f_{\phi}) = \sum_{\phi \in i, f} \int d\Pi_{i_{1}} ... d\Pi_{i_{n}} d\Pi_{f_{1}} ... d\Pi_{f_{m}} (2\pi)^{4} \delta^{(4)} (\Sigma p_{i} - \Sigma p_{f}) 
\times \left( |\mathcal{M}_{i \to f}|^{2} f_{i_{1}} ... f_{i_{n}} \bar{f}_{f_{1}} ... \bar{f}_{f_{m}} - |\mathcal{M}_{f \to i}|^{2} f_{f_{1}} ... f_{f_{m}} \bar{f}_{i_{1}} ... \bar{f}_{i_{n}} \right).$$
(3.8)

Here we wrote i, f for the initial and final states that contain n and m particles, respectively. We sum over all initial and final states that contain at least one particle  $\phi$ , and integrate over the phase space of all participating particles. Here  $d\Pi = \frac{d^3p}{(2\pi)^32E}$  is the phase space element, and  $(2\pi)^4\delta^{(4)}(\Sigma p_i - \Sigma p_f)$  accounts for energy momentum conservation. The phase space distribution of  $\psi$  is  $f_{\psi}$ . We denote as  $\bar{f}_{\psi} = (1 \pm f_{\psi})$  the final state distribution, which includes the effect of finite density in the final state. The sign depends on whether particle  $\psi$  is a boson (+) or fermion (-), and its effect is known as Bose enhancement and Pauli blocking, respectively.

A few comments regarding the matrix element  $\mathcal{M}_{i\to f}$  for the reaction  $i\to f$  are in order. In general, the phase space distributions for the same particle, but with different internal configurations, such as different spin states, are different. However, in many situations and all those we are interested in, the different internal degrees of freedom have identical distributions in phase space. Thus, instead of treating them separately, we can combine the reactions.

In this convention, the matrix element is summed over initial and final spin states, not averaged. For n identical particles in the initial or final state, the phase space integration overcounts physically identical configurations that only differ by mere exchange of identical particles [166]. This can be remedied with a symmetry factor 1/n!, which we absorb in the matrix element in our convention. Thus, the matrix element we use for Boltzmann equations is, in general, different from typical matrix elements used in unpolarized cross section computations and other observables that require an averaging of internal degrees of freedom.

#### 3.2 Neutrinos in the early Universe

At early times, where temperatures satisfy  $T \gg \text{MeV}$ , weak interactions were efficient and neutrinos thermalized with the remaining SM particles. In the epoch after EW symmetry breaking, interactions of neutrinos with the thermal bath proceed via effective Four-Fermi interactions dictated by the Fermi constant  $G_F$ . While the details of the underlying interactions are involved, including charged current induced flavor effects, we can identify the Fermi constant as the relevant scale of interaction strength. From dimensional analysis, we infer an interaction rate

$$\Gamma_{\text{weak}} = \langle \sigma v \rangle \, n \sim G_F^2 T^5 \,,$$
(3.9)

which is to be compared with the Hubble rate  $H \sim \sqrt{G}T^2$ , where G is Newton's constant, and we dropped order one factors and the effective number of relativistic degrees of freedom, which is also  $\mathcal{O}(1)$  for  $T \sim \text{MeV}$ . Equating the two rates gives the decoupling temperature of

neutrinos

$$T_{\rm dec} \sim \left(\frac{\sqrt{G}}{G_F^2}\right)^{1/3} \sim \text{MeV},$$
 (3.10)

thus implying that neutrinos decouple from the SM around that temperature. From there on, the relic neutrinos interact predominantly through their gravitational interaction, which, despite its feebleness, leaves traceable imprints on the appearance of the Universe to us, thus allowing us to study primordial neutrinos directly from cosmological observations.

#### 3.2.1 Neutrino decoupling and $\Delta N_{\rm eff}$

While the thermal history of the Universe at  $T \gg T_{\rm BBN} \sim 1 \,\mathrm{MeV}$  is mostly unprobed, our previous estimate suggests that the active neutrinos have been in thermal equilibrium with the SM at these temperatures. They subsequently decoupled at temperatures  $T \sim \mathrm{MeV}$ . Therefore, the  $\Lambda\mathrm{CDM}$  model generically predicts the existence of a large abundance of relic neutrinos.

Crucially, neutrinos decouple when they are relativistic, and so they approximately maintain their equilibrium Fermi-Dirac distribution [168]. The decoupling takes place prior to  $e^+e^-$  annihilation, and the total radiation density after decoupling and  $e^+e^-$  annihilation can be written as

$$\rho_{\rm rad} = \rho_{\gamma} \left( 1 + \frac{7}{8} \left( \frac{11}{4} \right)^{4/3} N_{\rm eff} \right),$$
(3.11)

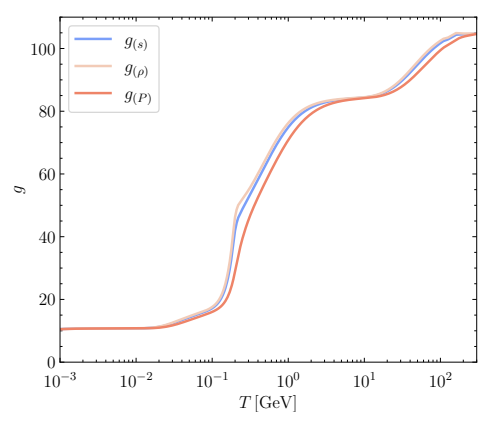
where  $\rho_{\gamma}$  is the energy density of photons and  $N_{\rm eff}$  parametrizes additional light relics including neutrinos. The numerical prefactor is obtained from separate entropy conservation in the photon and the neutrino sector when  $e^+e^-$  annihilate. We call  $N_{\rm eff}$  the effective number of neutrino species, since it normalizes the energy density to that of one active neutrino flavor. Thus, in the SM and in the instantaneous decoupling approximation, the prediction is  $N_{\rm eff}=3$ .

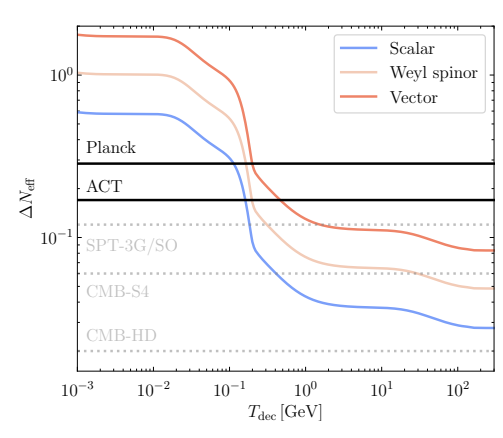
In reality, the decoupling process of neutrinos is neither instantaneous nor universal among flavors, as electron flavors also undergo charged current interactions. Moreover, finite temperature effects and QED corrections to weak processes give a small but significant contribution. A more precise value of  $N_{\rm eff}$  can be computed by solving the relevant Boltzmann equations. All of the above combined, the current theoretical prediction  $[48-51]^1$  is

$$N_{\text{eff}} = 3.044 + \Delta N_{\text{eff}},$$
 (3.12)

where we separate any possible deviation from the theoretical prediction by defining the excess in the effective number of neutrinos  $\Delta N_{\rm eff}$ . A deviation from the expected null result on  $\Delta N_{\rm eff}$  is a powerful probe of non-standard neutrino properties that affect the decoupling process, or signals the presence of additional light degrees of freedom. The idea to use  $\Delta N_{\rm eff}$  to probe additional light relics is old and predates the precision era of cosmological measurements [169–171].

<sup>&</sup>lt;sup>1</sup>Here we omit the theoretical uncertainty and slightly older concurring studies that prefer  $N_{\text{eff}} = 3.045$ . The effect of this uncertainty on later results is negligible.





- (A) Effective relativistic degrees of freedom.
- (B) Contributions of light relics to  $\Delta N_{\rm eff}$

FIGURE 3.1: Left: Effective relativistic degrees of freedom of the SM as a function of SM temperature for entropy, energy density, and pressure. Values from Ref. [172]. Right: Contributions to  $\Delta N_{\rm eff}$  from an additional light real scalar, Weyl fermion, and light but massive vector boson, computed from Eq. (3.13). For comparison, we show current and forecasted limits on  $\Delta N_{\rm eff}$ . Details on these values are discussed in the main text.

If extra light degrees of freedom are present and in chemical equilibrium with the SM at early times, their relic abundance can be estimated from their decoupling temperature. This gives a correction to the effective neutrino number [43]

$$\Delta N_{\text{eff}} \simeq 0.027 \, g_x \left( \frac{106.75}{g_{\star}(T_{\text{dec}})} \right)^{4/3} \,.$$
 (3.13)

We write  $g_x$  for the (effective) internal degrees of freedom for a new light species x, i.e.  $g_x = 1$  for a real scalar or  $g_x = 7/8 \times 2$  for a Weyl spinor. Fig 3.1 illustrates both, the effective degrees of freedom of the SM as well as excess contributions to  $\Delta N_{\text{eff}}$  from selected new light relics.

Excess radiation in the early Universe is observationally accessible at BBN and from the CMB, and to a lesser extent also in large scale structure data. The former constrains the total radiation budget through the primordial element abundances that can be computed from Boltzmann equations (see Ref. [173] for a review). Thus, BBN provides a measurement of any deviation in the expected radiation budget at that time.

The determination from the CMB is less direct and happens at lower temperatures. Here, excess radiation affects the CMB spectrum in a complicated manner. In simplified terms, it is in particular the experimentally very precise determination of the angular scales of acoustic peaks and the CMB damping tail [174]. However, these effects can be compensated for by parameter degeneracies in the CMB. Thus, the effect of neutrinos can be masked, as some effects are compensated by varying less strongly constrained parameters. It is not possible to fully eliminate the effect of extra radiation by parameter degeneracies. Therefore, CMB ultimately does provide a constraint on extra radiation. We illustrate this in Fig. 3.2.

While early measurements of  $\Delta N_{\rm eff}$  were not yet precise enough to put stringent limits on BSM physics, the situation improved with Planck providing the competitive limit  $\Delta N_{\rm eff} < 0.285$  at 95% C.L. [42, 43]. The recent data release six of the Atacama Cosmology Telescope

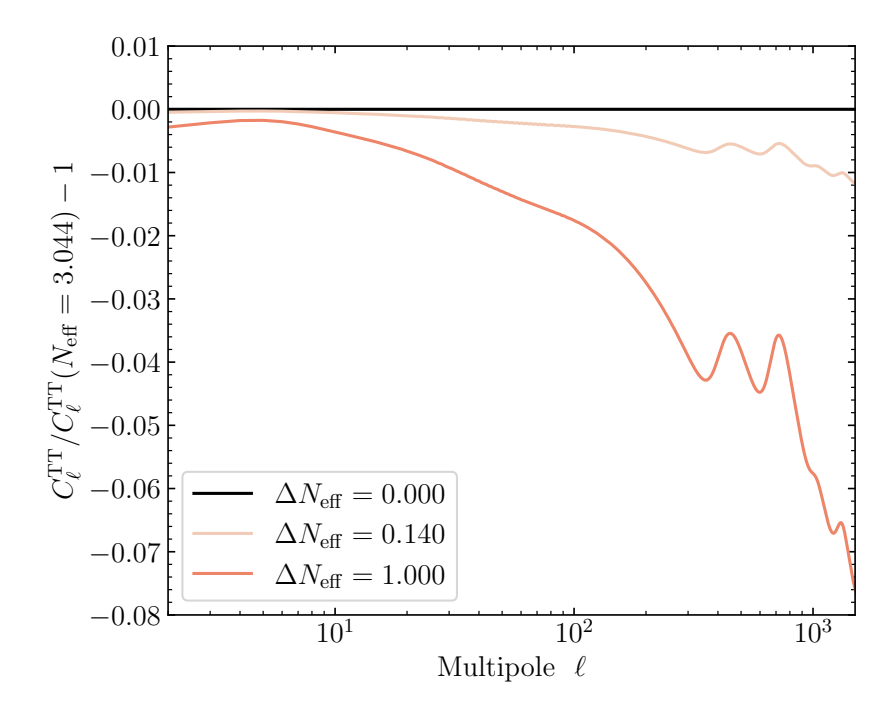


FIGURE 3.2: Illustration of the effect of  $\Delta N_{\rm eff} \neq 0$ . We show the relative change of the CMB power spectrum compared to  $\Delta N_{\rm eff} = 0$ . For simplicity, we neglect neutrino masses. The presented values correspond to the case of three thermalized Dirac neutrinos, and a ruled out benchmark value  $\Delta N_{\rm eff} = 1$  for illustration. Cosmological parameters are fixed to the Planck best-fit otherwise, apart from a rescaling of the matter density by  $\alpha = (1 + 0.2271 \, N_{\rm eff})$ . This keeps the well-constrained redshift of matter-radiation equality fixed, and the difference between the spectra results from a change in the damping scale and the direct effect of neutrino perturbations. For more details on this, see the discussion in Chapter 5.3 in Ref. [175]. Spectra computed with CLASS [176].

(ACT) [44, 45] tightened the limit to  $\Delta N_{\rm eff} < 0.17$  at 95% C.L. Using the full primary CMB data from ACT in combination with large and medium scale data from earlier Planck measurements, this provides the strongest CMB-only limit on relativistic degrees of freedom.

Joint CMB+BBN analyses corroborate this result. Bringing together the data from different cosmological epochs, limits of  $\Delta N_{\rm eff} < 0.180$  [46] and  $\Delta N_{\rm eff} < 0.163$  [47] at 95% C.L., respectively, were found. A partial data set of SPT-3G polarization and lensing data in junction with earlier Planck, ACT and BAO data, finds  $N_{\rm eff} = 2.86 \pm 0.13$  ( $\Delta N_{\rm eff} < 0.076$ ),  $N_{\rm eff} = 2.83 \pm 0.13$  ( $\Delta N_{\rm eff} < 0.046$ ), and  $N_{\rm eff} = 2.89 \pm 0.23$  ( $\Delta N_{\rm eff} < 0.306$ ) when allowing for extended  $\Lambda {\rm CDM} + N_{\rm eff}$ ,  $\Lambda {\rm CDM} + N_{\rm eff} + \sum m_{\nu}$ , and  $\Lambda {\rm CDM} + N_{\rm eff} + Y_p$  fits, respectively [177].<sup>2</sup> While these values should be taken with some caution due to combining different experiments and cosmological eras, they provide a strong indication that additional light relics are disfavored by data. Future surveys will only tighten these bounds unless a positive detection is made.

Indeed, the forecasted sensitivities of currently operating and other planned experiments anticipate ambitious limits. The Simons Observatory (SO) [178] and SPT-3G [179] expect to reach  $\Delta N_{\rm eff} < 0.12$  at 95% C.L. eventually. The CMB-S4 proposal [180] aims to reach  $\Delta N_{\rm eff} < 0.06$  at the same C.L. Notably, futuristic proposals such as CMB-HD [181] aim to surpass the

<sup>&</sup>lt;sup>2</sup>We provide these heuristic limits on  $\Delta N_{\rm eff}$  by adding the  $2\sigma$  uncertainty to the mean value, and subtracting the theoretical expectation of  $N_{\rm eff} = 3.044$ .

important  $\Delta N_{\rm eff} = 0.027$  threshold of a single Nambu-Goldstone boson in equilibrium with the SM prior to EWSB (see also Fig. 3.1).

#### 3.2.2Neutrino masses in cosmology

Although not central to this thesis, we will give a short overview of how neutrino masses affect the CMB and, perhaps more importantly, large scale structure formation for two reasons. First, neutrinos do play a vital role, and cosmic structure as we observe it cannot be explained without a relic neutrino background that provides feedback on the gravitational structure formation. Second, recent surveys of CMB and, in particular, large scale structure data give strong bounds on the sum of neutrino masses.

Current limits disfavor IO and even put some pressure on NO in light of the minimal neutrino mass required for oscillation experiments. DESI [40] and ACT [44] quote neutrino mass bounds as strong as

$$\sum m_{\nu} < 0.064 \,\text{eV} \,(95\% \,\text{DESI}) \,,$$
 (3.14)

$$\sum m_{\nu} < 0.064 \,\text{eV} \,(95\% \,\text{DESI}) \,, \tag{3.14}$$
$$\sum m_{\nu} < 0.089 \,\text{eV} \,(95\% \,\text{ACT}) \,. \tag{3.15}$$

Even though we do not make direct use of this probe here, it is clear how it provides valuable input on neutrino mass model building, especially should the disfavoring of IO continue. This also triggered considerable interest in the community and attempts to either resolve such a possible discrepancy or to put extra scrutiny on the cosmological parameter inference have been undertaken, e.g. Refs. [182, 183]. In the following, we briefly discuss how these cosmological probes test the neutrino mass due to their effect on large scale structure, and possible pitfalls when inferring parameters. For a detailed discussion, we refer to Refs. [175, 184].

The leading effect of massive neutrinos on the CMB and on large scale structure is of the same origin. Crucially, neutrinos are relativistic during photon decoupling and, therefore, they contribute as radiation before the CMB formed. Thus, they contribute to the radiation budget when determining matter-radiation equality,  $\rho_b + \rho_{cdm} = \rho_{\gamma} + \rho_{\nu}$ . However, some time after recombination at least two neutrinos transition to the non-relativistic regime and they participate as a warm dark matter candidate in structure formation. Thus, maintaining the well-constrained matter-radiation equality, an increase in neutrino mass corresponds to an increase in total matter today, as at least two neutrinos have turned non-relativistic by today.

Moreover, once neutrinos turn non-relativistic, they affect the expansion rate through the slower decay of energy density with expansion. This means the Hubble rate decreases slower, and structure formation is further hindered by the change in background evolution. In addition, the increase in expansion rate leads to more prominent photon damping, thus reducing the photon diffusion damping scale observable in the CMB spectrum.

At last, the scale of free-streaming for neutrinos depends on the neutrino mass. This scale determines the sizes of structures that are eradicated by the kinematic impossibility to confine or keep out neutrinos on these length scales. This change in the underlying neutrino density perturbations propagates through gravity to other species and therefore affects large scale structure and the CMB.

This is by no means a complete picture, but it should give a good indication as to how neutrinos affect the very appearance of the Universe today. It also clarifies how the era of precision cosmology allows us to put such substantial bounds on the neutrino mass. We do not discuss here possible parameter degeneracies or other systematic issues that may arise in cosmological probes. They are not relevant to the central topics of this thesis.

#### 3.3 Neutrinos in the late Universe

#### 3.3.1 Supernovae

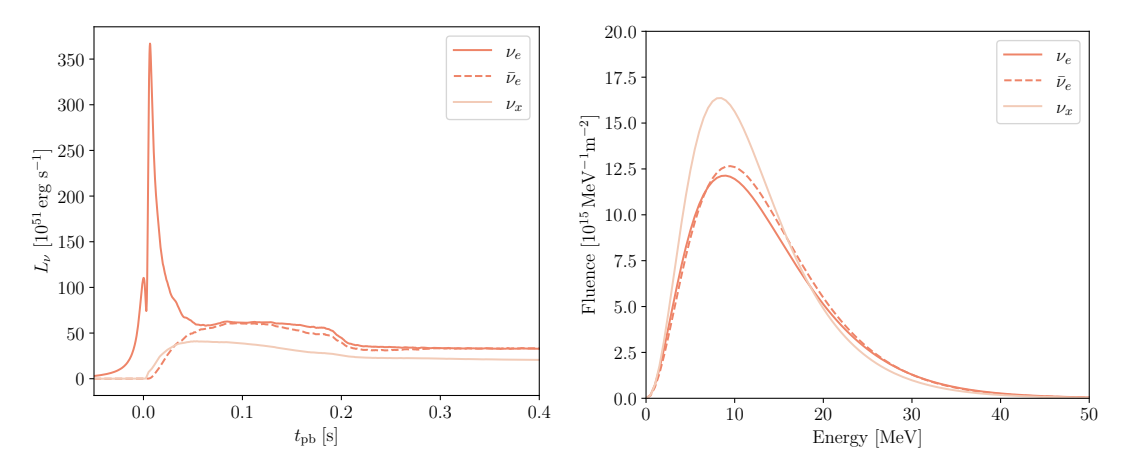
Core-collapse supernovae (CCSNe) are among the most violent and energetic processes that take place in the Universe. As massive stars transition to the fusion of increasingly heavier elements, the fusion process becomes energetically disfavored. The radiation pressure that originally supported the stellar structure ceases to stabilize the system, and gravitational collapse leads to the formation of a dense central object, such as a neutron star or a black hole. The shockwave of the collapsing star lunges stellar debris out into the Universe, and for a brief period only, a supernova may outshine entire galaxies in photons alone. However, almost  $\sim 99\%$  of the binding energy of the progenitor star is lost by the release of up to  $\sim 10^{58}$  neutrinos [185].

The physics of CCSNe is complex, and we can by no means give a satisfactory overview of the related hydrodynamics that is still an active field of research. We focus on the most important aspects from the view of neutrino physics and refer to the comprehensive review in Ref. [38, 185] for more details and other aspects.

Simulations reveal that the complicated dynamics of CCSNe can only be accounted for by neutrinos, as they not only carry away most of the energy but also provide feedback on the explosion itself. This is corroborated by the superior role that the supernova SN1987A in the Large Magellanic Cloud played in establishing the standard picture of CCSN physics. The detection of some  $\mathcal{O}(10)$  neutrinos [36, 37] gave first indications of the underlying CCSN physics as well as providing valuable input on (B)SM physics related to neutrinos.

While many of the details of the resulting neutrino spectrum ultimately depend on the underlying progenitor star, some universal properties can be found. We can identify three simplified but distinct emission regimes over the course of the CCSN event [38, 186].

- 1. The neutronization burst originates from the collapse shock wave as it moves outward through the degenerate (iron) core, breaking up heavy nuclei and releasing neutrons and protons in the process. A phase of rapid electron capture of free protons and nuclei leads to an enormous release of  $\nu_e$ , but the extremely dense environment keeps neutrinos trapped in the collapsing star. Once the shock crosses the neutrino sphere, the neutrinos trapped within this region can escape. This shock breakout gives rise to the characteristic  $\nu_e$  burst.
- 2. During the accretion phase, neutrinos provide additional support for the outflowing shock, and an explosion that ejects stellar debris is triggered. The dense core accretes and heats up material, and annihilation of primarily  $e^+e^-$  produces neutrinos of all flavors. The



(A) Neutrino luminosity over the course of a (B) Neutrino fluence at Earth assuming a distance CCSN. of 10 kpc.

FIGURE 3.3: Left: Supernova neutrino luminosity as a function of time post bounce. Simulation data for a  $27M_{\odot}$  progenitor star used also in Ref. [38]. The initial neutronization burst is clearly visible, followed by the accretion phase. The cooling phase is not visible and starts at even longer times after core bounce. Right: Fluence as the time integrated neutrino flux observed at Earth, based on the same simulation and an assumed distance of 10 kpc. Computed using SNEWPY [189].

signal tends to be dominated by (anti-)electron flavors, as non-electron flavor neutrinos can only be created in neutral current interactions.

3. Finally, the Kelvin-Helmholtz cooling phase is the longest stage and releases the most neutrinos due to its longer duration. The proto-neutron star at the center of the explosion cools down. It is said to de-leptonize, as the cooling releases neutrinos of all flavors. With progressing cooldown, the neutrino luminosity continuously decreases. The emission can last for considerable times, but typically becomes weak compared to initial neutrino fluxes after about  $\sim 10\,\mathrm{s}$  post bounce.

Fortunately for us, the neutrino energy spectrum as found by numerical simulations is well described by a simple analytic fit for each flavor [187, 188]

$$F_{\nu}(E,t) \propto \left(\frac{E}{\langle E_{\nu}(t)\rangle}\right)^{\alpha(t)} \exp\left(-\frac{(1+\alpha(t)E)}{\langle E_{\nu}(t)\rangle}\right),$$
 (3.16)

and the fit parameter  $\alpha(t)$  satisfies

$$\frac{\left\langle E_{\nu}^{2}\right\rangle}{\left\langle E_{\nu}\right\rangle^{2}} = \frac{2+\alpha(t)}{1+\alpha(t)}.$$
(3.17)

Called the pinching parameter,  $\alpha$  describes the deviations to a Maxwell-Boltzmann distribution ( $\alpha = 2$ ), e.g.  $\alpha \approx 2.3$  corresponds to a Fermi-Dirac distribution with zero chemical potential.

For many applications, it is sufficient to consider the time integrated neutrino spectrum or fluence. It is dominated by the cooling stage, and can be approximated by Eq. (3.16) using an effective time averaged pinching parameter and effective time averaged energy parameter. We illustrate the time dependence of neutrino emission and the fluence from a CCSN simulation in Fig. 3.3.

We note here in passing the complexity of neutrino flavor phenomena in supernova explosions, again referring to Ref. [38] for details. Neutrinos are not only copiously produced in a CCSN but also influence the explosion dynamics. The extreme densities of nuclei, electrons, and also neutrinos provide feedback on flavor distributions through matter effects and neutrino self-interactions. Neutrino densities can be so high as to themselves forming a background for neutrinos to propagate through, leading to non-linear effects. The other matter densities result in neutrinos being subjected to matter effects, and the ultimately observable neutrino flavor spectrum contains corrections from the MSW effect [190].

In many CCSN simulations, it is found that the matter profile that neutrinos traverse is sufficiently slowly changing, such that neutrino propagation is adiabatic and subject to adiabatic flavor conversion (see Ref. [190] and Sec. 2.2.4).

#### 3.3.2 Diffuse supernova neutrino background

CCSNe occur with a rate of about  $\sim 1/s$  in the entire observable Universe. The integrated flux of all past CCSNe that took place throughout cosmic history is known as the diffuse supernova neutrino background, or DSNB for short. It is expected to be a persistent, nearly isotropic flux of incoming neutrinos with energies  $E \sim \mathcal{O}(10\,\text{MeV})$ , that remains undetected for now (see Refs. [34, 35] for reviews).

Detection of the DSNB is considered a key objective for current and upcoming neutrino facilities, such as Super-Kamiokande (SK) [191], Hyper-Kamiokande (HK) [32], JUNO [31], and DUNE [192]. It is anticipated that, due to enrichment with gadolinium and the thereby increased sensitivity, SK could possibly detect the DSNB within the next decade [193–195]. Current experimental upper bounds on the DSNB flux are usually less than an order of magnitude weaker than theoretical expectations [191, 196]. Future experiments like Theia [197], and facilities for the study of  $CE\nu NS$  may have the potential to also detect the DSNB and perform precision measurements [198–200]. The timely detection of the DSNB is therefore not only likely, but highlights its importance within astro- and astroparticle physics and gives credibility to its potential to probe BSM physics [122, 201–208].

The DSNB spectrum is computed by adding the individual neutrino emission spectra  $F_{\nu}(E)$  of all past CCSN. For simplicity, we adopt the approximately thermal Fermi-Dirac distribution for the fluence, corresponding to  $\alpha \approx 2.3$  in Eq. (3.16). The reason is that the total neutrino output is dominated by the cooling stage, and hence the DSNB is predominantly fueled by these quasi-thermal neutrinos. We parametrize in terms of an effective temperature parameter [34]

$$F_{\nu}(E) = \frac{E_{\nu}^{\text{tot}}}{6} \frac{120}{7\pi^4} \frac{E^2}{T_{\nu}^4} \frac{1}{e^{E/T_{\nu}} + 1}.$$
 (3.18)

Here,  $E_{\nu}^{\rm tot}=3\times10^{53}\,{\rm erg}$  is the total emitted neutrino energy. Unless stated otherwise, we take  $T_{\nu_e}=6.6\,{\rm MeV}, T_{\bar{\nu}_e}=7\,{\rm MeV}$ , and  $T_{\nu_x}=10\,{\rm MeV}$ , where  $\nu_x\equiv\nu_{\mu,\tau}$  [122] which is on the higher end of viable temperatures. Generally, this parameter is constrained from non-observation of the DSNB flux by SK [196]. Recent studies like Ref. [209] prefer smaller values of the temperature, but we do not adopt these values here.

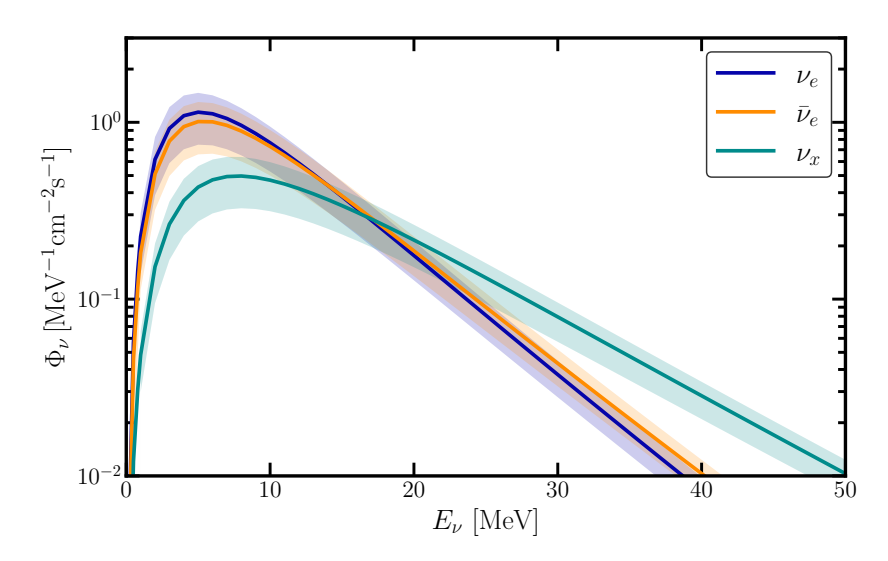


FIGURE 3.4: Differential spectrum of the diffuse supernova neutrino background (DSNB) as we adopt it here. We separate the spectrum by flavor, showing  $\nu_e$  (blue),  $\bar{\nu}_e$  (orange), and  $\nu_x$  (green). Shaded regions indicate the uncertainty estimated from the star formation rate. We adopt the effective Fermi-Dirac parametrization with temperature parameters explained in the main text. Adiabatic flavor MSW conversion for NO is adopted here. Published in Ref. [1].

We have to account for redshift, since neutrinos of past CCSNe travel cosmological distances. To obtain the rate, we need to weigh with the rate of CCSNe at any given time in cosmic history. The DSNB spectrum for a given neutrino flavor can be written as [34, 210]

$$\Phi_{\nu}(E) = \int_{0}^{z_{\text{max}}} \frac{dz}{H(z)} R_{\text{CCSN}}(z) F_{\nu}(E')|_{E'=E(1+z)}, \qquad (3.19)$$

where  $H(z) = H_0 \sqrt{\Omega_m (1+z)^3 + \Omega_\Lambda}$  is the Hubble rate as a function of redshift. The upper integration bound is the maximum redshift of supernovae we take into account, i.e. the time at which we have enough star formation to fuel the DSNB with CCSNe. In this thesis, unless stated otherwise, we assume  $z_{\text{max}} \simeq 6$ , in agreement with Ref. [122].

We can estimate the rate of CCSNe with the star formation rate (SFR)  $R_{\rm SFR}(z)$ . The SFR itself is rather difficult to compute, and it is informed by cosmological structure formation in the non-linear regime. We will adopt the empirical fitting formula of Ref. [211] (Ref. [212] for a more recent measurement), and take the otherwise difficult to model star formation rate as a given input. The adopted parametrization is

$$R_{\rm SFR}(z) = R_{0,\rm SFR} \left[ (1+z)^{-10\alpha} + \left(\frac{1+z}{B}\right)^{-10\beta} + \left(\frac{1+z}{C}\right)^{-10\gamma} \right]^{-1/10}, \tag{3.20}$$

and the fitting parameters are  $R_{0,\rm SFR} = 0.0178\,M_{\odot}{\rm yr}^{-1}{\rm Mpc}^{-3}$ ,  $\alpha = 3.4$ ,  $\beta = -0.3$ ,  $\gamma = -3.5$ , and  $B = (1+z_1)^{1-\alpha/\beta}$ ,  $C = (1+z_1)^{(\beta-\alpha)/\gamma} \times (1+z_2)^{1-\beta/\gamma}$ .

The SFR rate only captures the total rate at which mass is converted to stars per unit volume at any given redshift. We need to account for the mass distribution and also for stars being too heavy or too light to end up in a CCSN. The initial mass function  $\psi(M)$  models the distribution of stellar masses. We adopt the well-established power-law scaling

 $\psi \propto M^{-2.35}$  [213] and following Ref. [202] write

$$R_{\rm CCSN} \simeq R_{\rm SFR} \times \frac{\int_{8M_{\odot}}^{50M_{\odot}} \psi(M)dM}{\int_{0.1M_{\odot}}^{100M_{\odot}} M\psi(M)dM}$$
 (3.21)

The integration bounds are chosen such that we normalize to all stars up to a mass of  $M \sim 100 M_{\odot}$ , and we include stars in a range from  $8-50 M_{\odot}$  to undergo CCSN. Stars above  $50 M_{\odot}$  are expected to collapse to black holes directly [201], so we do not include them. The effective fraction of stars to undergo CCSN is obtained by performing the integral in Eq. (3.21), and we find  $0.007/M_{\odot}$ . Thus, we arrive at

$$R_{\rm CCSN} \simeq \frac{0.007}{M_{\odot}} \times R_{\rm SFR} \,.$$
 (3.22)

When performing BSM studies with the DSNB, we expect it to be sufficient to consider the neutrino spectra to be subject to adiabatic MSW flavor conversions (see also Sec. 2.2.4 and 3.3.1). We justify this due to the large uncertainty of up to  $\sim 40\%$  in the CCSN rate, which possibly obscures more subtle effects of supernova physics [210].

We show an example spectrum for the flavors in Fig. 3.4. Here, we assume NO of masses. Since we also assume MSW conversion, this implies  $\nu_e$  is mostly associated with  $\nu_3$ , and the  $\bar{\nu}_e$  with the lightest state  $\bar{\nu}_1$  [190]. The aforementioned uncertainty from the CCSN rate is also shown.

## Chapter 4

# The Monte Carlo approach to Boltzmann equations

In this Chapter, we present an alternative approach to integrated Boltzmann equations. Key feature of this implementation is the Monte Carlo integration of the collision operator. Commonly employed solution schemes often rely on a number of approximations to deal with the involved collision operator. These include neglecting the effect of final state statistics, i.e. Bose enhancement and Pauli blocking, relativistic effects, and simplified prescriptions for backreactions. While the aforementioned effects can be taken into account, the expressions are complicated and somewhat inconvenient to work with. Implementations are numerous in the literature, and some examples include Refs. [214–217].

The available schemes are usually also limited to  $2 \to 2$  processes or fewer particles and not readily extended to general  $m \to n$  processes. The Monte Carlo approach is an alternative. It is exact on the level of integrated Boltzmann equations, thus all relativistic effects as well as corrections from final state occupation are taken into account. We will see that the implementation is straightforward and convenient, as the central object encoding the underlying particle model is the Lorentz-invariant matrix element. More importantly, when going to larger  $m \to n$  processes, the increasing dimension of the phase space integrals is best dealt with by Monte Carlo integration over traditional numerical integration.

In the following, we first develop the general framework for brute force Monte Carlo integration of collision operators in general, where we use Ref. [218] as a starting point. While we use the formalism for calculating the energy densities of light relics in later Chapters, we note here that the entire approach is general and not limited to light relics. Indeed, the formalism can readily be adapted for computations of DM abundances, yields from leptogenesis, or any other quantity that is connected to moments of the Boltzmann equation.

We proceed with a brief discussion of finite temperature effects and how leading effects can be taken into account, and at last address the problem of s-channel resonances, mediators in thermal equilibrium, and the issue of over counting. We clarify some of the underlying issues and offer possible prescriptions to remedy these problems.

#### 4.1 General framework

Let us consider the following scenario, where we augment the thermal history of the SM by an additional species  $\phi$ . The generalization to multiple new species is straightforward. Here,

 $\phi$  need not be a single new particle. Within good approximation, it will often be possible to cluster different new degrees of freedom into a single effective species with  $g_{\phi}$  internal degrees of freedom. For example, light right-handed neutrinos  $\nu_R$  can be considered a single effective fluid, but also new fermions tightly coupled with a mediator particle can form such an effective fluid, similar to the effective baryon-photon fluid approximation in cosmology. In the same spirit, we treat the SM plasma as an effective species with  $g_{(\rho)}(T)$  internal degrees of freedom. We show the derivation for the first moment of the Boltzmann equation, i.e. the energy density, but the procedure can readily be adapted for any other moment.

The thermal history of the Universe is augmented by

$$\frac{d\rho_{\phi}}{dt} = -3H\rho_{\phi}(1+w_{\phi}) + \mathcal{C}_{\text{SM}\to\phi}^{(\rho)}, \qquad (4.1)$$

$$\frac{d\rho_{\rm SM}}{dt} = -3H(\rho_{\rm SM} + P_{\rm SM}) - \mathcal{C}_{\rm SM \to \phi}^{(\rho)}, \qquad (4.2)$$

with

$$H^2 = \frac{8\pi G}{3} (\rho_{\rm SM} + \rho_{\phi}). \tag{4.3}$$

Here,  $w_{\phi}$  is the equation of state parameter of species  $\phi$ , and  $C_{\text{SM}\to\phi}^{(\rho)}$  is the integrated collision operator, here for energy density  $\rho$ . In its most general form, it can be written as

$$C_{\text{SM}\to\phi}^{(\rho)} = \sum_{\phi\in i,f} \int d\Pi_{i_1}...d\Pi_{i_n} d\Pi_{f_1}...d\Pi_{f_m} (2\pi)^4 \,\delta^{(4)} \left(\Sigma \, p_i - \Sigma \, p_f\right)$$

$$\Delta E_{\phi} \times \left( \left| \mathcal{M}_{i\to f} \right|^2 f_{i_1}...f_{i_n} \bar{f}_{f_1}...\bar{f}_{f_m} - \left| \mathcal{M}_{f\to i} \right|^2 f_{f_1}...f_{f_m} \bar{f}_{i_1}...\bar{f}_{i_n} \right) .$$
(4.4)

The notation follows Eq. (3.8), but Eq. (4.4) contains the additional integration over  $d\Pi_1$ . The factor  $\Delta E_{\phi}$  is related to the moments we consider. Here, we deal with energy transfer from or to the  $\phi$ -sector, and  $\Delta E_{\phi}$  is the difference between the initial and final state energies of all occurring  $\phi$ . For number densities, we would include the multiplicity of number density change in the process, and for yet other moments of the Boltzmann equation, we need to introduce the appropriate phase space weighting factor for that quantity. The matrix element is denoted by  $\mathcal{M}_{i\to f}$ , and we adopt the symmetry factor convention discussed in Sec. 3.1.3.

We assume that the SM particles maintain internal thermal equilibrium at all times.<sup>1</sup> The effective SM plasma can be characterized by a well-defined thermodynamic temperature, and energy density and pressure can be written as

$$\rho_{\rm SM} = \frac{\pi^2}{30} g_{(\rho)} T^4, \qquad P_{\rm SM} = \frac{\pi^2}{90} g_{(P)} T^4.$$
(4.5)

Here we made manifest the subtle difference between  $g_{(\rho)}$  and  $g_{(P)}$  that can occur during freezeout of plasma constituents or phase transitions [219]. Numerical values for all subsequent analyses are from Ref. [172].

<sup>&</sup>lt;sup>1</sup>This is a reasonable approximation for the isolated SM. While not possible within the framework as we adopt it here, it would be interesting to study the situation where BSM physics, such as resonant enhancement, causes brief violations of the equilibrium assumption.

By considering integrated Boltzmann equations, we lose information on the underlying phase space distributions. By assumption, the SM remains in equilibrium, and the appropriate equilibrium distributions can be substituted by inverting Eq. (4.5). However, we do not have explicit knowledge of the phase space for species  $\phi$ , but argue in the following that we can also use equilibrium distributions to good approximation (see also Refs. [114, 218]).

First, we consider the limiting case of negligible  $\phi$  abundance and thermal equilibrium between  $\phi$  and the SM is never attained. Then,  $f_{\phi} \ll 1$  and  $\bar{f}_{\phi} \simeq 1$  holds. The backreaction and final state occupation effects are negligible, and the abundance of  $\phi$  is set by freeze-in production [220]. The only phase space distributions we are sensitive to are the SM ones, which are exactly known in this case.

The other limiting case is thermal equilibrium between  $\phi$  and the SM. The initial phase space distribution of  $\phi$  follows equilibrium up until decoupling and freeze-out of  $\phi$ . The prescription is therefore exact up to spectral distortions that are induced by the decoupling process (see e.g. discussion in Ref. [218]). Close to thermalization of  $\phi$ , the exact shape of the phase space distribution is important, but this is a narrow window in  $E_{\phi}/T$ . Thus, the prescription we adopt can be thought of as a smooth interpolation.

The framework as presented can readily be extended to general  $m \to n$  processes, however, we restrict our use to  $1 \leftrightarrow 2$  and  $2 \leftrightarrow 2$  processes, as we can often anticipate higher particle number processes to face extra suppression from additional powers of couplings or suppression from limited phase space. As far as the implementation is concerned, we first perform some integration steps analytically by eliminating the energy-momentum conserving  $\delta$ -distribution. The remaining integrations are rewritten in a way suitable for Monte Carlo integration. We illustrate how to implement the collision operator for the Monte Carlo scheme in Appendix A for  $1 \leftrightarrow 2$  and  $2 \leftrightarrow 2$ . The generalization to  $m \leftrightarrow n$  processes is straightforward.

#### 4.2 Thermal corrections

A dense plasma induces finite temperature and density corrections to fields, and particles have their dispersion relations and couplings modified by in-medium corrections. A full treatment at the level of thermal quantum field theory is possible, but for our considerations unnecessarily complicated as we tend to work in regimes where these corrections are subdominant. For a recent pedagogical introduction, see Ref. [221].

Therefore, for our goals it suffices to consider thermal masses [217, 222, 223]. We understand thermal masses as a prescription to capture the leading thermal effects without resorting to a full thermal QFT treatment. In principle, we could also prescribe other thermal couplings in interactions, but it is usually less important than the finite temperature correction on masses.

Prior to EWSB, the thermally induced masses for fermions are chiral due to the chiral nature of their interactions. Thus, left- and right-handed fermions have [223]

$$m_{l,L}^2 = \frac{m_Z^2 + 2m_W^2 + m_l^2}{2v_H^2} T^2, (4.6)$$

$$m_{l,R}^2 = \frac{m_Z^2 - m_W^2 + \frac{1}{2}m_l^2}{2v_H^2} T^2, (4.7)$$

$$m_{q,L}^2 = \frac{1}{6}g_s^2 T^2 + \frac{3m_W^2 + \frac{1}{9}(m_Z^2 - m_W^2) + m_u^2 + m_d^2}{2v_H^2},$$
(4.8)

$$m_{u,R}^2 = \frac{1}{6}g_s^2 T^2 + \frac{\frac{4}{9}(m_Z^2 - m_W^2) + \frac{1}{2}m_u^2}{2v_H^2},$$
(4.9)

$$m_{d,R}^2 = \frac{1}{6}g_s^2 T^2 + \frac{\frac{1}{9}(m_Z^2 - m_W^2) + \frac{1}{2}m_d^2}{2v_H^2},$$
(4.10)

before EWSB, and after EWSB, the mass from the Higgs mechanism dominates. It is subject to a small thermal correction for leptons and quarks [217]

$$\Delta m_l^2 = \frac{1}{8}e^2T^2\,, (4.11)$$

$$\Delta m_q^2 = \frac{1}{6} g_s^2 T^2 \,. \tag{4.12}$$

Here, we restrict ourselves to corrections from SM fields only. In Chapter 5, we consider an additional gauged U(1), and the corresponding Z' will also give a thermal correction unless we consider regimes in which the Z' is no longer part of the plasma, or corrections are negligible for other reasons, e.g. small couplings.

Likewise, all gauge bosons in the plasma receive an effective thermal mass. It can be written for a gauge boson G at leading order as [217]

$$m_G^2 = \frac{1}{6}g_G^2T^2(N_V + N_S + \frac{N_F}{2}),$$
 (4.13)

where  $N_{V,S,F}$  is the number of vector, scalar, and fermionic fields in the bath and coupled to G.

At last, thermal corrections to the Higgs effective potential, and possibly other scalar fields in extended models, are of great importance. This is less due to direct thermal corrections on mass terms, but more so due to the theory fundamentally changing between the two phases. The different phases give rise to different regimes in which processes are to be taken into account or not. For example, the presence or absence of trilinear scalar vertices can determine whether a decay is fundamentally allowed or not.

For the sake of completeness, we state here briefly the result for the effective Higgs potential in the high temperature limit  $\mu_H^2/T^2 \ll 1$  at one loop [224],

$$V_{\text{eff,T}} \simeq D(T^2 - T_0^2)\phi^2 - ET\phi^3 + \frac{\lambda(T)}{4}\phi^4,$$
 (4.14)

where  $\phi$  is the classical field value. The parameters in the equation are given in Ref. [224] and

4.3. Resonances 39

are fully determined by SM parameters, notably  $m_W$ ,  $m_Z$ , and  $m_t$ . In the high temperature regime, EW symmetry is restored and the minimum is at  $\phi = 0$ . The Higgs doublet acquires an effective thermal mass

$$m_H^2(T) = \frac{d^2 V_{\text{eff,T}}}{d\phi^2} \Big|_{\phi=0} \simeq 2D(T^2 - T_0^2).$$
 (4.15)

As the temperature drops, the potential develops a new minimum at  $\phi \neq 0$ , and it is possible to find approximate relations for the VEV and the mass of the physical Higgs boson as a function of temperature, see e.g. Ref. [224], although they break down for  $T \ll T_0$ .

### 4.3 Resonances

We address the issue of a mediator in the s-channel going on-shell, leading to a resonant enhancement of the production cross section. Besides the singular behavior of the propagator, we also face the problem of over counting if the mediator goes on-shell. The problem worsens if the mediator also happens to be in thermal equilibrium with the plasma [217, 222, 225]. In this case, the problem essentially amounts to the decay of thermalized mediators, the inverse decay and subsequent decay of the mediator, and the on-shell production in the  $2 \to 2$  process, being physically indistinguishable. Computation of the abundance requires both the  $2 \to 2$  process with possibly resonant enhancement, as well as the decay of the mediator to be taken into account. Naively adding these contributions, however, will lead to a double counting of physically equivalent processes. In this section, we expand on a prescription adapted from Ref. [217] to consistently take these processes into account and lay out how over-counting can be avoided.

#### 4.3.1 The narrow width approximation

Let us consider a scalar field  $\phi$  that mediates the process  $\psi \bar{\psi} \to \sigma \bar{\sigma}$ . We adopt the Breit-Wigner propagator to model the unstable mediator,

$$\frac{1}{(s - m_{\phi}^2)^2} \longrightarrow \frac{1}{(s - m_{\phi}^2)^2 + m_{\phi}^2 \Gamma_{\phi}^2}, \tag{4.16}$$

and make the assumption that  $\Gamma_{\phi} \ll m_{\phi}$  holds. Then, we can adopt the narrow width approximation (NWA)

$$\frac{1}{(s - m_{\phi}^2)^2 + m_{\phi}^2 \Gamma_{\phi}^2} \simeq \frac{\pi}{m_{\phi} \Gamma_{\phi}} \delta(s - m_{\phi}^2), \qquad (4.17)$$

which is exact in the limit  $\Gamma_{\phi}m_{\phi} \to 0$ . Physically, we make the assumption that the particle width is small against its mass, and so only a narrow width of momenta gives rise to on-shell production. Away from the resonance, the resonance peak quickly decays, and the  $2 \to 2$  amplitude will only receive negligible contributions from the finite width of  $\phi$ .

The squared amplitude for  $\psi \bar{\psi} \to \sigma \bar{\sigma}$  in the NWA readily factorizes to the amplitudes of decay and inverse decay of the mediator [217]

$$\left| \mathcal{M}_{\psi\bar{\psi}\to\sigma\bar{\sigma}} \right|^2 = \frac{\left| \mathcal{M}_{\psi\bar{\psi}\to\phi} \right|^2 \left| \mathcal{M}_{\phi\to\sigma\bar{\sigma}} \right|^2}{m_{\phi}\Gamma_{\phi}} \pi \delta(s - m_{\phi}^2). \tag{4.18}$$

This factorization is exact for a scalar mediator, but a complete factorization is, in general, not possible for non-scalar particles. In such cases, production and decay are correlated due to the spin or polarization states of the mediator [226, 227].

However, it is possible to introduce a decorrelated matrix element by averaging out the spin or polarization correlations. First, we observe that the matrix element for the same process but with a vector mediator in unitary gauge can be written as

$$\left| \mathcal{M}_{\psi\bar{\psi}\to\sigma\bar{\sigma}} \right|^{2} \propto \left| \mathcal{M}_{\psi\bar{\psi}\to\phi}^{\mu} \left( g_{\mu\nu} - \frac{k^{\mu}k^{\nu}}{m_{\phi}^{2}} \right) \mathcal{M}_{\phi\to\sigma\bar{\sigma}}^{\nu} \right|^{2}$$

$$= \left| \sum_{\lambda} \mathcal{M}_{\psi\bar{\psi}\to\phi}^{\mu} \varepsilon_{\mu}^{\star}(k,\lambda) \varepsilon_{\nu}(k,\lambda) \mathcal{M}_{\phi\to\sigma\bar{\sigma}}^{\nu} \right|^{2}, \tag{4.19}$$

where  $\varepsilon_{\mu}(k,\lambda)\mathcal{M}^{\mu}_{\phi\to\sigma\bar{\sigma}}$  is the partial amplitude for the decay of  $\phi$  with polarization vector  $\varepsilon_{\mu}(k,\lambda)$ . The NWA for a vector resonance is obtained by neglecting the correlation from polarizations of the vector resonance, and then averaging over the polarization states

$$\left| \sum_{\lambda} \mathcal{M}^{\mu}_{\psi\bar{\psi}\to\phi} \varepsilon^{\star}_{\mu}(k,\lambda) \varepsilon_{\nu}(k,\lambda) \,\mathcal{M}^{\nu}_{\phi\to\sigma\bar{\sigma}} \right|^{2} \to \frac{1}{3} \sum_{\lambda,\lambda'} \left| \mathcal{M}^{\mu}_{\psi\bar{\psi}\to\phi} \varepsilon^{\star}_{\mu}(k,\lambda) \right|^{2} \left| \varepsilon_{\nu}(k,\lambda) \,\mathcal{M}^{\nu}_{\phi\to\sigma\bar{\sigma}} \right|^{2} . \tag{4.20}$$

A completely analogous observation can be made for fermions. There, the NWA is found by neglecting the spin-spin correlations from production and decay, and averaging over the spin states of the fermionic mediator. Schematically, we can summarize this as

$$|\mathcal{M}_{i\to f}|^2 \propto \left| \mathcal{M}_{i\to\phi}(\not k + m_\phi) \mathcal{M}_{\phi\to i}^2 \right|^2 \propto \left| \sum_s \mathcal{M}_{i\to\phi} u_s(k) \bar{u}_s(k) \mathcal{M}_{\phi\to f} \right|^2$$

$$\to \frac{1}{2} \sum_{s,s'} \left| \mathcal{M}_{i\to\phi} u_s \right|^2 \left| \bar{u}_{s'} \mathcal{M}_{\phi\to f} \right|^2. \tag{4.21}$$

For sufficiently inclusive processes, e.g. the total cross section from unpolarized initial states, it can be shown that the exact amplitude and the NWA are in good agreement [227]. We anticipate that matrix elements in the collision operator amount to sufficiently inclusive process. Indeed, prescribing f=1 for the phase space distributions recovers the definition of the total cross section up to possible symmetry factors. Since we typically assume production from a thermal bath and we prescribe identical phase space distributions for all internal degrees of freedom, we do not expect new sources of correlation and the general conclusion should still hold.

4.3. Resonances 41

#### 4.3.2 Mediators in thermal equilibrium

Returning to our toy model of  $\psi \bar{\psi} \to \sigma \bar{\sigma}$  via an s-channel  $\phi$ , we now address the complication of  $\phi$  being in thermal equilibrium with  $\psi$ . We assume that  $\psi, \bar{\psi}$  form the thermal bath that  $\phi$  is in equilibrium with. We follow Ref. [217] in our analysis of the resonant  $\psi \bar{\psi} \to \sigma \bar{\sigma}$  reaction. Assuming that the mediator is in thermal equilibrium and  $f_{\sigma} \ll 1$ , so we can neglect the backreaction, we reorganize the integrals in the collision operator to find

$$\mathcal{C}_{\psi\bar{\psi}\to\sigma\bar{\sigma}} = \int d\Pi_{\psi}d\Pi_{\bar{\psi}}d\Pi_{\bar{\sigma}}d\Pi_{\bar{\sigma}} (2\pi)^{4} \delta^{(4)}(p_{\psi} + p_{\bar{\psi}} - p_{\sigma} - p_{\bar{\sigma}}) 
\times \frac{\left|\mathcal{M}_{\psi\bar{\psi}\to\phi}\right|^{2} \left|\mathcal{M}_{\phi\to\sigma\bar{\sigma}}\right|^{2}}{2E_{\phi}m_{\phi}\Gamma_{\phi}} \pi\delta(E_{\psi} + E_{\bar{\psi}} - E_{\phi})f_{\psi}f_{\bar{\psi}}\bar{f}_{\sigma}\bar{f}_{\bar{\sigma}} 
= \int d\Pi_{\psi}d\Pi_{\bar{\psi}} \frac{2\pi \delta^{(1)}(E_{\psi} + E_{\bar{\psi}} - E_{\phi})}{4E_{\phi}\Gamma_{\phi}m_{\phi}} \left|\mathcal{M}_{\phi\to\psi\bar{\psi}}\right|^{2} f_{\psi}f_{\bar{\psi}} 
\times \int d\Pi_{\sigma}d\Pi_{\bar{\sigma}} (2\pi)^{4} \delta^{(4)}(p_{\psi} + p_{\bar{\psi}} - p_{\sigma} - p_{\bar{\sigma}}) \left|\mathcal{M}_{\phi\to\sigma\bar{\sigma}}\right|^{2} \bar{f}_{\sigma}\bar{f}_{\bar{\sigma}} .$$
(4.22)

We observe that the last line in Eq. (4.22) resembles the decay width of  $\phi \to \sigma \bar{\sigma}$  with four momentum  $p_{\phi} = p_{\psi} + p_{\bar{\psi}}$ , but weighted with phase space densities  $f_{\sigma}$  and  $f_{\bar{\sigma}}$ . Indeed, the expression can be understood as a decay width in medium, and so we define

$$\hat{\Gamma}_{\phi \to \sigma \bar{\sigma}} = \frac{1}{2m_{\phi}} \int d\Pi_{\sigma} d\Pi_{\bar{\sigma}} (2\pi)^4 \, \delta^{(4)} (p_{\sigma} + p_{\bar{\sigma}} - p_{\phi}) \, |\mathcal{M}_{\phi \to \sigma \bar{\sigma}}|^2 \, \bar{f}_{\sigma} \bar{f}_{\bar{\sigma}} \,, \tag{4.23}$$

and reserve the hat for distinguishing quantities in vacuum and in medium.

Regarding the  $\psi$ -related integrations in Eq. (4.22), we multiply by  $\bar{f}_{\phi}/\bar{f}_{\phi}=1$  and introduce a dummy integration  $d^3p_{\phi}\,\delta^{(3)}(p_{\psi}+p_{\bar{\psi}}-p_{\phi})$  to complete to the full four momentum conserving delta distribution. Since we assume thermal equilibrium between  $\phi$  and  $\psi$ , we also exploit the relation  $f_{\phi}\bar{f}_{\psi}\bar{f}_{\bar{\psi}}=f_{\psi}f_{\bar{\psi}}\bar{f}_{\phi}$  to find

$$\mathcal{C}_{\psi\bar{\psi}\to\sigma\bar{\sigma}} = \int d\Pi_{\psi} d\Pi_{\bar{\psi}} d\Pi_{\phi} \frac{2\pi \,\delta^{(4)}(p_{\psi} + p_{\bar{\psi}} - p_{\phi})}{4E_{\phi}\Gamma_{\phi}m_{\phi}} \left| \mathcal{M}_{\phi\to\psi\bar{\psi}} \right|^{2} \frac{f_{\phi}}{\bar{f}_{\phi}} \bar{f}_{\psi}\bar{f}_{\bar{\psi}} \\
\times \int d\Pi_{\sigma} d\Pi_{\bar{\sigma}} (2\pi)^{4} \,\delta^{(4)}(p_{\psi} + p_{\bar{\psi}} - p_{\sigma} - p_{\bar{\sigma}}) \left| \mathcal{M}_{\phi\to\sigma\bar{\sigma}} \right|^{2} \bar{f}_{\sigma}\bar{f}_{\bar{\sigma}} . \tag{4.24}$$

Notice that we brought the  $\psi$ -integrations in the same form as the  $\sigma$ -integrations before. Rearranging terms and switching the roles of  $\sigma$  and  $\psi$ , we finally arrive at

$$C_{\psi\bar{\psi}\to\sigma\bar{\sigma}} = \int d\Pi_{\sigma}d\Pi_{\bar{\sigma}}d\Pi_{\phi} (2\pi)^4 \,\delta^{(4)}(p_{\sigma} + p_{\bar{\sigma}} - p_{\phi}) \left| \mathcal{M}_{\phi\to\sigma\bar{\sigma}} \right|^2 \, f_{\phi}\bar{f}_{\sigma}\bar{f}_{\bar{\sigma}} \,\frac{\hat{\Gamma}_{\phi\to\psi\bar{\psi}}}{\bar{f}_{\phi}\Gamma_{\phi}}. \tag{4.25}$$

It is important to clarify the physical meaning of this result. By assuming on-shell production and thermal equilibrium for the mediator, we arrived at an expression for the collision operator  $C_{\psi\bar{\psi}\to\sigma\bar{\sigma}}$  that resembles the production from mediator decay up to the weight factor  $\hat{\Gamma}_{\phi\to\psi\bar{\psi}}/(\bar{f}_{\phi}\Gamma_{\phi})$ . Indeed, the general expectation is that decay from equilibrium and on-shell production are physically equivalent if equilibrium is also maintained by the exact same inverse decay. In accordance with Ref. [217], we identify  $\Gamma_{\phi} = \bar{f}_{\phi}^{-1} \sum_{f} \hat{\Gamma}_{\phi\to f}$  as the correct width

for the Breit-Wigner propagator in the plasma, where f includes all final states regardless of whether they are in equilibrium or not. The expression Eq. (4.25) then coincides with the mediator decay up to a rescaling involving the decay widths. This can be traced back to a deviation of the distribution of  $\phi$  from the equilibrium form in the presence of decays into non-equilibrated final states [217]. The distribution is no longer set by cancellations of decay and inverse decay rates of plasma particles, but rather between plasma particles and also the decay into out-of-equilibrium final states.

For a mediator not in thermal equilibrium, we can perform an analogous computation, however, we cannot use the relation  $f_{\phi}\bar{f}_{\psi}\bar{f}_{\bar{\psi}} \neq f_{\psi}f_{\bar{\psi}}\bar{f}_{\phi}$ , and  $f_{\phi} \ll 1$  can be used instead. The expression readily simplifies to

$$C_{\psi\bar{\psi}\to\sigma\bar{\sigma}} = \int d\Pi_{\psi} d\Pi_{\bar{\psi}} d\Pi_{\phi} (2\pi)^4 \delta^{(4)} (p_{\psi} + p_{\bar{\psi}} - p_{\phi}) \left| \mathcal{M}_{\psi\bar{\psi}\to\phi} \right|^2 \hat{\mathrm{Br}}_{\phi\to\sigma\bar{\sigma}}. \tag{4.26}$$

Again, the hat indicates that  $\hat{\mathrm{Br}}_{\phi\to\sigma\bar{\sigma}}$  is the branching ratio in the medium that includes final state occupations. Thus, in this limit, resonant production simplifies to inverse decay of mediators weighted by the branching ratio in the medium. Note that even if production of  $\sigma\bar{\sigma}$  proceeds in the freeze-in regime, we can be sensitive to final state effects from plasma constituents as their decay widths and, therefore, the above branching ratio, are subject to Pauli blocking or Bose enhancement.

## Chapter 5

# Cosmology of Dirac neutrinos with a Z'

Models of Dirac neutrinos with an additional gauge symmetry and the respective gauge boson, here referred to as a generic Z' boson, are well-motivated and have been studied widely in the literature. These models include, but are not limited to, gauge symmetries that protect the Dirac nature. For an incomplete list of recent examples of such models, see Refs. [70–72, 76, 87, 96].

It is well-known that, in principle, these models are strongly constrained from cosmological excess radiation due to gauge interactions coupled to the right-handed neutrino.<sup>1</sup> Previous limits focusing specifically on a gauged  $U(1)_{B-L}$  were competitive with laboratory and collider constraints [43, 113, 114, 116]. Since then, cosmological bounds have tightened, and an update on these limits is needed. Although these studies were pushing towards precision, they still rely on a few simplifications regarding the implementation of the relevant Boltzmann equations.

A more pressing issue is the underlying assumptions regarding cosmology. The validity of limits and forecasts relies on the Universe reaching temperatures of the order of the gauge boson mass. While not necessarily troubling when limits probe masses on the order of  $\sim 1\,\text{TeV}$  as we may perfectly envision a hot big bang reaching such temperatures, the issue becomes more apparent when considering forecasts for future experiments. Here, masses  $m_{Z'}\gg \text{TeV}$  and even up to the GUT scale appear testable. However, the effect of reheating and modified thermal histories in general on these limits has not been carefully studied before.

In the following, we will systematically study deviations from changing cosmological assumptions. We first introduce the B-L benchmark model, and briefly discuss how the results we find are generic and apply to a wide range of models that introduce new gauge interactions. We update previous constraints with the new ACT limit on  $\Delta N_{\rm eff} < 0.17$ , finding the strongest limits on such models thus far. For this, we utilize the framework we developed in Chapter 4, and in the process also eliminate some of the approximations made in previous implementations. We then turn to the systematic study of non-standard cosmologies in Dirac neutrino models with gauge interactions.

 $<sup>^1</sup>$ We only consider an exact Dirac nature of neutrinos here. However, our results also apply to light right-handed neutrinos in the Majorana case, as long as  $m_{\nu_R} < T_{\rm CMB}$  and the  $\nu_R$  contribute as cosmological radiation at that time. In particular, this includes Pseudo-Dirac neutrinos with a small mass-splitting between active and sterile neutrinos.

#### 5.1 A minimal B-L model

Many gauge group extensions to protect the Dirac nature of neutrinos exist. Our benchmark model is a  $U(1)_{B-L}$  extension, and we will discuss how bounds translate approximately to other Z' models by a rescaling of the gauge coupling. While other representatives for a Z' extension are perfectly fine candidates, we consider a B-L extension particularly well motivated. It arises as a building block of more involved models, that e.g. also account for the presence and production of DM candidates. Moreover, the introduction of three right-handed neutrinos with suitable charge assignment automatically renders B-L anomaly free and makes it a good candidate for a gauged symmetry.

#### 5.1.1 Particle content

The model of gauged  $U(1)_{B-L}$  we adopt here is minimal. We introduce only the three necessary generations of  $\nu_R$  for gauge anomaly cancellation and the massive gauge boson. In particular, we remain agnostic of the origin of the Z' mass. Both a Stueckelberg mass or a massive gauge boson from a broken  $U(1)_{B-L}$  is feasible, provided that the spontaneous breaking violates  $\Delta(B-L) \neq 2$  as to forbid a Majorana mass term. The relevant addition to the SM Lagrangian is given by

$$\mathcal{L} \supset \frac{1}{4} F'_{\mu\nu} F'^{\mu\nu} + \frac{1}{2} m_{Z'}^2 Z'_{\mu} Z'^{\mu} + g' Z'_{\mu} \sum_{f \in \text{SM}} Q_{\text{B-L}}^{(f)} \bar{f} \gamma^{\mu} f + g' Z'_{\mu} Q_{\text{B-L}}^{(\nu_R)} \bar{\nu}_R \gamma^{\mu} \nu_R , \qquad (5.1)$$

where  $f \in SM$  runs over all SM fermions including  $\nu_L$ . The gauge charges are 1/3 for quarks and -1 for leptons. Without any additional fields charged under B-L, the charges of  $\nu_R$  are either  $Q_{B-L}^{(\nu_R)} = -1$  or  $Q_{B-L}^{(\nu_R)} = -4$ , -4, 5 to make a consistent theory. We will only consider the former charge assignment, but discuss the other option in light of other Z' extensions. We note in passing that this charge assignment allows for Dirac neutrino masses directly from a Yukawa term with the SM Higgs doublet, although we stay agnostic also about the precise mechanism giving rise to neutrino masses. All constraints we obtain are either unaffected or conservative when adding additional fields, as their effect on  $\Delta N_{\rm eff}$  is either negligible or additional channels for populating the  $\nu_R$  abundance are introduced.

Equation (5.1) is not necessarily complete for an unbroken B-L and should contain a kinetic mixing term  $\mathcal{L} \supset \frac{\epsilon}{2} Y_{\mu\nu} F'^{\mu\nu}$ . Note that this term will inevitably be generated from radiative corrections, so its absence cannot be justified. However, limits we derive are expected to be only marginally altered by the presence of gauge boson mixing. Any exact cancellation from destructively interfering amplitudes is fine tuned and not stable under running. Moreover, in the high mass regimes we are predominantly interested in, it is the mixing to the Z that is expected to be relevant. Due to the chiral nature of weak interactions, an exact cancellation with a vector-like interaction poses no problem. Thus, kinetic mixing will at most provide a minor correction to limits obtained, and such corrections can be approximately absorbed in an effective coupling that is probed.

The total decay width in vacuum is given by [114]

$$\Gamma_{Z'} = \frac{g^2}{12\pi} m_{Z'} \left( 3 + \sum_{f \neq \nu}^{m_{Z'} > 2m_f} \frac{Q_{B-L}^2}{N_c(f)} \left( 1 + \frac{2m_f}{m_{Z'}} \right) \sqrt{1 - \frac{4m_f^2}{m_{Z'}^2}} \right) , \tag{5.2}$$

where the factor 3 comprises the contribution of left- and right-handed neutrinos. We neglect the complications of hadronization and assume decay into free quarks only.

#### 5.1.2 Cosmology

Computations are performed within the framework developed in Chapter 4. We do not distinguish between  $\nu_R$  and  $\bar{\nu}_R$ , but instead treat the right-handed neutrinos as an effective fermion fluid with  $g_{\nu_R} = 3 \times 2$  internal degrees of freedom [43, 114, 218, 228]. Thus, we effectively take Eq. (4.2) with  $\phi = \nu_R$ . The collision operator is calculated from a single process  $f\bar{f} \to \nu_R\bar{\nu}_R$ , but we note that we have possible on-shell Z' contributions. Since the process is resonantly enhanced, the rate of the on-shell contribution dominates over the  $2 \to 2$  process due to the additional suppression in the coupling constant. Moreover, we explicitly checked whether Z' thermalizes with the SM from  $f\bar{f} \leftrightarrow Z'$ , which applies for almost all of parameter space we consider. Thus, unless  $T \lesssim m_{Z'}$ , the (inverse) decay involving Z' dominates over  $2 \to 2$  scattering. We generically avoid the issue of overcounting, since  $1 \to 2$  processes dominate unless they are kinematically forbidden.

For temperatures below the gauge boson mass, decays become inefficient, and  $2 \to 2$  processes start to take over. We can address this similarly to Ref. [222] by cutting the resonant region. The error we introduce is marginal, as we checked explicitly, since the  $2 \to 2$  process is relevant only in a region where the now cut resonant regime is kinematically inaccessible anyways. This limit is only relevant for UV sensitive freeze-in at temperatures much below the gauge boson mass, or if we consider the decoupling process from the SM plasma, again at temperatures smaller than the boson mass.

The effect of (quasi-)elastic scattering, such as  $f \nu_R \to f \nu_R$  is negligible. Deep in the freeze-in limit,  $f_{\nu_R} \ll 1$  and scattering is suppressed by the phase space densities. Thus, it can only play a role when the  $\nu_R$  density becomes relevant. When fully coupled, however, the energy transfer is subdominant compared to the s-channel process and will not have a resonant enhancement.

#### 5.1.3 Results

We present an overview of the current experimental constraints on a heavy Z' with light right-handed neutrinos in Fig. 5.1, in particular constraints from collider searches as well as previous cosmological limits. We include the updated limit for  $\Delta N_{\rm eff} = 0.17$  from DESI DR6 that we compute, as well as a refined forecast for the benchmark value  $\Delta N_{\rm eff} = 0.06$  also calculated here.

We provide an exact limit based on this benchmark value by tracking the energy density throughout the decoupling process without additional assumptions beyond the prescribed phase space distributions. We also include thermally corrected masses before and after the EW phase

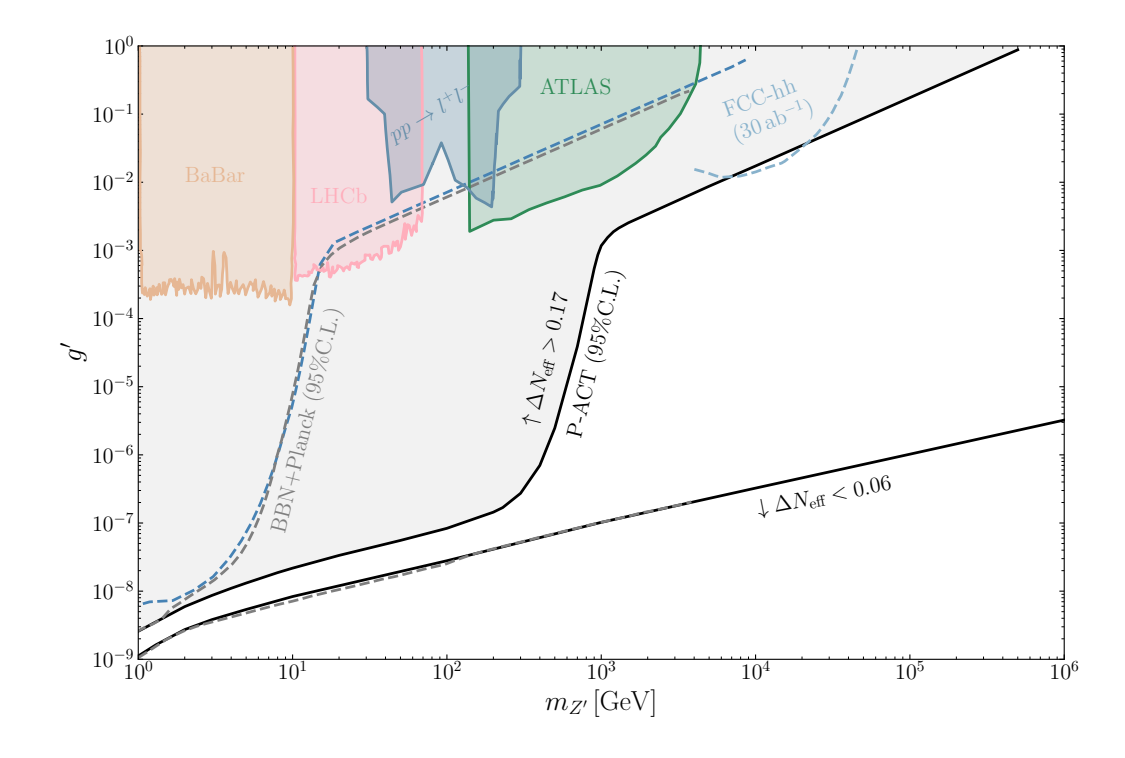


FIGURE 5.1: Constraints on  $U(1)_{B-L}$  gauge bosons in presence of light right-handed neutrinos. The upper black curve corresponds to  $\Delta N_{\rm eff} = 0.17$ , excluded by ACT [45] at 95% C.L. and disfavored by BBN+CMB combinations [46, 47]. The lower black curve is a benchmark value  $\Delta N_{\rm eff} = 0.06$  for future CMB surveys. We show forecasts and Planck+BBN limits from Refs. [114](grey dashed) and [43](blue dashed). We show complementary limits from ATLAS [229], the Drell-Yan process in ATLAS [230, 231], recasted LHCb limits [231, 232], and dark photon decays from BaBar [231, 233]. For comparison, we also show the projected reach of FCC-hh for Z' searches from Ref. [234]. Figure published in Ref. [2].

transition, in accordance with the results of Sec. 4.2. In comparison to the results of Refs. [218, 235], which use a simplified prescription for the backreaction term, no final state statistics, and no thermal effects, we find percent level corrections. This is in agreement with analytic estimates of the uncertainty done in those References.

The constrained value  $\Delta N_{\rm eff} \simeq 0.17$  implies a decoupling temperature of the three right-handed neutrinos of about  $T_{\rm dec} \sim 40\,{\rm GeV}$  from Eq. (3.13) if thermal equilibrium between the SM and  $\nu_R$  has been established at higher temperatures. For sufficiently small gauge boson masses, the inverse decay is still efficient at  $T < 40\,{\rm GeV}$  and can maintain equilibrium for longer. Consequently, limits are much stronger due to the resonant enhancement. We transition to freeze-in production, since we cannot have  $\nu_R$  thermalized below 40 GeV for even smaller masses. Since the freeze-in is also dominated by the resonantly enhanced inverse decay channel, limits remain strong in this low mass regime.

The CMB-S4 forecast ( $\Delta N_{\rm eff} = 0.06$ ) computed here is consistent with the result from Ref. [114], which we also show for comparison. The inclusion of thermal masses and final state statistics provides a minor correction. In the freeze-in regime, decays to fully thermalized SM fermions are subject to Pauli blocking from final state statistics and receive a minor reduction, however, decays to  $\nu_R$  are not. Therefore, the in medium branching ratio receives a small

enhancement, and accordingly, we can expect a small boost to  $\nu_R$  production. Taking all effects into account, corrections do not generally exceed the percent level. We note the presence of a disagreement of up to  $\sim 10\%$  above  $m_{Z'} \sim 1 \,\text{GeV}$  when compared to the previous forecast. We cannot reproduce this discrepancy, even when fully replicating the approximations from that study, and attribute this mismatch to numerical difficulties in Ref. [114].

Some extra care is needed for very small gauge couplings in the low mass regime. Here, the Z' can be cosmologically long-lived  $\Gamma_{Z'} \lesssim H$ . Produced gauge bosons redshift as matter and therefore slower than the ambient radiation bath and the extra right-handed neutrinos. The energy they inject into  $\nu_R$  as well as SM fermions upon decay is enhanced [114, 236, 237]. We explicitly checked this by tracking the energy density of a non-relativistic Z'. For the masses and couplings shown in Fig. 5.1, this only provides a minor correction of sub percent level that becomes largest close to  $m_{Z'} \sim 1 \text{ GeV}$ , in agreement with similar estimates from Ref. [114].

#### 5.1.4 Probing Dirac neutrinos up to the GUT scale?

The forecasts we compute are not limited to the parameter values shown in Fig. 5.1 – indeed, they can be safely extrapolated to much higher masses, as confirmed by explicit computation. Curiously, we find that  $m_{Z'} \sim \Lambda_{\rm GUT} \sim 10^{16} \, {\rm GeV}$  implies that a gauge coupling  $g' \sim \mathcal{O}(1)$  is close to future experimental limits. This seems to suggest that GUT scale physics is testable in  $\Delta N_{\rm eff}$  surveys, and perhaps more importantly, natural realizations with gauge coupling values  $g' \sim \mathcal{O}(1)$  are accessible and will be tested on all scales up to  $\Lambda_{\rm GUT}$ .

Such a prospect deserves extra scrutiny, and it is important that we recall the explicit and implicit assumptions made in the computation. Experiments like CMB-S4 and others probe the regime  $\Delta N_{\rm eff} < 0.14$ , i.e. if we have three light  $\nu_R$ , they can never attain thermal equilibrium with the SM prior to the electroweak phase transition. However, we make the implicit assumption of reheating to at least  $T_{\rm reh} \sim m_{Z'}$ , which for  $m_{Z'} \sim \Lambda_{\rm GUT}$  is in tension with limits on the scale of inflation [238]. Thus, unless we wish to break with the inflationary paradigm in a rather drastic manner, it seems unlikely that GUT scale realizations of a Z' in conjunction with light right-handed neutrinos are testable by  $\Delta N_{\rm eff}$  alone.

A similar consideration applies to limits at smaller masses, too. It shows that the limits found here need to be thought of jointly with the underlying cosmological assumptions. The initial reheating is just as important as any secondary phase of reheating that could possibly dilute a primordial  $\nu_R$  abundance. Turning the argument around, if we were to establish the Dirac nature of neutrinos otherwise, the Z' limits turn into a powerful test of the thermal history of the Universe long before BBN – an era that is notoriously difficult to probe. In the next section, we focus on the effect of the reheating temperature and some frequently considered non-standard thermal histories on the limits of our model.

## 5.2 Cosmology revisited

We begin with a few general remarks on how non-standard thermal histories affect  $\Delta N_{\rm eff}$  for light  $\nu_R$  models, before considering in more detail the effect of lowered reheating temperatures,

extra relativistic degrees of freedom in the Universe, phase transitions and vacuum energies, and an early matter dominated era.

Let us assume that couplings are sufficiently large to keep the three  $\nu_R$  in thermal equilibrium with the SM at high temperatures, so that they decouple at some lower temperature. Then, whatever process may inject entropy into the SM plasma will not affect  $\Delta N_{\rm eff}$ , as any injection is quickly equilibrated between the two sectors. It is only after decoupling of the right-handed neutrinos that changes to the SM plasma remain isolated and affect the ratio  $\rho_{\nu_R}/\rho_{\rm SM}$  and thus  $\Delta N_{\rm eff}$ . Although it is feasible that production of  $\nu_R$  falls into a non-standard era, e.g. an early matter era, we do not consider this case in detail. Since we know the Universe must have been radiation dominated around the time of BBN, this itself implies any such non-standard period must be accompanied by a second phase of reheating. If the  $\nu_R$  population is decoupled, this will imply a dilution of  $\nu_R$  abundances, possibly beyond detection thresholds. Therefore, changes to  $\Delta N_{\rm eff}$  in such scenarios are predominantly set by processes after such a second phase of reheating. It is worthwhile to consider the effect of lowered reheating temperatures on the production process for the sake of an outright lowered reheating temperature, as well as accommodate for non-standard thermal histories accompanied by a second phase of reheating.

From  $\Delta N_{\rm eff} \propto \rho_{\nu_R}/\rho_{\rm SM}$ , and  $\rho \propto s^{4/3}$ , we can define an entropy dilution factor connecting the thermal baths before and after entropy injection,  $D_s = S_{\rm after}/S_{\rm before}$ . The effect of entropy injection can be written as

$$\Delta N_{\text{eff}} \to \Delta N_{\text{eff}} \times \left(\frac{D_{s,\nu_R}}{D_{s,\text{SM}}}\right)^{4/3}$$
 (5.3)

We usually assume negligible entropy injection into the  $\nu_R$  sector and set  $D_{s,\nu_R} = 1$ . Eq. (5.3) provides a convenient way to rescale limits if additional entropy is being injected. We provide approximate expressions for the dilution factors in various modified thermal histories, which enables the recasting of our limits for entropy injection after  $\nu_R$  production. If the secondary reheating event is dominant in any given cosmology, and  $D_s \gg 1$  holds, the limits for explicitly lowered reheating temperatures we compute later in this section will apply.

Many modified thermal histories can be parametrized by means of a fiducial energy density  $\rho_{\phi}$ , with possibly time dependent equation of state parameter  $w_{\phi}$ , a decay rate  $\Gamma_{\phi}$ , and the fraction  $\kappa$  of energy density injection into the SM and  $\nu_R$  sector. Moreover, we need to specify the amount of energy density in  $\phi$ , e.g. by specifying the ratio  $\rho_{\phi}/\rho_{\rm SM}$  at some initial time. In many cases, this is done by defining a time of equality, at which  $\rho_{\phi} = \rho_{\rm SM}$  holds.

This parametric family of cosmologies includes, among others, variations of early dark energy, an early matter era, and more. Our master equations containing  $\rho_{\phi}$  are,<sup>2</sup>

$$\frac{d\rho_{\phi}}{dt} + 3H(1+w_{\phi})\rho_{\phi} = -\Gamma_{\phi}\rho_{\phi}, \qquad (5.4)$$

$$\frac{d\rho_{\phi}}{dt} + 3H(1+w_{\phi})\rho_{\phi} = -\Gamma_{\phi}\rho_{\phi}, \qquad (5.4)$$

$$\frac{d\rho_{\rm SM}}{dt} + 3H(\rho_{\rm SM} + P_{\rm SM}) = (1-\kappa)\Gamma_{\phi}\rho_{\phi} - C_{f\bar{f}\to\nu_R\bar{\nu}_R}, \qquad (5.5)$$

$$\frac{d\rho_{\nu_R}}{dt} + 4H\rho_{\nu_R} = C_{f\bar{f}\to\nu_R\bar{\nu}_R} + \kappa \Gamma_{\phi}\rho_{\phi}. \qquad (5.6)$$

$$\frac{d\rho_{\nu_R}}{dt} + 4H\rho_{\nu_R} = \mathcal{C}_{f\bar{f}\to\nu_R\bar{\nu}_R} + \kappa \,\Gamma_{\phi}\rho_{\phi} \,. \tag{5.6}$$

We do not solve the system explicitly within a given modified cosmology, but rather take the equations as the starting point of a more general discussion of how the modifications alter  $\nu_R$ -genesis.

#### 5.2.1Extra degrees of freedom

An extended theory may contain other degrees of freedom that are thermalized with the SM at high temperatures. In terms of the  $\rho_{\phi}$  parametrization, this corresponds to a radiationlike extra density that is tightly coupled to the SM, and has  $g_{\phi}^{(s)}$  internal degrees of freedom. During freeze-out, the comoving entropy of the  $SM + \phi$  plasma is conserved, and its temperature increases. The dilution factor is given by

$$D_s = \left(\frac{g_{\rm SM}^{(s)} + g_{\phi}^{(s)}}{g_{\rm SM}^{(s)}}\right), \tag{5.7}$$

if  $\phi$  becomes non-relativistic after  $\nu_R$ -genesis. Any disappearing degrees of freedom from before  $\nu_R$  production do not affect  $\Delta N_{\rm eff}$ . It is evident that, unless there is a large number of degrees of freedom freezing out after the abundance of right-handed neutrinos has been set, the dilution factor is small and detection prospects are not severely affected. Notably, even the initial presence and complete disappearance of the entire spectrum of many supersymmetric extensions [239] would dilute the energy density of  $\nu_R$  by little more than a factor two. This does not pose a severe challenge to the limits we put.

#### 5.2.2Phase transitions and other early dark energies

A phase of early dark energy, or a (strong) first order phase transition, is characterized by a stage of vacuum energy domination. In the language of the fiducial energy density  $\rho_{\phi}$ , we adopt an equation of state parameter  $w_{\phi} = -1$ , which at a later time proceeds to decay with rate  $\Gamma_{\phi}$  into an intermediate matter-like component with equation of state  $w_{\phi} = 0$ . Thus, such a period is characterized by an initial radiation-like era, followed by an episode of vacuum energy domination, before reheating to SM and other final states during an entropy injection phase.

Depending on the details of the injection, such a phase may either be prolonged due to a slowly decaying matter-like intermediate stage, or almost instantaneous if the decay rate

<sup>&</sup>lt;sup>2</sup>In general, it is expected that  $\Gamma_{\phi} = \Gamma_{\phi}(w_{\phi})$  for  $w_{\phi} > 0$ , i.e. the effective width can be energy dependent for (semi-)relativistic matter. We do not consider this subtle effect here.

dominates over the Hubble rate. The analytic estimates of this section follow Ref. [240], with the appropriate changes made to apply results to our scenario.

The stage of vacuum domination starts once  $\rho_{\phi} = \rho_{\rm rad} \simeq \rho_{\rm SM}$  holds. It transitions into the entropy injection phase at temperature  $T_e$ , when the evolution of the SM plasma ceases to be adiabatic due to the injected energy. The injection phase concludes once the SM evolves adiabatically and radiation-like again at temperature  $T_r$  and can approximately be defined from  $\Gamma_{\phi} = H$ . However, decay of the vacuum-like component may be triggered at temperature  $T_e$  and if  $\Gamma_{\phi} \gg H(T_e)$  holds, the decay is very efficient and can be considered instantaneous to good approximation.

The latter case is particularly simple to estimate. Assuming that injection into right-handed neutrinos is negligible, we readily estimate the dilution factor by adding the vacuum energy to the SM energy at  $T_e$  to find  $T_r$ . This gives the dilution factor

$$D_s = \frac{T_r^3}{T_e^3} = \left(1 + \frac{30\Delta V}{\pi^2 g_{(\rho)} T_e^4}\right)^{3/4} \simeq (1 + \alpha)^{3/4} , \qquad (5.8)$$

where  $\alpha = \Delta V/\rho_{\rm SM}(T_e)$  denotes the ratio of vacuum to SM radiation energy at  $T_e$ .<sup>3</sup>

In case that the intermediate matter-like stage is long-lived, the estimate changes somewhat, and since the matter-like component redshifts slower than its radiation counterpart, injection is enhanced. Such a situation might occur during a phase transition, where the field oscillates around a new minimum and these oscillations decay slowly compared to the Hubble rate.

Adopting the result from Ref. [240], we find

$$D_s = \left(\frac{90}{8\pi^3 g_{(\rho)}(T_r)}\right)^{3/4} \left(\frac{2}{5}\Gamma_\phi M_P\right)^{1/2} \left(\frac{8\pi\Delta V}{3}\right) \frac{1}{T_e^3}.$$
 (5.9)

However, we anticipate that in most situations of interest the instantaneous approximation gives a good estimate, and an extended period of e.g. long-lived oscillations may better be captured by an early stage of matter domination altogether.

In either case, it is evident from Eq. (5.8) and (5.9) that, unless the vacuum energy dominates significantly prior to its decay, the  $\nu_R$  abundance and hence  $\Delta N_{\rm eff}$  is not diluted by more than a factor  $\mathcal{O}(1)$ . Any stronger vacuum energy will likely dilute right-handed neutrinos beyond detection, unless reheating into the  $\nu_R$  sector is also present. Such a situation requires a more careful analysis, and like the explicit production during such a stage, will likely involve solving the system in Eq. (5.6). In case of strong dilution, considering a secondary phase of  $\nu_R$  production starting from the lowered second reheating temperature will provide conservative limits.

We note here in particular that a BSM induced first order EW phase transition or modified QCD transitions are unlikely to make significant alterations to our forecasts, since they are typically expected to fall in the  $\alpha < 1$  regime. For more details, see e.g. the discussion in Ref. [241].

<sup>&</sup>lt;sup>3</sup>We follow a similar notation here as is often used in the phase transition literature [241].

#### 5.2.3 Early matter dominated era

Next, we consider the effect of an era of early matter domination (EMD). We remain agnostic as to the origin of such an era and characterize it entirely by its phenomenological description. These non-standard cosmological interludes are widely studied and an active field of research. The deviations from the radiation dominated Universe can result from a variety of mechanisms, including the aforementioned field oscillations, but also production of long-lived particles, the presence of string moduli, and more. Therefore, we instead refer to Refs. [242, 243] for comprehensive and recent reviews on the subject. Indeed, we note here that our results are independent of the precise workings of the matter dominated era, as we are only sensitive to the phenomenological consequences of such an interlude. Namely, it is the deviation of the Hubble parameter and the reheating stage at the end of an EMD that affects our results.

In terms of the fiducial energy density  $\rho_{\phi}$ , we set w=0 and define  $T_{\rm eq}$  through the relation  $\rho_{\phi}=\rho_{\rm rad}\simeq\rho_{\rm SM}$ . This defines a temperature of equality and the beginning of the era of EMD. Initially, the energy transfer from the matter sector to the radiation sector is inefficient. Therefore, the SM and all other radiation-like additional sectors continue to evolve adiabatically. Of course, the Hubble rate evolves differently compared to a standard radiation dominated era. We find  $H \propto a^{-3/2} \propto T_{\rm SM}^{3/2}$  in this case [244]. Adiabatic expansion implies  $\rho \propto a^{-4}$  and therefore the ratio  $\rho_{\nu_R}/\rho_{\rm SM}$  remains unaffected. This assumes that  $\nu_R$  and the SM are decoupled at this time and  $\nu_R$ -genesis is completed.

Production throughout such an era gives a non-trivial abundance. A few general remarks, however, can be made. Considering the freeze-in production of  $\nu_R$ , it is evident how the ratio  $\mathcal{C}/H$  is crucial for the yield that can be obtained. We could, in principle, study this production by adopting our fiducial cosmology and solving the system of equations explicitly. It turns out that this is not necessary, as the end of EMD must encompass strong reheating and therefore dilute  $\nu_R$  beyond detection. Only production during the reheating process itself may leave some traceable amounts of  $\nu_R$ . DM production during EMD is widely studied (e.g. [245]), but it is also known that at least the UV-sensitive freeze-in contribution is negligible in such cases [240].

Eventually, decays of the matter component become efficient in transferring entropy to the SM. Thus, the SM deviates from adiabatic expansion. Let us assume that  $\phi$  continues to scale like matter and is the dominant species in the Universe. It follows that  $\rho_{\rm SM} \propto a^{-3/2}$  and  $T_{\rm SM} \propto g_{(\rho)}^{-1/4} a^{-3/8}$  holds [244], manifesting the deviation from adiabatic expansion of the SM plasma.

As alluded to before, we can define the end of EMD by  $H(T_r) \simeq \Gamma_{\phi}$ . Physically, it means the decays become efficient compared to the expansion rate, thus entropy injection from decays dominates over the adiabatic Hubble expansion – the matter component quickly disappears and reheats the SM. We can readily estimate the dilution factor that must depend on  $T_{\rm eq}$  and  $T_r$  and find [244]

$$D_s = \frac{T_{\text{eq}}}{T_r} \frac{g_{(\rho)}(T_{\text{eq}})g_{(s)}(T_r)}{g_{(\rho)}(T_r)g_{(s)}(T_{\text{eq}})} \simeq \frac{T_{\text{eq}}}{T_r},$$
 (5.10)

which implies dilution is, up to matters of counting the correct degrees of freedom for the plasma, given by the ratio of temperatures between beginning and end of the matter era. Therefore, dilution at the end of EMD generically yields  $D_s \gg 1$ . Any primordial abundance

of  $\nu_R$  is diluted beyond detection. As for the vacuum case studied before, we can obtain conservative bounds by considering production after reheating of the matter era has completed.

#### 5.2.4 Reheating

At last, we consider the situation of a lowered reheating temperature, by which we mean  $T_{\rm reh} < m_{Z'}$ . This situation is worthwhile to consider for two reasons. First of all, a lowered reheating temperature from inflation is possible, and in cases where extremely high temperatures are at play, the possibility of outright overlap of the reheating process with our  $\nu_R$ -genesis needs to be acknowledged. In addition, we find that for many modified thermal histories, enough reheating to dilute  $\Delta N_{\rm eff}$  is present. Thus, production after some  $T_{\rm reh} < m_{Z'}$  gives a conservative but reliable bound.

Low mass scenarios with extremely low reheating temperatures below the EW scale ( $T_{\rm reh} \ll T_{\rm EWSB}$ ) were considered in Ref. [246]. Here we take a different approach. Motivated by the strong forecasts up to very high scales, we consider a lowered reheating temperature for masses all the way up to the GUT scale. The dynamics of reheating are involved, and we do not attempt to incorporate the entire reheating process and possible light relics from this period. Instead, we neglect the reheating dynamics and simply integrate the evolution equations from some initial temperature  $T_{\rm reh}$ . This gives a conservative limit, as possible contributions from reheating itself are neglected.

For selected values  $m_{Z'}$ , we show the dependence of  $\Delta N_{\rm eff}$  on the reheating temperature in Fig. 5.2. We focus on values that are within reach of near-future and very futuristic colliders, but also GUT scale physics and in between. In all cases, we observe some general trends. If the reheating temperature obeys  $T_{\rm reh} \lesssim m_{Z'}$ , limits are still shaped by the resonant production of on-shell gauge bosons and their subsequent decay. As we progress to smaller values in mass relative to the reheating temperature, limits weaken drastically as we shift away from the resonant regime, which becomes kinematically inaccessible. Production is dominated by the UV-sensitive effective operator obtained from integrating out Z' in the  $f\bar{f} \to \nu_R \bar{\nu}_R$  process. Thus, the abundance will explicitly depend on  $T_{\rm reh}$ , and is to good approximation controlled by the parameter combination  $g^4 T_{\rm reh}^3 M_P/m_{Z'}^4$ . For a benchmark value  $\Delta N_{\rm eff} \sim 0.1$ , we find the empirical relations

$$g \sim 1.8 \left(\frac{T_{\rm reh}/m_{Z'}}{10^{-3}}\right)^{-3/4} \left(\frac{m_{Z'}}{10^9 \,\text{GeV}}\right),$$
 (5.11)

$$\frac{T_{\text{reh}}}{m_{Z'}} \sim 0.05 \left(\frac{m_{Z'}}{10^9 \,\text{GeV}}\right)^{1/3} \left(\frac{g'}{0.1}\right)^{-4/3},$$
(5.12)

to estimate parametric dependencies.

Note how, in particular, the seemingly testable high-scale realizations in the GUT regime or somewhat below are substantially affected. It is clear that reheating temperatures consistent with Planck [238] or somewhat below directly imply g>1, and we approach the non-perturbative regime. Even for smaller masses, just going two to three orders of magnitude below the mass will suppress abundances of  $\nu_R$  unless g is close to the non-perturbative regime. Going to even smaller masses  $m_{Z'}\sim 1000\,\text{TeV}$ , the conclusions change. Here we would need to

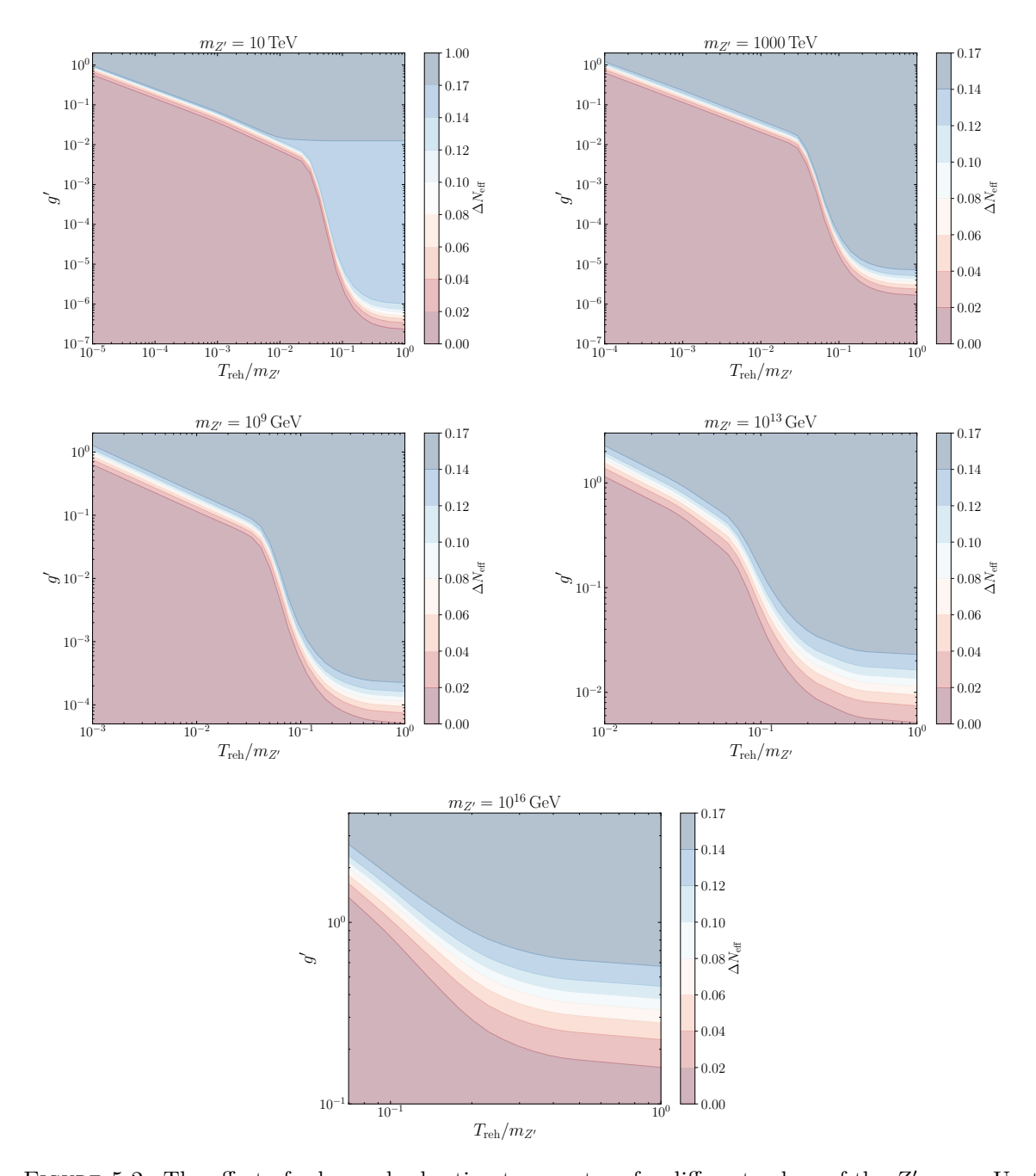


FIGURE 5.2: The effect of a lowered reheating temperature for different values of the Z' mass. Up to masses of thousands of TeV, limits can only be significantly weakened for a lowered reheating temperature. We can still have a Z' within reach of future colliders, if there was strong reheating at temperatures as low as  $T_{\rm reh} \lesssim 100$  MeV. For larger masses, strong limits on  $\mathcal{O}(1)$  gauge coupling may be avoided by having (inflationary or secondary) reheating at temperatures a few orders of magnitude below the gauge boson mass. We note that for scales as high as the GUT scale, a seemingly natural realization with  $\mathcal{O}(1)$  gauge coupling becomes testable. However, reheating to just an order of magnitude below the mass will suppress any signal from  $\Delta N_{\rm eff}$ . We note that detectable amounts of  $\nu_R$  produced at the GUT scale require reheating to temperatures in tension with upper limits on the inflationary scale. Published in Ref. [2].

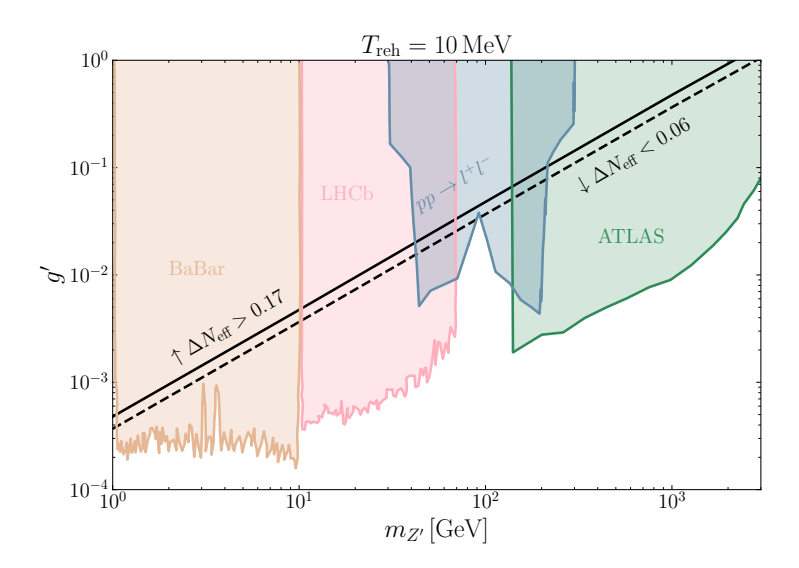


FIGURE 5.3: Irreducible constraints on  $U(1)_{B-L}$  gauge bosons in presence of light right-handed neutrinos. These limits assume a reheating temperature  $T_{\rm reh}=10\,{\rm MeV}$ , which is the minimum value required for successful BBN and therefore cannot be avoided. We show the same complementary limits as in Fig. 5.1 for comparison. The upper black curve corresponds to  $\Delta N_{\rm eff}=0.17$ , excluded by ACT [45] at 95% C.L. and disfavored by BBN+CMB combinations [46, 47]. The lower dashed curve is a benchmark value  $\Delta N_{\rm eff}=0.06$  for future CMB surveys.

reheat to temperatures in the GeV range and lower to avoid limits – a regime that is testable in principle also by collider experiments.

The implications in terms of a lowered reheating temperature are of particular interest here. We stress again that we should view our benchmark model as a representative of other Z' extensions, and as a building block of more complex models. Such models often incorporate other features, such as a suitable DM candidate or they account for Dirac leptogenesis [247]. Then, an irreducible  $\nu_R$  abundance has profound consequences on the viability of such models, as the generic bounds can only be avoided by lowered reheating temperatures or non-standard cosmological interludes – which is a potentially limiting factor for DM production or leptogenesis.

To complement this analysis, we also provide a maximally conservative limit by the requirement that the Universe was radiation dominated at BBN. We assume a minimal reheating temperature  $T_{\rm reh} = 10\,{\rm MeV}$  and show these irreducible limits that cannot be avoided in Fig. 5.3.

## 5.3 The future of gauge symmetries and Dirac neutrinos

A central issue for models of Dirac neutrinos is how to protect their Dirac nature. A widely adopted and well-motivated approach from a theoretical perspective is to forbid Majorana terms by means of a symmetry. Key advantage of the gauge symmetry variant is that the symmetry and therefore the Dirac nature are expected to remain intact when confronted with quantum gravity – for global symmetries, there is the possibility of them being broken by gravity [248].

Here, we considered a gauged B-L variant that, as long as  $\Delta(B-L) \neq 2$ , is a well-suited candidate for such a gauge symmetry protection. However, other Z' extensions can achieve the same feat, and moreover, UV complete models of Dirac neutrinos may just include any number of gauged U(1) extensions that couple light right-handed neutrinos to other SM fermions. Thus, the setup we study deserves extra scrutiny, since bounds related to the effective number of neutrino species  $\Delta N_{\rm eff}$  are generic and robust even when the complete model contains additional degrees of freedom.

New constraints from the latest ACT DR6 data release put  $\Delta N_{\rm eff} < 0.17$  (95% C.L.) and the implied constraints on the  $m_{Z'}-g'$  parameter space surpass previous cosmological bounds from Planck and BBN by orders of magnitude. Laboratory and collider limits are also surpassed by orders of magnitude across all mass scales, and even forecasts for the FCC are barely competitive with these updated cosmological limits. Notably, for the first time, limits in the previously unexplored regime  $m_{Z'} > 4$  TeV are being placed. We exclude gauge boson masses of up to  $m_{Z'} \sim 100$  TeV for  $g' \sim \mathcal{O}(1)$ .

Forecasts of future CMB surveys show the enormous potential of  $\Delta N_{\rm eff}$  to test Dirac neutrino models. Natural realizations with  $g \sim \mathcal{O}(1)$  are subject to strong constraints for  $m_{Z'} \lesssim \Lambda_{\rm GUT}$  and below, provided the Universe reached temperatures close to the gauge boson mass and no significant entropy injection occurred between  $\nu_R$ -genesis and the formation of the CMB. Our analysis shows that even if  $T_{\rm reh} < m_{Z'}$ , all but the highest mass scales are still subject to similarly constraining limits on natural realizations. Moreover, scenarios with non-standard interludes of the thermal history, or an outright low reheating temperature may face difficulties when trying to account also for DM abundances or Dirac leptogenesis. A picture emerges in which the possibility of gauge protected Dirac neutrinos will be put under strong pressure by future CMB observations if no excess in  $\Delta N_{\rm eff}$  is detected. Should such a non-detection prevail, while being put under pressure, the Dirac hypothesis may still be viable.

As shown in our analysis, we need to think about these limits in tandem with the underlying cosmological assumptions. Thus, a non-observation may be an indication of a non-standard thermal history. In light of growing cosmological tensions, this may be an attractive option to address cosmological tensions within a consistent model of Dirac neutrinos. For example, it is known that extra radiation can at least alleviate the Hubble tension to some degree [249]. Alternatively, solving a cosmological tension may just introduce the change of thermal history needed so that Dirac neutrinos with a gauge symmetry can evade detection.

If the existence of a Z' and a light right-handed neutrino were to be established in the laboratory or it seems plausible from theoretical considerations, we would find ourselves equipped with a powerful probe of pre-BBN physics – a notoriously difficult to probe era of the early Universe. We should also stress that, while particularly attractive, a gauge symmetry is not the only way to protect the Dirac nature of neutrinos. Indeed, a mere global symmetry will achieve the same. As we do not have a theory of quantum gravity yet, the breaking of global symmetries, while plausible and well-motivated, is only conjectured, and we do not have a theory of quantum gravity to precisely quantify the effect of breaking. Indeed, we will address the possibility of global symmetry protected Dirac neutrinos in the next Chapter. In either case, future surveys will give valuable limits that either provide us with a possible clue to the

nature of neutrinos or may even be the herald of a new cosmological paradigm if such a model can be established in the laboratory.

## Chapter 6

# The Dirac Type-I seesaw family

Global symmetries are an attractive feature of Dirac neutrino models. They can forbid the generation of a Majorana mass term, and in extended models, they can also guarantee DM stability and more. Global symmetries appear in a variety of shapes, including continuous and discrete symmetries, exactly or approximately realized and sometimes spontaneously broken. Recent publications involving Dirac neutrinos and a related global symmetries are numerous and cannot be completely summarized here. Instead, we refer to Refs. [106–112] for some selected recent examples.

The case of a spontaneously broken continuous symmetries is particularly interesting. The associated Nambu-Goldstone boson is physical, and for exact symmetries exists as a massless degree of freedom. As a light degree of freedom, it can give corrections to  $\Delta N_{\rm eff}$  and due to the charge assignment, lepton flavor violation (LFV) in SM particle decays is predicted and offers additional probes of Dirac neutrino models.

It is well-motivated that gravity breaks all symmetries unless they are gauged [248]. Thus, if a global symmetry protecting the Dirac nature of neutrinos is explicitly broken by gravitational effects, the exact Dirac nature may be spoiled and neutrinos end up being Majorana particles. The only guarantee to avoid this problem is promotion to a gauge symmetry if possible. As we showed in Chapter 5, Dirac neutrinos with new gauge interactions face strong and generic constraints from  $\Delta N_{\rm eff}$  that can only be avoided in a non-standard thermal history. It is natural to ask if a minimal global symmetry option can avoid bounds, despite possible complications from quantum gravity.

In the following, we first introduce the Type-I Dirac seesaw family as a generalization of similar results for the Majorana Type-I seesaw [159]. This is a general result for model building with applicability beyond the minimal models we study in the following. We discuss two realizations that have minimal particle content, generate a small Dirac mass, and protect the Dirac nature with a global symmetry. We proceed to study the phenomenology and cosmology of these models in great detail and draw general conclusions on the viability of this approach to Dirac masses and conjecture on consequences for models beyond the Type-I family. We also discuss our findings in light of the role of gravity in symmetry violation and how minimal models with global symmetries avoid strong constraints compared to their gauged counterparts.

## 6.1 The Type-I Dirac seesaw family

We will study in more detail two models belonging to what we refer to as the Dirac Type-I seesaw family. This classification is an adaption of the Majorana Type-I seesaw family [159], which understands a wide class of Majorana mass models as specific realizations of a generalized framework and that we already introduced in Sec. 2.3.2. Here, we develop a suitable analogue for the Dirac case, and we make manifest the similarities and differences of the two seesaw families.

For a model to belong to the Dirac Type-I seesaw family, we require the neutral fermion mass matrix to be of the form

$$\mathcal{L} \supset \begin{pmatrix} \bar{\nu}_L & \bar{N}_L \end{pmatrix} \begin{pmatrix} 0 & M_1 \\ M_2 & M_N \end{pmatrix} \begin{pmatrix} \nu_R \\ N_R \end{pmatrix} + \text{h.c.} \equiv \begin{pmatrix} \bar{\nu}_L & \bar{N}_L \end{pmatrix} \mathcal{M} \begin{pmatrix} \nu_R \\ N_R \end{pmatrix} + \text{h.c.}, \qquad (6.1)$$

where  $\nu_L$  is the active neutrino flavors included in the SM, and  $\nu_R$  and  $N_{L,R}$  are new BSM fermions and SM singlets. We tentatively separate  $\nu_R$  from  $N_{L,R}$ , as the  $\nu_R$  coming in  $n_{\nu_R} \leq 3$  generations are the light Dirac partners of  $\nu_L$  and we consider  $n_N$  additional generations of  $N_{L,R}$ . We do not consider further the case of  $n_{\nu_R} > 3$ , but note that it would still make for a perfectly consistent theory – the additional  $\nu_R$  remain unpaired to the active neutrino flavors, and consequently can remain massless after neutrino mass generation, with possible phenomenological consequences.

Moreover, we impose two seesaw conditions  $(M_1 M_N^{-1})_{ij} \ll 1$  and  $(M_2 M_N^{-1})_{ij} \ll 1 \ \forall i, j$  for a model to belong to the Dirac Type-I seesaw family. We refer to  $\epsilon_1 = \mathcal{O}(M_1 M_N^{-1})$  and  $\epsilon_2 = \mathcal{O}(M_2 M_N^{-1})$  as seesaw expansion parameters, which turn out to be the correct small parameters for a perturbative mass matrix diagonalization. We also assume that Majorana mass terms are prohibited by symmetry, such that the light neutrinos are truly Dirac in nature.

The conditions define a generic setup, with virtually infinitely many BSM completions to realize such a Dirac Type-I seesaw. In the following, we study the generated neutrino mass matrix in more detail, and illustrate how it generically leads to small Dirac masses  $M_{\nu} \ll \Lambda_{\rm EW}$ . We define two unitary matrices  $U_L$  and  $U_R$  acting on the left-handed and right-handed fermions by the transformation

$$U_L^{\dagger} \mathcal{M} U_R = \widehat{\mathcal{M}} = \operatorname{diag} (m_1, m_2, \dots, m_{3+n_N}) .$$
(6.2)

Here and in the following, we use the hat symbol to denote quantities in the mass basis, and note that  $m_1, m_2, m_3 \ll \Lambda_{EW} \ll m_4...m_{3+n_N}$  necessarily follows from the seesaw conditions. The two matrices  $U_{L,R}$  are of shape  $(3+n_N)\times(3+n_N)$  and  $(n_{\nu_R}+n_N)\times(n_{\nu_R}+n_N)$ , respectively. We parametrize them as

$$U_{L,R} = \begin{pmatrix} \sqrt{1_{3,n} - P_{L,R}(P_{L,R})^{\dagger}} & P_{L,R} \\ -P_{L,R}^{\dagger} & \sqrt{1_n - (P_{L,R})^{\dagger} P_{L,R}} \end{pmatrix} \begin{pmatrix} (U_{\ell})_{L,R} & 0 \\ 0 & (U_h)_{L,R} \end{pmatrix}, \tag{6.3}$$

and separate the block diagonalization into the light/heavy sectors from subsequent diagonalization of the respective sector. The block rotation matrices of the left light and heavy blocks are of dimension  $3 \times 3$  for  $(U_\ell)_L$ , and  $n_N \times n_N$  for  $(U_h)_L$ . Similarly, for the right-handed fields we have  $(U_\ell)_R$  and  $(U_h)_R$  of dimensions  $n_{\nu_R} \times n_{\nu_R}$  and  $n_N \times n_N$ , respectively. The auxiliary matrices  $P_{L,R}$  have dimension  $3 \times n_N$  and  $n_{\nu_R} \times n_N$ . Since in the seesaw expansion we first block diagonalize into light/heavy sectors,  $(U_\ell)_L$  can be identified with the usual lepton mixing matrix inferred from neutrino oscillations at first order in the seesaw expansion.

The block-diagonalization is analogous to the Majorana case that we discussed in detail in Sec. 2.3.2. We define the auxiliary matrices  $P_{L,R}$  in terms of a power series in the seesaw expansion parameters,

$$P_{L,R} = \sum_{n} P_{L,R}^{(n)}, \qquad P_{L,R}^{(n_1+n_2)} = \mathcal{O}(\epsilon_1^{n_1} \epsilon_2^{n_2}) \equiv \mathcal{O}(\epsilon_{1,2}^{n_1+n_2}). \tag{6.4}$$

Then,  $\sqrt{1 - P_{L,R}(P_{L,R})^{\dagger}} = 1 + \mathcal{O}(\epsilon_{1,2}^2)$  at leading order in the seesaw expansion. When applied to a general mass matrix of the Dirac Type-I seesaw family from Eq. (6.1), we find at leading order

$$\widehat{\mathcal{M}}_{\text{block}} \stackrel{!}{=} \begin{pmatrix} 1 & -P_L \\ P_L^{\dagger} & 1 \end{pmatrix} \begin{pmatrix} 0 & M_1 \\ M_2 & M_N \end{pmatrix} \begin{pmatrix} 1 & P_R \\ -P_R^{\dagger} & 1 \end{pmatrix} + \mathcal{O}(\epsilon_{1,2}^2)$$

$$= \begin{pmatrix} -M_1 P_R^{\dagger} - P_L M_2 & M_1 - P_L M_N \\ M_2 - M_N P_R^{\dagger} & M_N \end{pmatrix} + \mathcal{O}(\epsilon_{1,2}^2).$$

$$(6.5)$$

Requiring the off-diagonal blocks to vanish leads to

$$P_L = M_1 M_N^{-1}, P_R^{\dagger} = M_N^{-1} M_2. (6.6)$$

We find for the not yet diagonalized mass matrix of the light neutrinos

$$M_{\nu} = -M_1 \, M_N^{-1} \, M_2 \,, \tag{6.7}$$

whereas the heavy fermion mass matrix is given by  $M_N$  to leading order in the seesaw expansion. We note that it is convenient to express the model parameter  $M_1$  in terms of the physical parameters  $M_N$ ,  $U_\ell$ , and the neutrino masses  $\widehat{M}_{\nu}$ , as well as the model parameters  $M_2$  and  $U_{\ell R}$ ,

$$M_1 = -U_\ell^{\dagger} \, \widehat{M}_{\nu} \, U_{\ell R} \, M_2^{-1} \, M_N \,. \tag{6.8}$$

We can make the analogy to the Majorana seesaw family from Ref. [159] and Sec. 2.3.2 manifest, by noting that it corresponds to the replacement  $\nu_R = \nu_L^c$ ,  $N_R = N_L^c$ , and, therefore,  $M_2 = M_1^T$ .

UV-complete realizations of the Dirac Type-I seesaw family differ by means of how the three mass matrices constituting  $\mathcal{M}_{\nu}$  are generated. In particular, Eq. (6.7) holds regardless of the details of  $M_1$ ,  $M_N$  and  $M_2$ . The  $N_{R,L}$  can belong to multiplets of different charges in any UV-complete realization and the details are not important for a model to belong to this family. Such models have been realized before, e.g. in Refs. [82, 250–253]. They all constitute a realization the Dirac Type-I seesaw family.

At last, we discuss the new physics scales that enter the seesaw relation. To this end, we first note that

$$M_{\nu} = -\epsilon_1 M_2 \,, \tag{6.9}$$

and  $\epsilon_1$  simply is a measure of mixing between light SM neutrinos and the heavy BSM fermions. Since the new fermions are SM singlets and in absence of other new interactions, any new physics effect arises from this mixing, and hence is similarly suppressed as the active neutrino masses. However, it is important also to observe that

$$\epsilon_1 \sim \frac{\mathcal{M}_{\nu}}{M_2} \,, \tag{6.10}$$

i.e. the mixing explicitly depends on  $M_2$ . It is evident how small mixing in the seesaw expansion arises from our naive expectations of a high-scale  $M_2$ . However, it would be perfectly consistent with all our previously stated requirements to impose also

$$M_2 \ll M_1 \ll M_N \,. \tag{6.11}$$

Then, a small  $\mathcal{M}_{\nu}$  is still realized, but the mixing parameter can be sizable. We refer to the first case with suppressed mixing as high-scale Dirac Type-I seesaw, and the second case with large mixing as low-scale variant. Out of the large class of UV-completions, we study two minimal representatives of the Dirac Type-I seesaw in more detail, and in particular their flavor phenomenology and cosmological probes in case of a global symmetry protecting the Dirac nature. We highlight the complementarity of the two probes, and also conceptual and phenomenological differences that arise when compared to the gauged variants. Due to the minimal nature of the models, the general expectation is that phenomenology is suppressed by the mixing parameter.

### 6.2 Minimal realizations

In the following, we study two minimal realizations of the Dirac Type-I seesaw family, which we will refer to as the *canonical* and the *enhanced* model. At the heart of both realizations is a global and chiral symmetry  $U(1)_D$ , where first and foremost the charge assignment constitutes the main difference between the models and is chosen such that all Majorana mass terms are forbidden and hence the Dirac nature of neutrinos is protected [254]. By chiral, we mean that charges between left-handed and right-handed fermions can differ, and in particular, we can arrange for the bilinear  $\bar{\nu}_L \nu_R + \text{h.c.}$  to be forbidden at tree-level, hence giving rise to neutrino masses only from higher-order operators [253].

We introduce a new complex scalar field  $\sigma$  which will spontaneously break  $U(1)_D \to \mathbb{Z}_3$ , and the associated exact Nambu-Goldstone boson is referred to as the Diracon. In the canonical model, we introduce three singlets  $\nu_R$  carrying  $U(1)_D$  charges (-4, -4, 5), and two generations of  $N_{L,R}$  with charges -1, which is required to generate the correct pattern of neutrino masses to be consistent with oscillation experiments. We note here that introducing the third  $\nu_R$  with charge 5 is not necessary for this. In fact, it completely decouples and remains massless

		Canonical	Enhanced
Fields	$SU(2)_L \otimes U(1)_Y$	$U(1)_D$	$U(1)_D$
H	$(2,rac{1}{2})$	0	0
$\sigma$	(1,0)	3	3
L	$(2,- frac{1}{2})$	-1	-1
$\nu_R$	(1,0)	(-4, -4, 5)	2
$N_L$	(1,0)	-1	2
$N_R$	(1,0)	-1	-1

TABLE 6.1: Fields and charge assignments for the two minimal Dirac Type-I seesaw models studied here. The  $U_D(1)$  charge of  $N_R$  is fixed by the  $M_1$  term in Eq. (6.1), while that of  $\sigma$  is model-dependent and sequentially fixes the charges of  $N_L$  and  $\nu_R$ . Here we choose the simplest case with a charge of 3.

due to the charge assignment. However, we chose to include it here explicitly and make the aforementioned charge assignment motivated by the results of Chapter 5. Such an assignment makes the  $U_D(1)$  anomaly-free. Hence, it would be possible to promote it to a gauge symmetry, the phenomenological consequences of which we studied in Chapter 5, and the two cases can be compared more directly.

The enhanced model comes with an identical scalar sector, and we introduce three generations of  $\nu_R$  and  $N_{L,R}$  each, carrying  $U_D(1)$  charges 2 in case of  $\nu_R$  and 2, -1 for  $N_{L,R}$ . Again, a different choice of charges would be possible, but we motivate this assignment by an appeal to anomaly-cancellation, so that a direct comparison to the gauged version of the model is possible. We summarize the models in Tab. 6.1.

We note here that this charge assignment can be identified with B-L. Indeed, since L and H carry charges -1 and 0 respectively, and the quark sector remains unaffected from this model, we could indeed make the identification, as was done e.g. in Ref. [66]. However, we stress here that this identification is not strictly necessary, and we will remain agnostic and hence continue to refer to D-charge or D-symmetry.

#### 6.2.1 Scalar sector

We consider the most general scalar potential under the symmetry group  $SU(3)_C \times SU(2)_L \times U(1)_Y \times U(1)_D$  for the complex scalar  $\sigma$ , and the EW doublet H

$$V(H,\sigma) = -\mu^{2}(H^{\dagger}H) - \mu_{\sigma}^{2}(\sigma^{\dagger}\sigma) + \lambda(H^{\dagger}H)(H^{\dagger}H) + \lambda_{\sigma}(\sigma^{\dagger}\sigma)(\sigma^{\dagger}\sigma) + \lambda_{H\sigma}(H^{\dagger}H)(\sigma^{\dagger}\sigma).$$
(6.12)

We define  $\langle H^0 \rangle = v_H/\sqrt{2}$  and  $\langle \sigma \rangle = v_\sigma/\sqrt{2}$  for the VEVs of the neutral component of H and  $\sigma$ , respectively. Then, the scalar sector admits a parametrization

$$H = \begin{pmatrix} G_W^+ \\ \frac{1}{\sqrt{2}} \left( v + S_H + i G_Z \right) \end{pmatrix}, \qquad \sigma = \frac{1}{\sqrt{2}} \left( v_\sigma + S_\sigma + i \mathcal{D} \right). \tag{6.13}$$

Of course, the former is responsible for EWSB, just as the SM EW scalar doublet, while  $\sigma$  breaks the global  $U(1)_D$ . The scalar sector separates into a CP-even and a CP-odd sector. In the former, a mass matrix

$$\mathcal{M}_S^2 = \begin{pmatrix} 2v^2 \lambda & v_\sigma v \lambda_{H\sigma} \\ v_\sigma v \lambda_{H\sigma} & 2v_\sigma^2 \lambda_\sigma \end{pmatrix}, \tag{6.14}$$

gives rise to two massive states  $S_H$  and  $S_\sigma$ . The matrix is straightforwardly diagonalized by

$$U^{\dagger} \mathcal{M}_{S}^{2} U = \begin{pmatrix} m_{h}^{2} & 0\\ 0 & m_{S}^{2} \end{pmatrix}, \quad \text{with} \quad U = \begin{pmatrix} \cos \alpha & \sin \alpha\\ -\sin \alpha & \cos \alpha \end{pmatrix}.$$
 (6.15)

We identify two physical mass eigenstates with masses  $m_h$  and  $m_s$ , and we redefine the parameters of the potential in terms of the physical masses and mixing angle  $\alpha$ . We find

$$2v_H^2 \lambda = \cos^2 \alpha \, m_h^2 + \sin^2 \alpha \, m_S^2 \,, \tag{6.16}$$

$$2v_{\sigma}^2 \lambda_{\sigma} = \sin^2 \alpha \, m_h^2 + \cos^2 \alpha \, m_{\mathcal{S}}^2 \,, \tag{6.17}$$

$$v_{\sigma}v_{H}\lambda_{H\sigma} = \cos\alpha \sin\alpha \left(m_{\mathcal{S}}^{2} - m_{h}^{2}\right), \tag{6.18}$$

and in the limit  $\alpha \ll 1$ , we readily identify  $h \simeq S_H$  as the SM-like Higgs of  $m_h \simeq 125$  GeV, and an additional massive scalar  $\mathcal{S}$  with a mass proportional to  $v_{\sigma}$ . Similarly, the charged and CP-odd states of the doublet H are identified as the would-be Goldstones that give rise to the longitudinal modes of the electroweak SM gauge bosons  $G_W^+$  and  $G_Z$ . The remaining Goldstone from  $\sigma$  is physical and connected to the spontaneous breaking of  $U_D(1)$ . It is commonly referred to as the Diracon  $\mathcal{D}$  [255].

The presence of the massless scalar Diracon constitutes a main difference of global symmetry protection schemes over protection of the Dirac nature due to a gauge symmetry. Indeed, such a massless mode is not only affecting  $\Delta N_{\rm eff}$  if copiously produced in the early Universe, but due to its connection to a symmetry of the extended lepton sector, it has phenomenological implications in the high-energy regime. These include contributions to the Higgs invisible decays, but also rare flavor violating low-energy processes like  $\mu \to e\mathcal{D}$  are possible. Both signatures provide valuable constraints on model parameter space.

#### 6.2.2 Canonical model

The charge assignment of the canonical model (see Tab. 6.1) allows us to write the Lagrangian density

$$\mathcal{L} \supset Y \bar{L} \tilde{H} N_R + Y' \bar{N}_L \sigma \nu_R^{(1,2)} + M_N \bar{N}_L N_R + \text{h.c.}$$
 (6.19)

Here we made explicit that, due to  $U(1)_D$  charges, only two right-handed neutrinos are subject to Yukawa couplings. Consequently, the Yukawa matrices Y' and Y are of dimensions  $2 \times 2$  and  $3 \times 2$ , and the heavy mass matrix  $M_N$  is of shape  $2 \times 2$ . A different charge assignment would allow for  $\nu_R^{(3)}$  to be part of the Yukawa sector. Again, we stress here that this charge assignment is chosen to make the differences to a gauge protected variant manifest. Especially cosmological constraints from  $\Delta N_{\rm eff}$  on this model variant are expected to be weakened, as we have fewer light degrees of freedom coupled to the SM and, therefore, a smaller contribution to

the total expansion rate. This model also constitutes a minimal realization in light of oscillation experiments, as they only require two massive active neutrinos.

Upon symmetry breaking, the above Yukawa sector gives rise to a mass matrix for the neutral fermions

$$\mathcal{M}_n = \begin{pmatrix} 0 & \frac{v}{\sqrt{2}}Y\\ \frac{v_{\sigma}}{\sqrt{2}}Y' & M_N \end{pmatrix}. \tag{6.20}$$

We demand the model to be a realization of the Dirac Type-I seesaw family, and therefore the hierarchy  $Yv, Y'v_{\sigma} \ll M_N$ , required for the perturbative seesaw diagonalization, is imposed. The resulting neutrino mass matrix from Eq. (6.7) reads

$$M_{\nu} = \frac{v \, v_{\sigma}}{2} \, Y \, M_N^{-1} \, Y' \,, \tag{6.21}$$

which is of dimension  $3 \times 2$ , again making explicit that one of the active neutrinos remains massless in this model. The corresponding diagrammatic representation of the seesaw mechanism is shown in Fig. 6.1. We refer to this model variant as the canonical version, since the mass generating diagram clearly resembles the Type-I seesaw for Majorana neutrinos. We note here that neutrino masses are necessarily small as a consequence of the seesaw expansion. Transforming to the mass basis, we find the useful Casas-Ibarra-like relation

$$Y = \frac{2}{v v_{\sigma}} U_{\ell} \widehat{M}_{\nu} U_{\ell R}^{\dagger} (Y')^{-1} M_{N}.$$
 (6.22)

We can choose the charged lepton mass matrix  $M_{\ell}$  and the heavy neutral fermion mass matrix  $M_N$  to be diagonal, real, and positive. The former works completely analogous to the SM, where the charged lepton mass matrix can also be made diagonal. The latter follows from rotating an arbitrary  $M_N$  into diagonal form, and then absorbing the excess rotations in a redefinition of the free Yukawa matrices.

Following our discussion around Eq. (6.10), we identify a low-scale regime of the model by the hierarchy  $v_{\sigma} \ll v$ , which allows for sizable mixing between the active neutrinos and the heavy neutral fermions. We expect phenomenological signatures to be stronger in this limit, due to larger mixing. On the other hand, we approach the high-scale limit for  $v_{\sigma} > v_H$  with a suppressed phenomenology.

#### 6.2.3 Enhanced model

For the enhanced model, we find the Yukawa sector

$$\mathcal{L} \supset Y \bar{L} \tilde{H} N_R + M_2 \bar{N}_L \nu_R + Y' \bar{N}_L \sigma N_R + \text{h.c.}, \qquad (6.23)$$

which, after symmetry breaking, yields

$$\mathcal{M}_n = \begin{pmatrix} 0 & \frac{v}{\sqrt{2}}Y\\ M_2 & \frac{v_{\sigma}}{\sqrt{2}}Y' \end{pmatrix} , \qquad (6.24)$$

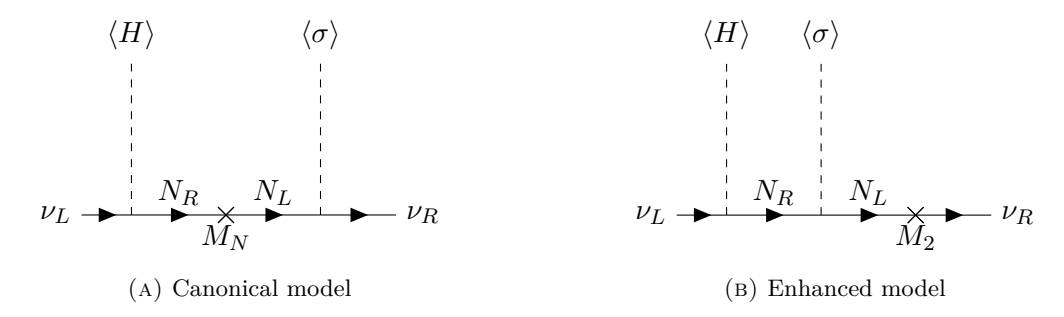


FIGURE 6.1: Feynman diagrams for neutrino mass generation for the canonical and the enhanced model. Both models belong to the Dirac Type-I seesaw family and have formally the same particle content, but differ in their charge assignments and symmetry breaking patterns.

for the neutral fermion mass matrix. Once more, we impose the seesaw conditions which for the enhanced model read Yv,  $M_2 \ll Y'v_{\sigma}$ . From Eq. (6.7), we find the mass matrix and Casas-Ibarra-like relation

$$M_{\nu} = -\frac{v}{v_{\sigma}} Y (Y')^{-1} M_2 \quad \rightarrow \quad Y = -\frac{v_{\sigma}}{v} U_{\ell} \widehat{M}_{\nu} U_{\ell R}^{\dagger} M_2^{-1} Y'.$$
 (6.25)

A diagrammatic representation is given in Fig. 6.1. The hierarchy required for the seesaw expansion naturally gives rise to suppressed neutrino masses, even if Yukawa couplings Y and Y' are sizable. Following the discussions near Eq. (6.10), we can identify a low- and high-scale variant of the model. Here, the low-scale regime is identified as  $M_2 \ll Yv$ , which gives rise to significant deviations from SM phenomenology at low energy scales. The high-scale regime is given by the opposite limit, and is expected to come with suppressed BSM signatures.

We note here that the seesaw expansion also implies a suppression of the bilinear  $\bar{N}_L \nu_R$  compared to  $\bar{N}_L N_R$ . While mixing to the SM remains largely unaffected, the interactions induced from couplings to  $\sigma$  change the phenomenology and, in particular, physics related to the Diracon. We will find that this structure leads to an enhancement of Diracon related signals compared to the canonical version. Hence, we refer to it as the enhanced model.

# 6.3 Phenomenology of the Dirac Type-I seesaw

In the following, we discuss two promising probes of the Dirac Type-I seesaw family in the laboratory. We focus on Higgs related physics, as well as rare flavor violating decays, most notably the "golden" signatures  $\mu \to e \gamma$  and  $\mu \to e \mathcal{D}$ .

#### 6.3.1 Invisible Higgs decays

Due to their identical scalar sectors, the Diracon contribution to the Higgs invisible decay in both models is given by [256, 257]

$$\Gamma(h \to \mathcal{D}\mathcal{D}) = \frac{m_h^3}{32\pi} \frac{\sin^2 \alpha}{v_\sigma^2} \,, \tag{6.26}$$

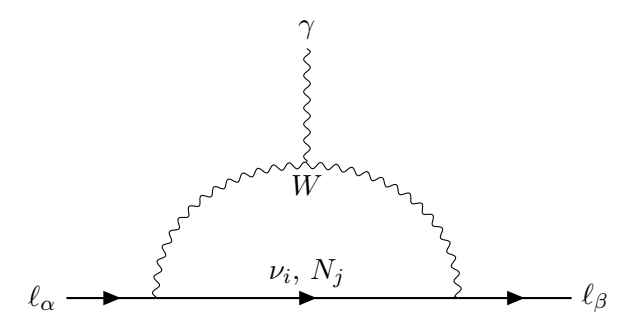


FIGURE 6.2: Feynman diagram relevant for the muon decay  $\mu \to e\gamma$ . The fermion mediators include the light and heavy neutral fermions.

and if kinematically possible, also a decay into the radial mode  $\mathcal{S}$ 

$$\Gamma(h \to \mathcal{SS}) \simeq \frac{\left(m_h^2 + 2m_{\mathcal{S}}^2\right)^2}{32\pi m_h} \frac{\sin^2 \alpha}{v_\sigma^2} \sqrt{1 - 4\frac{m_{\mathcal{S}}^2}{m_h^2}}.$$
 (6.27)

The decay into the radial modes must not necessarily contribute to the Higgs invisible decay width. However, as is evident from our investigation of the Yukawa sectors of both models, the radial scalar has only tree-level couplings to neutrinos and the Diracon. Hence, its decays are – to good approximation – invisible.

Thus, we find the limit

$$\Gamma(h \to \mathcal{D}\mathcal{D}) + \Gamma(h \to \mathcal{S}\mathcal{S}) < \Gamma^{\text{inv}},$$
(6.28)

where  $\Gamma^{\rm inv}$  is the 95% C.L. limit on the invisible Higgs decay and we use  $\Gamma^{\rm inv} < 0.39\,{\rm MeV}$  [144]. We note here that this scalar sector is not restricted to our Dirac Type-I seesaw family, but rather provides a universal limit on a large class of models with a broken global Abelian symmetry.

#### 6.3.2 Lepton flavor violation

Many BSM models introduce new sources of LFV. We consider the processes  $\ell_{\alpha} \to \ell_{\beta} \gamma$  and  $\ell_{\alpha} \to \ell_{\beta} \mathcal{D}$ . More concretely, we are interested in direct searches in muon decays. These processes receive a 1-loop correction from the BSM neutral fermions that is possibly larger than the SM contribution.

We illustrate the diagram in Fig. 6.2. We will not perform the full loop calculation here, as it is a well-known standard result that has been computed in full generality for many possible loop constituents [258]. Here we start from the result of Ref. [259], which provides a simplified but exact expression for the case of general neutral fermions in the loop.

We rewrite the result of Ref. [259] as

$$\Gamma(l_{\alpha} \to l_{\beta} \gamma) = \frac{\alpha_W^3 \sin^2 \theta_W}{64\pi^2} \frac{m_{l_{\alpha}}^5}{m_W^4} \times \left( \left| \sum_{i} U_{i\alpha} U_{i\beta}^{\star} \left[ F_1^{(i)} + F_2^{(i)} \right] \right|^2 + \frac{m_{l_{\beta}}}{m_{l_{\alpha}}} \left| \sum_{i} U_{i\alpha} U_{i\beta}^{\star} \left[ F_1^{(i)} - F_1^{(i)} \right] \right|^2 \right) , \tag{6.29}$$

where the sum runs over light and heavy neutral fermions in the loop. In the limit  $m_{\alpha,\beta} \ll m_W$ , Ref. [259] finds that  $F_2^{(i)}$  becomes negligible over  $F_1^{(i)}$  and for light neutrinos  $m_i \ll m_W$  holds and we find  $F_1^{(i)} \to -7/24$ . In the limit  $m_i \gg m_W$ , which applies for the heavy neutral fermions due to the seesaw limit, we have  $F_1^{(i)} \to 1/24$ . Hence, we may separate the sum over i into a heavy and a light block and find

$$\sum_{i} U_{i\alpha} U_{i\beta}^{\star} \left[ F_{1}^{(i)} + F_{2}^{(i)} \right] = \frac{7}{24} \sum_{i \sim \text{light}} U_{i\alpha} U_{i\beta}^{\star} + \frac{1}{24} \sum_{i \sim \text{heavy}} U_{i\alpha} U_{i\beta}^{\star}$$

$$= \frac{7}{24} \sum_{i \sim \text{all}} U_{i\alpha} U_{i\beta}^{\star} - \frac{6}{24} \sum_{i \sim \text{heavy}} U_{i\alpha} U_{i\beta}^{\star}, \tag{6.30}$$

where to arrive in the second line we have added  $0 = (7/24 - 7/24) \sum_{i \sim \text{heavy}} U_{i\alpha} U_{i\beta}^{\star}$ . We note that from unitarity of the lepton mixing matrix, we have  $\sum_{i \sim \text{all}} U_{i\alpha} U_{i\beta}^{\star} = \delta_{\alpha\beta}$ , and the first term does not contribute to LFV. Courtesy of Eq. (6.6), we can write to leading order  $\sum_{i \sim \text{heavy}} U_{\alpha i} U_{i\beta}^{\dagger} = P_L P_L^{\dagger} = M_1 M_N^{-1} (M_N^{-1})^{\dagger} M_1^{\dagger}$ . Putting all together, we obtain the master formula for the branching ratio of the leptonic decays

$$BR(\ell_{\alpha} \to \ell_{\beta} \gamma) = \frac{\alpha_W^3 s_W^2}{1024\pi^2} \left(\frac{m_{\ell_{\alpha}}}{m_W}\right)^4 \frac{m_{\ell_{\alpha}}}{\Gamma_{\ell_{\alpha}}} \left| \left(M_1 M_N^{-1} (M_N^{-1})^{\dagger} M_1^{\dagger}\right)_{\alpha\beta} \right|^2.$$
 (6.31)

The dependence on specific realizations is given by the respective model realizations of  $M_1$  and  $M_N$ . We focus on the so-called "golden" flavor signal  $\mu \to e\gamma$ , which is tightly constrained by the MEG collaboration. They report the current limit [260]

BR 
$$(\mu \to e \gamma)_{\text{current}} \lesssim 1.5 \cdot 10^{-13}$$
, (6.32)

at 90% C.L. with a projected improvement to reach [261]

BR 
$$(\mu \to e \gamma)_{\text{future}} \lesssim 6 \cdot 10^{-14}$$
. (6.33)

Interactions of the Diracon with the SM are, apart from its direct coupling to the Higgs, not present at tree-level. However, mixing of the neutral fermions with SM fermions gives rise to new gauge interactions of the Diracon at loop-level. The most important contributions come from W and Z bosons. We illustrate two diagrams in Fig. 6.3. In Ref. [262], the general 1-loop coupling of Majorons to charged leptons is calculated. The results are readily adapted also to the case of a Diracon. The interactions are model dependent for any specific realizations, as they depend on interactions of the Diracon with new fields that mix with SM leptons. More details on the derivation are presented in Appendix B.

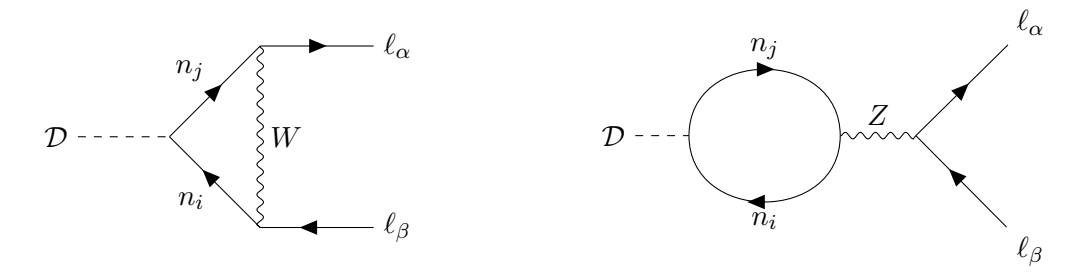


FIGURE 6.3: Diagrams contributing to the interactions of the Diracon and charged leptons.

The effective interaction between the Diracon and charged leptons can be written as

$$\mathcal{L}_{\ell\ell\mathcal{D}} = \mathcal{D}\,\bar{\ell}\left(S_L P_L + S_R P_R\right)\ell + \text{h.c.} = \mathcal{D}\,\bar{\ell}\left(S P_L + S^{\dagger} P_R\right)\ell\,,\tag{6.34}$$

where  $S = S_L + S_R^{\dagger}$  varies between model realizations and is given in Appendix B.

We consider flavor violating as well as flavor conserving couplings, as both can be tightly constrained [263]. Flavor conserving couplings are predominantly constrained by energy loss in astrophysical systems. Pulsating white dwarfs on the Diracon-electron coupling [264–266] constrain the Diracon-electron coupling to approximately  $|S_{ee}| < 3.1 \times 10^{-13}$ . Slightly stronger still are more recent bounds from the tip of the red giant branch at  $|S_{ee}| < 1.6 \times 10^{-13}$  [267], and  $|S_{ee}| < 1.48 \times 10^{-13}$  [268] The Diracon-muon coupling is constrained by additional energy loss in supernovae [264, 269–271]. For our analysis, we adopt the numerical values

$$|\operatorname{Im}(S_{ee}^{\operatorname{exp}})| < 1.5 \times 10^{-13},$$
 (6.35)

$$\left| \text{Im} \left( S_{\mu\mu}^{\text{exp}} \right) \right| < 3.1 \times 10^{-9} \,, \tag{6.36}$$

and we explicitly write the imaginary part to emphasize that we probe the pseudo-scalar part of the interaction. The scalar part vanishes, since the Diracon is a true pseudoscalar. The off-diagonal couplings cause LFV with an invisible final state. In particular, Eq. (6.34) shows that there is a Diracon analogue to the LFV muon decay, i.e.  $\mu^+ \to e^+ \mathcal{D}$ . The decay width can readily be written as

$$\Gamma(\ell_{\alpha} \to \ell_{\beta} \mathcal{D}) = \frac{m_{\ell_{\alpha}}}{32 \pi} \left| \widetilde{S}^{\alpha \beta} \right|^{2}, \qquad (6.37)$$

where we defined the shorthand

$$\left| \widetilde{S}^{\alpha\beta} \right| = \left( \left| S_L^{\alpha\beta} \right|^2 + \left| S_R^{\alpha\beta} \right|^2 \right)^{1/2} . \tag{6.38}$$

We use the limits put forward by TRIUMF [272]. Translation into couplings of the Diracon requires a proper addressing of the chiral structures of the interaction. We use the estimated bounds from Ref. [273]

$$BR(\mu \to e \mathcal{D}) \lesssim 10^{-5}. \tag{6.39}$$

Future experiments will tighten this bound. In particular, we compare results to the projected bounds from Mu3e [274, 275] and COMET [276, 277]. We use the values

$$BR(\mu \to e \mathcal{D})_{Mu3e} \lesssim 6 \cdot 10^{-7},$$
 (6.40)

BR 
$$(\mu \to e \mathcal{D})_{\text{COMET}} \lesssim 4.6 \cdot 10^{-9}$$
. (6.41)

LFV in other leptonic decay modes is not studied here, but may offer additional insights. For example,  $\tau$  decays would be a perfect candidate, although it is experimentally challenging. When going beyond 2-body decays, a wide array of decay processes becomes accessible and have been studied to some extent. To name only a few, the models also give rise to  $\mu \to e\mathcal{D}\gamma$  [262, 273, 278],  $\mu \to eee\mathcal{D}$  [279] and  $\mu \to e\mathcal{D}\mathcal{D}$ . While these are promising targets for future surveys, we usually expect either additional suppression of the already small branching ratios, or a phase space suppression of these 3-body decays. Hence, they are not expected to be the dominant signal for us, but could offer additional hints in the event of a possible signal.

### 6.4 Cosmology of the Dirac Type-I seesaw

The two models we consider make profound changes to the thermal history of the Universe. Courtesy of the two (three) light right-handed neutrinos, as well as the exact massless Nambu-Goldstone boson, these new light degrees of freedom cause observable changes in  $\Delta N_{\rm eff}$ . Each model comes with significant complexity, as we introduce many new degrees of freedom, all with interactions between each other and the SM spectrum. We are explicitly confronted with the electroweak phase transition and a new phase transition associated with the breaking of  $U(1)_D$ . In the following, we introduce some well-motivated simplifications to reduce this complexity.

#### 6.4.1 General setup

As we did in Chapter 5 for the case of  $\nu_R$  coupled to a Z', we treat the right-handed neutrinos and anti-neutrinos as a single common species with the same justification as before. In addition, we make the same ansatz for the new scalar sector. We motivate this as follows. Prior to  $U(1)_D$  breaking, the theory has a complex scalar  $\sigma$  with  $g_{\sigma} = 2$  internal degrees of freedom. After the phase transition, the two degrees of freedom separate into a massive radial mode  $\mathcal{S}$  and the massless Diracon  $\mathcal{D}$ . Now, we are by assumption generically in the regime  $\lambda_{\sigma} \gg \lambda_{H\sigma}$ . After symmetry breaking, the hierarchy of couplings suggests that the radial mode and Diracon are primarily coupled to each other, and interactions with the SM in comparison are negligible. Thus, for  $T \gg m_{\mathcal{S}}$  we have  $g_{\sigma} = 2$  degrees of freedom, and if  $T \ll m_{\mathcal{S}}$  only the Diracon mode can be excited. Upon freeze-out of  $\mathcal{S}$ , we assume negligible energy transfer back to the SM, and the energy remains confined in the scalar sector.

<sup>&</sup>lt;sup>1</sup>Having  $\lambda_{H\sigma} \ll 1$  is fine-tuned in light of RG considerations, but necessary to avoid bounds, e.g. Higgs invisible decay. We consider  $\lambda_{\sigma} \sim \mathcal{O}(1)$  exclusively, again since any small fine-tuned value will not remain stable under the RG. Hence, albeit fine-tuned, we always resort to the implied hierarchy.

We add to the standard thermal history two new effective sectors, denoted here  $\nu_R$  and  $\sigma$ and solve the system

$$\frac{d\rho_{\nu_R}}{dt} = -4H\rho_{\nu_R} + \mathcal{C}_{\text{SM}\to\nu_R}^{(\rho)} + \mathcal{C}_{\sigma\to\nu_R}^{(\rho)}, 
\frac{d\rho_{\sigma}}{dt} = -4H\rho_{\sigma} + \mathcal{C}_{\text{SM}\to\sigma}^{(\rho)} - \mathcal{C}_{\sigma\to\nu_R}^{(\rho)},$$
(6.42)

$$\frac{d\rho_{\sigma}}{dt} = -4H\rho_{\sigma} + \mathcal{C}_{SM\to\sigma}^{(\rho)} - \mathcal{C}_{\sigma\to\nu_R}^{(\rho)}, \qquad (6.43)$$

$$\frac{d\rho_{\rm SM}}{dt} = -3H(\rho_{\rm SM} + P_{\rm SM}) - \mathcal{C}_{\rm SM \to \nu_R}^{(\rho)} - \mathcal{C}_{\rm SM \to \sigma}^{(\rho)}. \tag{6.44}$$

For details on definitions of appearing quantities, we refer to Chapter 4. For each of the two realizations, we take into account all  $1 \leftrightarrow 2$  and  $2 \leftrightarrow 2$  processes that can be constructed from all new scalar and Yukawa terms. We separate into four possible regimes, taking into account all possible phases of the scalar potential, i.e. both scalar sectors can be (un-)broken, or only one sector respectively. In addition, we include processes from mixing of  $\mathcal S$  with the SM-like Higgs h in the phase where both symmetries are broken.

#### 6.4.2Phase transition dynamics

A complete treatment of the double phase transition would require a self-consistent solution of the scalar field dynamics, and it may be feasible in the framework of lattice computations of cosmological phase transitions. However, we will see that we do not need to invoke lattice simulations to capture the important effects of the phase transition here.

A crucial observation is the assumed hierarchy  $\lambda_{H\sigma} \ll \lambda_{\sigma}$ , which makes us conjecture a weak coupling between the EW sector and the  $\sigma$ -sector overall. Corrections to the EW part of the scalar potential only face portal suppressed contributions, and we thus assume a SM-like phase transition – we assume here a crossover at  $T_H^c \simeq 160 \,\mathrm{GeV}$ . The  $\sigma$ -transition is somewhat more involved, as Higgs related thermal corrections can dominate even for small portal couplings if the associated energy scale is small, i.e. the low-scale regimes.

It is important to note that the details of the phase transition have little effect on the expected result. Indeed, the dominant effect of the phase transition is its control on the presence or absence of processes, most importantly decay modes (see also our discussion in Sec. 4.2). Thus, unless the phase transition coincides somewhat with the peak production in, say decays, at  $T \sim m/3$ , the details of the phase transition have little impact on the resulting abundance. We have explicitly varied the onset of the phase transitions and found subdominant effects on final results. This is confirmed by a similar approach to phase transitions in Ref. [222]. We highlight that this also means we are agnostic to the order of the phase transition.

We prescribe the following thermal corrections to the scalar potential [280, 281]

$$-\mu_H^2(T) \simeq -\mu_H^2 + \left(\frac{3}{16}g^2 + \frac{1}{16}g'^2 + \frac{1}{4}y_t^2 + \frac{1}{2}\lambda\right)T^2, \tag{6.45}$$

$$-\mu_{\sigma}^{2}(T, T_{\sigma}) \simeq -\mu_{\sigma}^{2} + \frac{1}{3}\lambda_{\sigma}T_{\sigma}^{2} + \frac{1}{6}\lambda_{H\sigma}T^{2}.$$
 (6.46)

Here, g and g' are the couplings to W and Z bosons,  $y_t$  is the top Yukawa and  $\lambda$  is the Higgs quartic scalar coupling. We define the approximate temperature of the  $\sigma$ -transition  $T_{\sigma}^{c}$  by

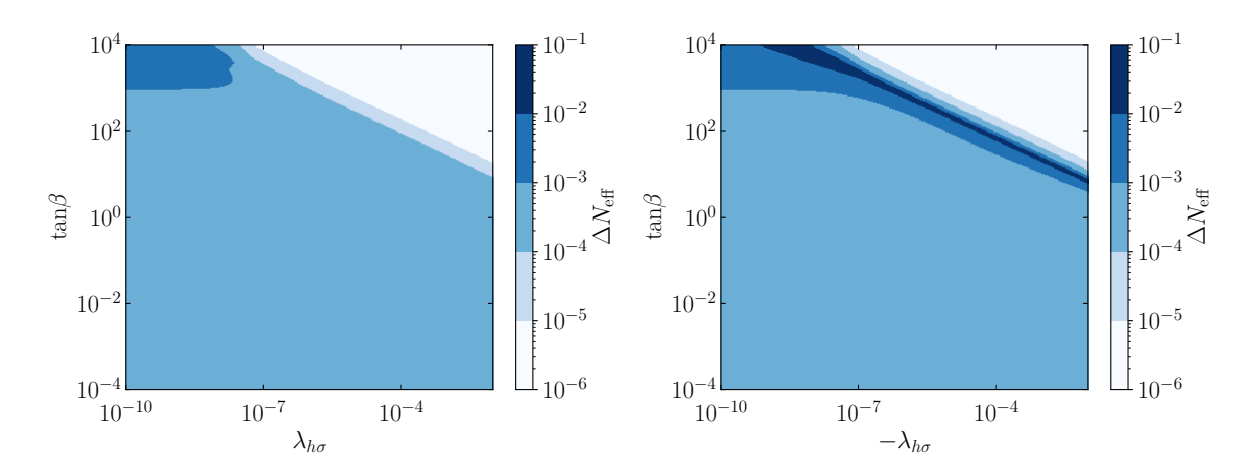


FIGURE 6.4: Energy release in the  $\sigma$ -phase transition, but normalized to a fictitious  $\Delta N_{\rm eff} = \Delta V/\rho_{\rm SM}(T_\sigma^c)$ , where  $T_\sigma^c$  is the critical temperature we define from Eq. (6.46) and  $\Delta V \sim \lambda_\sigma v_\sigma^4$ . This is the maximum possible increase of  $\Delta N_{\rm eff}$  due to the phase transition. Except for a small region in the low-scale model with negative portal coupling, we do not expect a significant correction to  $\Delta N_{\rm eff}$  from the phase transition. The non-negligible contributions arise from a relative sign in thermal corrections that lead to a substantially lowered critical temperature, therefore enhancing the ratio of vacuum energy to SM energy at that time.

equating absolute values of thermal corrections and the vacuum term in Eq. (6.46).

The phase transition releases energy of the order  $\Delta V \sim \lambda_{\sigma} v_{\sigma}^4$  that becomes dynamical. For crossover or similar transitions, we expect this energy to be released as excitations of the field around the new minimum, and in case of a first order transition, some of the energy may be transferred to the bubbles and later gravitational waves. We do not make any specific assumptions here, since we show below that corrections to our numerical results are in either case subdominant. Due to the suppressed portal coupling, we expect the bulk of it to reheat the  $\sigma$ -sector and not SM states. If this happens while the hidden sector is coupled to the SM, or it couples to the SM at some later time, the effect is washed out. If the transition occurs after decoupling of the sectors (or if it remains in the freeze-in limit), the hidden sector is reheated. Consequently, we obtain an extra contribution to  $\Delta N_{\rm eff}$ . Comparing  $\Delta V$  to the energy density of  $\sigma$  and the SM at  $T_{\sigma}^c$  shows that these corrections are subdominant, unless there is partial or full cancellation of thermal corrections in Eq. (6.46). We show in Fig. 6.4 that indeed, we expect small corrections to  $\Delta N_{\rm eff}$  unless for a negligibly small chunk of parameter space, where the partial cancellation leads to a large ratio  $\Delta V/\rho_{\rm SM}(T_{\sigma}^c)$ .

#### 6.4.3 Process details and the degenerate BSM approximation

In this section, we make further steps to simplify the problem before presenting results for the cosmologically relevant interactions. Although the grouping of species already poses a convenient simplification, we still have to include a large number of processes and parameters to scan, e.g. scalar couplings, mass scales, two Yukawa matrices, and a priori unconstrained rotation matrices. Performing a full scan over all of these free parameters is numerically costly. To this end, we employ an approximation we refer to as the degenerate BSM approximation, which is a convenient way to reduce especially the number of parameters in the Yukawa sector.

Without loss of generality, we can always choose a basis in which the charged lepton mass matrix and the heavy neutral fermion mass matrix  $M_N$  are diagonal. Now we make the ansatz of a degenerate heavy mass matrix, i.e.  $M_N = m_N 1_{n \times n}$ , as well as degenerate  $M_2 = m_2 1_{n \times n}$ . For both models, this implies a diagonal and degenerate Yukawa matrix  $Y' = y' 1_{n \times n}$ , and from the Casas-Ibarra-like formulas Eq. (6.22) and (6.25), it follows that Y is diagonal, albeit not degenerate because the eigenvalues of  $\mathcal{M}_{\nu}$  are not degenerate. From now on, we refer to the degenerate value of the matrices by the corresponding lower case letters.

#### Scalar sector

The scalar sector for both models is identical. Since we assume a tightly coupled secluded sector, the relevant amplitudes involve either the Higgs doublet or the physical Higgs, depending on phase, and the additional scalars. We provide results for a general theory of three scalars  $\phi$ ,  $\varphi$ , and  $\sigma$ . The  $2 \leftrightarrow 2$  and  $1 \leftrightarrow 2$  amplitudes can generally be written as

$$\mathcal{A}(\phi\phi \to \varphi\varphi) = \lambda_{\phi^{2}\varphi^{2}} + \lambda_{\phi^{3}}\lambda_{\phi\varphi^{2}}P(s, m_{\phi}) + \lambda_{\varphi^{3}}\lambda_{\phi^{2}\varphi}P(s, m_{\varphi}) + \lambda_{\phi^{2}\sigma}\lambda_{\sigma\varphi^{2}}P(s, m_{\sigma}) + \lambda_{\phi\varphi^{2}}^{2}\left(P(t, m_{\varphi}) + P(u, m_{\varphi})\right) + \lambda_{\phi^{2}\varphi}^{2}\left(P(t, m_{\phi}) + P(u, m_{\phi})\right) + \lambda_{\phi\sigma\varphi}^{2}\left(P(t, m_{\sigma}) + P(u, m_{\sigma})\right),$$

$$\mathcal{A}(\phi \to \varphi\varphi) = \lambda_{\phi\varphi^{2}}.$$

$$(6.48)$$

Here,  $P(p, m_i)$  denotes the Breit-Wigner propagator,

$$P(p, m_i) = \frac{1}{p^2 - m_i^2 + i \, m_i \, \Gamma_i}, \tag{6.49}$$

since the scalar particles are not stable in general. We denote dimensional coupling constants as  $\kappa$  and dimensionless couplings by  $\lambda$ . They can readily be obtained by expanding the Lagrangian and sorting by terms.

For the completely unbroken phase, the theory is straightforwardly read from the potential in Eq. (6.12). We also need to consider the case where either phase is broken and the other is unbroken. We find the relevant coupling between Higgs sector and BSM scalars to be

$$\kappa_{h\sigma\bar{\sigma}} = v_H \lambda_{H\sigma} \,, \tag{6.50}$$

$$\lambda_{h^2\sigma\bar{\sigma}} = \frac{\lambda_{H\sigma}}{2} \,, \tag{6.51}$$

(6.52)

in the case of EWSB but restored  $U(1)_D$ , and the case of unbroken EW symmetry and broken  $U(1)_D$  reads

$$\kappa_{H\bar{H}S} = v_{\sigma} \lambda_{H\sigma} \,, \tag{6.53}$$

$$\lambda_{H\bar{H}S^2} = \lambda_{H\sigma}/2\,, (6.54)$$

$$\lambda_{H\bar{H}D^2} = \lambda_{H\sigma}/2\,, (6.55)$$

(6.56)

where we omit all vertices coupling BSM degrees of freedom or the SM Higgs only.

In the completely broken phase, we identify  $\phi = h$ ,  $\varphi = \mathcal{D}$ ,  $\mathcal{S}$ , and  $\sigma = \mathcal{S}$ ,  $\mathcal{D}$ . Moreover, we use only the physical degrees of freedom, such that  $h = \cos \alpha S_H + \sin \alpha S_\sigma$  and  $S = \cos \alpha S_H + \sin \alpha S_\sigma$  $-\sin\alpha S_H + \cos\alpha S_\sigma$ , which allows us to collect all relevant terms with correct scalar mixing from the scalar potential. We summarize all resulting vertices at leading order and use the shorthand  $\tan \beta = v/v_{\sigma}$ . Once more, we omit all couplings between  $\mathcal{S}$  and  $\mathcal{D}$  only and find

$$\kappa_{h^2S} = \frac{\sin \alpha \sqrt{G_F}}{2^{3/4}} \left( 2m_h^2 + m_S^2 \right) , \qquad (6.57)$$

$$\kappa_{hS^2} = -\frac{\sin \alpha \sqrt{G_F} \tan \beta}{2^{3/4}} \left( m_h^2 + 2m_S^2 \right) , \qquad (6.58)$$

$$\kappa_{hDD} = -\frac{\sin \alpha \sqrt{G_F m_h^2 \tan \beta}}{2^{3/4}}, \qquad (6.59)$$

$$\lambda_{h^3S} = \frac{\sin \alpha G_F m_h^2}{\sqrt{2}} \,, \tag{6.60}$$

$$\lambda_{h^2S^2} = -\frac{\sin \alpha G_F \tan \beta \left(m_h^2 - m_S^2\right)}{2\sqrt{2}},$$

$$\lambda_{hS^3} = -\frac{\sin \alpha G_F m_S^2 \tan^2 \beta}{\sqrt{2}},$$
(6.61)

$$\lambda_{hS^3} = -\frac{\sin \alpha G_F m_S^2 \tan^2 \beta}{\sqrt{2}}, \qquad (6.62)$$

$$\lambda_{h^2D^2} = -\frac{\sin \alpha G_F \tan \beta \left(m_h^2 - m_S^2\right)}{2\sqrt{2}},$$

$$\lambda_{hSD^2} = -\frac{\sin \alpha G_F m_S^2 \tan^2 \beta}{\sqrt{2}}.$$
(6.63)

$$\lambda_{hSD^2} = -\frac{\sin \alpha G_F m_S^2 \tan^2 \beta}{\sqrt{2}}.$$
 (6.64)

(6.65)

For example, the scattering of two physical Higgs bosons into new scalars is readily found to be

$$\mathcal{A}(hh \to \mathcal{D}\mathcal{D}) = \frac{\sqrt{\sqrt{2}G_F}}{4} m_h^2 \frac{\sin \alpha}{v_\sigma} \times \left[ \left( 2 + \frac{m_S^2}{m_h^2} \right) \frac{m_S^2}{s - m_S^2 + im_S \Gamma_S} - 1 + \frac{m_S^2}{m_h^2} - \frac{m_h^2}{s - m_h^2 + im_h \Gamma_h} \right], \tag{6.66}$$

for annihilation to Diracons and

$$\mathcal{A}(hh \to SS) = -\frac{\sqrt{\sqrt{2}G_F}}{4} m_h^2 \frac{\sin \alpha}{v_\sigma} \left[ \frac{m_h^2 + 2m_S^2}{s - m_h^2 + im_h \Gamma_h} + 1 - \frac{m_S^2}{m_h^2} \right], \tag{6.67}$$

for annihilation into the radial mode. Similarly, we can construct all other relevant amplitudes, including decays, with the effective vertex couplings listed above.

We note here also the partial decay widths of the scalar fields to two scalars

$$\Gamma(\phi \to \varphi \varphi) = \frac{\kappa_{\phi \varphi^2}^2}{8\pi m_{\phi}} \sqrt{1 - \frac{4m_{\varphi}^2}{m_{\phi}^2}}, \qquad (6.68)$$

and to two fermions in the absence of Dirac matrix structures

$$\Gamma(\phi \to \bar{\psi}\psi) = \frac{Y^2 m_\phi}{8\pi} \left(1 - 4\frac{m_\psi^2}{m_\phi^2}\right)^{3/2} .$$
 (6.69)

We use these results to find an approximate total decay width for the BSM fields by using the sum of the dominant decay widths. For the radial mode S, this usually corresponds to  $S \to DD$ , as we assume  $\alpha \ll 1$  throughout and any SM final state faces suppression by mixing.

#### Yukawa sector

For the (partially) unbroken case, Yukawa couplings can directly be read off the Lagrangians in Eqs. (6.19) and (6.23) by expanding terms. In the broken phase, it is convenient to parametrize the interacting part of the Lagrangian in a way that allows us to handle the canonical and the enhanced models simultaneously. We consider the general scalar-fermion-fermion interaction

$$\mathcal{L}_{\text{int}} = \begin{pmatrix} \bar{\nu}_L & \bar{N}_L \end{pmatrix} \cdot \begin{pmatrix} 0 & \frac{1}{\sqrt{2}} Y S_h \\ \frac{1}{\sqrt{2}} Y_2 \left( S_\sigma + i \mathcal{D} \right) & \frac{1}{\sqrt{2}} Y_M \left( S_\sigma + i \mathcal{D} \right) \end{pmatrix} \cdot \begin{pmatrix} \nu_R \\ N_R \end{pmatrix} + \text{h.c.}$$
 (6.70)

Here  $S_h = h \cos \alpha + S \sin \alpha$ ,  $S_\sigma = S \cos \alpha - h \sin \alpha$  holds, since mixing is present in the broken phase. The canonical model can be identified as the case where  $Y_2 = Y'$  and  $Y_M = 0$ , whereas the enhanced model is given by the assignment  $Y_2 = 0$  and  $Y_M = Y'$ .

We are interested in the Yukawa interactions in the mass basis. Therefore, after rotating the fields accordingly, we find in the mass basis

$$\mathcal{L}_{\text{int}} = \begin{pmatrix} \overline{\widehat{\nu}}_L & \overline{\widehat{N}}_L \end{pmatrix} \cdot U_L^{\dagger} \cdot \begin{pmatrix} 0 & \frac{1}{\sqrt{2}} Y S_h \\ \frac{1}{\sqrt{2}} Y_2 \left( S_{\sigma} + i \mathcal{D} \right) & \frac{1}{\sqrt{2}} Y_M \left( S_{\sigma} + i \mathcal{D} \right) \end{pmatrix} \cdot U_R \cdot \begin{pmatrix} \widehat{\nu}_R \\ \widehat{N}_R \end{pmatrix} + \text{h.c.}$$
 (6.71)

From Eq. (6.3) we use  $P_L = M_1 M_N^{-1}$ ,  $P_R^{\dagger} = M_N^{-1} M_2$  and  $U_{hL} = U_{hR} = I$  at leading order. Moreover, we neglect interactions manifestly suppressed by the neutrino mass, and find

$$\mathcal{L}_{\text{int}} \supset \overline{\widehat{\nu}}_L U_{lL}^{\dagger} \left( S_h \frac{Y}{\sqrt{2}} - \frac{S_{\sigma}}{\sqrt{2}} M_1 M_N^{-1} Y_M \right) \widehat{N}_R + \overline{\widehat{N}}_L \frac{S_{\sigma}}{\sqrt{2}} \left( Y_2 - M_2 M_N^{-1} Y_M \right) U_{lR} \widehat{\nu}_R + \text{h.c.}$$

$$(6.72)$$

This Lagrangian describes the Yukawa interactions between heavy and light fermions in the mass basis. We summarize all interaction vertices we find in the Yukawa sector for both, the canonical and the enhanced model, in Tab. 6.2.

Fields	Canonical	Enhanced Diracon
$N_R \nu_L h$	$U_{lL}^{\dagger}Y\cos{\alpha}/\sqrt{2}$	$U_{\ell}^{\dagger} Y(\frac{v}{v_{\sigma}} \sin \alpha + \cos \alpha) / \sqrt{2}$
$N_R \nu_L S$	$U_{lL}^{\dagger}Y\sin{\alpha}/\sqrt{2}$	$U_{\ell}^{\dagger} Y(\sin \alpha - \frac{v}{v_{\sigma}} \cos \alpha) / \sqrt{2}$
$N_R \nu_L \mathcal{D}$	0	$-i \frac{v}{v_{\sigma}} U_{\ell}^{\dagger} Y / \sqrt{2}$
$N_L \nu_R h$	$-Y'U_{lR}\sin\alpha/\sqrt{2}$	$\frac{\mu}{v_{\sigma}}U_{lR}\sin\alpha$
$N_L \nu_R S$	$Y'U_{lR}\cos\alpha/\sqrt{2}$	$-\frac{\mu}{v_{\sigma}}U_{lR}\cos\alpha$
$N_L   u_R  \mathcal{D}$	$iY'U_{lR}/\sqrt{2}$	$-i\frac{\mu}{v_{\sigma}}U_{lR}$

TABLE 6.2: Yukawa couplings in the broken phase after rotation to the mass basis.

We have one additional observation regarding the enhanced model. We can use Eq. (6.25) to find  $\mu/v_{\sigma}U_{lR}$ . This implies

$$\frac{\mu U_{\ell R}}{v_{\sigma}} = \frac{1}{v_H} Y' Y^{-1} U_{\ell} \widehat{M}_{\nu}. \tag{6.73}$$

Here we showed explicitly that this expression is neutrino-mass suppressed. The significance of this is that some interaction vertices in the enhanced model are directly proportional to this quantity, and therefore, these interactions are neutrino mass suppressed, which is not manifest upon first inspection.

#### 6.5 Results

In the following, we discuss the phenomenological and cosmological probes introduced in Sec. 6.3 and 6.4. We investigate both models separately and put particular focus on the complementarity of lepton flavor signals and cosmological bounds.

#### 6.5.1 Model I: Canonical model

We perform general scans of LFV processes without additional approximations, but it is instructive to first discuss some analytic estimates. In particular, we employ the degenerate BSM approximation introduced in Sec. 6.4.3. Within this approximation, the interaction of charged leptons and the Diracon simplifies to

$$\mathcal{L}_{\ell\ell\mathcal{D}} = -\frac{i\,\mathcal{D}}{96\pi^2} \frac{y'^2 v_\sigma}{m_N^2} \bar{\ell} \left[ M_\ell \operatorname{Tr}(YY^\dagger) \,\gamma_5 + 5\,M_\ell \,YY^\dagger \,P_L - 5\,YY^\dagger \,M_\ell \,P_R \right] \ell \,. \tag{6.74}$$

This interaction is neutrino mass suppressed. We can make this manifest by considering the limit  $m_N \to \infty$  or  $y' \to 0$ , both of which yield  $m_\nu \to 0$  and from Eq. (6.74) a branching ratio  $\text{Br}(\mu \to e\mathcal{D}) \to 0$ . Note that this dependence is in the global prefactor of Diracon-lepton interaction, i.e. it is not possible to make the limit  $m_\nu \to 0$  while maintaining a non-vanishing interaction as long as the seesaw relation Eq. (6.22) is enforced. Thus, the interaction is neutrino mass suppressed, which is confirmed in explicit numerical scans.

6.5. Results 75

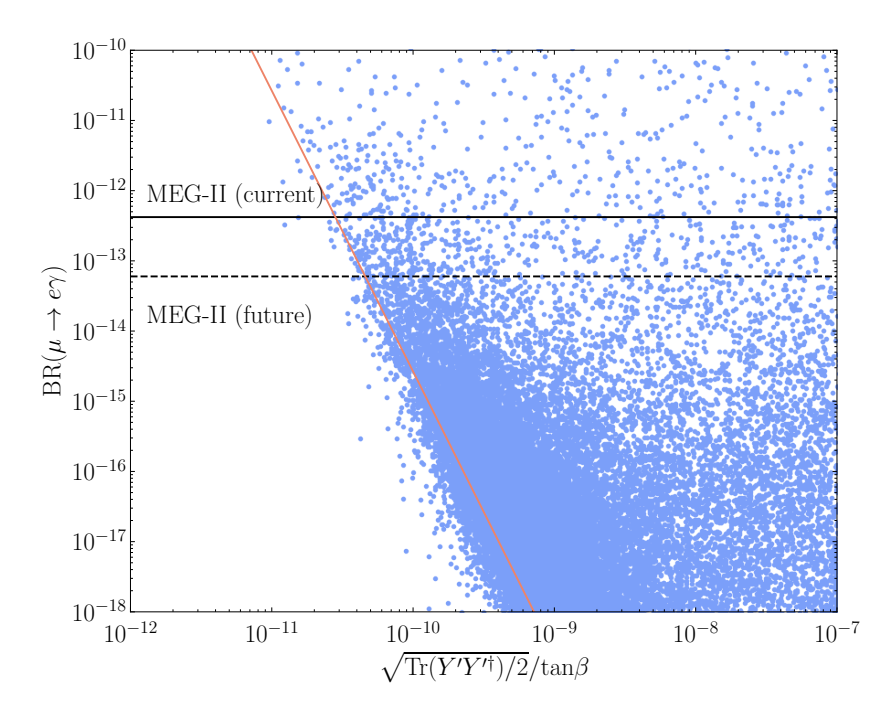


FIGURE 6.5: Parameter scan for the canonical model. We show the branching ratio for  $\mu \to e\gamma$ , and an effective parameter for the Yukawa matrix Y'. This effective parameter is defined such that in the degenerate BSM approximation, it corresponds to  $y'v_{\sigma}/v_{H}$ . Blue dots represent a general scan over the entire parameter range allowed by the seesaw expansion and perturbativity. The orange curve represents the degenerate BSM approximation. Note that it reduces to a simple line, as one of the neutrinos in the canonical model is exactly massless. All data points shown are consistent with oscillation parameters [28]. Only a small fraction of points will be tested by MEG and MEG-II, respectively.

For the decay  $\mu \to e\gamma$ , we use the master formula Eq. (6.31) and employ the degenerate BSM approximation. We find

$$BR(\ell_{\alpha} \to \ell_{\beta} \gamma) = \frac{\alpha_W^3 s_W^2}{1024\pi^2} \left(\frac{m_{\ell_{\alpha}}}{m_W}\right)^4 \frac{m_{\ell_{\alpha}}}{\Gamma_{\ell_{\alpha}}} \frac{\left|\left(M_{\nu} M_{\nu}^{\dagger}\right)_{\alpha\beta}\right|^2}{m_2^4}, \tag{6.75}$$

which we apply to the canonical model variant

$$BR(\mu \to e \gamma) = \frac{\alpha_W^3 s_W^2}{1024 \pi^2} \left(\frac{m_\mu}{m_W}\right)^4 \frac{m_\mu}{\Gamma_\mu} \left(\frac{\sqrt{2}}{v_\sigma y'}\right)^4 \left| \left(U_\ell \widehat{M}_\nu \widehat{M}_\nu^T U_\ell^\dagger\right)_{21} \right|^2. \tag{6.76}$$

Recall our discussion of low- and high-scale variants of the models around Eq. (6.10). The branching ratio for  $\mu \to e \gamma$  receives an enhancement in the limit  $y'v_{\sigma} \ll v$ , which according to our previous classification corresponds to the low-scale variant.

Likewise, we can use Eq. (6.37) and the result from Appendix B to find an analogous degenerate BSM expression for the decay to Diracons. We use this to evaluate the ratio of  $BR(\mu \to e \gamma)$  and  $BR(\mu \to e \mathcal{D})$ 

$$\frac{\mathrm{BR}(\ell_{\alpha} \to \ell_{\beta} \mathcal{D})}{\mathrm{BR}(\ell_{\alpha} \to \ell_{\beta} \gamma)} \approx \left(\frac{5}{12\pi^{3/2} \alpha_w^{3/2} s_w}\right)^2 \left(\frac{M_W^2}{v \, m_{\ell_{\alpha}}}\right)^2 \frac{y'^2}{2} \frac{m_2^2}{v^2} \lesssim 1.02 \cdot 10^{-14} \, y'^2 \,. \tag{6.77}$$

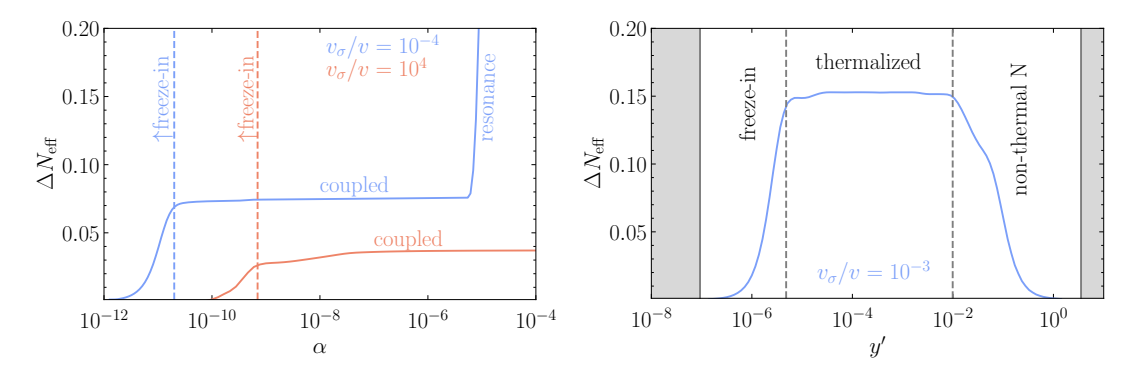


FIGURE 6.6: Left: Contributions to  $\Delta N_{\rm eff}$  from the scalar sector only, and two representative values  $v_{\sigma}/v=10^{-4}$  and  $v_{\sigma}/v=10^4$ . Production of Diracons follows freeze-in production in the limit  $\alpha \to 0$ , as small mixing implies a suppressed portal coupling at fixed  $v_{\sigma}$ . For larger mixing angles, the scalar sector couples to the SM, predominantly through SM Higgs related interactions. Low and high-scale realizations differ in their contribution due to thermalization of the radial mode. In the low-scale regime, resonant production of Diracons is possible with strongly enhanced limits. Right: Contributions of  $\nu_R$  only, coming from the fermionic sector with  $m_N=1\,{\rm TeV}$  and  $v_{\sigma}/v=10^{-3}$ . Grey shaded regions indicate non-perturbative Y and Y' respectively. For small y', the heavy fermions thermalize due to increased Y. Subsequently, light degrees of freedom are populated from freeze-in due to small y'. At larger coupling,  $\nu_R$  and  $\mathcal D$  are coupled to the SM due to their interactions with the also coupled heavy fermions. At even larger values of y', the heavy fermions fall out of equilibrium and production is again suppressed. Published in Ref. [3].

In the last step, we require consistency with the MEG-II limit in Eq. (6.32). Thus potential observation of  $\mu \to e\gamma$  implies unobservable  $\mu \to e\mathcal{D}$ . We could try to improve this ratio and make both processes accessible at the same time. This would require an increase of  $m_2 = y'v_{\sigma}/\sqrt{2}$ , or by the neutrino mass relation Eq. (6.21), a decrease of Y or an increase of  $m_N$ . This is disadvantageous for observation of  $\mu \to e\mathcal{D}$  and, therefore, we cannot make both signals simultaneously observable in this model variant. Hence, we conclude that  $\mu \to e\gamma$  is the only viable LFV signal for this model.

We present the relation between BR( $\mu \to e\gamma$ ) and a proxy quantity  $\sqrt{\text{Tr}(Y'Y'^{\dagger})/2}v_{\sigma}/v_{H}$  in Fig. 6.5. The latter is chosen such that in the degenerate BSM case, it corresponds to the degenerate value y' divided by the new scale  $v_{\sigma}$ . The result confirms that only a small fraction of realizations lead to observable  $\mu \to e\gamma$  and the canonical model mostly evades flavor bounds.

For the cosmological analysis, we fully rely on the degenerate BSM approximation as discussed in Sec. 6.4.3. In addition, we split the analysis into two limiting cases. Case one assumes that all contributions to  $\Delta N_{\rm eff}$  arise from the scalar sector only, i.e.  $\mathcal{D}$  and possibly  $\mathcal{S}$  contribute to  $\Delta N_{\rm eff}$ . The other limiting case is that of negligible scalar contributions, and  $\Delta N_{\rm eff}$  is affected only by processes related to new heavy fermions.

We show two benchmark points in Fig. 6.6. The scalar only limit gives negligible contributions to  $\Delta N_{\rm eff}$ , as both the Diracon and the radial mode are only produced from freeze-in in the regime of small mixing. As mixing increases, we transition to a fully coupled scalar sector. The internal degrees of freedom depend on whether we find ourselves fully in the low- or high-scale regimes and on the mass of the radial mode. We observe moderate increases of  $\Delta N_{\rm eff}$  at most, as increased couplings can merely move the scalar sector to a lowered decoupling temperature with moderate increases in  $\Delta N_{\rm eff}$ . Especially in high-scale variants, contributions flatten out

6.5. Results 77

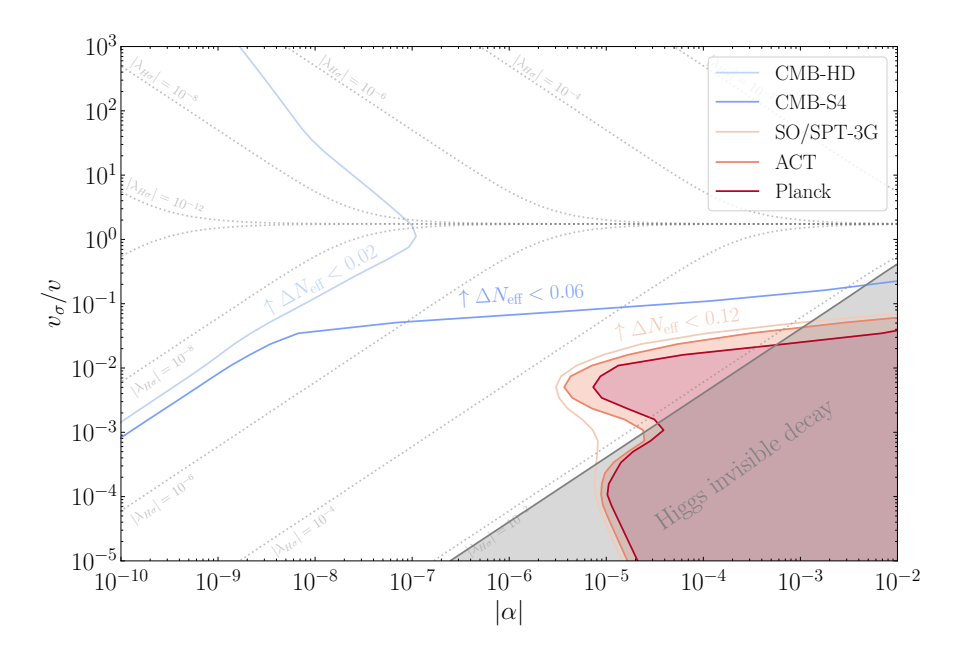


FIGURE 6.7: Limits and forecasts on the scalar sector. We neglect contributions arising from the Yukawa sector. Current constraints are given by Planck and ACT and tend to be weaker than invisible Higgs decays with the exception of a small region in the low-scale regime that is dominated by resonant on-shell radial scalars. CMB-S4 will put constraints on the low-scale realizations of the model, with high-scale variants largely unconstrained. Only when going to a proposal such as CMB-HD, we start putting limits on all mass scales, since this experiment would potentially be sensitive to a single Nambu-Goldstone boson. Note that, to leading order, the sign of  $\alpha$  does not affect constraints here. We fix the scalar self coupling to  $\lambda_{\sigma} = 0.1$ , and show contours of constant  $|\lambda_{H\sigma}|$  for comparison. Published in Ref. [3].

eventually due to feebleness of the interactions, and larger couplings cannot compensate for this. Low-scale variants may stay coupled to the SM until significantly lower temperatures. The regime  $v_{\sigma}/v \sim 10^{-2} - 10^{-3}$  with a light radial mode is particularly interesting, as a resonant enhancement from on-shell radial modes is possible.

This general behavior is reflected in the constraints we put on the  $\alpha - v_{\sigma}/v_{H}$ -plane, as we show in Fig. 6.7. For large modulus of the mixing angle, we can put constraints on low-scale variants of the model. In general, these are not significantly stronger or even weaker than existing constraints from invisible Higgs decay.

The situation is different for future experiments like CMB-S4. For the anticipated reach of  $\Delta N_{\rm eff} = 0.06$ , a fully thermalized Diracon and a thermalized light radial mode below the EW scale are testable. We observe an asymptotic limit for small mixing, which directly follows from the relation between mixing and portal coupling. Indeed, the decoupling process is determined by the portal coupling. For the benchmark limit  $\Delta N_{\rm eff} = 0.02$  that is the goal of CMB-HD, a single scalar degree of freedom, even if not fully thermalized above the EW scale, is detectable.

We now consider constraints coming from the Yukawa sector only. Here, we can produce both the two light  $\nu_R$  fields as well as the new scalar particles through their interactions with the heavy fermions. The neutrino mass relation effectively fixes  $YY' \propto v/v_{\sigma}$ . This induces an effective seesaw relation between the Yukawa matrices Y and Y' that gives a characteristic shape to our exclusion contours. Contributions to  $\Delta N_{\rm eff}$  fall into three distinct regimes. At

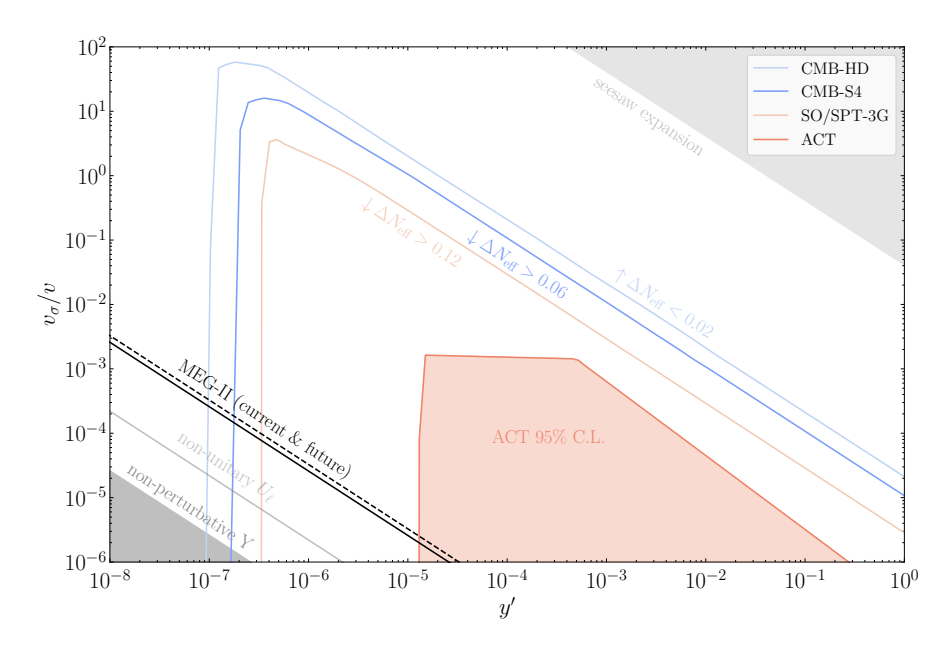


FIGURE 6.8: Canonical model constraints under the assumption of negligible scalar mixing  $\alpha=0$ . Results are shown for a benchmark  $m_N=1\,\mathrm{TeV}$  in the degenerate BSM approximation, as discussed in the main text. The shape of the constraints follows directly from the seesaw-like relation between the Yukawa matrices and the different production regimes this defines. Details are given in the main text. ACT based constraints rely on thermalization of the Diracon and two right-handed neutrinos with the SM, but due to  $m_N=1\,\mathrm{TeV}$  we can maintain equilibrium somewhat below the EW scale. We also indicate limits from MEG and MEG-II computed in the degenerate BSM approximation. In addition, we show internal consistency conditions, namely, non-perturbative Yukawas and the seesaw expansion condition, and a non-unitary lepton mixing matrix. Published in Ref. [3]

small y', we proceed from a freeze-in production of light degrees of freedom from thermalized heavy fermions. For larger y', the light degrees of freedom thermalize with the heavy fermions, which remain in contact with the SM. At even larger Y, the heavy fermions cannot achieve equilibrium from suppressed interactions, thus secluding the light degrees of freedom from the SM. They cannot be produced efficiently and  $\Delta N_{\rm eff}$  is suppressed. The width in parameter space that defines the window of efficient production is given by the seesaw relation. We exemplify this general behavior for a benchmark point in Fig. 6.6.

We show limits for selected cases in Fig. 6.8 and Fig. 6.9. The characteristic shape of the limits can be directly understood from our discussion on the role of the seesaw relation and Fig. 6.6. For regions of parameter space where cosmological limits are present, they dominate over LFV. However, the seesaw relation restricts limits to a particular region of parameter space. LFV observables can partially probe regions inaccessible to cosmology, in particular regions of extremely small y'.

We note here that cosmology currently provides mostly forecasts. This is because the canonical model has only two coupled  $\nu_R$  degrees of freedom as well as a single Nambu-Goldstone boson.<sup>2</sup> Only for relatively light new fermions  $m_N = 1 \,\mathrm{TeV}$ , we have limits from ACT from thermalization of Diracons and neutrinos below the EW scale. Larger masses do not allow for such low temperature thermalization. Moreover, constraints shift to larger values of y' in

<sup>&</sup>lt;sup>2</sup>Which in some circumstances contributes as two scalar degrees of freedom due to the structure of the hidden sector and the hierarchy of couplings.

6.5. Results

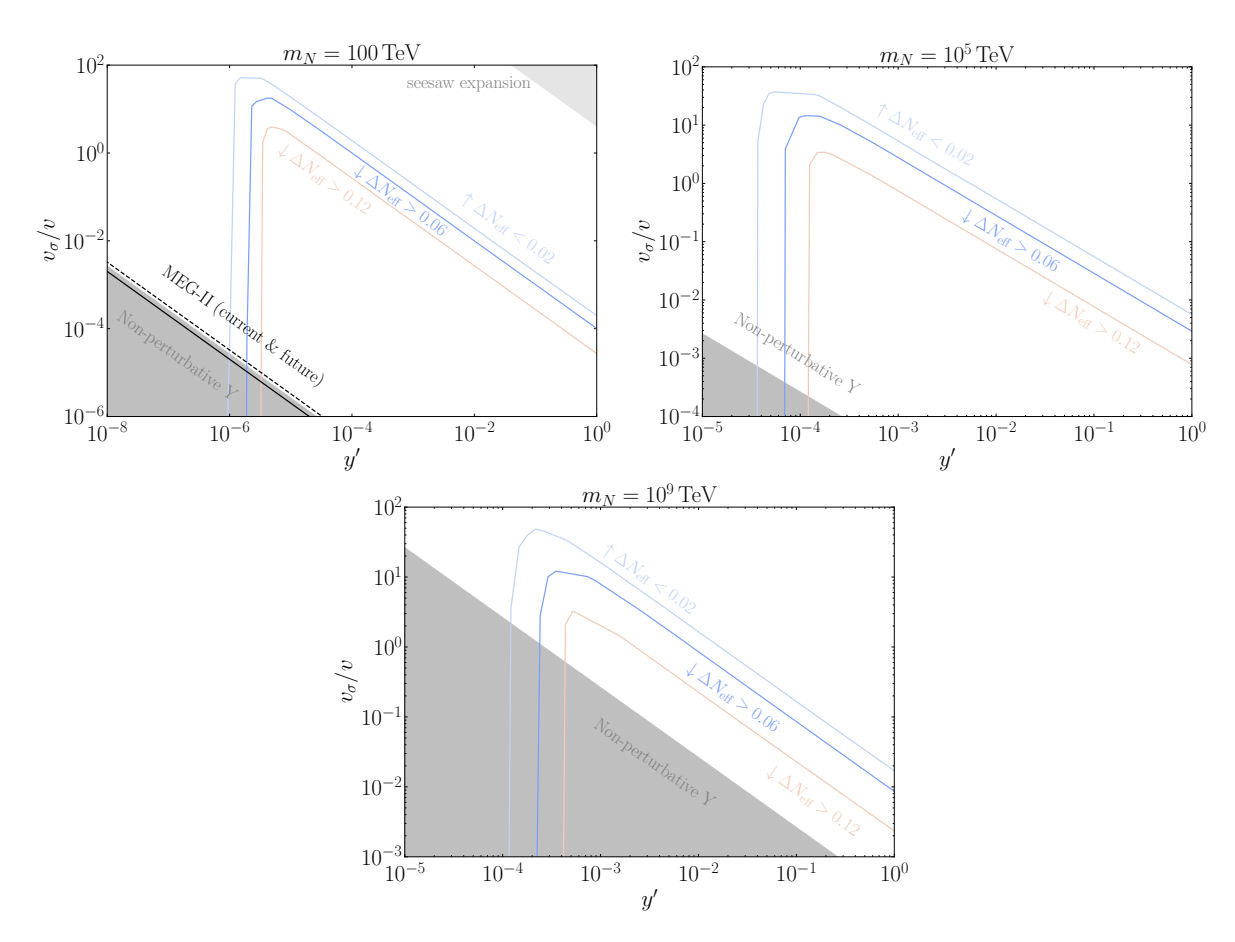


FIGURE 6.9: Canonical model constraints under the assumption of negligible scalar mixing  $\alpha=0$ . Results are shown for different values of  $m_N$  and computed in the degenerate BSM approximation. As before, the shape of the constraints follows directly from the seesaw-like relation between the Yukawa matrices and the associated production regimes. We also indicate limits from MEG and MEG-II computed in the degenerate BSM approximation, if relevant. Also, theoretical consistency conditions such as the seesaw expansion and non-perturbative Yukawa matrices are indicated. As we progress to heavier fermion masses, the required Yukawa couplings also increase. Published in Ref. [3].

general, which again can be understood from the seesaw relation and the leading dependence of the production amplitudes, here decays of heavy fermions, on the Yukawa matrices.

We provide a combined scan for a benchmark of  $\alpha=10^{-6}$  in Fig. 6.10. Adding the scalar contributions can at most increase limits by a moderate amount in the region of parameter space where limits are strongest. This is simply because the region already features a nearly thermalized Goldstone mode. However, we can keep the Goldstone coupled to the SM for longer, hence leading to a moderate increase in limit strength. In regions where Yukawa contributions to  $\Delta N_{\rm eff}$  are weak, the limit is dominated by the scalar sector contribution. Thus, to good approximation, we can separate the two sectors. For any given model realization, we can therefore apply the limits of each sector independently. This leads at most to a mild underestimation of limits.

As we already observed in Chapter 5, at first sight and for futuristic proposals, we can probe high scales for the scalar sector and the new fermions, although we acknowledge here that these probes are much weaker compared to the results of that Chapter. Indeed, the Dirac nature of neutrinos and the exact Nambu-Goldstone boson guarantee the existence of multiple light

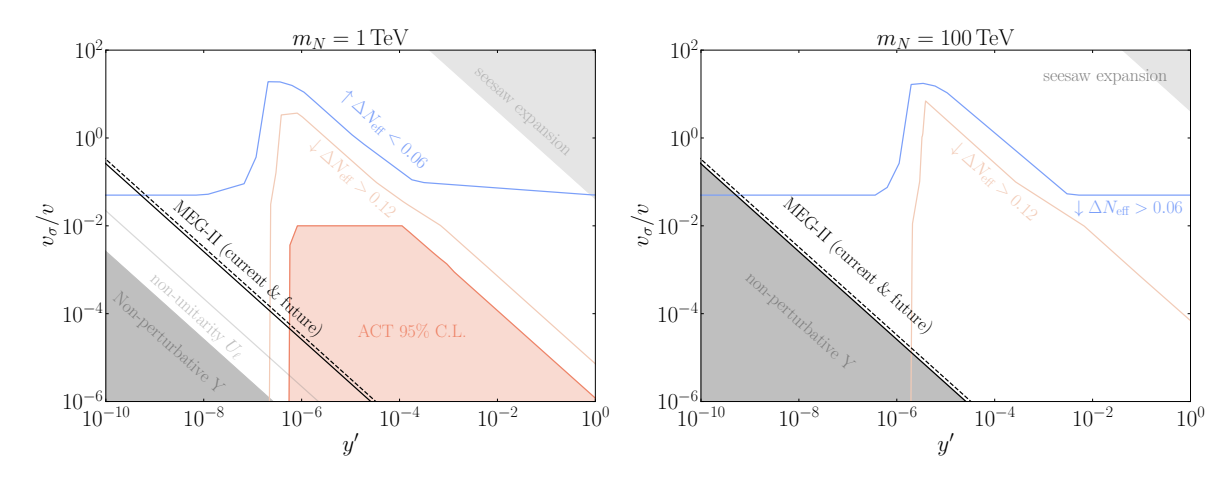


FIGURE 6.10: Results for selected full scans with fixed mixing angle  $\alpha=10^{-6}$ . We show limits for  $m_N=1\,\mathrm{TeV}$  (left) and 100 TeV (right). For large values of  $\Delta N_{\mathrm{eff}}$ , limits are slightly stronger when compared to the case of negligible mixing. For smaller values, here represented by  $\Delta N_{\mathrm{eff}}=0.06$ , constraints flatten out as the scalar contribution alone gives the dominant contribution in the low-scale regime. There is no limit for CMB-HD as it would be ruled out for the chosen mixing angle. Published in Ref. [3].

degrees of freedom no matter the scale of new physics. These limits are subject to the same cosmological caveats we discussed for the Z' model. Therefore, the same limitations imply, and we stress again the necessity of reheating to reach temperatures  $T_{\rm reh} \gg \max(v_{\sigma}, M_N)$ . We can use the approximate relation developed in Sec. 5.2 to make the same mapping of limits to the case of non-standard cosmologies.

While we do not perform a detailed study of lowered reheating temperatures for this model variant, it is reasonable to assume that the scaling will show great similarity to the gauge boson case. After all, the shape in Fig. 5.2 seems to originate purely from kinematic considerations. Hence, moving to reheating temperatures of  $T_{\rm reh} \sim 10^{-2} \, m_{N/S}$  should delegate this particular channel to a UV type freeze-in like in the Z' case, and going to even smaller values may fully escape the limits we can place here. Thus, we stress once again that these limits need to be thought of in tandem with the thermal history.

#### 6.5.2 Model II: Enhanced Diracon model

The enhanced model has no suppressed Diracon interactions. The interaction between charged leptons and the Diracon is given by

$$\mathcal{L}_{\ell\ell\mathcal{D}} = -\frac{i\,\mathcal{D}}{32\pi^2 v_{\sigma}} \bar{\ell} \left[ M_{\ell} \operatorname{Tr}(Y\,Y^{\dagger}) \,\gamma_5 + 2M_{\ell}\,Y\,Y^{\dagger}\,P_L - 2Y\,Y^{\dagger}\,M_{\ell}\,P_R \right] \ell\,, \tag{6.78}$$

where we applied the results from Appendix B to the enhanced model variant.

We again consider LFV in leptonic decays into Diracons as well as the golden signal  $\mu \to e\gamma$ . While all scans are performed with exact formulas, we once more employ the degenerate BSM approximation to gain some insight and allow for comparison to cosmological results. For this model, the approximation amounts to a degenerate explicit breaking parameter  $M_2$  and

6.5. Results

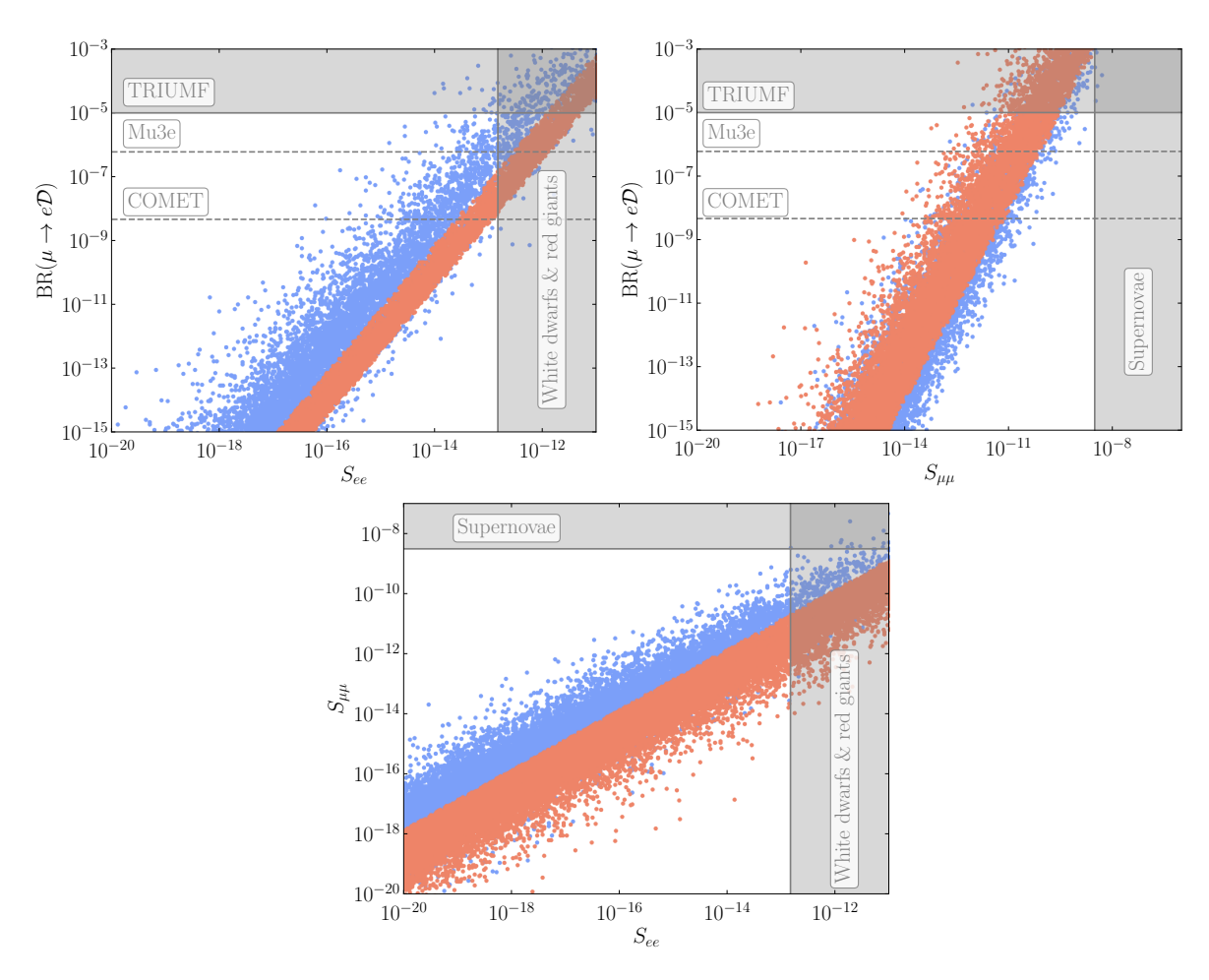


FIGURE 6.11: Scans of selected observables related to the Diracon for the enhanced model variant. We show astrophysical limits from white dwarf and supernova energy loss, as well as laboratory constraints on LFV in muon decays. Blue dots correspond to general scans, and orange dots to scans employing the degenerate BSM approximation. All points shown satisfy neutrino oscillation parameters [28] and the sum of masses bound [40], as well as enforcing internal consistency by requiring that Yukawa matrices conform with perturbativity and the seesaw expansion as discussed in the main text. Due to the strong limit of DESI on IO, we restrict the analysis to NO. The degenerate BSM approximation for which we explicitly compute cosmological limits captures a significant portion of the parameter space that is covered in an unconstrained scan.

Yukawa matrix Y'. The resulting branching ratio for decays to Diracons is then given by

$$BR(\mu \to e \mathcal{D}) = 4 \left(\frac{1}{8\pi}\right)^5 \frac{m_{\mu}^3}{v^2 \Gamma_{\mu}} \left(\frac{m_N}{m_2}\right)^4 \frac{\left|\left(U_{\ell} \widehat{M_{\nu}}^2 U_{\ell}^{\dagger}\right)_{21}\right|^2}{v^2 v_{\sigma}^2}, \tag{6.79}$$

where we used the neutrino mass relation Eq. (6.25). Similarly, we adopt the degenerate BSM result for  $\mu \to e\gamma$  for the enhanced model and compare their ratios

$$\frac{\mathrm{BR}(\mu \to e \,\mathcal{D})}{\mathrm{BR}(\mu \to e \,\gamma)} \approx 2.3 \cdot 10^8 \,y'^2 \,\left(\frac{m_N}{\mathrm{TeV}}\right)^2 \,. \tag{6.80}$$

It is evident how this ratio can be sizable even for small Yukawa couplings. Thus, searches for LFV with invisible final states can be more constraining for this model, even though limits on  $\mu \to e\gamma$  are orders of magnitude stronger.

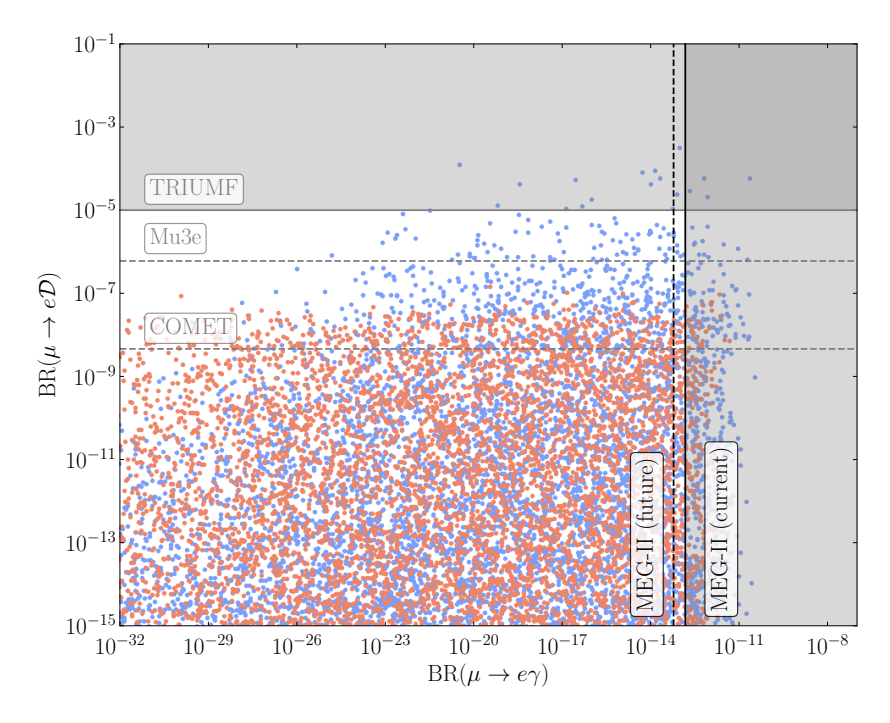


FIGURE 6.12: Scan results for the two most promising muon decays with LFV in direct comparison. Blue corresponds to a general scan and orange to the degenerate BSM approximation. As before, all points shown are consistent with neutrino flavor oscillation data [28] and the DESI neutrino mass bound [40], again assuming NO only. Moreover, all data points shown here are compatible with astrophysical energy loss and satisfy the conditions on perturbativity and the seesaw expansion discussed in the main text.

Decays of charged leptons to Diracon final states constitute an energy loss mechanism in astrophysical systems. Hence, the quantity  $S_{ee}$  from Eq (6.35) and Eq. (6.34) is of particular interest. Using the results from App. B, we find in the degenerate BSM approximation

$$S_{ee} = i \frac{m_e}{16\pi^2} \left(\frac{m_N}{m_2}\right)^2 \frac{1}{v^2 v_\sigma} \left[ 2 \left( U_\ell \widehat{M}_\nu^2 U_\ell^\dagger \right)_{11} - \sum_i m_i^2 \right]. \tag{6.81}$$

We note that both Eq. (6.79) and (6.81) depend on  $m_N^2/(m_2^2v_\sigma)$ . Hence, we do not expect them to give much complimentary information.

We show the relation between  $|S_{ee}|$ ,  $|S_{\mu\mu}|$ , and BR( $\mu \to e\mathcal{D}$ ) decay in Fig. 6.11 for a general scan and for the degenerate BSM approximation. The points fall largely on a diagonal, which is due to the lack of complementary information in the two probes. Stronger cooling also implies stronger LFV. However, the experimental limits have different reaches in parameter space. For comparison, we also show the region that is populated by the degenerate BSM approximation, for which we also find cosmological limits. The width of the region is determined by the lightest neutrino mass and would shrink to a line for a lightest neutrino with negligible mass.

Fig. 6.12 shows the relation between the two branching ratios  $\mu \to e\gamma$  and  $\mu \to e\mathcal{D}$ . Points in this plot include correct neutrino masses and mixing, a bound on the sum of neutrino masses from DESI [40], as well as consistency conditions from perturbativity of the Yukawas, and non-unitarity constraints on the lepton mixing matrix. We generally expect the Diracon decay to be as accessible as the  $\gamma$  decay. This can also be seen from Eqs. (6.79) and (6.80).

6.5. Results 83

The enhanced model provides a rich phenomenology and is subject to current and projected limits. Cosmological signatures, on the other hand, are surprisingly suppressed. While dominant for the canonical model, the picture changes in the enhanced model. First, we note that the scalar sectors are identical and the same limits as before apply. One caveat is that the scale  $v_{\sigma}$  is related to  $M_N$  in the enhanced model. Thus, the VEV cannot be taken too low. This pushes us further into the high-scale regime that favors suppressed contributions to  $\Delta N_{\rm eff}$  and may only ever be probed in futuristic experiments. For more details, see the detailed discussions of Fig. 6.7 in Sec. 6.5.1.

Even though the enhanced model has three coupled light  $\nu_R$ , interactions that may populate the neutrino sector are neutrino mass suppressed. To see this, we consider the mass basis interaction terms between heavy fermions and neutrinos,

$$\sum_{\phi \in \{h, \mathcal{S}, \mathcal{D}\}} C_{\phi} \widehat{\bar{N}_L} \phi \frac{M_2}{v_{\sigma}} \widehat{\nu_R} . \tag{6.82}$$

Here,  $C_{\phi}$  specifies couplings and mixing of scalars, but the details are not important for the general conclusion. Courtesy of the neutrino mass relation Eq. (6.25), we observe that

$$\frac{M_2}{v_{\sigma}} = -Y'Y^{-1}\frac{M_{\nu}}{v} \tag{6.83}$$

is explicitly suppressed by the neutrino mass. The only compensation for small neutrino mass could come from sufficiently small Y. However, this would suppress the interaction of heavy fermions with the SM, see Tab. 6.2, suppressing their abundance and consequently preventing population of the light sector.

We note that Diracon final states from N decays into SM particles are possible. However, this does not provide a meaningful enhancement of the cosmological signature. We may capture the cosmological limit in an effective energy scale for the benchmark  $\Delta N_{\rm eff} = 0.02$ . Production predominantly comes from decay of heavy fermions, i.e. is proportional to  $(Yv/v_{\sigma})^2/M_N$ . With  $M_N = Y'v_{\sigma}/\sqrt{2}$ , it follows that

$$\Lambda_{\rm enh}^{-1} = \frac{y^2 \sqrt{2}v^2}{y'v_{\sigma}^3} \approx 10^{-15} \,\text{TeV}^{-1} \,,$$
(6.84)

where the numerical value corresponds to  $\Delta N_{\rm eff}=0.02$  and was determined by solving the Boltzmann equation. This is an approximate effective limit in the case of negligible scalar contributions. We show a comparison of this approximate future reach of CMB-HD to the promising decay  $\mu \to e\mathcal{D}$  in Fig. 6.13. Even for such a futuristic experiment, limits would be expected to be of similar strength as near future flavor observables, albeit to some extent in non-overlapping regions of parameter space. Therefore, our conclusion stands that flavor observables are more promising than limits on  $\Delta N_{\rm eff}$  for the enhanced model. Future cosmological surveys can yield a level of complementarity.

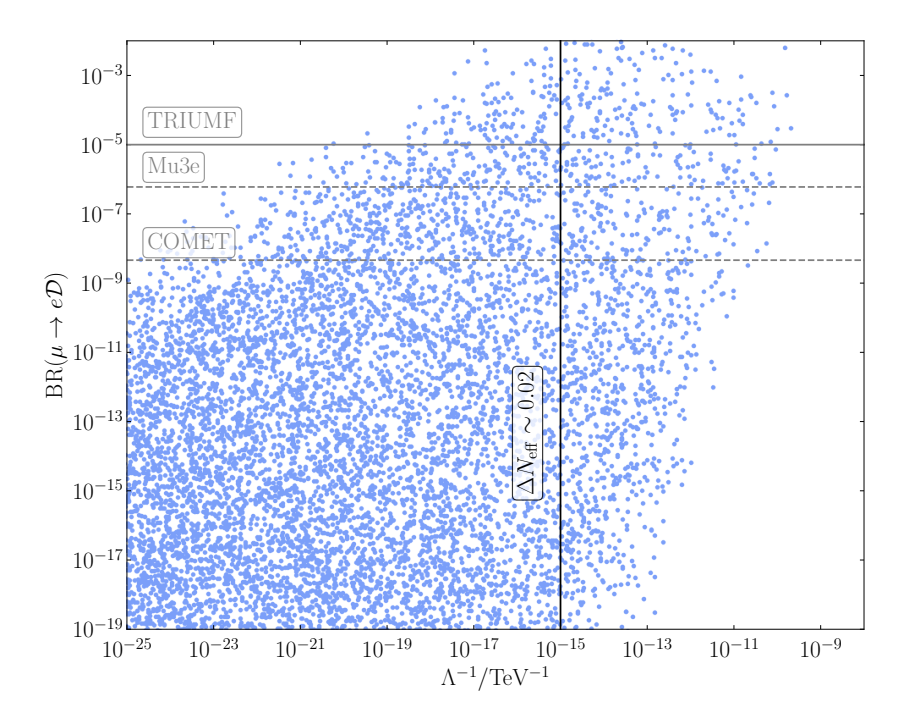


FIGURE 6.13: Comparison of the promising decay  $\mu \to e\mathcal{D}$  with an approximate estimate for what a potential futuristic CMB survey like CMB-HD could probe. It could cover a similar size of relevant parameter space as current and near future LFV experiments, although we note that non-overlapping regions of parameter space are being tested. Therefore, cosmology could provide complementary information.

## 6.6 Summary and future directions

Let us summarize the results of this chapter on a technical level, but also in the grander scheme of the viability of protecting Dirac neutrinos by means of a global symmetry.

We have generalized the notion of a seesaw family from the Type-I seesaw family to that of a Dirac Type-I seesaw family. This constitutes a generalization of different Dirac-seesaw models under a unified framework. Further, we considered two minimal extensions of the SM that belong to this family. Both models feature a new global  $U(1)_D$  that is spontaneously broken and gives rise to Dirac neutrino masses. The spectrum of the theory contains a massless Nambu-Goldstone boson referred to as the Diracon. Smallness of the neutrino mass is further ensured by a seesaw mechanism. We note here that by making the appropriate charge assignments to the new heavy fermions and the new scalar, the  $U(1)_D$  can be identified as B-L, but our considerations are more general. We make this identification, and moreover assign charges such that B-L is anomaly free. This makes it suitable for gauging and allows for the direct comparison with the results from Chapter 5.

Both realizations have the same particle content and scalar potential, but differ in their symmetry breaking patterns. The canonical model features Diracon interactions with charged leptons that are neutrino mass suppressed, and the implied LFV observables are suppressed. Cosmology allows for significant production of two of the right-handed neutrinos and the Nambu-Goldstone boson. This proceeds predominantly from decays of the heavy fermions that, in turn, can be produced from their Yukawa interactions in the early Universe. The

interplay between the production of heavy fermions N is controlled by the Yukawa matrix Y coupling  $\nu_L$  and the Higgs to N. The decay of N into  $\nu_R$  is controlled by a second Yukawa matrix Y', and they are subject to the neutrino mass relation  $M_{\nu} \propto YY'$ . Low-scale realizations of the canonical model lead to constraints from non-zero contributions to  $\Delta N_{\text{eff}}$ .

The enhanced model has, in some sense, an opposite phenomenology. Production of  $\nu_R$  from the Yukawa sector in the early Universe is explicitly neutrino mass suppressed. Diracons can be produced copiously, but since this is only a single degree of freedom, it usually avoids even future projections for  $\Delta N_{\rm eff}$ . Flavor observables, however, are found to be enhanced, hence the name of the model. Indeed, the decay  $\mu \to e\mathcal{D}$  is even expected to be observed before the golden signal  $\mu \to e\gamma$ , although this is not general and the complicated Yukawa structure allows for a variety of configurations. However, a general picture emerges where flavor is more constraining than cosmology as far as the enhanced model is concerned.

From a model building perspective, these models are minimal and well-motivated SM extensions. The complementarity between cosmological probes and flavor observables is striking, and highlights open directions including collider phenomenology, non-standard neutrino propagation from mixing with heavy fermions, or a continuation of Diracon phenomenology, and evaluating the possibility of Dirac leptogenesis in the models [247, 282–284].

However, we want to put not only the model studied here into context, but also raise some points about general models that protect the Dirac nature with a global symmetry. We already referred to the conjectured breaking of global symmetries by gravity at the beginning of this Chapter and a possible spoiling of an exact Dirac nature, to e.g a pseudo-Dirac nature, if breaking and the subsequently generated Majorana mass of right-handed neutrinos is sufficiently small. While neutrinos would end up as fundamentally Majorana in such a case, the model as such remains an interesting and well-motivated UV-completion, and such gravitational effects may also have phenomenological implications, e.g. by promoting the exactly massless Diracon to a pseudo-Nambu-Goldstone boson. Here, we want to remain agnostic to the role of gravity and contrast this with what we can infer from Dirac neutrino models based on our analysis.

Since we adopted anomaly-free models, a direct comparison between the results here and those of Chapter 5 is possible. Indeed, the gauge variant is subject to generic and strong constraints from future CMB surveys. The only way to reliably avoid these limits is a non-standard thermal history. Here, the situation is different. Indeed, we find that a minimal, realistic model of Dirac neutrinos without additional gauge bosons is only constrained by cosmology in low-scale regimes, if at all. High-scale realizations show systematically weaker constraints from  $\Delta N_{\rm eff}$ . We can attribute this to the smallness of neutrino masses. Interactions that would populate light degrees of freedom are either explicitly neutrino mass suppressed or the seesaw relation enforces such a suppression. In other words, the neutrino mass, the population of light degrees of freedom, and also flavor observables are suppressed by the mixing of neutrinos with the heavy fermions. This means that cosmological constraints are weaker than in an otherwise equivalent model where  $U(1)_D$  is promoted to a gauge symmetry.

We conjecture that other minimal models of Dirac neutrinos face similar issues. If right-handed neutrinos are minimally coupled, i.e. only the relevant couplings to produce light masses

are present, we can anticipate that similar mixing-related suppression takes place. While this would need to be shown on more general terms, it would imply that a large class of models can hardly be constrained by cosmology or even the laboratory if the new physics is high-scale. We note, however, that this must not hold in non-minimal models, where phenomenology and cosmology are affected beyond mixing. Thus, protecting the Dirac nature by a global symmetry, especially in minimal models, would be an attractive way to escape the stringent bounds from gauge symmetry protection.

# Chapter 7

# Boosted Dark Matter from the Diffuse Supernova Neutrino Background

In the last main Chapter of this thesis, we study hypothetical interactions of neutrinos, regardless of whether they are Majorana or Dirac particles, with DM by utilizing the concept of boosted dark matter (BDM). BDM was originally conceived as a proposal to overcome the sub-GeV suppression of DM direct detection signals in current noble gas detectors [121, 285]. In this Chapter, we utilize the boosting of MeV-scale DM through upscattering by the DSNB to study not only DM itself, but also the otherwise difficult to probe neutrino-DM interactions required for boosting.

DM forms a virialized halo in which the galaxy is embedded. Ambient DM particles move with velocities of order  $v_{\rm DM} \sim 10^{-3}c$  relative to Earth. For  $m_{\rm DM} \ll M_{\rm target}$ , the recoil energy is limited by  $E_{\rm rec}^{\rm max} = 2m_{\rm DM}^2v_{\rm DM}^2/M_{\rm target}$ . Indeed, supplementing typical DM velocities for a sub-GeV candidate implies recoil energies in liquid xenon experiments of order keV – too small to be detected. If a sub-dominant fraction of DM were boosted to energies  $T \gg m_{\rm DM}v_{\rm DM}$ , this kinematic suppression would be avoided, and even light DM candidates become potentially detectable in currently operating experiments. One might worry that BDM signals are conditional on additional assumptions. However, the existence of an irreducible boosted sub-component is often inevitable. Once we assume an interaction channel for detection, say scattering on nucleons for concreteness, the very same interaction will boost DM in astrophysical systems where energetic nucleons are present. This was the premise of the original proposals [121, 285], where DM is upscattered by nuclear cosmic rays (CR).

Thus, the question is not so much whether such a component exists, but whether the boosted component is of sufficiently large flux and energy to make direct detection in current experiments feasible. The arguably best studied mechanism for boosting is that of upscattering by charged cosmic rays [121, 285–299]. Subsequently, other mechanisms for boosting the DM candidate have been explored. This includes upscattering by neutrinos, and more complicated dark sectors that allow for inelastic DM interactions or heavy particle decays that produce boosted populations among others [122, 123, 126, 300–312].

Apart from its DM direct detection application, the proposal of DSNB upscattered DM fits into a larger body of research regarding neutrino-DM interactions. In addition to the

widely studied neutrino portal options for DM [313], such interactions have also been studied extensively in the CMB and other cosmological data [117–120] and are also discussed in context of persisting cosmological tensions [314].

Some of the aforementioned studies even find a mild preference of neutrino-DM interactions. However, their drawback is that these probes are necessarily indirect. Directly detecting particles that took part in these interactions is therefore an intriguing possibility to move one step closer to a direct probe. This includes direct DSNB imprints [315] or detection of the boosted DM component [122, 123]. The latter is complemented by a wider class of possibilities to upscatter DM by alternative neutrino sources, including upscattering in the vicinity of a CCSN [124–130].

In the remainder of this Chapter, we first discuss in detail the boosting, attenuation of the BDM flux and detection in liquid xenon experiments. We then introduce toy models of leptophilic DM to study not only BDM from the DSNB but also the role of energy dependence. We discuss our results in light of the anticipated DSNB detection and implications for neutrino-DM interactions, and the search for BDM more generally.

#### 7.1 From boost to detection

We begin with some general kinematic considerations that will be useful throughout this section. Let a particle B of mass  $m_B$  be at rest initially before scattering on another particle A. Upon scattering, B is boosted to

$$T_B = T_B^{\text{max}} \left( \frac{1 - \cos \theta_{AB}}{2} \right) \,, \tag{7.1}$$

$$T_B^{\text{max}} = \frac{T_A^2 + 2m_A T_A}{T_A + (m_B + m_A)^2 / 2m_B} \,. \tag{7.2}$$

Here, we denote the kinetic energy of particle i in the laboratory frame by  $T_i = E_i - m_i$ , and  $\theta$  is the scattering angle in the center of mass frame. This expression for the maximum kinetic energy is what we refer to as the maximum kinetic energy throughout this Chapter.

#### 7.1.1 Upscattering

The flux of BDM upscattered by the DSNB is calculated as the local upscattering rate integrated along all possible line-of-sights from Earth. We use the DSNB spectrum discussed in Sec. 3.3.2 and presented in Fig. 3.4. Combining the contributions from all possible directions gives the isotropic<sup>1</sup> BDM spectral flux [121–123, 295]

$$\frac{d\Phi_{\chi}}{dT_{\chi}} = \int \frac{d\Omega}{4\pi} \int_{\text{l.o.s.}} dl \int_{E_{\nu}^{\text{min}}}^{E_{\nu}^{\text{max}}} dE_{\nu} \frac{\rho_{\chi}(l)}{m_{\chi}} \frac{d\Phi_{\nu}}{dE_{\nu}} \frac{d\sigma_{\nu\chi}}{dT_{\chi}} \equiv D_{\text{halo}} \int_{E_{\nu}^{\text{min}}}^{E_{\nu}^{\text{max}}} dE_{\nu} \frac{1}{m_{\chi}} \frac{d\Phi_{\nu}}{dE_{\nu}} \frac{d\sigma_{\nu\chi}}{dT_{\chi}} . \tag{7.3}$$

<sup>&</sup>lt;sup>1</sup>A small level of anisotropy is expected but neglected here, since our Earth is not located in the center of the Milky Way.

In the second equality, we have used that halo dependence and local upscattering rate factorize, and thus it is convenient to define an effective halo parameter

$$D_{\text{halo}} = \int \frac{d\Omega}{4\pi} \int_{l, \alpha, s} \rho_{\chi}(l) dl. \qquad (7.4)$$

The precise value of the halo parameter is model dependent. A commonly adopted parametrization of the DM halo is given by the parametric family [316]

$$\rho_{\chi}(r) = \rho_{\odot} \left(\frac{r}{r_{\odot}}\right)^{-\gamma} \left(\frac{1 + (r_{\odot}/r_s)^{\alpha}}{1 + (r/r_s)^{\alpha}}\right)^{\frac{\beta - \gamma}{\alpha}}, \tag{7.5}$$

special cases of which include the cored isothermal sphere or the widely used Navarro-Frenk-White (NFW) profile [317] for  $(\alpha, \beta, \gamma, r_s) = (1, 3, 1, 20 \,\mathrm{kpc})$ , which we will adopt for the following study. We fix the distance of our Sun to the galactic center to  $r_{\odot} = 8.5 \,\mathrm{kpc}$  and the local DM density to  $\rho_{\odot} = 0.4 \,\mathrm{GeV}\,\mathrm{cm}^{-3}$ . Like Ref. [123], we probed slightly different values and parametrizations for the halo and find a mild dependence on the effective halo parameter. Therefore, for the remainder of this study we fix  $D_{\mathrm{halo}} = 2 \times 10^{25} \,\mathrm{MeV}\,\mathrm{cm}^{-2}$ .

#### 7.1.2 Attenuation

BDM particles may scatter off ambient targets along their line of travel, predominantly inside the Earth on their way to underground detector sites. This leads to a distortion and attenuation of the BDM flux at the detector. To take this effect into account, we calculate the mean energy loss of a single DM particle traveling through a medium and scattering (quasi-)elastically [121, 285, 287],

$$\frac{dT_{\chi}}{dx}(x) = -\sum_{i} n_{i}(x) \int_{0}^{T_{i}^{\max}} dT_{i} T_{i} \frac{d\sigma_{i\chi}}{dT_{i}}.$$
 (7.6)

We add the contributions from all target species and their respective target densities in the medium, and determine the energy transfer in a single interaction. We tentatively labeled the integration variable  $T_i$ , since in the case of elastic scattering the energy transfer approximately equals the recoil energy. In general, effects from binding energies and other inelasticities from DM and medium need to be taken into account.

Once solutions to Eq. (7.6) of the form  $T_{\chi}(z, T_{\chi}^{0})$ , where  $T_{\chi}^{0}$  is the energy at surface level, are found, we can transform the BDM flux at the surface of Earth to the one at the detector site. We invert the solutions to find  $T_{\chi}^{0}(T_{\chi}(z), z)$ . The attenuated DM flux is found by a simple transformation of variables

$$\frac{d\Phi_{\chi}}{dT_{\chi}} = \int \frac{d\Omega}{4\pi} \frac{d\Phi_{\chi}^{0}}{dT_{\chi}^{0}} \frac{dT_{\chi}^{0}}{dT_{\chi}}.$$
 (7.7)

We need to take into account that DM particles arriving at the detector from different solid angles traveled different distances in the medium. The distance traveled for DM coming from a particular angle  $\beta$ , where  $\beta$  is the angle between the DM path and the line of shortest distance between detector and the surface of Earth, can be written as [123]

$$z = -(R_E - h_d)\cos\beta(z) + \sqrt{R_E^2 - (R_E - h_d)^2 \sin^2\beta(z)},$$
(7.8)

which we take into account when performing the angular averaging procedure in Eq. (7.7).

It is possible to find approximate solutions to (7.6) [121, 222]. If we assume  $T_{\chi} \ll m_i$  and write  $d\sigma_{i\chi}/dT_i = \sigma_i/T_i^{\rm max}$ , the problem simplifies to

$$\frac{dT_{\chi}}{dz} = -\frac{1}{2} \sum_{i} n_i \sigma_i T_i^{\text{max}} \approx -\frac{T_{\chi}^2 + 2m_{\chi} T_{\chi}}{2m_{\chi} l}, \qquad (7.9)$$

$$l^{-1} = \sum_{i} n_i \sigma_i \frac{2m_i m_{\chi}}{(m_i + m_{\chi})^2} \,, \tag{7.10}$$

with the solution

$$T_{\chi}(z) = T_{\chi}^{0} \frac{e^{-z/l}}{1 + \frac{T_{\chi}^{0}}{2m_{\chi}} \left(1 - e^{-z/l}\right)}.$$
 (7.11)

This solution, although frequently used, is not applicable here. It relies on two key assumptions that we cannot guarantee. First, the simple form of the cross section. In more generalized settings, such an easy form is not obtainable. More severely, finding the solution requires the assumption of  $T_{\chi} \ll m_i$ . We focus on minimal models of leptophilic DM later on and do not incorporate interactions beyond neutrinos and charged leptons. Therefore, our situation reduces to that of scattering on electrons in the Earth only. For example,  $T_{\chi} \sim T_{\chi}^{\text{max}} = E_{\nu}^2/(E_{\nu} + m_{\chi}/2)$  violates the assumed hierarchy of energies strongly for typical DSNB energies and  $m_{\chi} \sim \mathcal{O}(1-10)$  MeV.

These two considerations naturally lead us to a numerical solution of the problem for scattering on electrons only. From now on, we assume a constant electron density of  $n_e = 8 \times 10^{23} \, \mathrm{cm}^{-3}$  in the Earth [123]. We solve Eq. (7.6) repeatedly for different initial energies  $T_\chi^0$ , which gives us a dense grid of  $T_\chi^x(x, T_\chi^0)$ . For fixed z, which is the distance from surface to detector under a given angle  $\beta$ , we can determine  $T_0^\chi(T_\chi)$  and the Jacobian  $\frac{dT_\chi}{dT_\chi^0}(T_\chi^0(T_\chi, z), z)$ , and exploit the relation  $\frac{dT_\chi}{dT_\chi^0} = \left(\frac{dT_\chi^0}{dT_\chi}\right)^{-1}$ .

#### 7.1.3 Detection and statistical analysis

We compare our predicted event rates with the published electron recoil data of XENONnT [318], LZ [319, 320], and PandaX [321, 322]. The differential event rate can be conveniently written as

$$\frac{dR}{dT_e} = N_e \int dT_\chi \frac{d\Phi_\chi}{dT_\chi^2} \frac{d\sigma_{e\chi}}{dT_e} \,, \tag{7.12}$$

where  $N_e = M_{\rm det}/m_{\rm Xe}Z_{\rm eff}(T_e)$  is the effective number of electron targets in the detector volume. It is simply the number of xenon atoms and the effective charge number, i.e. the electrons that can be ionized upon scattering. Instead of approximating  $Z_{\rm eff}$  as a series of step functions, we simplify to a constant  $Z_{\rm eff}(T_e) \approx 40$ , which gives a good approximation for the contribution from electrons with binding energies  $E_b < 1.15 \, {\rm keV}$  [323].

We model the uncertainties of energy reconstruction by convoluting the predicted signal with a Gaussian shaped energy resolution function

Res
$$(E_R, T_e) = \frac{1}{\sqrt{2\pi\sigma(T_e)^2}} \exp\left(-\frac{(T_e - E_R)^2}{2\sigma(T_e)^2}\right),$$
 (7.13)

where  $T_e$  is the deposited energy and  $E_R$  is the reconstructed energy. The energy resolutions are provided by the respective collaborations with  $\sigma_{\rm XE}/{\rm keV} = 0.31 \sqrt{E/{\rm keV}} + 0.0037 E/{\rm keV}$  for XENONnT [324],  $\sigma_{\rm LZ}/{\rm keV} = 0.323 \times 10^{-1.5} \sqrt{E/{\rm keV}}$  for the LZ experiment [319], and finally  $\sigma_{\rm PA}/{\rm keV} = 0.073 + 0.173 E/{\rm keV} - 6.5 \times 10^{-3} (E/{\rm keV})^2 + 1.1 \times 10^{-4} (E/{\rm keV})^3$  for PandaX [321]. Inefficiencies in the reconstruction are captured by a multiplicative efficiency function that is also published by the collaborations.

We analyze the parameter spaces of interest with a  $\chi^2$  statistic

$$\chi^2 = \sum_{E_i} \frac{\left(R_i^{\text{pred}}(E_i) - R_i^{\text{exp}}(E_i)\right)^2}{\sigma_i^2(E_i)}, \tag{7.14}$$

where the predicted event rate is a *total* event rate consisting of BDM contributions and experimental background. We fix the background to the best-fit background model, implying conservative limits since a simultaneous fit of background and prediction is not performed. The total uncertainty is

$$\sigma_i^2(E_i) = R_i^{\text{pred}}(E_i) + \sigma_E^2(E_i), \qquad (7.15)$$

where we estimate the event rate uncertainties  $\sigma_i$  by combining a Poissonian counting error on the total predicted event rate, including background, with the experimental uncertainty as published by the collaborations. We exclude regions of parameter space based on a  $\chi^2$  difference to the best-fit background model, i.e.  $\Delta\chi^2 = \chi^2 - \chi^2_{\rm bkg}$  and reject regions with  $\Delta\chi^2 > 4.61$  at 90% C.L.

# 7.2 Models and the role of energy dependence

Studies of DM direct detection and BDM detection often employ a constant cross section, where  $\frac{d\sigma}{dT} = \frac{\bar{\sigma}}{T_{\text{max}}} \Theta(T_{\text{max}} - T)$ . While this is a good approximation for traditional direct detection searches, the case of BDM is conceptually different. BDM can be (semi-)relativistic upon arrival in the detector, which means we also probe the energy dependence of the underlying interaction beyond the deep non-relativistic limit. This effect is expected to be more pronounced in the case of scattering of BDM on electrons, since the kinetic energy of incoming DM can easily be of the order or above the mass of the recoil target in this case. First studies suggest that this effect is indeed significant and alters limits we put on DM parameter space by orders of magnitude [295].

We study the specifics of energy dependence and compare to previous limits from DSNB boosted DM [122, 123], and at the same time, also employ an improved scheme for the treatment of attenuation. As we demonstrated in Sec. 7.1.2, the commonly employed approximations do

not apply in the case of light BDM scattering on electrons. For concreteness, we focus on two representative toy models of  $\nu$ -DM and e-DM interactions, where the interaction is mediated by exchange of vector and scalar mediators, respectively.

We note here that this provides a simplified setup, and that the naive realizations of these models are already constrained in large parts of the relevant parameter space [325–329]. Nevertheless, they serve as a useful testing ground to highlight the necessity of the model-dependent approach. Moreover, they could serve as part of larger realizations that involve multiple channels for DM boosting. Thus, they deserve scrutiny as building blocks of more complete models of neutrino-DM interactions and more generally, boosting of DM. As future DM experiments improve in sensitivity, bounds from boosting will improve. We also note the relevance with regard to the irreducibility of a boosted component. Should future surveys find the non-relativistic bulk component of a light DM candidate, the interactions that lead to detection are the same interactions that produce an irreducible, albeit sub-dominant, boosted component. Hence, the search for BDM can offer a valuable cross check.

We note here that we are oblivious to the Majorana or Dirac nature of neutrinos. We will assume that all additional interactions we introduce couple to  $\nu_L$  only. As a reference model, we compute results under the assumption of a constant, energy-independent cross section. These limits are expected to differ from previous results insofar as we take into account attenuation beyond the analytic approximation. Since this approximation is not applicable to begin with, deviations are expected.

In the first toy model, we couple a fermion singlet  $\chi$  with a massive vector boson Z' that also couples to charged and neutral leptons,

$$\mathcal{L} \supset g_e \,\bar{e}\gamma^{\mu}eZ'_{\mu} + g_{\nu}\,\bar{\nu}\gamma^{\mu}\nu Z'_{\mu} + g_{\chi}\,\bar{\chi}\gamma^{\mu}\chi Z'_{\mu}. \tag{7.16}$$

It could easily be integrated into a UV-complete model for  $g_{\nu} = g_e = g$ , but varying couplings are also possible. Unless specifically stated otherwise, we chose equal couplings. The matrix elements relevant to us are given by

$$|\mathcal{M}|_{\nu\chi\to\nu\chi}^2 = \frac{2\,g_{\nu}^2 g_{\chi}^2}{(t - m_{Z'}^2)^2} \left[ 2(m_{\chi}^2 - s)^2 + 2st + t^2 \right] \,, \tag{7.17}$$

$$|\mathcal{M}|_{e\chi \to e\chi}^2 = \frac{2 g_e^2 g_\chi^2}{(t - m_{Z'}^2)^2} \left[ 2(m_e^2 + m_\chi^2 - s)^2 + 2st + t^2 \right] , \tag{7.18}$$

for upscattering by neutrinos and interaction with electrons, respectively.

Our second model introduces two scalar mediators  $\Phi^0$  and  $\Phi^-$ . The relevant interactions are given by

$$\mathcal{L} \supset g_{\nu}\bar{\nu}\chi\Phi^{0} - g_{e}\bar{e}\chi\Phi^{-}. \tag{7.19}$$

As for the previous model, the couplings to electrons and neutrinos can, in principle, be different. Once more, we opt for the assignment  $g_e = g_{\nu} = g$ . Possible UV-completions could then proceed via introduction of a new scalar doublet  $\Phi = (\Phi^-, \Phi^0)^T$ . The amplitudes of interest

7.3. Results 93

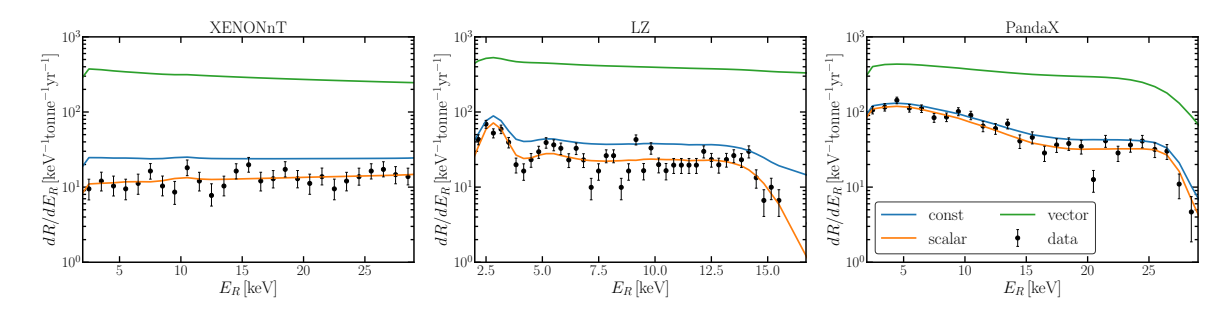


FIGURE 7.1: Event rates for the electron recoil in the three experiments we consider here. We show the released data and background for XENONnT (left), LZ (middle), and PandaX (right) and also our theoretical prediction for a benchmark point of  $\bar{\sigma}_{e\chi} = 10^{-30} \, \mathrm{cm}^2$ , mediator mass 1MeV and  $m_{\chi} = 0.5 \mathrm{MeV}$ . We predict rates for a constant cross section (blue), vector mediated interaction (green), and scalar mediator (orange). Couplings are chosen such that the mediator models are mapped on an effective cross section of the same magnitude, i.e. they would have been considered equivalent and subject to the same constraints. For more details, see the main text. Published also in Ref. [1].

can be written as

$$|\mathcal{M}|_{\nu\chi\to\nu\chi}^2 = g_{\nu}^2 g_{\chi}^2 \frac{(t - m_{\chi}^2)^2}{2(t - m_{\Phi}^2)^2} \,, \tag{7.20}$$

$$|\mathcal{M}|_{e\chi \to e\chi}^2 = g_e^2 g_\chi^2 \frac{\left[ (m_\chi + m_e)^2 - t \right]^2}{(t - m_\Phi^2)^2} \,. \tag{7.21}$$

We would like to note a few peculiarities of our scalar toy model. We necessarily require  $m_{\chi} < m_{\Phi} + m_e^2$ , as otherwise DM efficiently decays. Moreover, interactions of the new scalar introduce a conversion of species at each vertex. We note that this gives rise to thresholds on the t-channel.

#### 7.3 Results

Results from the literature typically assume a constant interaction cross section. To translate these constraints on specific model parameter spaces, an effective cross section prescription is used. It is given by [121, 295]

$$\bar{\sigma}_{e\chi} = \frac{g^4}{\pi} \frac{\mu_{e\chi}^2}{(q_{\text{ref}}^2 + m_{\text{med}}^2)^2},$$
 (7.22)

where the reference momentum transfer is most usually taken as  $q_{\text{ref}} = \alpha m_e$  with fine structure constant  $\alpha$ .

Indeed, this prescription proves useful in the context of traditional direct detection searches, where all DM is expected to have a similar order of magnitude in kinetic energy  $T_{\chi} \sim m_{\chi} v^2$  such that a suitable reference momentum transfer may be defined. In the case of BDM, however, the energy spectrum is spread out over orders of magnitude, and incoming DM particles have kinetic energies that go far above the energies of virialized cold DM. Thus, in addition to the explicit energy dependence of the underlying interaction, we have an additional distortion of

<sup>&</sup>lt;sup>2</sup>Technically it is  $m_{\Phi^-}$ , but for the sake of concreteness and alluding to ideas of UV-completion, we have implicitly adopted  $m_{\Phi^-} = m_{\Phi^0}$ .

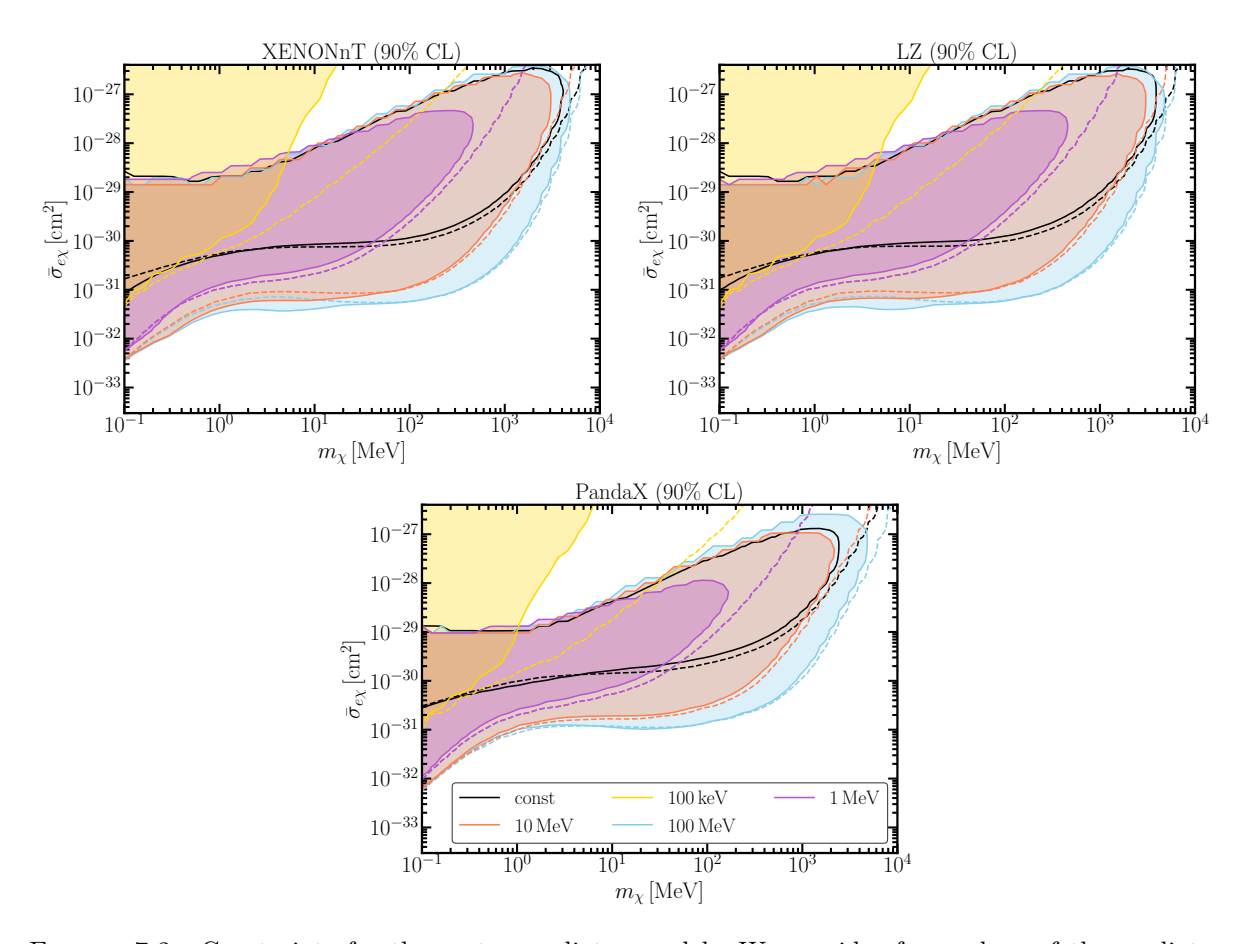


FIGURE 7.2: Constraints for the vector mediator model. We consider four values of the mediator mass  $m_{Z'}=0.1$  (yellow), 1 (purple), 10 (orange), and 100MeV (blue). Shaded regions are excluded at 90% C.L. The updated constant cross section computation is shown in black for reference. We also indicate the effect of attenuation by showing in dashed lines the results without attenuation. Published in Ref. [1].

limits on parameter space, since we usually map models naively onto an unsuitably defined reference cross section.

We show examples of the expected signals in the three experiments we consider in Figure 7.1, where we consider the constant cross section case, as well as models of vector and scalar mediated interaction that are equivalent in the sense of Eq. (7.22). Here we can already see a drastic difference in the expected signal, although these benchmark points would usually all be mapped on the same value of  $\bar{\sigma}_{e\chi}$ .

We perform systematic scans of the parameter space spanned by  $m_{\chi}$  and  $\bar{\sigma}_{e\chi}$  for different masses of the mediator. The  $\nu$  – DM cross section is fixed to  $\sigma_{\nu\chi} = \sigma_{e\chi}$  in the case of constant cross section. For the mediator models, any choice of mediator, DM mass, and effective cross section implies a coupling constant  $g = \sqrt{g_{\chi}g_e}$  from Eq. (7.22). We use the same value of coupling for the upscattering of DM by DSNB neutrinos. Note that this almost always implies  $\sigma_{e\chi} \neq \sigma_{\nu\chi}$ , contrary to assumptions from previous studies [122, 123]. However, from a point of view of possible UV-completions, we deem this scenario more plausible and, therefore, of particular interest for this study.

7.3. Results

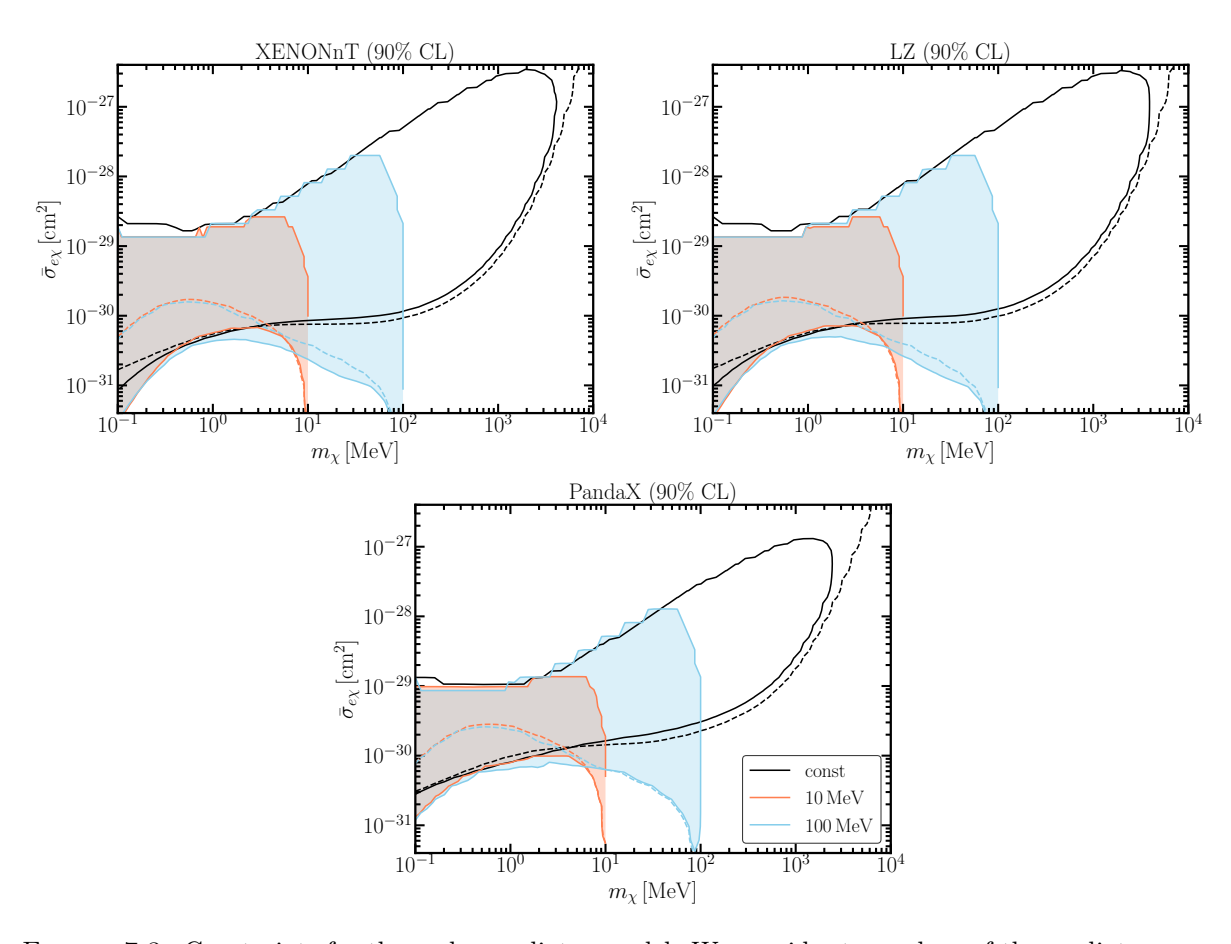


FIGURE 7.3: Constraints for the scalar mediator model. We consider two values of the mediator mass only, 10 (orange), and 100MeV (blue). Shaded regions are excluded at 90% C.L. The updated constant cross section computation is shown in black for reference. We also indicate the effect of attenuation by showing in dashed lines the results without attenuation. Published in Ref. [1].

We show the limits we find in Fig. 7.2 and Fig. 7.3 for the vector and scalar case, respectively. The shaded regions correspond to exclusion at 90% C.L. for fixed mediator masses. We also show the limits we would find for neglected attenuation in the Earth as dashed lines. For reference, we show the result for constant cross section. We attribute the differences to previous results [123], especially in the upper part of the contour, to our improved treatment of attenuation.

Let us focus on the vector mediator case first. Even in the absence of attenuation, the effect of mediator mass dependence is very pronounced and the dominant effect on differing exclusion contours. In general, the energy-dependent limits are stronger in the sense that they probe smaller values of the effective cross-section. The reason for this is multifold. Being mindful of plausible UV-completions introduces different cross sections for  $\nu$  – DM and e – DM interactions, thus leading to an asymmetry in upscattering, attenuation, and detection. This could partially be compensated by introducing different cross sections also for the constant case. However, the underlying energy dependence changes the nature of the interaction quite significantly, an effect that is enhanced by a misrepresentation of the underlying cross section in the effective cross section prescription.

For heavy mediator masses, we approach a regime of effectively constant cross section, albeit

different ones for upscattering and detection. In the intermediate regime, limits change noticeably in shape and tend to become weaker at higher DM masses and stronger for smaller values of DM mass. The light to massless mediator regime is different qualitatively and quantitatively. Coincidentally, it is the case where the misrepresentation of  $\bar{\sigma}_{e\chi}$  is the most pronounced, on top of the explicit energy-dependence.

Apart from the very light mediator case, we observe the presence of an attenuation ceiling. Interactions of DM and electrons become so frequent that effectively no BDM particle can reach the detector site anymore. The location of the attenuation ceiling is almost universal and largely unaffected by the underlying model parameters. For example, this can be understood by Eq. (7.6). The details of the energy dependence are smoothed out by integration, and the energy loss profile we find with Eq. (7.6) is approximately exponential. Thus, any model dependence is obstructed by these conditions and, therefore, barely noticeable. We conclude that the energy dependence that arises in a particular model is still important, indeed, it is the dominant effect on the shape and position of the exclusion contours that we can place.

The situation is different for scalar mediated interactions. Here, the limits are qualitatively very different from the constant and the vector case. Considerations of DM stability already limit the available parameter space. Nevertheless, the results show two important features that deserve a more careful consideration. The inclusion of attenuation has a much more pronounced effect here. While in the vector case the most noticeable difference was the presence of the attenuation ceiling, here we find on top of the attenuation ceiling also significantly stronger limits in the low DM mass case. This can be attributed to interactions with electrons in the Earth, which scatter BDM to lower energies. Thus, the distortion of the flux will not only suppress signals, but if it leads to an enhancement of flux in kinetic energy ranges that the experiments are particularly sensitive to, it leads to a sizable enhancement of limits.

Another concern is the strong enhancement in the limit  $m_{\chi} \to m_{\Phi}$ , which is the result of the mass differences on the vertices and leads to a t-channel resonance. It signals the presence of unstable states, and it leads to a resonant enhancement of the matrix element.

# 7.4 Summary and future directions

We conclude that BDM from the DSNB is a unique probe of neutrino-DM interactions. Contrary to other studies of DM upscattered by neutrinos, we can utilize the near isotropy and temporal stability of the DSNB as a cosmological signal of past CCSN. Before discussing the larger implications of our findings, we summarize several key technical findings of this analysis concerning not only DSNB upscattered DM but BDM more generally.

First, obtaining reliable limits from BDM implies a strong model dependence of such limits. This dependence extends beyond energy scaling of the interaction, which can be probed due to the (semi-)relativistic nature of BDM. More complex interaction types, such as those mediated by scalars in our toy model, cannot be accurately captured by assuming a constant cross section at all. Thus, reliable limits on the parameter space of leptophilic BDM can only be obtained on a model by model basis. However, the energy dependence would also allow for discrimination between different proposed models in the case of a positive signal.

Second, the correct modeling of attenuation, especially for BDM, is crucial. Commonly used approximations fail in the presence of BDM, in particular if DM predominantly interacts with leptons. The results depend on attenuation in a non-trivial way, leading to suppression of flux at the detector site, but also to reallocation of DM towards energies beneficial for direct detection. The correct implementation of the detector overburden remains an issue that goes beyond studies of BDM and has implications also for more conventional direct detection searches, yet to a smaller extent.

Here, we considered the mean energy loss of BDM from scattering on electrons in the Earth without resorting to extra approximations beyond the ballistic ansatz. Our approach is an improvement to this semi-analytic approximation. The limitations of the mean energy loss or ballistic approach are known, e.g. Refs. [293, 330] for the case of relativistic BDM and Refs. [305, 331] for non-relativistic DM. Monte Carlo simulations of the energy loss in medium constitute an improvement [293, 305, 322, 330, 332]. However, they are computationally costly and still require simplifications to reduce the computational load. The ballistic ansatz, on which we improved here, allows us to simplify the problem and it gives good agreement in many situations [332].

Beyond the technical level, interactions between neutrinos and DM remain an intriguing possibility. In light of tensions between different cosmological data sets, new physics related to neutrinos and, in particular, neutrino-DM interactions are regarded as a possible solution for their reconciliation [314]. We note again the mild preference for such interactions in CMB [118–120] and Lyman- $\alpha$  data [117]. Interestingly, these studies find similar preferences for an interaction strength of  $u \sim 10^{-6} - 10^{-4}$ , where

$$u = \frac{\sigma_{\nu-\text{DM}}}{\sigma_{\text{Thomson}}} \left(\frac{m_{\text{DM}}}{100 \,\text{GeV}}\right)^{-1} \,, \tag{7.23}$$

and  $\sigma_{\text{Thomson}} \simeq 6.7 \times 10^{-29} \,\text{m}^2$  is the Thomson cross section used for reference. While current BDM analyses have not yet reached this sensitivity, as we see from our results, ongoing and future experiments can close this gap. Thus, the possibility of observing DM upscattered by neutrinos offers a unique window into these interactions, and despite their limitation towards lighter DM candidates, they, therefore, offer complementary information when constraining the parameter space of neutrino-DM interactions.

We note here also that such interactions could leave an imprint in the DSNB itself [315], similar to how upscattering by cosmic rays could leave its imprint in the cosmic ray spectrum. In addition, detecting the BDM component implies other interaction channels, either electrons or nucleons, and therefore additional sources of boosting to a wide range of possible kinetic energies. This motivates future comprehensive studies combining all boosting sources, incorporating full energy dependence and propagation effects. Such work should include DSNB spectral alterations and possible DM-induced modifications of other boosting sources – and to push current and near future experiments to sensitivities where it might become feasible to detect a BDM component and perhaps directly probe neutrino-DM interactions as currently preferred by cosmology.

Experiments with lower detection thresholds will be crucial to establish the connection

between detecting a boosted component and the bulk abundance of light cold DM. Likewise, pushing towards lower thresholds allows for the detection of heavier BDM for which upscattering is less pronounced. We can envision the combination of all sources of boosting for a given DM model in something akin to a grand-unified spectrum of BDM. A definite prediction of a persistent, energetic component of DM for a given DM model that, in some circumstances, is within experimental reach and offers a valuable cross check for traditional direct detection searches.

### Chapter 8

# Summary and Outlook

The absence of neutrino masses in the SM is among the strongest hints of physics beyond the SM. Due to their feeble interactions, however, their study remains challenging. Although the situation is not as pessimistic as Pauli had originally feared, and neutrinos have not only been experimentally established but are also routinely observed in terrestrial detectors, many questions remain open.

Despite the numerous theoretical ideas to explain neutrino masses and mixing, we do not have a clear experimental signature favoring or disfavoring any particular ansatz to explain them. Particularly noteworthy is that we still do not have a clear signal discriminating between a Majorana or Dirac nature of neutrinos. While observation of  $0\nu\beta\beta$ -decay would clarify the situation, the inverse is not true – we cannot rule out a Majorana nature even if  $0\nu\beta\beta$ -decay is not observed any time soon. This is where we turn to cosmology and astrophysics, in the hope of identifying other smoking gun signatures of a possible Dirac nature of neutrinos. One option is the extra degrees of freedom of a Dirac neutrino. If a complete model of the neutrino sector allows for copious production of these light states, it can affect the effective neutrino number  $N_{\rm eff}$ , which is experimentally constrained.

In Chapter 4, we developed a complementary ansatz to solve integrated Boltzmann equations. These Boltzmann equations can be used to compute the cosmological abundance of such light particles. We opt for a Monte Carlo integration of the high-dimensional collision operator. This allows for an approximation-free solution of the integrated Boltzmann equation, which includes all relativistic and spin-statistical effects. We present a formalism that is straightforward to implement for different models, and we present prescriptions to include leading thermal effects, as well as s-channel resonances. The framework is complementary to existing Boltzmann codes that are often tailored to dark matter relic abundance calculations. Our implementation is used for energy densities and abundances of light relativistic species, but it could just as well be used for dark matter relic density, leptogenesis calculations, and more.

We employed this Boltzmann scheme to study the cosmology of models of Dirac neutrinos. The focus is on the abundance of light relics, here the light right-handed partners of the SM neutrino, as well as possible additional light degrees of freedom such as Nambu-Goldstone bosons. In Chapter 5, we focused on generic extensions that protect the Dirac nature of neutrinos by a gauged U(1). Our benchmark model is  $U(1)_{B-L}$ , but similar limits apply to other gauge group extensions that couple  $\nu_R$  and a subset of SM fermions.

We present the  $\nu_R$  relic abundance in a Z'-model that includes all relativistic and spinstatistical effects, a correct treatment of on-shell mediators from resonant production, and thermal masses as a leading correction. We provide an update of limits for the new CMB-only limit  $\Delta N_{\rm eff} < 0.17$  from ACT. This limit is the strongest limit on  $\nu_R + Z'$ -extensions thus far. Focusing on  $m_{Z'} > 1 \,\text{GeV}$ , we find that for the first time, cosmological limits surpass laboratory and collider constraints on all mass scales, including the previously untested regime  $m_{Z'} \sim 100 \,\text{TeV}$ . We also confirm forecasts for future CMB surveys and results indicate that, for gauge coupling  $g \sim \mathcal{O}(1)$ , gauge boson masses close to  $m_{Z'} \sim \Lambda_{\rm GUT}$  are testable.

These results are deeply entangled with underlying cosmological assumptions. Production of  $\nu_R$  peaks around  $T \sim m_{Z'}/3$ , thus reheating to  $T_{\rm reh} \gg m_{Z'}$  is required to maximize yield. We systematically studied the effect of a lowered reheating temperature on  $\Delta N_{\rm eff}$  and find that  $T_{\rm reh} < 10^{-2} m_{Z'}$  severely reduces the effectiveness of the production as we transition to a UV-sensitive effective operator freeze-in. Notably, the seemingly testable GUT scale gauge boson can no longer yield detectable  $\Delta N_{\rm eff}$  if upper bounds on the reheating temperature from inflation are taken into account. For lower masses, constraints can be avoided for a sufficiently low reheating temperature. We also consider the effect of non-standard thermal histories, in particular a phase of early matter domination, new degrees of freedom freezing out, and early phase transitions. We present prescriptions to translate our bounds to such non-standard cosmologies and the accompanying phase of reheating. The assumption of  $\nu_R + Z'$  turns  $\Delta N_{\rm eff}$  into a powerful probe of pre-BBN cosmology, an otherwise difficult to probe era. We highlight especially the tremendous implications of a near-future collider signature of such models as a smoking gun signal for non-standard cosmologies.

In Chapter 6, we generalized the notion of a Type-I seesaw family to the Dirac case. It offers a unified framework to study a variety of specific seesaw realizations for Dirac neutrino models. We studied two minimal realizations in more detail. Named the canonical and the enhanced version, these models have the same particle content but differ in charge assignments. The Dirac nature is protected by a global  $U(1)_D$  symmetry. The theory contains an exact Nambu-Goldstone boson commonly referred to as the Diracon, leading to additional constraints from flavor observables. We generally note that cosmological limits from  $\Delta N_{\rm eff}$  are weaker than what we would expect from their gauged counterpart, based on our analysis in Chapter 5. We observe that production of  $\nu_R$  is usually suppressed either by mixing, explicitly by neutrino mass, or by a parameter relation induced by the seesaw relation that further suppresses  $\nu_R$  production. Only low-scale variants of the canonical model are within reach of future experiments, and the enhanced version remains virtually invisible to forecasted sensitivities. The presence of the Diracon is crucial, and leads to LFV that can still probe regions of parameter space complementary to cosmology.

We anticipate that a similar suppression will occur in other minimal models of Dirac seesaws with a global symmetry. Especially if contributions to  $\Delta N_{\rm eff}$  mainly arise from mixing to heavy fermions, which can be sizable only for low-scale variants in the Type-I family. Still, limits are generally weaker than for gauged model variants. This makes a global symmetry protection an attractive alternative to gauged variants despite the conjectured breaking of global symmetries by gravity, which could potentially spoil an exact Dirac nature.

Many models that aim to explain the neutrino mass often predict suitable dark matter candidates and interactions between neutrinos and a dark sector. Some cosmological data sets prefer such neutrino-dark matter interactions, but evidence remains indirect. In the case of MeV-scale dark matter candidates, a direct approach is given by upscattering of cold dark matter by energetic neutrinos. Such boosted dark matter becomes observable with unique signatures in Earth-bound direct detection experiments. The observation of one of the scattering partners makes a direct probe of neutrino-dark matter interactions feasible.

We turned to such direct probes of neutrino-dark matter interactions in Chapter 7. We consider MeV-scale DM with interactions to neutrinos and charged leptons. Using the DSNB as a source of energetic neutrinos with  $E_{\nu} \sim \mathcal{O}(10)\,\mathrm{MeV}$ , we studied the flux of BDM at terrestrial laboratories and found that neutrino upscattered BDM leaves unique signatures in direct detection facilities. Here, the often overlooked energy dependence of the interaction and overburden effects near the detector plays a crucial role. The results we find can vary by orders of magnitude when compared to results from standard approximations. This has implications for BDM beyond upscattering by the DSNB. Especially, the energy dependence will allow for model discrimination if a signal is to be found.

Current limits are not quite there yet to probe the cosmologically preferred regime. However, future experiments in combination with imprints on the DSNB from such interactions, or implications for a local CCSN, may allow us to explore the currently preferred interaction strength. Combining all of the above aspects could give a promising indication not only for neutrino-DM interactions, but also towards the nature of DM itself. Upscattering on neutrinos beyond the DSNB embeds into a large body of BDM research. Models that generate neutrino-DM interactions often generate other interaction terms too, which allow for additional boosting. We highlighted how this creates synergy in searches for BDM, and how the combination of different sources of upscattering provides a means to discriminate models. The creation of a small BDM component is inevitable for MeV-scale DM, and would offer a valuable cross check for the detection of the unboosted bulk component in future low-threshold experiments.

In the end, we want to briefly advocate for the potential that a galactic CCSN could have beyond neutrino-DM interactions and in light of the other research projects presented in this thesis. The effect of Dirac neutrinos and other light degrees of freedom in supernovae has been studied before. In combination with the results of this thesis, however, new opportunities arise. Supernovae may offer a complementary clue to the Dirac or Majorana nature of neutrinos. For instance, the presence of light particles in CCSNe is already well-constrained. However, the models we discussed with regard to the Type-I seesaw family not only have a Nambu-Goldstone boson, but also potentially large interactions between left- and right-handed neutrinos or charged leptons with the Diracon. A future galactic CCSN could, therefore, be a strong indicator in favor or disfavor of such models.

Similarly, we already hinted at how Dirac neutrinos with a new gauge interaction are a powerful probe of the very early Universe. Different future directions are open, and we only highlight here the potential of addressing cosmological problems like the Hubble tension in Dirac neutrino model building, or how solutions to cosmological tensions may offer a natural way out of the strong projected limits on Dirac neutrino models with a gauge symmetry by

means of drastically altering the thermal history.

It is by using all of the cosmological and astrophysical *laboratories* at our disposal that we can fully utilize the power of astroparticle physics to unravel open fundamental questions in neutrino physics. From the early thermal history to the messengers of stellar collapse, this thesis has explored how cosmology and astroparticle physics can be turned into a neutrino experiment that could give us a clue to the nature of neutrinos, how they interact with dark matter, and how they fit into a more complete theory of particle physics. As experiment and observation progress to unprecedented precision, the idea of the Universe as a neutrino laboratory will continue to evolve, offering both guidance and new insights in the ongoing attempt to understand this most elusive particle.

## Appendix A

# Collision operator

### A.1 Implementation

Here we give more details on solving for the collision operator by means of Monte Carlo integration. To this end, we bring relevant collision operators in a form that is particularly useful for integration. We use the VEGAS framework [333, 334] for the numerical implementation. Due to its adaptive sampling strategy, we can quickly achieve convergence for the integrals and reach a desirable level of numerical precision.

We give the details on  $2 \to 2$  and the  $1 \to 2$  processes, but a generalization to general  $m \to n$  collision operators can be achieved by using the same approach.

### A.1.1 $2 \rightarrow 2$ processes

We can analytically reduce the collision operator from 12 to 5 dimensions without further assumptions. A similar parameterization was adopted in Ref. [335], but our implementation deviates in a number of steps.

We begin with the integral of an arbitrary function on four particle phase space

$$C_{(F)} = \int \frac{d^3p_1}{(2\pi)^3 2E_1} \frac{d^3p_2}{(2\pi)^3 2E_2} \frac{d^3p_3}{(2\pi)^3 2E_3} \frac{d^3p_4}{(2\pi)^3 2E_4} (2\pi)^4 \delta^{(4)} \left(p_1 + p_2 - p_3 - p_4\right) F(p_i) . \quad (A.1)$$

Rotational invariance implies it is always possible to go to a coordinate system where  $\vec{p}_1 = (0,0,p_1)^T$ , and the angular integration of the first momentum is trivial. Thus, we may write for the first momentum  $d^3p_1 = 4\pi p_1^2 dp_1$  and for the remaining momenta we adopt the relations  $\vec{p}_2 = p_2(\sin\beta,0,\cos\beta)^T$  and  $\vec{p}_3 = p_3(\sin\theta\cos\phi,\sin\theta\sin\phi,\cos\theta)^T$ . All angles are defined relative to the direction of  $\vec{p}_1$ .

After performing the azimuthal integration of  $p_2$ ,

$$C^{(F)} = 2(2\pi)^2 \int_0^\infty \frac{dp_1 p_1^2}{(2\pi)^3 2E_1} \int_{-1}^1 d\cos\beta \int_0^\infty \frac{dp_2 p_2^2}{(2\pi)^3 2E_2} \int_0^{2\pi} d\phi \int_{-1}^1 d\cos\theta$$

$$\int_0^\infty \frac{dp_3 p_3^2}{(2\pi)^3 2E_3} \int \frac{d^3 p_4}{(2\pi)^3 2E_4} (2\pi)^4 \delta^{(4)} \left( p_1 + p_2 - p_3 - p_4 \right) \times F(p_i) .$$
(A.2)

The next step concerns dealing with the  $\delta$ . The spatial part is readily eliminated by the  $p_4$ -integration, and  $\delta(E_1 + E_2 - E_3 - E_4)$  remains. Here,  $E_4$  is a shorthand for

$$E_4 = \sqrt{m_4^2 + (\vec{p}_1 + \vec{p}_2 - \vec{p}_4)^2} \tag{A.3}$$

$$= (m_4^2 + p_1^2 + p_2^2 + p_3^3 + 2p_1p_2\cos\beta - 2p_1p_2\cos\beta - 2p_1p_3\cos\theta$$
(A.4)

$$-2p_2p_3(\sin\beta\sin\theta\cos\phi + \cos\beta\cos\theta))^{1/2}.$$
 (A.5)

The change variables in the  $\delta$ -distribution,

$$\delta(E_1 + E_2 - E_3 - E_4) = \frac{E_1 + E_2 - E_3}{2p_2 p_3 \sin \beta \sin \theta} \delta(\cos \phi - \cos \phi_c), \qquad (A.6)$$

where

$$\cos \phi_c = \frac{m_1^2 + m_2^2 + m_3^2 - m_4^2 + 2(E_1 E_2 - E_1 E_3 - E_2 E_3) - 2p_1 p_2 \cos \beta}{2p_2 p_3 \sin \beta \sin \theta}$$
(A.7)

The integral over  $\phi$  is symmetric around  $\phi = \pi$ , so we replace  $\int_0^{2\pi} d\phi = 2 \int_0^{\pi} d\phi$ . All combined, we arrive at

$$\mathcal{C}_{(F)} = 4(2\pi)^4 \int_0^\infty \frac{dp_1 p_1^2}{(2\pi)^3 2E_1} \int_0^\infty \frac{dp_2 p_2^2}{(2\pi)^3 2E_2} \int_0^\infty \frac{dp_3 p_3^2}{(2\pi)^3 2E_3} \int_{-1}^1 d\cos\beta \int_{-1}^1 d\cos\beta \times \frac{1}{2E_4} \frac{E_1 + E_2 - E_3}{2p_2 p_3 \sin\beta \sin\theta} \times \Theta(0 \leqslant \cos^2\phi_c \leqslant 1) \times F(\vec{p}_1, \vec{p}_2, \vec{p}_3, \vec{p}_4),,$$
(A.8)

We understand  $E_4$  and  $\vec{p}_4$  as functions of the remaining integration variables defined by the above relations, and note that  $\cos \phi = \cos \phi_c$  holds.

The integrations  $d \cos \beta$  and  $d \cos \theta$  are well suited for Monte Carlo integration. We perform a change of variables,  $p_i = -\Lambda_i \log x_i$ , where  $x_i$  is the new integration variable. The dimensional constant  $\Lambda_i$  can be chosen freely, but we note that we found good convergence for  $\Lambda_i = \mathcal{O}(1 - 10) T_{\text{SM}}$  (see also Ref. [218]). Eq. A.8 is the collision integral implemented in our code.

#### A.1.2 $1 \rightarrow 2$ processes

We reduce the 9-dimensional integral to 2, which could also be implemented with traditional numerical integration. The steps are similar to the previous case.

Again, we chose  $\vec{p}_1 = p_1(0,0,1)^T$ , and  $\vec{p}_1$  and  $\vec{p}_2$  form a plane. We can write  $\vec{p}_2 = p_2(\sin\theta,0,\cos\theta)^T$ . As before, the spatial part of the  $\delta$ -distribution eliminates the  $d^3p_3$  integration. Momentum conservation now enforced, we have  $E_3 = \sqrt{m_3^2 + (\vec{p}_1 - \vec{p}_2)^2}$ . After changing variables in the remaining energy conserving  $\delta$ -distribution to an angular relation  $\delta(\cos\theta - \cos\theta_c)$ , where now

$$\cos \theta_c = \frac{m_3^2 + p_1^2 + p_2^2 - (E_1 - E_2)^2}{2p_1 p_2},$$
(A.9)

Using an indicator function  $\Theta(0 \le \cos^2 \phi \le 1)$ , we restrict integration to physically allowed kinematics, but explicit bounds could be derived in principle. We find for the final collision

integral

$$C_{(F)} = 8\pi^2 \int_0^\infty \frac{dp_1 p_1^2}{(2\pi)^3 2E_1} \int_0^\infty \frac{dp_2 p_2^2}{(2\pi)^3 2E_2} \times \frac{1}{2E_3} \frac{E_3}{p_1 p_2} \times F(p_i). \tag{A.10}$$

The remaining integrations make use of the same variable transformation as before, i.e. substituting  $p_i = -\Lambda_i \log x_i$ .

## Appendix B

## Diracon-charged lepton interactions

We follow the notation of Ref. [262], where the original computation for general interactions of charged leptons and a Majoron generated at the loop-level were discussed. Here, we sketch the analogous results for charged lepton interactions with a Diracon.

The general interaction is written as [263]

$$\mathcal{L}_{\ell\ell\mathcal{D}} = \mathcal{D}\,\bar{\ell}_{\beta} \left[ S^{\beta\alpha} P_L + \left( S^{\alpha\beta} \right)^* P_R \right] \ell_{\alpha} \,. \tag{B.1}$$

We write  $P_{L,R} = \frac{1}{2} (1 \mp \gamma_5)$  for the usual chiral projection operators, and denote the charged leptons as  $\ell_{\alpha,\beta}$ , where the index indicates the fermion generation. The matrix S has contributions from both, the Z and W bosons, which we label  $\Gamma_Z$  and  $L_W$ , respectively. Thus,

$$S^{\beta\alpha} = \frac{1}{8\pi^2} \left( \delta^{\beta\alpha} \, \Gamma_Z^{\alpha} + L_W^{\beta\alpha} \right) \,, \tag{B.2}$$

giving rise to both flavor conserving and flavor violating terms.

In the following, we write  $M_{\ell} = \text{diag}\left(m_{\ell_e}, m_{\ell_{\mu}}, m_{\ell_{\tau}}\right)$  for the charged lepton mass matrix, and we write the Lagrangian terms coupling the Diracon to neutrinos in the flavor basis with corresponding Yukawa matrix  $\mathcal{Y}$  as

$$\mathcal{L} \subset \mathcal{D} \left( \bar{\nu}_L \quad \bar{N}_L \right) \mathcal{Y} \begin{pmatrix} \nu_R \\ N_R \end{pmatrix} + \text{h.c.},$$
 (B.3)

or,

$$\mathcal{L} \subset \mathcal{D}\,\bar{n}\left(U_L^{\dagger}\,\mathcal{Y}\,U_R\,P_R + U_R^{\dagger}\,\mathcal{Y}^{\dagger}\,U_L\,P_L\right)n\,,\tag{B.4}$$

where n contains all neutral leptons  $\nu$  and N. Written in this form, we have similar terms as in Ref. [262] and their results can readily be used by plugging in our definitions. The leading contributions to  $\Gamma_Z^{\alpha}$  and  $L_W^{\beta\alpha}$  are found, and we denote by  $\sum_{j\sim l}$  and  $\sum_{j\sim h}$  the sum over light and heavy neutral leptons. The leading contributions from W and Z are then given by

$$\Gamma_Z^{\alpha} \simeq -i \frac{m_{\ell_{\alpha}}}{6v^2} \operatorname{Im} \left[ \sum_{s=1}^3 \left( \Gamma_{ss} - 2\Delta_{ss} \right) \right],$$
(B.5)

$$L_W^{\beta\alpha} \simeq \frac{m_{\ell_\beta}}{12 v^2} \left[ \left( \Gamma_{\alpha\beta}^* + 8 \Gamma_{\beta\alpha} \right) - \left( 2 \Delta_{\alpha\beta}^* + 7 \Delta_{\beta\alpha} \right) \right] , \tag{B.6}$$

where  $\Gamma$  and  $\Delta$  are defined as follows:

$$\Gamma_{\beta\alpha} = \sum_{k,r} \mathcal{Y}_{kr} \mathcal{M}_{r\alpha}^{\dagger} \sum_{j \sim l} (U_L)_{\beta j} \left( U_L^{\dagger} \right)_{jk} , \qquad (B.7)$$

$$\Delta_{\beta\alpha} = \sum_{k,r} \mathcal{Y}_{kr} \left( \mathcal{M} \mathcal{M}^{\dagger} \right)_{\beta k} \sum_{j \sim h} \left( U_R \right)_{rj} m_j^{-1} \left( U_L^{\dagger} \right)_{j\alpha} . \tag{B.8}$$

Interactions between the Diracon and charged leptons at loop level are then fully determined from charged lepton masses, Diracon Yukawa interactions, and the mixing matrices.

## Acknowledgements

Pursuing a PhD in physics was a humbling and shaping experience, and I wish to thank the many people who were beside me on this journey. First of all, I would like to express my gratitude to my supervisor Manfred Lindner. For giving me to opportunity to do my doctoral studies at the Max-Planck-Institut für Kernphysik, but also for his role as mentor and guide, for his encouragement and his trust, and for all the advise and the many discussions – physics and sometimes beyond – that were a great personal enrichment for me.

I am very thankful to Joerg Jaeckel for agreeing to be my second examiner, and to Bjoern-Malte Schaefer and Loredana Gastaldo to be part of my defense committee.

Science is a cooperative endeavor and I wish to thank my collaborators for the things we achieved together. I want to thank in particular Salvador Centelles Chuliá, again Manfred Lindner, and Manibrata Sen not only for the collaboration, but also their roles as mentors during these projects. My thanks for the enriching collaboration also goes to Anirban Das, Antonio Herrero-Broccal, Volodymyr Takhistov, and Avelino Vicente. Although our project is not finished yet, I also want to thank Thomas Rink for the great collaboration thus far.

The unique and extraordinary environment of the Max-Planck-Institut für Kernphysik is, of course, only possible because of all the wonderful people there, and it has been a joy to meet you and spend time with you. Whether it is the scientific discussion, the somewhat less scientific discussion mostly over coffee, or the extracurricular activities – all the ingredients for a great time were there. Special thanks to my long time office mates, Paul Frederik Depta and Oliver Scholer, and to Frederik also my gratitude for his advise on all coding related things. Also to Thede de Boer for the many scientific and unscientific discussions we had.

Special thanks to my (successful) proofreaders for spotting even more typos after I convinced myself there should not have been any left: Salvador Centelles Chuliá, Paul Frederik Depta, Sophie Klett, Philipp Saake, Oliver Scholer, and Ann Cathrin Wesener.

I am extremely grateful to all the new friends I made here, and my flat mates, all of who made my transition to Heidelberg so smooth and made me find a new home here. To my friends from university and before, who are still part of my life although we do not share the same location anymore. Special thanks to Lukas for almost two decades of friendship.

My heartfelt gratitude also to my spectacular Gizem, who crashed into my life without a warning and just made everything so much better. I could not imagine being here now without you. Thank you for everything you have done for me, and all the support and your believe in me.

I cannot put in words my gratitude to my family for their support and all the opportunities the made possible. To my parents, Hubert and Brigitte, who laid the foundation for the path I later chose, and who always encouraged me on my journey and made sure I never lacked wanting. I could not wish for more. My sister Nina, for her open ears and her unwavering support and believe in me. Thank you!

- [1] Anirban Das et al. "Energy-dependent boosted dark matter from diffuse supernova neutrino background". In: JCAP 07 (2024), p. 045. DOI: 10.1088/1475-7516/2024/07/045. arXiv: 2403.15367 [hep-ph].
- [2] Tim Herbermann and Manfred Lindner. "Improved cosmological limits on Z' models with light right-handed neutrinos". In: accepted for publication in JCAP (May 2025). arXiv: 2505.04695 [hep-ph].
- [3] Salvador Centelles Chuliá et al. "Flavour and cosmological probes of Diracon models". In: accepted for publication in JHEP (June 2025). arXiv: 2506.06449 [hep-ph].
- [4] Tim Herbermann, Manfred Lindner, and Manibrata Sen. "Attenuation of cosmic ray electron boosted dark matter". In: *Phys. Rev. D* 110.12 (2024), p. 123023. DOI: 10.1103/PhysRevD.110.123023. arXiv: 2408.02721 [hep-ph].
- [5] Anirban Das et al. "Energy-dependent boosted DM from DSNB". In: PoS NOW2024 (2025), p. 014. DOI: 10.22323/1.473.0014.
- [6] Fred Hoyle. "Concluding Remarks". In: Proceedings of the Royal Society of London. Series A, Mathematical and Physical Sciences 301 (1967), pp. 171–176. DOI: 10.1098/rspa.1967.0199. URL: https://doi.org/10.1098/rspa.1967.0199.
- [7] C. L. Cowan et al. "Detection of the free neutrino: A Confirmation". In: *Science* 124 (1956), pp. 103-104. DOI: 10.1126/science.124.3212.103.
- [8] Raymond Davis Jr., Don S. Harmer, and Kenneth C. Hoffman. "Search for neutrinos from the sun". In: Phys. Rev. Lett. 20 (1968), pp. 1205–1209. DOI: 10.1103/PhysRevLett. 20.1205.
- [9] R. Davis. "A review of the Homestake solar neutrino experiment". In: Prog. Part. Nucl. Phys. 32 (1994), pp. 13–32. DOI: 10.1016/0146-6410(94)90004-3.
- [10] Y. Fukuda et al. "The Super-Kamiokande detector". In: Nucl. Instrum. Meth. A 501 (2003). Ed. by V. A. Ilyin, V. V. Korenkov, and D. Perret-Gallix, pp. 418–462. DOI: 10.1016/S0168-9002(03)00425-X.
- [11] S. Fukuda et al. "Solar B-8 and hep neutrino measurements from 1258 days of Super-Kamiokande data". In: *Phys. Rev. Lett.* 86 (2001), pp. 5651–5655. DOI: 10.1103/PhysRevLett.86.5651. arXiv: hep-ex/0103032.
- [12] S. Fukuda et al. "Determination of solar neutrino oscillation parameters using 1496 days of Super-Kamiokande I data". In: *Phys. Lett. B* 539 (2002), pp. 179–187. DOI: 10.1016/S0370-2693(02)02090-7. arXiv: hep-ex/0205075.

[13] J. Boger et al. "The Sudbury neutrino observatory". In: *Nucl. Instrum. Meth. A* 449 (2000), pp. 172–207. DOI: 10.1016/S0168-9002(99)01469-2. arXiv: nucl-ex/9910016.

- [14] Q. R. Ahmad et al. "Direct evidence for neutrino flavor transformation from neutral current interactions in the Sudbury Neutrino Observatory". In: *Phys. Rev. Lett.* 89 (2002), p. 011301. DOI: 10.1103/PhysRevLett.89.011301. arXiv: nucl-ex/0204008.
- [15] Y. Fukuda et al. "Evidence for oscillation of atmospheric neutrinos". In: *Phys. Rev. Lett.* 81 (1998), pp. 1562–1567. DOI: 10.1103/PhysRevLett.81.1562. arXiv: hep-ex/9807003.
- [16] Y. Ashie et al. "A Measurement of atmospheric neutrino oscillation parameters by SUPER-KAMIOKANDE I". In: *Phys. Rev. D* 71 (2005), p. 112005. DOI: 10.1103/PhysRevD.71.112005. arXiv: hep-ex/0501064.
- [17] Takaaki Kajita. "Nobel Lecture: Discovery of atmospheric neutrino oscillations". In: Rev. Mod. Phys. 88.3 (2016), p. 030501. DOI: 10.1103/RevModPhys.88.030501.
- [18] Arthur B. McDonald. "Nobel Lecture: The Sudbury Neutrino Observatory: Observation of flavor change for solar neutrinos". In: Rev. Mod. Phys. 88.3 (2016), p. 030502. DOI: 10.1103/RevModPhys.88.030502.
- [19] F. Ardellier et al. "Double Chooz: A Search for the neutrino mixing angle theta(13)". In: (June 2006). arXiv: hep-ex/0606025.
- [20] Y. Abe et al. "Indication of Reactor  $\bar{\nu}_e$  Disappearance in the Double Chooz Experiment". In: *Phys. Rev. Lett.* 108 (2012), p. 131801. DOI: 10.1103/PhysRevLett.108.131801. arXiv: 1112.6353 [hep-ex].
- [21] Xinheng Guo et al. "A Precision measurement of the neutrino mixing angle  $\theta_{13}$  using reactor antineutrinos at Daya-Bay". In: (Jan. 2007). arXiv: hep-ex/0701029.
- [22] F. P. An et al. "Observation of electron-antineutrino disappearance at Daya Bay". In: *Phys. Rev. Lett.* 108 (2012), p. 171803. DOI: 10.1103/PhysRevLett.108.171803. arXiv: 1203.1669 [hep-ex].
- [23] S. Abe et al. "Precision Measurement of Neutrino Oscillation Parameters with Kam-LAND". In: *Phys. Rev. Lett.* 100 (2008), p. 221803. DOI: 10.1103/PhysRevLett.100. 221803. arXiv: 0801.4589 [hep-ex].
- [24] K. Abe et al. "The T2K Experiment". In: *Nucl. Instrum. Meth. A* 659 (2011), pp. 106–135. DOI: 10.1016/j.nima.2011.06.067. arXiv: 1106.1238 [physics.ins-det].
- [25] K. Abe et al. "Measurements of neutrino oscillation parameters from the T2K experiment using  $3.6\times10^{21}$  protons on target". In: Eur. Phys. J. C 83.9 (2023), p. 782. DOI: 10.1140/epjc/s10052-023-11819-x. arXiv: 2303.03222 [hep-ex].
- [26] G. L. Fogli et al. "Global analysis of neutrino masses, mixings and phases: entering the era of leptonic CP violation searches". In: *Phys. Rev. D* 86 (2012), p. 013012. DOI: 10.1103/PhysRevD.86.013012. arXiv: 1205.5254 [hep-ph].
- [27] Ivan Esteban et al. "Global analysis of three-flavour neutrino oscillations: synergies and tensions in the determination of  $\theta_{23}$ ,  $\delta_{CP}$ , and the mass ordering". In: *JHEP* 01 (2019), p. 106. DOI: 10.1007/JHEP01(2019)106. arXiv: 1811.05487 [hep-ph].

[28] P. F. de Salas et al. "2020 global reassessment of the neutrino oscillation picture". In: *JHEP* 02 (2021), p. 071. DOI: 10.1007/JHEP02(2021)071. arXiv: 2006.11237 [hep-ph].

- [29] N. Ackermann et al. "First observation of reactor antineutrinos by coherent scattering". In: (Jan. 2025). arXiv: 2501.05206 [hep-ex].
- [30] D. Akimov et al. "Observation of Coherent Elastic Neutrino-Nucleus Scattering". In: Science 357.6356 (2017), pp. 1123–1126. DOI: 10.1126/science.aao0990. arXiv: 1708.01294 [nucl-ex].
- [31] Fengpeng An et al. "Neutrino Physics with JUNO". In: *J. Phys. G* 43.3 (2016), p. 030401. DOI: 10.1088/0954-3899/43/3/030401. arXiv: 1507.05613 [physics.ins-det].
- [32] K. Abe et al. "Hyper-Kamiokande Design Report". In: (May 2018). arXiv: 1805.04163 [physics.ins-det].
- [33] R. Acciarri et al. "Long-Baseline Neutrino Facility (LBNF) and Deep Underground Neutrino Experiment (DUNE): Conceptual Design Report, Volume 2: The Physics Program for DUNE at LBNF". In: (Dec. 2015). arXiv: 1512.06148 [physics.ins-det].
- [34] John F. Beacom. "The Diffuse Supernova Neutrino Background". In: *Ann. Rev. Nucl. Part. Sci.* 60 (2010), pp. 439–462. DOI: 10.1146/annurev.nucl.010909.083331. arXiv: 1004.3311 [astro-ph.HE].
- [35] Shin'ichiro Ando et al. "Diffuse neutrino background from past core-collapse super-novae". In: June 2023. arXiv: 2306.16076 [astro-ph.HE].
- [36] K. Hirata et al. "Observation of a Neutrino Burst from the Supernova SN 1987a". In: Phys. Rev. Lett. 58 (1987). Ed. by K. C. Wali, pp. 1490–1493. DOI: 10.1103/PhysRevLett.58.1490.
- [37] R. M. Bionta et al. "Observation of a Neutrino Burst in Coincidence with Supernova SN 1987a in the Large Magellanic Cloud". In: *Phys. Rev. Lett.* 58 (1987), p. 1494. DOI: 10.1103/PhysRevLett.58.1494.
- [38] Alessandro Mirizzi et al. "Supernova Neutrinos: Production, Oscillations and Detection". In: Riv. Nuovo Cim. 39.1-2 (2016), pp. 1-112. DOI: 10.1393/ncr/i2016-10120-8. arXiv: 1508.00785 [astro-ph.HE].
- [39] B. P. Abbott et al. "Multi-messenger Observations of a Binary Neutron Star Merger". In: Astrophys. J. Lett. 848.2 (2017), p. L12. DOI: 10.3847/2041-8213/aa91c9. arXiv: 1710.05833 [astro-ph.HE].
- [40] M. Abdul Karim et al. "DESI DR2 Results II: Measurements of Baryon Acoustic Oscillations and Cosmological Constraints". In: (Mar. 2025). arXiv: 2503.14738 [astro-ph.CO].
- [41] Max Aker et al. "Direct neutrino-mass measurement based on 259 days of KATRIN data". In: Science 388.6743, adq9592 (2025). DOI: 10.1126/science.adq9592. arXiv: 2406.13516 [nucl-ex].

[42] N. Aghanim et al. "Planck 2018 results. VI. Cosmological parameters". In: Astron. Astro-phys. 641 (2020). [Erratum: Astron. Astrophys. 652, C4 (2021)], A6. DOI: 10.1051/0004-6361/201833910. arXiv: 1807.06209 [astro-ph.C0].

- [43] Kevork N. Abazajian and Julian Heeck. "Observing Dirac neutrinos in the cosmic microwave background". In: *Phys. Rev. D* 100 (2019), p. 075027. DOI: 10.1103/PhysRevD. 100.075027. arXiv: 1908.03286 [hep-ph].
- [44] Erminia Calabrese et al. "The Atacama Cosmology Telescope: DR6 Constraints on Extended Cosmological Models". In: (Mar. 2025). arXiv: 2503.14454 [astro-ph.C0].
- [45] Thibaut Louis et al. "The Atacama Cosmology Telescope: DR6 Power Spectra, Likelihoods and ΛCDM Parameters". In: (Mar. 2025). arXiv: 2503.14452 [astro-ph.C0].
- [46] Tsung-Han Yeh et al. "Probing physics beyond the standard model: limits from BBN and the CMB independently and combined". In: *JCAP* 10 (2022), p. 046. DOI: 10.1088/1475-7516/2022/10/046. arXiv: 2207.13133 [astro-ph.CO].
- [47] Brian D. Fields et al. "Big-Bang Nucleosynthesis after Planck". In: *JCAP* 03 (2020). [Erratum: JCAP 11, E02 (2020)], p. 010. DOI: 10.1088/1475-7516/2020/03/010. arXiv: 1912.01132 [astro-ph.CO].
- [48] Julien Froustey, Cyril Pitrou, and Maria Cristina Volpe. "Neutrino decoupling including flavour oscillations and primordial nucleosynthesis". In: *JCAP* 12 (2020), p. 015. DOI: 10.1088/1475-7516/2020/12/015. arXiv: 2008.01074 [hep-ph].
- [49] Miguel Escudero Abenza. "Precision early universe thermodynamics made simple:  $N_{\rm eff}$  and neutrino decoupling in the Standard Model and beyond". In: JCAP 05 (2020), p. 048. DOI: 10.1088/1475-7516/2020/05/048. arXiv: 2001.04466 [hep-ph].
- [50] Pablo F. de Salas and Sergio Pastor. "Relic neutrino decoupling with flavour oscillations revisited". In: JCAP 07 (2016), p. 051. DOI: 10.1088/1475-7516/2016/07/051. arXiv: 1606.06986 [hep-ph].
- [51] Kensuke Akita and Masahide Yamaguchi. "A precision calculation of relic neutrino decoupling". In: JCAP 08 (2020), p. 012. DOI: 10.1088/1475-7516/2020/08/012. arXiv: 2005.07047 [hep-ph].
- [52] J. Schechter and J. W. F. Valle. "Neutrinoless Double beta Decay in SU(2) x U(1) Theories". In: *Phys. Rev. D* 25 (1982), p. 2951. DOI: 10.1103/PhysRevD.25.2951.
- [53] Frank T. Avignone III, Steven R. Elliott, and Jonathan Engel. "Double Beta Decay, Majorana Neutrinos, and Neutrino Mass". In: *Rev. Mod. Phys.* 80 (2008), pp. 481–516. DOI: 10.1103/RevModPhys.80.481. arXiv: 0708.1033 [nucl-ex].
- [54] Boris Kayser. "Majorana Neutrinos and their Electromagnetic Properties". In: *Phys. Rev. D* 26 (1982), p. 1662. DOI: 10.1103/PhysRevD.26.1662.
- [55] Peter Minkowski. " $\mu \to e \gamma$  at a Rate of One Out of 10<sup>9</sup> Muon Decays?" In: *Phys. Lett.* B 67 (1977), pp. 421–428. DOI: 10.1016/0370-2693(77)90435-X.
- [56] S. L. Glashow. "The Future of Elementary Particle Physics". In: NATO Sci. Ser. B 61 (1980). Ed. by Maurice Lévy et al., p. 687. DOI: 10.1007/978-1-4684-7197-7\_15.

[57] Murray Gell-Mann, Pierre Ramond, and Richard Slansky. "Complex Spinors and Unified Theories". In: Conf. Proc. C 790927 (1979), pp. 315–321. arXiv: 1306.4669 [hep-th].

- [58] Tsutomu Yanagida. "Horizontal gauge symmetry and masses of neutrinos". In: *Conf. Proc. C* 7902131 (1979). Ed. by Osamu Sawada and Akio Sugamoto, pp. 95–99.
- [59] M. Magg and C. Wetterich. "Neutrino Mass Problem and Gauge Hierarchy". In: Phys. Lett. B 94 (1980), pp. 61–64. DOI: 10.1016/0370-2693(80)90825-4.
- [60] T. P. Cheng and Ling-Fong Li. "Neutrino Masses, Mixings and Oscillations in SU(2) x U(1) Models of Electroweak Interactions". In: *Phys. Rev. D* 22 (1980), p. 2860. DOI: 10.1103/PhysRevD.22.2860.
- [61] George Lazarides, Q. Shafi, and C. Wetterich. "Proton Lifetime and Fermion Masses in an SO(10) Model". In: Nucl. Phys. B 181 (1981), pp. 287–300. DOI: 10.1016/0550-3213(81)90354-0.
- [62] Rabindra N. Mohapatra and Goran Senjanovic. "Neutrino Masses and Mixings in Gauge Models with Spontaneous Parity Violation". In: *Phys. Rev. D* 23 (1981), p. 165. DOI: 10.1103/PhysRevD.23.165.
- [63] Robert Foot et al. "Seesaw Neutrino Masses Induced by a Triplet of Leptons". In: Z. Phys. C 44 (1989), p. 441. DOI: 10.1007/BF01415558.
- [64] Salvador Centelles Chuliá, Rahul Srivastava, and José W. F. Valle. "CP violation from flavor symmetry in a lepton quarticity dark matter model". In: *Phys. Lett. B* 761 (2016), pp. 431–436. DOI: 10.1016/j.physletb.2016.08.028. arXiv: 1606.06904 [hep-ph].
- [65] Salvador Centelles Chuliá, Rahul Srivastava, and José W. F. Valle. "Generalized Bottom-Tau unification, neutrino oscillations and dark matter: predictions from a lepton quarticity flavor approach". In: *Phys. Lett. B* 773 (2017), pp. 26–33. DOI: 10.1016/j.physletb. 2017.07.065. arXiv: 1706.00210 [hep-ph].
- [66] Cesar Bonilla et al. "Dark matter stability and Dirac neutrinos using only Standard Model symmetries". In: *Phys. Rev. D* 101.3 (2020), p. 033011. DOI: 10.1103/PhysRevD. 101.033011. arXiv: 1812.01599 [hep-ph].
- [67] Salvador Centelles Chuliá, Rahul Srivastava, and José W. F. Valle. "Seesaw Dirac neutrino mass through dimension-six operators". In: *Phys. Rev. D* 98.3 (2018), p. 035009. DOI: 10.1103/PhysRevD.98.035009. arXiv: 1804.03181 [hep-ph].
- [68] Salvador Centelles Chuliá et al. "Systematic classification of two loop d=4 Dirac neutrino mass models and the Diracness-dark matter stability connection". In: *JHEP* 10 (2019), p. 093. DOI: 10.1007/JHEP10(2019)093. arXiv: 1907.08630 [hep-ph].
- [69] Eduardo Peinado et al. "Dirac neutrinos from PecceiQuinn symmetry: A fresh look at the axion". In: Mod. Phys. Lett. A 35.21 (2020), p. 2050176. DOI: 10.1142/S021773232050176X. arXiv: 1910.02961 [hep-ph].
- [70] Zhi-Long Han and Weijian Wang. "Z' Portal Dark Matter in B-L Scotogenic Dirac Model". In: Eur. Phys. J. C 78.10 (2018), p. 839. DOI: 10.1140/epjc/s10052-018-6308-9. arXiv: 1805.02025 [hep-ph].

[71] Weijian Wang et al. "The B-L Scotogenic Models for Dirac Neutrino Masses". In: Eur. Phys. J. C 77.12 (2017), p. 889. DOI: 10.1140/epjc/s10052-017-5446-9. arXiv: 1705.00414 [hep-ph].

- [72] Debasish Borah and Arnab Dasgupta. "Naturally Light Dirac Neutrino in Left-Right Symmetric Model". In: JCAP 06 (2017), p. 003. DOI: 10.1088/1475-7516/2017/06/003. arXiv: 1702.02877 [hep-ph].
- [73] Sudip Jana, P. K. Vishnu, and Shaikh Saad. "Minimal realizations of Dirac neutrino mass from generic one-loop and two-loop topologies at d=5". In: JCAP 04 (2020), p. 018. DOI: 10.1088/1475-7516/2020/04/018. arXiv: 1910.09537 [hep-ph].
- [74] Sudip Jana, P. K. Vishnu, and Shaikh Saad. "Minimal dirac neutrino mass models from U(1)<sub>R</sub> gauge symmetry and leftright asymmetry at colliders". In: *Eur. Phys. J. C* 79.11 (2019), p. 916. DOI: 10.1140/epjc/s10052-019-7441-9. arXiv: 1904.07407 [hep-ph].
- [75] Julian Calle, Diego Restrepo, and Óscar Zapata. "Dirac neutrino mass generation from a Majorana messenger". In: *Phys. Rev. D* 101.3 (2020), p. 035004. DOI: 10.1103/PhysRevD. 101.035004. arXiv: 1909.09574 [hep-ph].
- [76] Dibyendu Nanda and Debasish Borah. "Connecting Light Dirac Neutrinos to a Multi-component Dark Matter Scenario in Gauged B-L Model". In: Eur. Phys. J. C 80.6 (2020), p. 557. DOI: 10.1140/epjc/s10052-020-8122-4. arXiv: 1911.04703 [hep-ph].
- [77] Ernest Ma. "Two-loop  $Z_4$  Dirac neutrino masses and mixing, with self-interacting dark matter". In: *Nucl. Phys. B* 946 (2019), p. 114725. DOI: 10.1016/j.nuclphysb.2019. 114725. arXiv: 1907.04665 [hep-ph].
- [78] Ernest Ma. "Scotogenic cobimaximal Dirac neutrino mixing from  $\Delta(27)$  and  $U(1)_{\chi}$ ". In: Eur. Phys. J. C 79.11 (2019), p. 903. DOI: 10.1140/epjc/s10052-019-7440-x. arXiv: 1905.01535 [hep-ph].
- [79] S. S. Correia, R. G. Felipe, and F. R. Joaquim. "Dirac neutrinos in the 2HDM with restrictive Abelian symmetries". In: *Phys. Rev. D* 100.11 (2019), p. 115008. DOI: 10. 1103/PhysRevD.100.115008. arXiv: 1909.00833 [hep-ph].
- [80] Shaikh Saad. "Simplest Radiative Dirac Neutrino Mass Models". In: Nucl. Phys. B 943 (2019), p. 114636. DOI: 10.1016/j.nuclphysb.2019.114636. arXiv: 1902.07259 [hep-ph].
- [81] Ernest Ma. "Scotogenic  $U(1)_{\chi}$  Dirac neutrinos". In: *Phys. Lett. B* 793 (2019), pp. 411–414. DOI: 10.1016/j.physletb.2019.05.006. arXiv: 1901.09091 [hep-ph].
- [82] Salvador Centelles Chuliá, Rahul Srivastava, and Avelino Vicente. "The inverse seesaw family: Dirac and Majorana". In: *JHEP* 03 (2021), p. 248. DOI: 10.1007/JHEP03(2021) 248. arXiv: 2011.06609 [hep-ph].
- [83] Salvador Centelles Chuliá et al. "Natural axion model from flavour". In: JHEP 09 (2020),
   p. 137. DOI: 10.1007/JHEP09(2020)137. arXiv: 2005.13541 [hep-ph].

[84] Shu-Yuan Guo and Zhi-Long Han. "Observable Signatures of Scotogenic Dirac Model". In: *JHEP* 12 (2020), p. 062. DOI: 10.1007/JHEP12(2020)062. arXiv: 2005.08287 [hep-ph].

- [85] Leon M. G. de la Vega, Newton Nath, and Eduardo Peinado. "Dirac neutrinos from Peccei-Quinn symmetry: two examples". In: *Nucl. Phys. B* 957 (2020), p. 115099. DOI: 10.1016/j.nuclphysb.2020.115099. arXiv: 2001.01846 [hep-ph].
- [86] Happy Borgohain and Debasish Borah. "Survey of Texture Zeros with Light Dirac Neutrinos". In: *J. Phys. G* 48.7 (2021), p. 075005. DOI: 10.1088/1361-6471/abde9b. arXiv: 2007.06249 [hep-ph].
- [87] Julio Leite et al. "Scotogenic dark matter and Dirac neutrinos from unbroken gauged B L symmetry". In: *Phys. Lett. B* 807 (2020), p. 135537. DOI: 10.1016/j.physletb. 2020.135537. arXiv: 2003.02950 [hep-ph].
- [88] Salvador Centelles Chuliá. "Theory and phenomenology of Dirac neutrinos". In: (Oct. 2021). arXiv: 2110.15755 [hep-ph].
- [89] Nicolás Bernal and Diego Restrepo. "Anomaly-free Abelian gauge symmetries with Dirac seesaws". In: Eur. Phys. J. C 81.12 (2021), p. 1104. DOI: 10.1140/epjc/s10052-021-09918-8. arXiv: 2108.05907 [hep-ph].
- [90] Subhasmita Mishra et al. "Scalar dark matter and radiative Dirac neutrino mass in an extended U(1)B-L model". In: *Nucl. Phys. B* 981 (2022), p. 115855. DOI: 10.1016/j.nuclphysb.2022.115855. arXiv: 2112.12569 [hep-ph].
- [91] Anirban Biswas, Debasish Borah, and Dibyendu Nanda. "Light Dirac neutrino portal dark matter with observable  $\Delta$ Neff". In: JCAP 10 (2021), p. 002. DOI: 10.1088/1475-7516/2021/10/002. arXiv: 2103.05648 [hep-ph].
- [92] Devabrat Mahanta and Debasish Borah. "Low scale Dirac leptogenesis and dark matter with observable  $\Delta N_{\rm eff}$ ". In: Eur. Phys. J. C 82.5 (2022), p. 495. DOI: 10.1140/epjc/s10052-022-10443-5. arXiv: 2101.02092 [hep-ph].
- [93] Nilavjyoti Hazarika and Kalpana Bora. "A new viable mass region of Dark matter and Dirac neutrino mass generation in a scotogenic extension of SM". In: (May 2022). arXiv: 2205.06003 [hep-ph].
- [94] Salvador Centelles Chuliá, Rahul Srivastava, and Sushant Yadav. "CDF-II W boson mass in the Dirac Scotogenic model". In: *Mod. Phys. Lett. A* 38.7 (2023), p. 29. DOI: 10.1142/S0217732323500499. arXiv: 2206.11903 [hep-ph].
- [95] Maximilian Berbig. "Freeze-In of radiative keV-scale neutrino dark matter from a new  $U(1)_{B-L}$ ". In: *JHEP* 09 (2022), p. 101. DOI: 10.1007/JHEP09(2022)101. arXiv: 2203.04276 [hep-ph].
- [96] Siddharth P. Maharathy, Manimala Mitra, and Agnivo Sarkar. "An alternate left-right symmetric model with Dirac neutrinos". In: *Eur. Phys. J. C* 83.6 (2023), p. 480. DOI: 10.1140/epjc/s10052-023-11653-1. arXiv: 2211.09675 [hep-ph].

[97] Talal Ahmed Chowdhury, Md. Ehsanuzzaman, and Shaikh Saad. "Dark Matter and  $(g-2)_{\mu,e}$  in radiative Dirac neutrino mass models". In: (Mar. 2022). arXiv: 2203.14983 [hep-ph].

- [98] Anirban Biswas et al. "Freeze-in Dark Matter and  $\Delta N_{eff}$  via Light Dirac Neutrino Portal". In: (May 2022). arXiv: 2205.01144 [hep-ph].
- [99] Maximilian Berbig. "Type II Dirac seesaw portal to the mirror sector: Connecting neutrino masses and a solution to the strong CP problem". In: *Phys. Rev. D* 106.11 (2022), p. 115018. DOI: 10.1103/PhysRevD.106.115018. arXiv: 2209.14246 [hep-ph].
- [100] Satyabrata Mahapatra et al. "Self-interacting dark matter and Dirac neutrinos via lepton quarticity". In: Phys. Rev. D 109.5 (2024), p. 055036. DOI: 10.1103/PhysRevD.109.055036. arXiv: 2312.12322 [hep-ph].
- [101] Debasish Borah et al. "Discrete dark matter with light Dirac neutrinos". In: (June 2024). arXiv: 2406.17861 [hep-ph].
- [102] Salvador Centelles Chuliá, Rahul Srivastava, and Sushant Yadav. "Comprehensive phenomenology of the Dirac Scotogenic Model: Novel low-mass dark matter". In: *JHEP* 04 (2025), p. 038. DOI: 10.1007/JHEP04(2025)038. arXiv: 2409.18513 [hep-ph].
- [103] Labh Singh, Monal Kashav, and Surender Verma. "Minimal Type-I Dirac seesaw and Leptogenesis under  $A_4$  modular invariance". In: (May 2024). arXiv: 2405.07165 [hep-ph].
- [104] Ranjeet Kumar et al. "Dirac Scoto Inverse-Seesaw from  $A_4$  Flavor Symmetry". In: (May 2025). arXiv: 2505.01407 [hep-ph].
- [105] A. Batra et al. "Axion framework with color-mediated Dirac neutrino masses". In: (Jan. 2025). arXiv: 2501.13156 [hep-ph].
- [106] Debasish Borah, Pritam Das, and Dibyendu Nanda. "Observable  $\Delta$ Neff in Dirac scotogenic model". In: Eur. Phys. J. C 84.2 (2024), p. 140. DOI: 10.1140/epjc/s10052-024-12440-2. arXiv: 2211.13168 [hep-ph].
- [107] Anirban Biswas, Dilip Kumar Ghosh, and Dibyendu Nanda. "Concealing Dirac neutrinos from cosmic microwave background". In: *JCAP* 10 (2022), p. 006. DOI: 10.1088/1475-7516/2022/10/006. arXiv: 2206.13710 [hep-ph].
- [108] Maximilian Berbig. "S.M.A.S.H.E.D.: Standard Model Axion Seesaw Higgs inflation Extended for Dirac neutrinos". In: JCAP 11 (2022), p. 042. DOI: 10.1088/1475-7516/ 2022/11/042. arXiv: 2207.08142 [hep-ph].
- [109] Anirban Biswas et al. "Phenomenology of Dirac neutrino EFTs up to dimension six". In: (Nov. 2024). arXiv: 2411.17414 [hep-ph].
- [110] Debasish Borah et al. "Singlet-doublet fermion Dark Matter with Dirac neutrino mass, (g-2) and  $\Delta N_{eff}$ ". In: *JHEP* 05 (2024), p. 096. DOI: 10.1007/JHEP05(2024)096. arXiv: 2310.03721 [hep-ph].
- [111] Zafri Ahmed Borboruah et al. "Minimal Dirac seesaw dark matter". In: (Dec. 2024). arXiv: 2412.12267 [hep-ph].

[112] Debasish Borah et al. "Effective theory of light Dirac neutrino portal dark matter with observable  $\Delta N_{\rm eff}$ ". In: (Feb. 2025). arXiv: 2502.10318 [hep-ph].

- [113] Julian Heeck. "Unbroken B L symmetry". In: *Phys. Lett. B* 739 (2014), pp. 256–262. DOI: 10.1016/j.physletb.2014.10.067. arXiv: 1408.6845 [hep-ph].
- [114] Peter Adshead, Pranjal Ralegankar, and Jessie Shelton. "Dark radiation constraints on portal interactions with hidden sectors". In: *JCAP* 09 (2022), p. 056. DOI: 10.1088/1475-7516/2022/09/056. arXiv: 2206.13530 [hep-ph].
- [115] Debasish Borah et al. "Collider and CMB complementarity of leptophilic dark matter with light Dirac neutrinos". In: *JHEP* 01 (2025), p. 074. DOI: 10.1007/JHEP01(2025)074. arXiv: 2408.14548 [hep-ph].
- [116] Dilip Kumar Ghosh et al. "Neff at CMB challenges U(1)X light gauge boson scenarios".
  In: Phys. Rev. D 110.7 (2024), p. 075032. DOI: 10.1103/PhysRevD.110.075032. arXiv: 2404.10077 [hep-ph].
- [117] Deanna C. Hooper and Matteo Lucca. "Hints of dark matter-neutrino interactions in Lyman- $\alpha$  data". In: *Phys. Rev. D* 105.10 (2022), p. 103504. DOI: 10.1103/PhysRevD. 105.103504. arXiv: 2110.04024 [astro-ph.CO].
- [118] William Giarè et al. "Hints of neutrino dark matter scattering in the CMB? Constraints from the marginalized and profile distributions". In: *Phys. Rev. D* 109.6 (2024), p. 063516. DOI: 10.1103/PhysRevD.109.063516. arXiv: 2311.09116 [astro-ph.CO].
- [119] Philippe Brax et al. "Extended analysis of neutrino-dark matter interactions with small-scale CMB experiments". In: *Phys. Dark Univ.* 42 (2023), p. 101321. DOI: 10.1016/j.dark.2023.101321. arXiv: 2305.01383 [astro-ph.CO].
- [120] Lei Zu et al. "Can  $\nu$ DM interactions solve the  $S_8$  discrepancy?" In: (Jan. 2025). arXiv: 2501.13785 [astro-ph.CO].
- [121] Torsten Bringmann and Maxim Pospelov. "Novel direct detection constraints on light dark matter". In: *Phys. Rev. Lett.* 122.17 (2019), p. 171801. DOI: 10.1103/PhysRevLett. 122.171801. arXiv: 1810.10543 [hep-ph].
- [122] Anirban Das and Manibrata Sen. "Boosted dark matter from diffuse supernova neutrinos". In: *Phys. Rev. D* 104.7 (2021), p. 075029. DOI: 10.1103/PhysRevD.104.075029. arXiv: 2104.00027 [hep-ph].
- [123] Valentina De Romeri et al. "XENONnT and LUX-ZEPLIN constraints on DSNB-boosted dark matter". In: JCAP 03 (2024), p. 028. DOI: 10.1088/1475-7516/2024/03/028. arXiv: 2309.04117 [hep-ph].
- [124] Yue Zhang. "Speeding Up Dark Matter With Solar Neutrinos". In: (Jan. 2020). arXiv: 2001.00948 [hep-ph].
- [125] Diptimoy Ghosh, Atanu Guha, and Divya Sachdeva. "Exclusion limits on dark matterneutrino scattering cross section". In: *Phys. Rev. D* 105.10 (2022), p. 103029. DOI: 10. 1103/PhysRevD.105.103029. arXiv: 2110.00025 [hep-ph].

[126] Yongsoo Jho et al. "Cosmic-Neutrino-Boosted Dark Matter ( $\nu$ BDM)". In: (Jan. 2021). arXiv: 2101.11262 [hep-ph].

- [127] Wei Chao, Tong Li, and Jiajun Liao. "Connecting Primordial Black Hole to boosted sub-GeV Dark Matter through neutrino". In: (Aug. 2021). arXiv: 2108.05608 [hep-ph].
- [128] Yen-Hsun Lin et al. "Searching for Afterglow: Light Dark Matter Boosted by Supernova Neutrinos". In: *Phys. Rev. Lett.* 130.11 (2023), p. 111002. DOI: 10.1103/PhysRevLett. 130.111002. arXiv: 2206.06864 [hep-ph].
- [129] Yen-Hsun Lin et al. "Signatures of afterglows from light dark matter boosted by supernova neutrinos in current and future large underground detectors". In: *Phys. Rev. D* 108.8 (2023), p. 083013. DOI: 10.1103/PhysRevD.108.083013. arXiv: 2307.03522 [hep-ph].
- [130] Yen-Hsun Lin and Meng-Ru Wu. "Supernova-Neutrino-Boosted Dark Matter from All Galaxies". In: *Phys. Rev. Lett.* 133.11 (2024), p. 111004. DOI: 10.1103/PhysRevLett. 133.111004. arXiv: 2404.08528 [hep-ph].
- [131] S. L. Glashow. "Partial Symmetries of Weak Interactions". In: Nucl. Phys. 22 (1961), pp. 579–588. DOI: 10.1016/0029-5582(61)90469-2.
- [132] Steven Weinberg. "A Model of Leptons". In: *Phys. Rev. Lett.* 19 (1967), pp. 1264–1266. DOI: 10.1103/PhysRevLett.19.1264.
- [133] Abdus Salam. "Weak and Electromagnetic Interactions". In: Conf. Proc. C 680519 (1968), pp. 367–377. DOI: 10.1142/9789812795915\_0034.
- [134] F. Englert and R. Brout. "Broken Symmetry and the Mass of Gauge Vector Mesons". In: *Phys. Rev. Lett.* 13 (1964). Ed. by J. C. Taylor, pp. 321–323. DOI: 10.1103/PhysRevLett. 13.321.
- [135] Peter W. Higgs. "Broken symmetries, massless particles and gauge fields". In: *Phys. Lett.* 12 (1964), pp. 132–133. DOI: 10.1016/0031-9163(64)91136-9.
- [136] Peter W. Higgs. "Broken Symmetries and the Masses of Gauge Bosons". In: *Phys. Rev. Lett.* 13 (1964). Ed. by J. C. Taylor, pp. 508–509. DOI: 10.1103/PhysRevLett.13.508.
- [137] Nicola Cabibbo. "Unitary Symmetry and Leptonic Decays". In: *Phys. Rev. Lett.* 10 (1963), pp. 531–533. DOI: 10.1103/PhysRevLett.10.531.
- [138] Makoto Kobayashi and Toshihide Maskawa. "CP Violation in the Renormalizable Theory of Weak Interaction". In: Prog. Theor. Phys. 49 (1973), pp. 652–657. DOI: 10.1143/PTP.49.652.
- [139] Manibrata Sen and Alexei Y. Smirnov. "Refractive neutrino masses, ultralight dark matter and cosmology". In: JCAP 01 (2024), p. 040. DOI: 10.1088/1475-7516/2024/ 01/040. arXiv: 2306.15718 [hep-ph].
- [140] A. Yu. Smirnov. "Solar neutrinos: Oscillations or No-oscillations?" In: (Sept. 2016). arXiv: 1609.02386 [hep-ph].
- [141] Evgeny K. Akhmedov. "Neutrino physics". In: *ICTP Summer School in Particle Physics*. June 1999, pp. 103–164. arXiv: hep-ph/0001264.

[142] B. Pontecorvo. "Inverse beta processes and nonconservation of lepton charge". In: Zh. Eksp. Teor. Fiz. 34 (1957), p. 247.

- [143] Ziro Maki, Masami Nakagawa, and Shoichi Sakata. "Remarks on the unified model of elementary particles". In: *Prog. Theor. Phys.* 28 (1962), pp. 870–880. DOI: 10.1143/PTP. 28.870.
- [144] S. Navas et al. "Review of particle physics". In: *Phys. Rev. D* 110.3 (2024), p. 030001. DOI: 10.1103/PhysRevD.110.030001.
- [145] Evgeny Akhmedov. "Quantum mechanics aspects and subtleties of neutrino oscillations". In: *International Conference on History of the Neutrino: 1930-2018*. Jan. 2019. arXiv: 1901.05232 [hep-ph].
- [146] Evgeny Kh. Akhmedov and Joachim Kopp. "Neutrino Oscillations: Quantum Mechanics vs. Quantum Field Theory". In: JHEP 04 (2010). [Erratum: JHEP 10, 052 (2013)], p. 008. DOI: 10.1007/JHEP04(2010)008. arXiv: 1001.4815 [hep-ph].
- [147] C. Giunti, C. W. Kim, and U. W. Lee. "When do neutrinos really oscillate?: Quantum mechanics of neutrino oscillations". In: *Phys. Rev. D* 44 (1991), pp. 3635–3640. DOI: 10.1103/PhysRevD.44.3635.
- [148] L. Wolfenstein. "Neutrino Oscillations in Matter". In: Phys. Rev. D 17 (1978), pp. 2369–2374. DOI: 10.1103/PhysRevD.17.2369.
- [149] S. P. Mikheyev and A. Yu. Smirnov. "Resonance Amplification of Oscillations in Matter and Spectroscopy of Solar Neutrinos". In: Sov. J. Nucl. Phys. 42 (1985), pp. 913–917.
- [150] Frank F. Deppisch, Martin Hirsch, and Heinrich Pas. "Neutrinoless Double Beta Decay and Physics Beyond the Standard Model". In: *J. Phys. G* 39 (2012), p. 124007. DOI: 10.1088/0954-3899/39/12/124007. arXiv: 1208.0727 [hep-ph].
- [151] Michael Duerr, Manfred Lindner, and Alexander Merle. "On the Quantitative Impact of the Schechter-Valle Theorem". In: *JHEP* 06 (2011), p. 091. DOI: 10.1007/JHEP06(2011) 091. arXiv: 1105.0901 [hep-ph].
- [152] Evgeny Akhmedov. "On chirality and chiral neutrino oscillations". In: (May 2025). arXiv: 2505.20982 [hep-ph].
- [153] A. Yu. Smirnov. "Chiral interactions, chiral states and "chiral neutrino oscillations"". In: (May 2025). arXiv: 2505.06116 [hep-ph].
- [154] Michael E. Peskin and Daniel V. Schroeder. An Introduction to quantum field theory. Reading, USA: Addison-Wesley, 1995. ISBN: 978-0-201-50397-5, 978-0-429-50355-9, 978-0-429-49417-8. DOI: 10.1201/9780429503559.
- [155] K. J. F. Gaemers, R. Gandhi, and J. m. Lattimer. "Neutrino Helicity Flips via Electroweak Interactions and SN1987A". In: Phys. Rev. D 40 (1989), p. 309. DOI: 10.1103/PhysRevD.40.309.
- [156] Raj Gandhi and Adam Burrows. "Massive Dirac neutrinos and the SN1987A signal".
   In: Phys. Lett. B 246 (1990). [Erratum: Phys.Lett.B 261, 519–520 (1991)], pp. 149–155.
   DOI: 10.1016/0370-2693(90)91323-4.

[157] Michael S. Turner. "Dirac neutrinos and SN1987A". In: Phys. Rev. D 45 (1992), pp. 1066–1075. DOI: 10.1103/PhysRevD.45.1066.

- [158] Steven Weinberg. "Baryon and Lepton Nonconserving Processes". In: *Phys. Rev. Lett.* 43 (1979), pp. 1566–1570. DOI: 10.1103/PhysRevLett.43.1566.
- [159] Salvador Centelles Chuliá, Antonio Herrero-Brocal, and Avelino Vicente. "The Type-I Seesaw family". In: (Apr. 2024). arXiv: 2404.15415 [hep-ph].
- [160] Evgeny K. Akhmedov et al. "Left-right symmetry breaking in NJL approach". In: *Phys. Lett. B* 368 (1996), pp. 270–280. DOI: 10.1016/0370-2693(95)01504-3. arXiv: hep-ph/9507275.
- [161] Evgeny K. Akhmedov et al. "Dynamical left-right symmetry breaking". In: *Phys. Rev.* D 53 (1996), pp. 2752–2780. DOI: 10.1103/PhysRevD.53.2752. arXiv: hep-ph/9509255.
- [162] Michal Malinsky, J. C. Romao, and J. W. F. Valle. "Novel supersymmetric SO(10) see-saw mechanism". In: *Phys. Rev. Lett.* 95 (2005), p. 161801. DOI: 10.1103/PhysRevLett. 95.161801. arXiv: hep-ph/0506296.
- [163] R. N. Mohapatra and J. W. F. Valle. "Neutrino Mass and Baryon Number Nonconservation in Superstring Models". In: *Phys. Rev. D* 34 (1986), p. 1642. DOI: 10.1103/PhysRevD.34.1642.
- [164] M. C. Gonzalez-Garcia and J. W. F. Valle. "Fast Decaying Neutrinos and Observable Flavor Violation in a New Class of Majoron Models". In: *Phys. Lett. B* 216 (1989), pp. 360–366. DOI: 10.1016/0370-2693(89)91131-3.
- [165] Sofiane M. Boucenna, Stefano Morisi, and José W. F. Valle. "The low-scale approach to neutrino masses". In: Adv. High Energy Phys. 2014 (2014), p. 831598. DOI: 10.1155/2014/831598. arXiv: 1404.3751 [hep-ph].
- [166] Edward W. Kolb and Michael S. Turner. The Early Universe. Vol. 69. Taylor and Francis, May 2019. ISBN: 978-0-429-49286-0, 978-0-201-62674-2. DOI: 10.1201/9780429492860.
- [167] David Silva Pereira et al. "Thermodynamics of the Primordial Universe". In: *Entropy* 26.11 (2024), p. 947. DOI: 10.3390/e26110947. arXiv: 2411.03018 [gr-qc].
- [168] J. Bernstein. KINETIC THEORY IN THE EXPANDING UNIVERSE. Cambridge Monographs on Mathematical Physics. Cambridge, U.K.: Cambridge University Press, 1988. ISBN: 978-0-511-56418-5. DOI: 10.1017/CB09780511564185.
- [169] G. Steigman, K. A. Olive, and D. N. Schramm. "Cosmological Constraints on Superweak Particles". In: Phys. Rev. Lett. 43 (4 July 1979), pp. 239–242. DOI: 10.1103/PhysRevLett.43.239. URL: https://link.aps.org/doi/10.1103/PhysRevLett.43.239.
- [170] A. D. Dolgov. "Neutrinos in cosmology". In: *Phys. Rept.* 370 (2002), pp. 333–535. DOI: 10.1016/S0370-1573(02)00139-4. arXiv: hep-ph/0202122.
- [171] A. D. Dolgov and Ya. B. Zeldovich. "Cosmology and elementary particles". In: *Rev. Mod. Phys.* 53 (1 Jan. 1981), pp. 1–41. DOI: 10.1103/RevModPhys.53.1. URL: https://link.aps.org/doi/10.1103/RevModPhys.53.1.

[172] M. Laine and M. Meyer. "Standard Model thermodynamics across the electroweak crossover". In: *JCAP* 07 (2015), p. 035. DOI: 10.1088/1475-7516/2015/07/035. arXiv: 1503.04935 [hep-ph].

- [173] Richard H. Cyburt et al. "Big Bang Nucleosynthesis: 2015". In: *Rev. Mod. Phys.* 88 (2016), p. 015004. DOI: 10.1103/RevModPhys.88.015004. arXiv: 1505.01076 [astro-ph.CO].
- [174] Zhen Hou et al. "How massless neutrinos affect the cosmic microwave background damping tail". In: *Phys. Rev. D* 87.8, 083008 (Apr. 2013), p. 083008. DOI: 10.1103/PhysRevD. 87.083008. arXiv: 1104.2333 [astro-ph.CO].
- [175] Julien Lesgourgues et al. Neutrino Cosmology. Cambridge University Press, Feb. 2013. ISBN: 978-1-108-70501-1, 978-1-139-60341-6.
- [176] Diego Blas, Julien Lesgourgues, and Thomas Tram. "The Cosmic Linear Anisotropy Solving System (CLASS) II: Approximation schemes". In: *JCAP* 07 (2011), p. 034. DOI: 10.1088/1475-7516/2011/07/034. arXiv: 1104.2933 [astro-ph.CO].
- [177] F. Ge et al. "Cosmology From CMB Lensing and Delensed EE Power Spectra Using 2019-2020 SPT-3G Polarization Data". In: (Nov. 2024). arXiv: 2411.06000 [astro-ph.CO].
- [178] Adrian Lee et al. "The Simons Observatory". In: Bulletin of the American Astronomical Society. Vol. 51. Sept. 2019, 147, p. 147. DOI: 10.48550/arXiv.1907.08284. arXiv: 1907.08284 [astro-ph.IM].
- [179] B. A. Benson et al. "SPT-3G: A Next-Generation Cosmic Microwave Background Polarization Experiment on the South Pole Telescope". In: *Proc. SPIE Int. Soc. Opt. Eng.* 9153 (2014), 91531P. DOI: 10.1117/12.2057305. arXiv: 1407.2973 [astro-ph.IM].
- [180] Kevork Abazajian et al. "CMB-S4 Science Case, Reference Design, and Project Plan". In: (July 2019). arXiv: 1907.04473 [astro-ph.IM].
- [181] Neelima Sehgal et al. "CMB-HD: An Ultra-Deep, High-Resolution Millimeter-Wave Survey Over Half the Sky". In: (June 2019). arXiv: 1906.10134 [astro-ph.CO].
- [182] Toni Bertólez-Martnez et al. "Origin of cosmological neutrino mass bounds: background versus perturbations". In: *JCAP* 06 (2025), p. 058. DOI: 10.1088/1475-7516/2025/06/058. arXiv: 2411.14524 [astro-ph.CO].
- [183] William Giarè et al. "Neutrino mass tension or suppressed growth rate of matter perturbations?" In: (July 2025). arXiv: 2507.01848 [astro-ph.CO].
- [184] Julien Lesgourgues and Sergio Pastor. "Massive neutrinos and cosmology". In: Phys. Rept. 429 (2006), pp. 307-379. DOI: 10.1016/j.physrep.2006.04.001. arXiv: astro-ph/0603494.
- [185] H. -Th. Janka. "Neutrino Emission from Supernovae". In: (Feb. 2017). DOI: 10.1007/978-3-319-21846-5\_4. arXiv: 1702.08713 [astro-ph.HE].

[186] Rafael F. Lang et al. "Supernova neutrino physics with xenon dark matter detectors: A timely perspective". In: *Phys. Rev. D* 94.10 (2016), p. 103009. DOI: 10.1103/PhysRevD. 94.103009. arXiv: 1606.09243 [astro-ph.HE].

- [187] Mathias Th. Keil, Georg G. Raffelt, and Hans-Thomas Janka. "Monte Carlo study of supernova neutrino spectra formation". In: *Astrophys. J.* 590 (2003), pp. 971–991. DOI: 10.1086/375130. arXiv: astro-ph/0208035.
- [188] Irene Tamborra et al. "High-resolution supernova neutrino spectra represented by a simple fit". In: *Phys. Rev. D* 86 (2012), p. 125031. DOI: 10.1103/PhysRevD.86.125031. arXiv: 1211.3920 [astro-ph.SR].
- [189] Amanda L. Baxter et al. "SNEWPY: A Data Pipeline from Supernova Simulations to Neutrino Signals". In: *Astrophys. J.* 925.2 (2022), p. 107. DOI: 10.3847/1538-4357/ac350f. arXiv: 2109.08188 [astro-ph.IM].
- [190] Amol S. Dighe and Alexei Yu. Smirnov. "Identifying the neutrino mass spectrum from the neutrino burst from a supernova". In: *Phys. Rev. D* 62 (2000), p. 033007. DOI: 10.1103/PhysRevD.62.033007. arXiv: hep-ph/9907423.
- [191] H. Zhang et al. "Supernova Relic Neutrino Search with Neutron Tagging at Super-Kamiokande-IV". In: *Astropart. Phys.* 60 (2015), pp. 41–46. DOI: 10.1016/j.astropartphys. 2014.05.004. arXiv: 1311.3738 [hep-ex].
- [192] Babak Abi et al. "Deep Underground Neutrino Experiment (DUNE), Far Detector Technical Design Report, Volume II: DUNE Physics". In: (Feb. 2020). arXiv: 2002.03005 [hep-ex].
- [193] Masayuki Harada. "First result of a search for Diffuse Supernova Neutrino Background in SK-Gd experiment". In: *PoS* ICRC2023 (2023), p. 1173. DOI: 10.22323/1.444.1173.
- [194] John F. Beacom and Mark R. Vagins. "GADZOOKS! Anti-neutrino spectroscopy with large water Cherenkov detectors". In: *Phys. Rev. Lett.* 93 (2004), p. 171101. DOI: 10. 1103/PhysRevLett.93.171101. arXiv: hep-ph/0309300.
- [195] Charles Simpson. "Physics Potential of Super-K Gd". In: PoS ICHEP2018 (2019), p. 008.
  DOI: 10.22323/1.340.0008.
- [196] K. Abe et al. "Diffuse supernova neutrino background search at Super-Kamiokande". In: Phys. Rev. D 104.12 (2021), p. 122002. DOI: 10.1103/PhysRevD.104.122002. arXiv: 2109.11174 [astro-ph.HE].
- [197] M. Askins et al. "THEIA: an advanced optical neutrino detector". In: Eur. Phys. J. C 80.5 (2020), p. 416. DOI: 10.1140/epjc/s10052-020-7977-8. arXiv: 1911.03501 [physics.ins-det].
- [198] Luca Pattavina, Nahuel Ferreiro Iachellini, and Irene Tamborra. "Neutrino observatory based on archaeological lead". In: *Phys. Rev. D* 102.6 (2020), p. 063001. DOI: 10.1103/PhysRevD.102.063001. arXiv: 2004.06936 [astro-ph.HE].

[199] Anna M. Suliga, John F. Beacom, and Irene Tamborra. "Towards probing the diffuse supernova neutrino background in all flavors". In: *Phys. Rev. D* 105.4 (2022), p. 043008. DOI: 10.1103/PhysRevD.105.043008. arXiv: 2112.09168 [astro-ph.HE].

- [200] Sebastian Baum, Francesco Capozzi, and Shunsaku Horiuchi. "Rocks, water, and noble liquids: Unfolding the flavor contents of supernova neutrinos". In: *Phys. Rev. D* 106.12 (2022), p. 123008. DOI: 10.1103/PhysRevD.106.123008. arXiv: 2203.12696 [hep-ph].
- [201] Klaes Møller et al. "Measuring the supernova unknowns at the next-generation neutrino telescopes through the diffuse neutrino background". In: *JCAP* 05 (2018), p. 066. DOI: 10.1088/1475-7516/2018/05/066. arXiv: 1804.03157 [astro-ph.HE].
- [202] André De Gouvêa et al. "Fundamental physics with the diffuse supernova background neutrinos". In: *Phys. Rev. D* 102 (2020), p. 123012. DOI: 10.1103/PhysRevD.102.123012. arXiv: 2007.13748 [hep-ph].
- [203] Pilar Iváñez-Ballesteros and M. Cristina Volpe. "Neutrino nonradiative decay and the diffuse supernova neutrino background". In: *Physical Review D* 107.2 (Jan. 2023), p. 023017. ISSN: 2470-0029. DOI: 10.1103/physrevd.107.023017. arXiv: 2209.12465 [hep-ph]. URL: http://dx.doi.org/10.1103/PhysRevD.107.023017.
- [204] Nicole F. Bell, Matthew J. Dolan, and Sandra Robles. "Dark matter pollution in the Diffuse Supernova Neutrino Background". In: *JCAP* 11 (2022), p. 060. DOI: 10.1088/1475-7516/2022/11/060. arXiv: 2205.14123 [hep-ph].
- [205] André de Gouvêa et al. "Diffuse supernova neutrino background as a probe of late-time neutrino mass generation". In: *Phys. Rev. D* 106.10 (2022), p. 103026. DOI: 10.1103/PhysRevD.106.103026. arXiv: 2205.01102 [hep-ph].
- [206] Zahra Tabrizi and Shunsaku Horiuchi. "Flavor Triangle of the Diffuse Supernova Neutrino Background". In: JCAP 05 (2021), p. 011. DOI: 10.1088/1475-7516/2021/05/011. arXiv: 2011.10933 [hep-ph].
- [207] Anirban Das, Yuber F. Perez-Gonzalez, and Manibrata Sen. "Neutrino secret self-interactions: A booster shot for the cosmic neutrino background". In: *Phys. Rev. D* 106.9 (2022), p. 095042. DOI: 10.1103/PhysRevD.106.095042. arXiv: 2204.11885 [hep-ph].
- [208] Pablo Martnez-Miravé, Irene Tamborra, and Mariam Tórtola. "The Sun and corecollapse supernovae are leading probes of the neutrino lifetime". In: (Jan. 2024). arXiv: 2402.00116 [astro-ph.HE].
- [209] Darcy A. Newmark and Austin Schneider. "Sensitivity to supernovae average  $\nu_x$ x temperature with neutral current interactions in DUNE". In: *Phys. Rev. D* 108.4 (2023), p. 043005. DOI: 10.1103/PhysRevD.108.043005. arXiv: 2304.00035 [hep-ph].
- [210] Shunsaku Horiuchi, John F. Beacom, and Eli Dwek. "The Diffuse Supernova Neutrino Background is detectable in Super-Kamiokande". In: *Phys. Rev. D* 79 (2009), p. 083013. DOI: 10.1103/PhysRevD.79.083013. arXiv: 0812.3157 [astro-ph].

[211] Matthew D. Kistler, Hasan Yuksel, and Andrew M. Hopkins. "The Cosmic Star Formation Rate from the Faintest Galaxies in the Unobservable Universe". In: (May 2013). arXiv: 1305.1630 [astro-ph.CO].

- [212] Nick Ekanger et al. "Diffuse supernova neutrino background with up-to-date star formation rate measurements and long-term multidimensional supernova simulations". In: *Phys. Rev. D* 109.2 (2024), p. 023024. DOI: 10.1103/PhysRevD.109.023024. arXiv: 2310.15254 [astro-ph.HE].
- [213] Edwin E. Salpeter. "The Luminosity Function and Stellar Evolution." In: *The Astro-*physical Journal 121 (Jan. 1955), p. 161. DOI: 10.1086/145971.
- [214] Geneviève Bélanger et al. "micrOMEGAs5.0 : Freeze-in". In: *Comput. Phys. Commun.* 231 (2018), pp. 173–186. DOI: 10.1016/j.cpc.2018.04.027. arXiv: 1801.03509 [hep-ph].
- [215] Oleg Lebedev and Takashi Toma. "Relativistic Freeze-in". In: *Phys. Lett. B* 798 (2019), p. 134961. DOI: 10.1016/j.physletb.2019.134961. arXiv: 1908.05491 [hep-ph].
- [216] Giorgio Arcadi et al. "Real Scalar Dark Matter: Relativistic Treatment". In: *JHEP* 08 (2019), p. 050. DOI: 10.1007/JHEP08(2019)050. arXiv: 1906.07659 [hep-ph].
- [217] Torsten Bringmann et al. "Freezing-in a hot bath: resonances, medium effects and phase transitions". In: *JHEP* 02 (2022), p. 110. DOI: 10.1007/JHEP02(2022)110. arXiv: 2111. 14871 [hep-ph].
- [218] Xuheng Luo, Werner Rodejohann, and Xun-Jie Xu. "Dirac neutrinos and  $N_{eff}$ . Part II. The freeze-in case". In: JCAP 03 (2021), p. 082. DOI: 10.1088/1475-7516/2021/03/082. arXiv: 2011.13059 [hep-ph].
- [219] Lars Husdal. "On Effective Degrees of Freedom in the Early Universe". In: *Galaxies* 4.4 (2016), p. 78. DOI: 10.3390/galaxies4040078. arXiv: 1609.04979 [astro-ph.CO].
- [220] Lawrence J. Hall et al. "Freeze-In Production of FIMP Dark Matter". In: *JHEP* 03 (2010), p. 080. Doi: 10.1007/JHEP03(2010)080. arXiv: 0911.1120 [hep-ph].
- [221] Alberto Salvio. "Introduction to Thermal Field Theory: From First Principles to Applications". In: *Universe* 11.1 (2025), p. 16. DOI: 10.3390/universe11010016. arXiv: 2411.02498 [hep-ph].
- [222] Valentina De Romeri et al. "Neutrino dark matter and the Higgs portal: improved freeze-in analysis". In: *JHEP* 10 (2020), p. 137. DOI: 10.1007/JHEP10(2020)137. arXiv: 2003.12606 [hep-ph].
- [223] Per Elmfors, Kari Enqvist, and Iiro Vilja. "Thermalization of the Higgs field at the electroweak phase transition". In: *Nucl. Phys. B* 412 (1994), pp. 459–478. DOI: 10.1016/0550-3213(94)90512-6. arXiv: hep-ph/9307210.
- [224] Mariano Quiros. "Finite temperature field theory and phase transitions". In: *ICTP Summer School in High-Energy Physics and Cosmology*. Jan. 1999, pp. 187–259. arXiv: hep-ph/9901312.

[225] H. Arthur Weldon. "Simple Rules for Discontinuities in Finite Temperature Field Theory". In: *Phys. Rev. D* 28 (1983), p. 2007. DOI: 10.1103/PhysRevD.28.2007.

- [226] Torsten Bringmann et al. "Electroweak and Higgs Boson Internal Bremsstrahlung: General considerations for Majorana dark matter annihilation and application to MSSM neutralinos". In: *JHEP* 09 (2017), p. 041. DOI: 10.1007/JHEP09(2017)041. arXiv: 1705.03466 [hep-ph].
- [227] C. F. Uhlemann and N. Kauer. "Narrow-width approximation accuracy". In: Nucl. Phys. B 814 (2009), pp. 195–211. DOI: 10.1016/j.nuclphysb.2009.01.022. arXiv: 0807.4112 [hep-ph].
- [228] Xuheng Luo, Werner Rodejohann, and Xun-Jie Xu. "Dirac neutrinos and  $N_{\rm eff}$ ". In: JCAP 06 (2020), p. 058. DOI: 10.1088/1475-7516/2020/06/058. arXiv: 2005.01629 [hep-ph].
- [229] Morad Aaboud et al. "Search for new high-mass phenomena in the dilepton final state using 36 fb<sup>-1</sup> of proton-proton collision data at  $\sqrt{s}=13$  TeV with the ATLAS detector". In: *JHEP* 10 (2017), p. 182. DOI: 10.1007/JHEP10(2017)182. arXiv: 1707.02424 [hepex].
- [230] M. Aaboud et al. "Measurement of the Drell-Yan triple-differential cross section in pp collisions at  $\sqrt{s}=8$  TeV". In: JHEP 12 (2017), p. 059. DOI: 10.1007/JHEP12(2017)059. arXiv: 1710.05167 [hep-ex].
- [231] Miguel Escudero, Samuel J. Witte, and Nuria Rius. "The dispirited case of gauged  $U(1)_{B-L}$  dark matter". In: *JHEP* 08 (2018), p. 190. DOI: 10.1007/JHEP08(2018)190. arXiv: 1806.02823 [hep-ph].
- [232] Roel Aaij et al. "Search for Dark Photons Produced in 13 TeV pp Collisions". In: Phys. Rev. Lett. 120.6 (2018), p. 061801. DOI: 10.1103/PhysRevLett.120.061801. arXiv: 1710.02867 [hep-ex].
- [233] J. P. Lees et al. "Search for a Dark Photon in  $e^+e^-$  Collisions at BaBar". In: *Phys. Rev. Lett.* 113.20 (2014), p. 201801. DOI: 10.1103/PhysRevLett.113.201801. arXiv: 1406.2980 [hep-ex].
- [234] Wei Liu, Suchita Kulkarni, and Frank F. Deppisch. "Heavy neutrinos at the FCC-hh in the U(1)B-L model". In: *Phys. Rev. D* 105.9 (2022), p. 095043. DOI: 10.1103/PhysRevD. 105.095043. arXiv: 2202.07310 [hep-ph].
- [235] Peter Adshead et al. "Unraveling the Dirac neutrino with cosmological and terrestrial detectors". In: *Phys. Lett. B* 823 (2021), p. 136736. DOI: 10.1016/j.physletb.2021. 136736. arXiv: 2009.07852 [hep-ph].
- [236] Shao-Ping Li and Xun-Jie Xu. " $N_{eff}$  constraints on light mediators coupled to neutrinos: the dilution-resistant effect". In: *JHEP* 10 (2023), p. 012. DOI: 10.1007/JHEP10(2023) 012. arXiv: 2307.13967 [hep-ph].

[237] Haidar Esseili and Graham D. Kribs. "Cosmological implications of gauged U(1) $_{B-L}$  on  $\Delta$ N  $_{eff}$  in the CMB and BBN". In: JCAP 05 (2024), p. 110. DOI: 10.1088/1475-7516/2024/05/110. arXiv: 2308.07955 [hep-ph].

- [238] Y. Akrami et al. "Planck 2018 results. X. Constraints on inflation". In: *Astron. Astrophys.* 641 (2020), A10. DOI: 10.1051/0004-6361/201833887. arXiv: 1807.06211 [astroph.CO].
- [239] Stephen P. Martin. "A Supersymmetry primer". In: *Adv. Ser. Direct. High Energy Phys.* 18 (1998). Ed. by Gordon L. Kane, pp. 1–98. DOI: 10.1142/9789812839657\_0001. arXiv: hep-ph/9709356.
- [240] Cristina Benso, Felix Kahlhoefer, and Henda Mansour. "Dark matter phase-in: producing feebly-interacting particles after a first-order phase transition". In: (Apr. 2025). arXiv: 2504.10593 [hep-ph].
- [241] Chiara Caprini et al. "Detecting gravitational waves from cosmological phase transitions with LISA: an update". In: *JCAP* 03 (2020), p. 024. DOI: 10.1088/1475-7516/2020/03/024. arXiv: 1910.13125 [astro-ph.CO].
- [242] Rouzbeh Allahverdi et al. "The First Three Seconds: a Review of Possible Expansion Histories of the Early Universe". In: *Open J. Astrophys.* 4 (2021), astro.2006.16182. DOI: 10.21105/astro.2006.16182. arXiv: 2006.16182 [astro-ph.CO].
- [243] Brian Batell et al. "Conversations and deliberations: Non-standard cosmological epochs and expansion histories". In: *Int. J. Mod. Phys. A* 40.17 (2025), p. 2530004. DOI: 10. 1142/S0217751X25300042. arXiv: 2411.04780 [astro-ph.CO].
- [244] Mara Dutra and Yongcheng Wu. "EvoEMD: cosmic evolution with an early matter-dominated era". In: *Phys. Dark Univ.* 40 (2023), p. 101198. DOI: 10.1016/j.dark.2023. 101198. arXiv: 2111.15665 [hep-ph].
- [245] Manuel Drees and Fazlollah Hajkarim. "Dark Matter Production in an Early Matter Dominated Era". In: JCAP 02 (2018), p. 057. DOI: 10.1088/1475-7516/2018/02/057. arXiv: 1711.05007 [hep-ph].
- [246] Luca Caloni et al. "Constraining UV freeze-in of light relics with current and next-generation CMB observations". In: *JCAP* 10 (2024), p. 106. DOI: 10.1088/1475-7516/2024/10/106. arXiv: 2405.09449 [astro-ph.CO].
- [247] Karin Dick et al. "Leptogenesis with Dirac neutrinos". In: Phys. Rev. Lett. 84 (2000), pp. 4039–4042. DOI: 10.1103/PhysRevLett.84.4039. arXiv: hep-ph/9907562.
- [248] Marc Kamionkowski and John March-Russell. "Planck scale physics and the Peccei-Quinn mechanism". In: Phys. Lett. B 282 (1992), pp. 137–141. DOI: 10.1016/0370-2693(92)90492-M. arXiv: hep-th/9202003.
- [249] Eleonora Di Valentino et al. "In the realm of the Hubble tensiona review of solutions". In: *Class. Quant. Grav.* 38.15 (2021), p. 153001. DOI: 10.1088/1361-6382/ac086d. arXiv: 2103.01183 [astro-ph.CO].

[250] Ernest Ma et al. "Gauge B-L Model with Residual  $Z_3$  Symmetry". In: *Phys. Lett. B* 750 (2015), pp. 135–138. DOI: 10.1016/j.physletb.2015.09.010. arXiv: 1507.03943 [hep-ph].

- [251] Ernest Ma and Rahul Srivastava. "Dirac or inverse seesaw neutrino masses with B-L gauge symmetry and  $S_3$  flavor symmetry". In: *Phys. Lett. B* 741 (2015), pp. 217–222. DOI: 10.1016/j.physletb.2014.12.049. arXiv: 1411.5042 [hep-ph].
- [252] Salvador Centelles Chuliá et al. "Dirac Neutrinos and Dark Matter Stability from Lepton Quarticity". In: *Phys. Lett. B* 767 (2017), pp. 209–213. DOI: 10.1016/j.physletb.2017.
   01.070. arXiv: 1606.04543 [hep-ph].
- [253] Salvador Centelles Chuliá, Rahul Srivastava, and José W. F. Valle. "Seesaw roadmap to neutrino mass and dark matter". In: *Phys. Lett. B* 781 (2018), pp. 122–128. DOI: 10.1016/j.physletb.2018.03.046. arXiv: 1802.05722 [hep-ph].
- [254] Martin Hirsch, Rahul Srivastava, and José W. F. Valle. "Can one ever prove that neutrinos are Dirac particles?" In: *Phys.Lett.* B781 (2018), pp. 302–305. DOI: 10.1016/j. physletb.2018.03.073. arXiv: 1711.06181 [hep-ph].
- [255] Cesar Bonilla and Jose W. F. Valle. "Naturally light neutrinos in *Diracon* model". In: *Phys. Lett. B* 762 (2016), pp. 162–165. DOI: 10.1016/j.physletb.2016.09.022. arXiv: 1605.08362 [hep-ph].
- [256] Anjan S. Joshipura and Saurabh D. Rindani. "Majoron models and the Higgs search". In: *Phys. Rev. Lett.* 69 (1992), pp. 3269–3273. DOI: 10.1103/PhysRevLett.69.3269.
- [257] Anjan S. Joshipura and J. W. F. Valle. "Invisible Higgs decays and neutrino physics". In: Nucl.Phys.B 397 (1993), pp. 105–122. DOI: 10.1016/0550-3213(93)90337-0.
- [258] L. Lavoura. "General formulae for  $f_1 \rightarrow f_2 \gamma$ ". In: Eur. Phys. J. C 29 (2003), pp. 191–195. DOI: 10.1140/epjc/s2003-01212-7. arXiv: hep-ph/0302221.
- [259] Ernest Ma and A. Pramudita. "Exact Formula for  $(\mu \to e\gamma)$  Type Processes in the Standard Model". In: *Phys. Rev. D* 24 (1981), p. 1410. DOI: 10.1103/PhysRevD.24.1410.
- [260] K. Afanaciev et al. "New limit on the  $\mu+->e+\gamma$  decay with the MEG II experiment". In: (Apr. 2025). arXiv: 2504.15711 [hep-ex].
- [261] Alessandro M. Baldini et al. "The Search for  $\mu^+ \to e^+ \gamma$  with  $10^{-14}$  Sensitivity: The Upgrade of the MEG Experiment". In: *Symmetry* 13.9 (2021), p. 1591. DOI: 10.3390/sym13091591. arXiv: 2107.10767 [hep-ex].
- [262] Antonio Herrero-Brocal and Avelino Vicente. "The majoron coupling to charged leptons". In: *JHEP* 01 (2024), p. 078. DOI: 10.1007/JHEP01(2024)078. arXiv: 2311.10145 [hep-ph].
- [263] Pablo Escribano and Avelino Vicente. "Ultralight scalars in leptonic observables". In: JHEP 03 (2021), p. 240. DOI: 10.1007/JHEP03(2021)240. arXiv: 2008.01099 [hep-ph].
- [264] Luca Di Luzio et al. "The landscape of QCD axion models". In: *Phys. Rept.* 870 (2020), pp. 1–117. DOI: 10.1016/j.physrep.2020.06.002. arXiv: 2003.01100 [hep-ph].

[265] Maurizio Giannotti. "Hints of new physics from stars". In: PoS ICHEP2016 (2016),p. 076. DOI: 10.22323/1.282.0076. arXiv: 1611.04651 [astro-ph.HE].

- [266] Alejandro H. Córsico et al. "Pulsating white dwarfs: new insights". In: *Astron. Astrophys. Rev.* 27.1 (2019), p. 7. DOI: 10.1007/s00159-019-0118-4. arXiv: 1907.00115 [astro-ph.SR].
- [267] Francesco Capozzi and Georg Raffelt. "Axion and neutrino bounds improved with new calibrations of the tip of the red-giant branch using geometric distance determinations". In: *Phys. Rev. D* 102.8 (2020), p. 083007. DOI: 10.1103/PhysRevD.102.083007. arXiv: 2007.03694 [astro-ph.SR].
- [268] O. Straniero et al. "The RGB tip of galactic globular clusters and the revision of the axion-electron coupling bound". In: *Astron. Astrophys.* 644 (2020), A166. DOI: 10.1051/0004-6361/202038775. arXiv: 2010.03833 [astro-ph.SR].
- [269] Lorenzo Calibbi et al. "Looking forward to lepton-flavor-violating ALPs". In: *JHEP* 09 (2021), p. 173. DOI: 10.1007/JHEP09(2021)173. arXiv: 2006.04795 [hep-ph].
- [270] Djuna Croon et al. "Supernova Muons: New Constraints on Z' Bosons, Axions and ALPs". In: *JHEP* 01 (2021), p. 107. DOI: 10.1007/JHEP01(2021)107. arXiv: 2006.13942 [hep-ph].
- [271] Andrea Caputo, Georg Raffelt, and Edoardo Vitagliano. "Muonic boson limits: Supernova redux". In: Phys. Rev. D 105.3 (2022), p. 035022. DOI: 10.1103/PhysRevD.105.035022. arXiv: 2109.03244 [hep-ph].
- [272] A. Jodidio et al. "Search for Right-Handed Currents in Muon Decay". In: Phys. Rev. D 34 (1986). [Erratum: Phys.Rev.D 37, 237 (1988)], p. 1967. DOI: 10.1103/PhysRevD.34.1967.
- [273] M. Hirsch et al. "Majoron emission in muon and tau decays revisited". In: *Phys. Rev. D* 79 (2009). [Erratum: Phys.Rev.D 79, 079901 (2009)], p. 055023. DOI: 10.1103/PhysRevD. 79.055023. arXiv: 0902.0525 [hep-ph].
- [274] Gavin Hesketh et al. "The Mu3e Experiment". In: *Snowmass 2021*. Apr. 2022. arXiv: 2204.00001 [hep-ex].
- [275] Ann-Kathrin Perrevoort. "Charged lepton flavour violation Overview of current experimental limits and future plans". In: *PoS* DISCRETE2022 (2024), p. 015. DOI: 10. 22323/1.431.0015.
- [276] R. Abramishvili et al. "COMET Phase-I Technical Design Report". In: *PTEP* 2020.3 (2020), p. 033C01. DOI: 10.1093/ptep/ptz125. arXiv: 1812.09018 [physics.ins-det].
- [277] Tianyu Xing et al. "Search for Majoron at the COMET experiment\*". In: *Chin. Phys. C* 47.1 (2023), p. 013108. DOI: 10.1088/1674-1137/ac9897. arXiv: 2209.12802 [hep-ex].
- [278] Yongsoo Jho, Simon Knapen, and Diego Redigolo. "Lepton-flavor violating axions at MEG II". In: *JHEP* 10 (2022), p. 029. DOI: 10.1007/JHEP10(2022)029. arXiv: 2203. 11222 [hep-ph].
- [279] Simon Knapen et al. "A Robust Search for Lepton Flavour Violating Axions at Mu3e". In: (Nov. 2023). arXiv: 2311.17915 [hep-ph].

[280] Andrey Katz and Maxim Perelstein. "Higgs Couplings and Electroweak Phase Transition". In: *JHEP* 07 (2014), p. 108. DOI: 10.1007/JHEP07(2014)108. arXiv: 1401.1827 [hep-ph].

- [281] Oleksii Matsedonskyi and Geraldine Servant. "High-Temperature Electroweak Symmetry Non-Restoration from New Fermions and Implications for Baryogenesis". In: *JHEP* 09 (2020), p. 012. DOI: 10.1007/JHEP09(2020)012. arXiv: 2002.05174 [hep-ph].
- [282] Hitoshi Murayama and Aaron Pierce. "Realistic Dirac leptogenesis". In: *Phys. Rev. Lett.* 89 (2002), p. 271601. DOI: 10.1103/PhysRevLett.89.271601. arXiv: hep-ph/0206177.
- [283] D. G. Cerdeno, A. Dedes, and T. E. J. Underwood. "The Minimal Phantom Sector of the Standard Model: Higgs Phenomenology and Dirac Leptogenesis". In: JHEP 09 (2006), p. 067. DOI: 10.1088/1126-6708/2006/09/067. arXiv: hep-ph/0607157.
- [284] Julian Heeck, Jan Heisig, and Anil Thapa. "Testing Dirac leptogenesis with the cosmic microwave background and proton decay". In: *Phys. Rev. D* 108.3 (2023), p. 035014. DOI: 10.1103/PhysRevD.108.035014. arXiv: 2304.09893 [hep-ph].
- [285] Yohei Ema, Filippo Sala, and Ryosuke Sato. "Light Dark Matter at Neutrino Experiments". In: *Phys. Rev. Lett.* 122.18 (2019), p. 181802. DOI: 10.1103/PhysRevLett.122. 181802. arXiv: 1811.00520 [hep-ph].
- [286] Christopher V. Cappiello, Kenny C. Y. Ng, and John F. Beacom. "Reverse Direct Detection: Cosmic Ray Scattering With Light Dark Matter". In: *Phys. Rev. D* 99.6 (2019), p. 063004. DOI: 10.1103/PhysRevD.99.063004. arXiv: 1810.07705 [hep-ph].
- [287] James B. Dent et al. "Bounds on Cosmic Ray-Boosted Dark Matter in Simplified Models and its Corresponding Neutrino-Floor". In: *Phys. Rev. D* 101.11 (2020), p. 116007. DOI: 10.1103/PhysRevD.101.116007. arXiv: 1907.03782 [hep-ph].
- [288] Wenyu Wang et al. "Cosmic ray boosted sub-GeV gravitationally interacting dark matter in direct detection". In: *JHEP* 12 (2020). [Erratum: JHEP 02, 052 (2021)], p. 072. DOI: 10.1007/JHEP12(2020)072. arXiv: 1912.09904 [hep-ph].
- [289] James Alvey et al. "Detecting Light Dark Matter via Inelastic Cosmic Ray Collisions". In: Phys. Rev. Lett. 123 (2019), p. 261802. DOI: 10.1103/PhysRevLett.123.261802. arXiv: 1905.05776 [hep-ph].
- [290] Gang Guo et al. "Elastic and Inelastic Scattering of Cosmic-Rays on Sub-GeV Dark Matter". In: *Phys. Rev. D* 102.10 (2020), p. 103004. DOI: 10.1103/PhysRevD.102.103004. arXiv: 2008.12137 [astro-ph.HE].
- [291] Gang Guo et al. "Elastic and inelastic scattering of cosmic rays on sub-GeV dark matter". In: *Physical Review D* 102.10 (Nov. 2020). ISSN: 2470-0029. DOI: 10.1103/physrevd. 102.103004. URL: http://dx.doi.org/10.1103/PhysRevD.102.103004.
- [292] James B. Dent et al. "Present and future status of light dark matter models from cosmic-ray electron upscattering". In: *Phys. Rev. D* 103 (2021), p. 095015. DOI: 10. 1103/PhysRevD.103.095015. arXiv: 2010.09749 [hep-ph].

[293] Chen Xia, Yan-Hao Xu, and Yu-Feng Zhou. "Production and attenuation of cosmic-ray boosted dark matter". In: *JCAP* 02.02 (2022), p. 028. DOI: 10.1088/1475-7516/2022/02/028. arXiv: 2111.05559 [hep-ph].

- [294] Nicole F. Bell et al. "Cosmic-ray upscattered inelastic dark matter". In: *Phys. Rev. D* 104 (2021), p. 076020. DOI: 10.1103/PhysRevD.104.076020. arXiv: 2108.00583 [hep-ph].
- [295] Debjyoti Bardhan et al. "Bounds on boosted dark matter from direct detection: The role of energy-dependent cross sections". In: *Phys. Rev. D* 107.1 (2023), p. 015010. DOI: 10.1103/PhysRevD.107.015010. arXiv: 2208.09405 [hep-ph].
- [296] Tarak Nath Maity and Ranjan Laha. "Cosmic-ray boosted dark matter in Xe-based direct detection experiments". In: Eur. Phys. J. C 84.2 (2024), p. 117. DOI: 10.1140/epjc/s10052-024-12464-8. arXiv: 2210.01815 [hep-ph].
- [297] Atanu Guha and Jong-Chul Park. "Constraints on cosmic-ray boosted dark matter with realistic cross section". In: (Jan. 2024). arXiv: 2401.07750 [hep-ph].
- [298] Nicole F. Bell, Jayden L. Newstead, and Iman Shaukat-Ali. "Cosmic-ray boosted dark matter confronted by constraints on new light mediators". In: *Phys. Rev. D* 109.6 (2024), p. 063034. DOI: 10.1103/PhysRevD.109.063034. arXiv: 2309.11003 [hep-ph].
- [299] Christopher Cappiello et al. "Cosmic Ray-Boosted Dark Matter at IceCube". In: (Apr. 2024). arXiv: 2405.00086 [hep-ph].
- [300] Kaustubh Agashe et al. "(In)direct Detection of Boosted Dark Matter". In: *JCAP* 10 (2014), p. 062. DOI: 10.1088/1475-7516/2014/10/062. arXiv: 1405.7370 [hep-ph].
- [301] Joshua Berger, Yanou Cui, and Yue Zhao. "Detecting Boosted Dark Matter from the Sun with Large Volume Neutrino Detectors". In: *JCAP* 02 (2015), p. 005. DOI: 10.1088/1475-7516/2015/02/005. arXiv: 1410.2246 [hep-ph].
- [302] Haipeng An et al. "Directly Detecting MeV-scale Dark Matter via Solar Reflection". In: Phys. Rev. Lett. 120.14 (2018). [Erratum: Phys.Rev.Lett. 121, 259903 (2018)], p. 141801. DOI: 10.1103/PhysRevLett.120.141801. arXiv: 1708.03642 [hep-ph].
- [303] Wen Yin. "Highly-boosted dark matter and cutoff for cosmic-ray neutrinos through neutrino portal". In: *EPJ Web Conf.* 208 (2019). Ed. by B. Pattison et al., p. 04003. DOI: 10.1051/epjconf/201920804003. arXiv: 1809.08610 [hep-ph].
- [304] William DeRocco et al. "Supernova signals of light dark matter". In: *Phys. Rev. D* 100.7 (2019), p. 075018. DOI: 10.1103/PhysRevD.100.075018. arXiv: 1905.09284 [hep-ph].
- [305] Timon Emken and Chris Kouvaris. "How blind are underground and surface detectors to strongly interacting Dark Matter?" In: *Phys. Rev. D* 97.11 (2018), p. 115047. DOI: 10.1103/PhysRevD.97.115047. arXiv: 1802.04764 [hep-ph].
- [306] Yifan Chen et al. "Sun heated MeV-scale dark matter and the XENON1T electron recoil excess". In: *JHEP* 04 (2021), p. 282. DOI: 10.1007/JHEP04(2021)282. arXiv: 2006.12447 [hep-ph].
- [307] Haipeng An et al. "Solar reflection of dark matter". In: Phys. Rev. D 104.10 (2021),
   p. 103026. DOI: 10.1103/PhysRevD.104.103026. arXiv: 2108.10332 [hep-ph].

[308] Alessandro Granelli, Piero Ullio, and Jin-Wei Wang. "Blazar-boosted dark matter at Super-Kamiokande". In: *JCAP* 07.07 (2022), p. 013. DOI: 10.1088/1475-7516/2022/07/013. arXiv: 2202.07598 [astro-ph.HE].

- [309] Timon Emken. "Solar reflection of light dark matter with heavy mediators". In: Phys. Rev. D 105.6 (2022), p. 063020. DOI: 10.1103/PhysRevD.105.063020. arXiv: 2102.12483 [hep-ph].
- [310] Chen Xia, Chuan-Yang Xing, and Yan-Hao Xu. "Boosted Dark Matter From Centaurus A and Its Detection". In: (Jan. 2024). DOI: 10.1007/JHEP03(2024)076. arXiv: 2401.03772 [hep-ph].
- [311] Keyu Lu et al. "Inelastic Scattering of Dark Matter with Heavy Cosmic Rays". In: *Res. Astron. Astrophys.* 24.6 (2024), p. 065007. DOI: 10.1088/1674-4527/ad3c6f. arXiv: 2310.12501 [astro-ph.HE].
- [312] Yifan Chen et al. "Earth shielding and daily modulation from electrophilic boosted dark particles". In: *Phys. Rev. D* 107.3 (2023), p. 033006. DOI: 10.1103/PhysRevD.107.033006. arXiv: 2110.09685 [hep-ph].
- [313] Adam Falkowski, Jose Juknevich, and Jessie Shelton. "Dark Matter Through the Neutrino Portal". In: (Aug. 2009). arXiv: 0908.1790 [hep-ph].
- [314] Eleonora Di Valentino et al. "Reducing the  $H_0$  and  $\sigma_8$  tensions with Dark Matterneutrino interactions". In: *Phys. Rev. D* 97.4 (2018), p. 043513. DOI: 10.1103/PhysRevD. 97.043513. arXiv: 1710.02559 [astro-ph.CO].
- [315] Yasaman Farzan and Sergio Palomares-Ruiz. "Dips in the Diffuse Supernova Neutrino Background". In: *JCAP* 06 (2014), p. 014. DOI: 10.1088/1475-7516/2014/06/014. arXiv: 1401.7019 [hep-ph].
- [316] Torsten Bringmann and Christoph Weniger. "Gamma Ray Signals from Dark Matter: Concepts, Status and Prospects". In: *Phys. Dark Univ.* 1 (2012), pp. 194–217. DOI: 10.1016/j.dark.2012.10.005. arXiv: 1208.5481 [hep-ph].
- [317] Julio F. Navarro, Carlos S. Frenk, and Simon D. M. White. "The Structure of Cold Dark Matter Halos". In: *The Astrophysical Journal* 462 (May 1996), p. 563. ISSN: 1538-4357. DOI: 10.1086/177173. URL: http://dx.doi.org/10.1086/177173.
- [318] E. Aprile et al. "Search for New Physics in Electronic Recoil Data from XENONnT". In: Phys. Rev. Lett. 129.16 (2022), p. 161805. DOI: 10.1103/PhysRevLett.129.161805. arXiv: 2207.11330 [hep-ex].
- [319] J. Aalbers et al. "First Dark Matter Search Results from the LUX-ZEPLIN (LZ) Experiment". In: Phys. Rev. Lett. 131.4 (2023), p. 041002. DOI: 10.1103/PhysRevLett.131. 041002. arXiv: 2207.03764 [hep-ex].
- [320] J. Aalbers et al. "Background determination for the LUX-ZEPLIN dark matter experiment". In: *Phys. Rev. D* 108.1 (2023), p. 012010. DOI: 10.1103/PhysRevD.108.012010. arXiv: 2211.17120 [hep-ex].

[321] Dan Zhang et al. "Search for Light Fermionic Dark Matter Absorption on Electrons in PandaX-4T". In: *Phys. Rev. Lett.* 129.16 (2022), p. 161804. DOI: 10.1103/PhysRevLett. 129.161804. arXiv: 2206.02339 [hep-ex].

- [322] Xuyang Ning et al. "Search for Light Dark Matter from the Atmosphere in PandaX-4T". In: *Phys. Rev. Lett.* 131.4 (2023), p. 041001. DOI: 10.1103/PhysRevLett.131.041001. arXiv: 2301.03010 [hep-ex].
- [323] Bartosz Fornal et al. "Boosted Dark Matter Interpretation of the XENON1T Excess". In: *Phys. Rev. Lett.* 125.16 (2020), p. 161804. DOI: 10.1103/PhysRevLett.125.161804. arXiv: 2006.11264 [hep-ph].
- [324] E. Aprile et al. "Excess electronic recoil events in XENON1T". In: *Physical Review D* 102.7 (Oct. 2020). ISSN: 2470-0029. DOI: 10.1103/physrevd.102.072004. URL: http://dx.doi.org/10.1103/PhysRevD.102.072004.
- [325] David V. Nguyen et al. "Observational constraints on dark matter scattering with electrons". In: *Phys. Rev. D* 104.10 (2021), p. 103521. DOI: 10.1103/PhysRevD.104.103521. arXiv: 2107.12380 [astro-ph.CO].
- [326] Manuel A. Buen-Abad et al. "Cosmological constraints on dark matter interactions with ordinary matter". In: *Phys. Rept.* 961 (2022), pp. 1–35. DOI: 10.1016/j.physrep.2022. 02.006. arXiv: 2107.12377 [astro-ph.CO].
- [327] Prakruth Adari et al. "SENSEI: First Direct-Detection Results on sub-GeV Dark Matter from SENSEI at SNOLAB". In: (Dec. 2023). arXiv: 2312.13342 [astro-ph.C0].
- [328] I. Arnquist et al. "First Constraints from DAMIC-M on Sub-GeV Dark-Matter Particles Interacting with Electrons". In: *Phys. Rev. Lett.* 130.17 (2023), p. 171003. DOI: 10.1103/PhysRevLett.130.171003. arXiv: 2302.02372 [hep-ex].
- [329] Kensuke Akita and Shin'ichiro Ando. "Constraints on dark matter-neutrino scattering from the Milky-Way satellites and subhalo modeling for dark acoustic oscillations". In: *JCAP* 11 (2023), p. 037. DOI: 10.1088/1475-7516/2023/11/037. arXiv: 2305.01913 [astro-ph.CO].
- [330] Christopher V. Cappiello and John F. Beacom. "Strong new limits on light dark matter from neutrino experiments". In: *Phys. Rev. D* 100 (10 Nov. 2019), p. 103011. DOI: 10. 1103/PhysRevD.100.103011. URL: https://link.aps.org/doi/10.1103/PhysRevD.100. 103011.
- [331] Timon Emken et al. "Direct Detection of Strongly Interacting Sub-GeV Dark Matter via Electron Recoils". In: *JCAP* 09 (2019), p. 070. DOI: 10.1088/1475-7516/2019/09/070. arXiv: 1905.06348 [hep-ph].
- [332] Christopher V. Cappiello. "Analytic Approach to Light Dark Matter Propagation". In: *Phys. Rev. Lett.* 130.22 (2023), p. 221001. DOI: 10.1103/PhysRevLett.130.221001. arXiv: 2301.07728 [hep-ph].

[333] G Peter Lepage. "A new algorithm for adaptive multidimensional integration". In: Journal of Computational Physics 27.2 (1978), pp. 192–203. ISSN: 0021-9991. DOI: https://doi.org/10.1016/0021-9991(78)90004-9. URL: https://www.sciencedirect.com/science/article/pii/0021999178900049.

- [334] G. Peter Lepage. "Adaptive multidimensional integration: VEGAS enhanced". In: *J. Comput. Phys.* 439 (2021), p. 110386. DOI: 10.1016/j.jcp.2021.110386. arXiv: 2009. 05112 [physics.comp-ph].
- [335] Torsten Bringmann et al. "Minimal sterile neutrino dark matter". In: *Phys. Rev. D* 107.7 (2023), p. L071702. DOI: 10.1103/PhysRevD.107.L071702. arXiv: 2206.10630 [hep-ph].